Politecnico di Milano

Department of Civil and Environmental Engineering

Doctoral School in Structural, Seismic and Geotechnical Engineering

XXV Cycle

LIFETIME PERFORMANCE AND SEISMIC RESILIENCE OF CONCRETE STRUCTURES EXPOSED TO CORROSION

Doctoral Dissertation by

Elena Camnasio

Supervisor

Prof. Fabio Biondini

The Chair of the Doctoral Program

Prof. Roberto Paolucci

Milan, October 16, 2013

Doctoral School in Structural, Seismic and Geotechnical Engineering
Department of Civil and Environmental Engineering
Politecnico di Milano
XXV Cycle

Supervisor

Prof. Fabio Biondini

The Chair of the Doctoral Program

Prof. Roberto Paolucci

Board Committee

Prof. Raffaele Ardito
Prof. Fabio Biondini
Prof. Gabriella Bolzon
Prof. Claudia Comi
Prof. Alberto Corigliano
Prof. Dario Coronelli
Prof. Claudio di Prisco
Prof. Marco di Prisco
Prof. Liberato Ferrara
Prof. Attilio Frangi
Prof. Elsa Garavaglia
Prof. Cristina Jommi
Prof. Pier Giorgio Malerba
Prof. Anna Pandolfi
Prof. Roberto Paolucci
Prof. Umberto Perego
Prof. Federico Perotti
Prof. Lorenza Petrini
Prof. Gianpaolo Rosati
Prof. Luigi Zanzi

To those who never give up

ABSTRACT

Seismic design of concrete structures is currently based on time-invariant capacity design criteria that do not account for environmental hazard. However, corrosion-induced damage of both concrete and reinforcing steel may affect over time the structural performance at global level, by reducing the capability to withstand the effects of a seismic event and to recover efficiently the original functionality. Therefore, the long-term behavior of deteriorating structural systems has to be properly considered in the seismic design of resilient concrete structures.

This Thesis presents a probabilistic approach to lifetime assessment of seismic performance and resilience of concrete structures exposed to corrosion. A life-cycle analysis methodology is presented accounting for both seismic and environmental hazards. Criteria for a time-variant measure of seismic resilience are proposed in order to take into account the combined effects of mechanical and environmental stressors. In particular, suitable performance indicators of the lifetime seismic capacity are considered, and structural functionality and resilience are investigated over time with respect to different limit states, from damage limitation up to collapse.

The proposed procedure is applied to a multi-story frame and a continuous bridge. The results demonstrate that structures designed for the same functionality target could exhibit over time different seismic performance and resilience depending on the environmental exposure. This highlights the need of a life-cycle oriented seismic design approach and the importance of a lifetime resilience assessment of concrete structures in the perspective of seismic risk mitigation.

Keywords: Concrete structures; Corrosion; Environmental damage; Seismic hazard; Lifetime structural performance; Time-variant seismic resilience.

ACKNOWLEDGEMENTS

At the end of my PhD studies, I would like to thank all the people who contributed to the present work in many ways.

First of all, I gratefully thank Professor Fabio Biondini, who supervised me with his valuable knowledge and experience. During the development of the Thesis, he involved me in various and attractive research fields. By his example, I learnt the importance of precision and dedication in research. I thank also Dr. Alessandro Palermo, who encouraged me to undertake the PhD. His passion and positive attitude for work were always inspiring.

Within the PhD, I had the chance to spend a nine-month period as a visiting researcher at the University of Canterbury, New Zealand, in order to develop part of the Thesis under the supervision of Dr. Palermo. There I was also involved in the post-earthquake assessment activities after the seismic event that stroke Christchurch on February 22, 2011. The evidence of earthquake disruption (and the aftershocks still occurring) made me even more aware of the crucial role of a good Researcher and a responsible Engineer. I would also like to thank Prof. Athol Carr, Dr. Liam Wotherspoon and Dr. Allan Scott for the fruitful collaboration in the research activities and all the people in the Department of Civil and Natural Resources Engineering who made my time there a pleasant stay.

Special thanks go to Andrea and Roberto, who spent with me every endless day in the office at Politecnico (and every lunch break!). Their continuous support has been fundamental in the progress of this work. Day by day, they became good friends rather than colleagues.

Thanks to Manuel, Visar, Juan, Francesco and Bruno, who shared with me "joys and pains" of being a PhD student, and to all the people who gave me a hand. The life in the Department would not have been definitely the same without them all.

Thanks to Mustafa, Daniela, Maria, Rodolfo, Alex, Denjam, Lucas, Anton, Andrew, Francesco, Manuel, Robert, Janelle, Tanya and Andy for being co-workers, flatmates and, above all, friends beyond cultural differences. They each contributed in making the living in New Zealand one of the most incredible experiences in my life.

Thanks to Sara, Elda, Roberta and Gianluca, who encouraged me to pursue my goal. Nevertheless, they were always there when I needed a break. Thanks for every laugh and for the good times we spent together.

Finally, I wish to thank my family, Mum, Dad and Erica, for supporting me throughout my education. Their love and patience helped me in overcoming the difficulties I had to face during the last three years. At the end every effort was worth it.

TABLE OF CONTENTS

PREFACE

Structural systems suffer aging, fatigue and deterioration over lifetime. Depending on the environmental exposure, aggressive chemical attacks and other physical damage mechanisms affect the structural performance by reducing the material and mechanical properties. The effects over time of these complex phenomena depend on both the type of damage process and the structural scheme. In fact, the local damage at element level is reflected at global level by a time-variant structural response under service loadings or accidental actions. In particular, the assessment of the long time performance of deteriorating systems becomes critical when the structure is subjected to natural hazards, such as earthquakes, and other extreme events.

As a consequence, the evaluation of the condition of existing structures and infrastructures gained increasing attention over the past decade. Huge stocks of buildings, bridges, roads, railways, dams, ports and other construction facilities have been rated showing significant deterioration and structural deficiencies, which affect the serviceability of such structures. Moreover, maintenance costs have a considerably high economic impact, as assessed for example by the ASCE's 2013 *Report Card for America's Infrastructure*. The Federal Highway Administration (FHWA) estimates that an increased investment of about $10 billion annually is needed to improve the condition of the nation's bridge network by repair interventions, without considering indirect economic losses.

European and Italian design codes and standards recently included specific requirements related to the durability of reinforced concrete structures in the perspective of lifetime extension. In particular,

requirements for concrete cover, water/cement ratio, minimum cement content, amount and type of cement, among others, are established depending on environmental exposure, in order to limit local damage due to concrete degradation and steel corrosion. However, the current prescriptive approach, which discards the interactions between the parts of the structure and the environment, has to be considered incomplete. Current codes limit the checking of strength requirements at local analysis, without explicitly consider for the interaction between the structural system, the load conditions and the environmental exposure. Actually, a durability failure may be a partial reason for mechanical failure.

In this perspective, significant research advances have been accomplished recently in the fields of modeling, analysis and design of deteriorating Civil Engineering systems. These advances highlighted the need of incorporating life-cycle concepts in a global design approach to account for the effects of deterioration processes on the overall structural performance. Moreover, to this purpose a reliable assessment of the performance of structures over time has to be carried out in probabilistic terms, because of the uncertainty in material and geometrical properties, in the physical models of the deterioration process and in the mechanical and environmental stressors.

A reliable design combined to a proper maintenance planning may improve the long-term performance of the structures under environmental deterioration and time-variant loadings, thus reducing life-cycle costs. The importance of a performance-based design of new structures and the need of repair interventions of existing deteriorated structures are also emphasized by the recent growth of associations such as IABMAS (International Association of Bridge Maintenance and Safety, founded 1999, *www.iabmas.org*) and IALCCE (International Association for Life-Cycle Civil Engineering, founded 2006, *www.ialcce.org*).

In particular, engineering interest has increased in the evaluation of safety and serviceability of reinforced concrete structures in earthquake-prone regions. Current seismic design is based on time-invariant capacity design criteria that do not account for environmental hazard. However, the corrosion-induced damage of both concrete and reinforcing steel may increase the vulnerability of the structural system to seismic hazard over time. In fact, the progressive decay of the mechanical properties of corroded concrete members may lead at global level to a variation of the resisting hierarchy and to a shift in the failure mode. While the strength capacity is mainly related to the corrosion of the steel bars, the impacts on the overall stiffness and system ductility are associated with others mechanisms, such as a reduced confinement and bond deterioration between concrete and reinforcing steel.

These considerations emphasize the importance of new generation design procedures in which the structural behavior is related to both the seismic intensity level and the environmental aggressiveness.

A proper calibration of the design objectives and limit states should also be planned in order to ensure suitable levels of performance and safety over the required structural lifetime. In particular, when aging and deterioration are considered, the evaluation of the system performance should account for additional probabilistic indicators aimed to provide a comprehensive description of the lifetime seismic resources.

Due to their disruption potential for communities and infrastructures, earthquakes represent a dominant hazard. After catastrophic events, such as the Loma Prieta Earthquake in 1989 and the Northridge Earthquake in 1994, risk assessments and mitigation programs have been carried out in the attempt to reduce future losses and post-disasters recovery costs. Under these circumstances, the concept of seismic resilience emerged as the capability of a system, a community or a society, to withstand the effects of extreme events and to recover efficiently the original performance and functionality.

Resilience of critical facilities, such as hospitals and infrastructure networks, has been investigated with reference to damage and disruption caused by seismic events. However, for structural systems damage could also arise progressively in time due to aging and environmental aggressiveness. Consequently, the functionality loss at the occurrence of a seismic event of same magnitude may vary over lifetime due to the time-variant structural functionality, thus implying a reduced system resilience. The time-evolution of the actual functionality state of structures exposed to corrosion should then be considered in order to effectively assess and possibly enhance the lifetime resilience.

This Thesis presents a probabilistic approach to lifetime assessment of seismic performance and resilience of concrete structures under corrosion considering the mutual interaction of seismic and environmental hazards. The proposed approach is based on a general methodology for the analysis of deteriorating structures over time. A review of criteria and methods for environmental damage modeling and life-cycle analysis of concrete structures is presented. Measures and indices for the evaluation of seismic damage are also discussed in order to identify suitable performance indicators of the lifetime structural behavior. The general approach for lifetime seismic reliability analysis under uncertainty is presented, as well as criteria and methods for a time-variant measure of the seismic resilience of deteriorating structures.

In particular, the role of the environmental damage on seismic resilience is investigated by comparing the system functionality in the original state, in which the structure is fully intact, and in a perturbed state, in which a damage scenario is applied. The time-variant seismic capacity associated to different limit states, from damage limitation up to collapse, is assumed as functionality indicator, and seismic resilience is evaluated with respect to this indicator over the structural lifetime. The influence of recovery interventions and target functionality is also investigated by means of efficiency coefficients.

The effectiveness of the proposed procedure for the lifetime assessment of concrete structures is shown through applications, including a multi-story frame and a continuous bridge. The results show that structures designed for the same functionality target could exhibit over time different seismic performance and resilience depending on the environmental exposure. This highlights both the need of a life-cycle oriented seismic design approach and the importance of a lifetime resilience assessment in a perspective of seismic risk mitigation.

CHAPTER 1

TOWARDS A LIFE-CYCLE ORIENTED SEISMIC DESIGN OF RESILIENT STRUCTURES

1. Environmental risk assessment

Concrete structures are subjected over lifetime to aging and deterioration induced by the diffusion of aggressive agents, such as sulfates and chlorides. These processes are generally complex and their effects over time depend on both the damage process and the type of materials and structures. In general terms, deterioration mechanisms are classified in chemical, such as sulfate/chloride attacks, physical, such as freeze and thaw cycles and mechanical, such as cracking, abrasion and erosion (Bertolini *et al.* 2004, CEB 1992, Kilareski 1980). As a consequence, the material chemical composition is altered and the mechanical properties are modified. Among others, the main effects are a progressive loss of concrete strength and corrosion of the steel bars.

Environmental deterioration affects the structural performance and the serviceability of the structures. In fact, huge stocks of deteriorating buildings, bridges and other infrastructure facilities show structural deficiencies, as indicated by the poor condition rating of existing structures and infrastructures (ASCE 2013, NCHRP 2006). Moreover, the economic impact of the structural deterioration is considerably high in terms of maintenance costs. For example, in the United States

the direct annual cost is 10 billion dollars just regarding highway bridges, with a total of 22 billion dollars of maintenance interventions for the infrastructure system in general, without considering indirect economic losses (ASCE 2013).

The evaluation of the degrading properties of the materials and the assessment of the deterioration mechanisms are therefore essential in order to properly estimate the actual behavior of concrete structures over lifetime. To this aim, durability of concrete structures recently gained increasing importance at both design and maintenance stages (Biondini & Frangopol 2008, Chen *et al.* 2010, *Duracrete* 2000*,* ACI-365 2000, CEB 1992, 1997, *fib* 2006, Frederiksen *et al.* 1996, Strauss *et al.* 2012). The durability design of concrete structures is based on implicit rules for materials, material compositions and structural dimensions.

Table 1.1 – Exposure classes related to corrosion of the reinforcement (classes 2, 3 and 4) and prescriptions on concrete according to the EN 206 standard (EN 206-1 2001). The minimum strength class refers to the use of Portland cement of type CEM I 32.5.

Exposure class		Description of the environment	Maximum w/c	Minimum strength class [MPa]	Minimum cement content [kg/m^3]
1. No risk of corrosion or attack	X0	For concrete with reinforcement: very dry	-	C15/20	-
2. Corrosion induced by carbonation	XC1	Dry or permanently wet	0.65	C20/25	260
	XC2	Wet, rarely dry	0.60	C25/30	280
	XC3	Moderate humidity	0.55	C30/37	280
	XC4	Cyclic wet and dry	0.50	C30/37	300
3. Corrosion induced by chlorides other than from seawater	XD1	Moderate humidity	0.55	C30/37	300
	XD2	Wet, rarely dry	0.55	C30/37	300
	XD3	Cyclic wet and dry	0.45	C35/45	320
4. Corrosion induced by chlorides from seawater	XS1	Exposure to airborne salt	0.50	C30/37	300
	XS2	Permanently submerged	0.45	C35/45	320
	XS3	Tidal, splash and spray zones	0.45	C35/45	340

Table 1.2 – Values of minimum concrete cover requirements with regard to durability for reinforcing steel (CEN-EN 1992-1-1 2004) for the structural class S4 (design working life of 50 years).

Exposure class	X0	XC1	XC2/XC3	XC4	XD1/XS1	XD2/XS2	XD3/XS3
$c_{\min,dur}$	10	15	25	30	35	40	45

Requirements for minimum concrete cover, maximum water/cement (w/c) ratio, minimum cement content, crack limitation, air content and cement type, under proper casting and curing conditions are established by current design codes (CEN-EN 1992-1-1 2004, CEN-EN 1992-2 2006, EN 206-

1 2001, EN 1990 2002, ENV 13670-1 2000, UNI 11104 2004) in order to assure the serviceability of the structure subjected to different environmental exposure (Table 1.1, Table 1.2).

In this approach, the checking of system performance requirements is referred to the initial time of construction when the system is intact and the attention is focused only on the effects of local damage due to deterioration of concrete and corrosion of steel. In fact, the mechanical properties of steel and concrete are considered time invariant and the design rules do not take into account the structural effects of environmental damage. However, a purely prescriptive approach, discarding the interactions between both the parts of the structural system and the environment has to be considered incomplete. Current design rules should hence be considered as a necessary condition to meet durability requirements, but not sufficient regarding the actual lifetime performance of the structure (Biondini *et al.* 2004a).

In order to guarantee a proper lifetime behavior of the structure, simplified procedures for a quantitative evaluation of the service life of a structure have been proposed based on a probabilistic approach similar to that used in the performance-based structural design. (Duracrete 2000, *fib* 2006). For example, corrosion initiation or the need for repair are considered as serviceability limit states, indicating the boundary between the desired and the adverse durability condition of the structure. When the failure, i.e. the exceeding of a certain limit state, is caused by degradation of materials, the term "durability failure" is used as distinct from "mechanical failure", which is caused by mechanical loads (Sarja & Vesikari 1996). Actually, durability failure may be a partial reason for mechanical failure. Lifetime safety factors should then be introduced in addition to the ordinary safety factors (Sarja 2000)

Both European and Italian Standards (EN 1990 2002, DM 14 Gennaio 2008) have recently renewed their attention to the durability of reinforced concrete structures, in particular by prescribing the fulfillment of required levels of safety up to the end of the design working life of the structure. In fact, the design of durable concrete structures cannot rely just on indirect evaluations of the effects of the structural deterioration. Novel performance-based design criteria should follow a global approach that allows to relate the deterioration process and the structural lifetime performance with reference not just to the material properties but also to aspects such as the quality of the structural details, the structural scheme, the environmental loading, the maintenance and repairing interventions, as already indicated in CEN-EN 1992-1-1 (2004) and assessed by recent advances in this field (Biondini *et al.* 2004a, 2006, 2008, Biondini & Frangopol 2008, 2009).

2. Structural effects of environmental deterioration

The load-bearing capacity as well as the mode of failure of concrete members exposed to aggressive environments depend on degradation of concrete and corrosion of steel. This has been proved by numerous experimental tests carried out on corroded concrete elements (Almusallam *et al.* 1996, Apostolopoulos & Papadakis 2008, Ou *et al.* 2012, Ouglova *et al.* 2008, Oyado *et al.* 2011, Rodriguez *et al.* 1997). The results showed a reduced bending performance of deteriorated concrete elements in terms of ultimate strength reduction and curvature ductility, which is mainly due to the reduction of cross-sectional area and variation of ductility of corroded steel bars. Bond between concrete and steel and confinement are also affected. Moreover, the reduction of the shear strength due to corrosion of transverse reinforcement may lead to a brittle failure mechanisms.

The structural design of concrete members is generally performed with reference to cross-sectional performance indicators, such as strength, which are evaluated at the initial time, when the structure is intact and do not account for the progressive material deterioration. Moreover, concrete members designed to have the same initial performance and quality in terms of durability may exhibit different lifetime performance depending on geometrical parameter, such as the shape of the cross-section, the number of corners or the reinforcement layout, and the exposure condition, i.e. the free perimeter exposed to the aggressive agents, for example along one or more sides of the cross-section (Biondini & Frangopol 2009, 2010, Biondini *et al.* 2010).

Moreover, the local environmental damage is reflected at global level in terms of time-variant performance of the deteriorating structural systems. As a consequence, a reliable structural analysis should account for the redistribution of bending moments, shear and axial forces due to the long term behavior of the structural parts exposed to corrosion. The checking of strength requirements should not be limited to local analysis but should consider the structure as a whole, with particular reference to the structural scheme. A redistribution of stiffness among the structural elements may alter the resisting hierarchy in the structure, thus causing a shift in collapse mode (Biondini & Frangopol 2008a, Biondini *et al.* 2011). This generally occurs in redundant systems, where local deterioration mechanisms may lead to different failure scenarios. A lifetime structural analysis is then needed to predict the actual behavior of deteriorated structures with respect to different limit states (Biondini *et al.* 2013).

During the last decades, the research field of lifetime performance of structural systems has been widely investigated as far as modeling, analysis, design maintenance and management (Biondini *et al.* 2004a, 2006, Biondini & Frangopol 2008b, 2011, Estes & Frangopol 2005, Frangopol & Ellingwood 2010, Nowak & Frangopol 2005). The research trend showed that the lifetime performance of deteriorating concrete structures can be reliably predicted only in probabilistic terms due to the inherent randomness of both the materials and the environmental parameters. Stated that both the demand and the capacity may vary over time due to the effects of corrosion processes and external

loads modification, the on-going research on the lifetime performance of concrete structures highlights the need of new the design criteria, which account for the combined effects of environmental and mechanical stressors.

A life-cycle assessment of the structural performance can also allow to plan maintenance of the existing structures in order to achieve a prescribed target value of the structural performance over time. In particular, different scenarios of essential and/or preventive interventions can be selected, based on the perspective of reduction of the life-cycle costs and the extension of the service life of the structures (Frangopol & Furuta 2001, Frangopol *et al.* 1997, 2004a). To this purpose, the additional information obtained from monitoring activities on existing structures should be also taken into account (Ceravolo *et al.* 2008b). In fact, a proper evaluation of the current state and damage level of a structure is needed when estimating the residual lifetime. The reduction of stiffness and the increase in the energy dissipation, measured by dynamic testing, may be assumed as symptoms of structural degradation (Ceravolo *et al.* 2008a, 2009).

In particular, engineering interest has increased in the evaluation of safety and serviceability of reinforced concrete structures under earthquake excitations. In fact, the time-dependent variation of the structural response becomes of great concern for structures in earthquake-prone regions, where the system ductility and the actual collapse mechanism are main issues in safety assessment. The seismic behavior of corroded frame structures and bridges has been investigated by nonlinear static and dynamic analyses (Akiyama & Frangopol 2010, Akiyama *et al.* 2011, Alipour *et al.* 2011, Berto *et al.* 2009, Biondini *et al.* 2011, 2012, 2013, Choe *et al.* 2008, 2009, Ghosh & Padgett 2009, 2010, Kumar *et al.* 2009, Titi 2012).

These investigation showed that the capability of a structure to withstand a specific earthquake action with an adequate level of safety, according to a certain level of ductility and resistance, may not be preserved over time. In particular, the time evolution of the cyclic behavior of those critical cross-sections, where a plastic hinge is expected to develop at the occurrence of seismic event, may vary the energy dissipating mechanism claimed for a capacity design of the structure. Therefore, the combination of both the progressive decay of material properties due to deterioration and the sudden mechanical damage due to earthquakes has to be considered for a reliable assessment of the seismic performance of concrete structures in aggressive environments.

3. Probabilistic modeling of deteriorating structures

A lifetime assessment of concrete structures exposed to corrosion should account for the evolution of the structural degradation at both local and global level. To this aim, the understanding of the environmental factors that influence corrosion processes and the investigation of the deterioration mechanisms that affect the materials are essential. Over the last decades, several models have been formulated to simulate both the diffusion process and the corrosion-induced damage. Different exposure scenarios have been considered, and refined models accounting for bi-dimensional patterns of concentration gradients has been proved to reliably assess the diffusion process (Biondini *et al.* 2004, Titi & Biondini 2012). Simplified approaches can be effectively adopted as well under particular conditions (*fib* 2006). Corrosion-induced damage has been modeled by taking into account the effects on both concrete (Coronelli & Gambarova 2004, Wang & Liu 2004) and reinforcing steel, under uniform and pitting corrosion (Rodriguez *et al.* 1997, Saetta 2005, Val & Melchers 1997). These models have been implemented in nonlinear analysis procedures and validated by comparing numerical and experimental results, which demonstrated their capability to reproduce at the global level the local effects of corrosion damage (Biondini & Vergani 2012).

The analysis of concrete structures has to account for both mechanical and geometrical nonlinearities, due to nonlinear material properties and to second order effects respectively. The cross-sectional and structural analysis of nonlinear three-dimensional elements can be effectively carried out by the use of finite element methods and numerical integration (Biondini 2000, Biondini *et al.* 2004b, Bontempi 1992, Bontempi *et al.* 1995, Malerba 1998, Malerba & Bontempi 1989). Based on this approach, three-dimensional beam elements have been formulated, in which a time-variant element stiffness matrix accounts for the degradation of the strain-stress relationships due to concrete and reinforcing steel degradation over time. Such elements allow to reliably model the coupled mechanical-environmental damage at structural level by means of distributed plasticity. Moreover, the fiber distributed plasticity models are considerably accurate and able to account for particular local damage effects (Spacone & Limkatanyu 2000).

The lumped plasticity approach can also be selected for the structural analysis, by introducing material nonlinearity at element level and concentrating plasticity in limited zones (Giberson 1967, 1969, Kunnath & Reinhorn 1989). In this approach, the effects of the material degradation are considered by modifying the constitutive relationships of the plastic hinges as a function of the corrosion level, thus accounting for the time-variant behavior of deteriorating concrete members. This approach represents a good compromise between simplicity and accuracy in the nonlinear structural analysis, allowing for the understanding of the structural effects of deterioration with a reduced computational effort.

At global structural level, a general methodology for the lifetime assessment of concrete structures has been proposed in Biondini *et al.* (2004, 2006) and in Biondini & Frangopol (2008a). Based on the

time-variant properties of the concrete elements subjected to corrosion, the investigation of the effects of the deterioration processes on the overall structural performance can be effectively investigated. Novel approaches to time-variant assessment and optimization of concrete structures have been proposed in both deterministic and probabilistic terms (Biondini & Frangopol 2008b). In particular, a reliable analysis of the performance of deteriorating structures has to be carried out in probabilistic terms (Frangopol 2011, Frangopol *et al.* 2004b), because great uncertainties are related to both the physical models of the deterioration processes (*fib* 2006) and to the mechanical and structural properties of concrete structures (Ang & Tang 2007).

Uncertainties are unavoidable in Engineering problems. The inherent variability of the phenomena and the lack of knowledge of the adopted models do not allow a reliable analysis in a deterministic way. In the analysis of complex systems, uncertainties can be aleatory and epistemic. Aleatory uncertainty, or randomness, deals with an intrinsic variability of the phenomena, while epistemic uncertainty refers to the lack of knowledge and/or to the accuracy of the model (Der Kiureghian & Ditlevsen 2009). Considering aleatory uncertainties allows to evaluate the probability of occurrence of a realization in the random process, while epistemic uncertainties determine its distribution (Ang & Tang 2007).

In order to reliably quantify the role of uncertainties in the design and performance of the structural systems, a proper estimation of the random variables involved in both the deterioration processes and the structural behavior, according to a specific modeling, is needed. Correlation among the variables should also be considered if information is available. Considering the complexity and nonlinearity of the problem, numerical simulations provide the only practical and effective method. In particular, numerical process with repeated simulations can be based on Monte Carlo sampling technique, which is particularly effective in treatment of aleatory and epistemic uncertainties (Schueller & Pradlwarter 2009).

4. Seismic resilience of structural systems

Since every risk cannot be prevented, societies have to enhance their capability to sustain disasters such as earthquakes, floods, hurricanes or terroristic attack minimizing the losses in terms of human lives, disruption and costs. In this sense, during last decades the concept of risk mitigation gained increasingly attention. Risk assessments and mitigation programs have been carried out in the attempt to reduce future losses and post-disasters recovery cost (FEMA 2000, Wachtendorf *et al.* 2002).

In the United States this effort was developed in response to growing catastrophic losses from natural disaster events during the past decade, including the Loma Prieta Earthquake in 1989 and the Northridge Earthquake in 1994. Because of their potential for producing high losses and extensive community disruption, earthquakes have been given high priority in efforts to enhance community disaster resistance. Under this circumstance, the concept of seismic resilience recently emerged and significant research advances have been accomplished (Bocchini *et al.* 2012, Bocchini & Frangopol 2012, Bruneau *et al.* 2003, Bruneau & Reinhorn 2004, 2007, Cimellaro *et al.* 2006, 2010b, Decò *et al.* 2013).

In general terms, resilience means the ability to recover from shock or to resist being affected by disturbance. The root of the term resilience has to be found in the Latin word "*resilio*" that literary means "*to jump back*". The concept of resilience has been firstly applied in Material Engineering as the capacity of a material to absorb elastic energy under loading or impact before reaching failure. Later on, the concept has been extended in different fields, such as environmental research, psychology, sociology and economics, as the ability of a system to sustain and recover from a loss or a damage.

In Civil Engineering, resilience indicates the capacity of structures, infrastructure systems and entire communities to withstand and recover efficiently from extreme events. A resilient structure is robust, in the sense that the suffered damage is not unproportioned to the event that caused the damage itself, and recovers quickly re-establishing its normal performance. Regarding a structural system or an infrastructures network, resilience is related to the concept of redundancy and resourcefulness.

The research aimed to quantify resilience in the context of earthquake hazards is very active and a univocal set of procedures for its quantification has not been provided yet. Resilience is one of the main themes at the Multidisciplinary Center for Earthquake Engineering Research (MCEER). The framework proposed by MCEER aims to improve the resilience of infrastructure systems, hospitals and communities in general in terms of reduced probability of system failure, reduced consequences due to failure and reduced time to system restoration (Chang *et al.* 2008, Cimellaro *et al.* 2009, 2010a, Kafali & Grigoriu 2008, Renschler *et al.* 2010).

5. Motivation and objectives

The present work deals with the lifetime performance of concrete structures under multiple hazards. In particular, the combined effect of aggressive environmental exposure and earthquakes on the structural behavior of concrete buildings and bridges over the service life is herein investigated. This topic raised particular concern over the last decades related to both the deterioration of existing concrete structures and the occurrence earthquakes, which are still a dominant hazard to our Society. This is reflected in the active research field related to modeling, analysis, design maintenance and management of concrete structures in aggressive environments and earthquake-prone regions.

The present research offers a review of the available models for the assessment of environmental damage, with focus on chloride-induced corrosion. A probabilistic approach to predict the lifetime seismic performance of concrete structure exposed to aggressive environments is then proposed. The methodology is based on the evaluation of the time-variant structural properties of concrete members by means of a lumped plasticity modeling of critical cross-sections. The overall behavior of concrete structures is then investigated in order to clarify the interaction between environmental and seismic hazards. A reduced performance in terms of seismic capacity and displacement ductility is expected over time, as well as a shift in the collapse mechanism under seismic excitation due to the deterioration processes at local level. This indicates that time-invariant design criteria have to be revised and emphasizes the need of a life-cycle oriented performance-based design approach.

A reliable resilience assessment should account for the mutual effects of environmental and seismic damage as well. In current resilience analysis, the structural functionality is considered time-invariant, and a sudden loss of functionality is assumed at the occurrence of an extreme event. However, since the seismic capacity decreases over lifetime due to deterioration processes, the structural functionality is expected to vary accordingly depending on the environmental exposure. Moreover, the functionality loss at the occurrence of a seismic event of same magnitude may vary over lifetime due to the time-variant structural capacity.

The extension of the above mentioned probabilistic approach to the lifetime assessment of seismic resilience of deteriorating structures aims in particular at the evaluation of the residual functionality depending on the time of occurrence of the seismic event. Aspects such as the influence of the recovery functions and the target functionality are also considered for a reliable resilience assessment of concrete structures under deterioration and seismic damage.

6. Outline

The present work is subdivided as follows.

Chapter 2 presents a review of the deterioration processes affecting concrete structures exposed to aggressive environments, with focus on chloride-induced corrosion, being one of the most critical forms of damage. The diffusion mechanisms and the factors involved in the corrosion initiation and propagation are presented referring to the available literature. Basing on experimental tests, several numerical models have been proposed to describe the chloride diffusion in concrete. In order to account for the complexity of such mechanisms, a probabilistic approach is followed. The validity of these models is then discussed and a comparison between simplified (1D) and more refined (2D) formulations is presented. Moreover, the simulation of the diffusion process according to a specific scenario shows the influence of the environmental aggressiveness on the initiation time and on the chloride concentration inside concrete over lifetime.

Chapter 3 deals with the modeling of corrosion damage. Over the last decades, several models have been formulated for evaluating the effects of corrosion on concrete elements. Despite the complexity of the deterioration processes, simplified degradation models can be successfully adopted based on linear relationships. The effects of corrosion at material level are illustrated, with emphasis on the variation of the mechanical properties of concrete and steel over time. The effectiveness of the adopted damage models is validated with reference to experimental tests carried out on beams subjected to accelerated corrosion. A comparison between distributed and lumped plasticity modeling is provided. Finally, an application of the adopted damage model is proposed, accounting for uniform corrosion of steel bars and deterioration of concrete under a specified corrosion scenario.

In Chapter 4, a methodology for the probabilistic time-variant analysis of concrete structures under deterioration is proposed. The finite element method is adopted for the cross-sectional analysis which accounts for both mechanical nonlinearity and material deterioration. The formulation of the stiffness matrix is based on time-variant constitutive laws for concrete and steel according to the above mentioned damage models. Lumped plasticity models have been selected to perform the structural analysis at element level, being this formulation less computationally expensive in a probabilistic approach. Measures and indices for the evaluation of seismic damage are then reviewed in order to identify suitable performance indicators of the structural behavior of concrete structures over lifetime. The probabilistic approach to predict the lifetime seismic performance of concrete structures exposed to aggressive environments is then applied to the case studies of a 2D multistory frame and a 3D continuous bridge. Nonlinear static and dynamic analyses are carried out. A reduction of the seismic capacity and a possible variation of the failure mode under seismic excitation are the main

detrimental effects of local deterioration on the overall seismic performance of concrete structures over lifetime. The investigation demonstrates the need of taking the severity of the environmental exposure and the required structural lifetime into account in both the seismic assessment of existing structures and the seismic design of new structures.

Chapter 5 introduces the concept of resilience as the capacity of structures, infrastructure systems and entire communities to withstand and recover efficiently from extreme events, such as earthquakes. First, the definitions of resilience given for network systems, critical facilities and structures are presented. Aspects involved in the resilience assessment, such as the estimation of the losses and the choice of recovery models, are discussed. The novel concept of time dependence of structural functionality and seismic resilience is proposed. In fact, deterioration processes affect the lifetime functionality of the structures in terms of seismic capacity, which causes a reduction of resilience at the occurrence of an earthquake event. The probabilistic approach for the assessment of the performance of concrete structures over time is extended to the evaluation of lifetime seismic resilience and applied to the concrete bridge investigated in Chapter 4. The effectiveness of post-event recovery interventions as well as the influence of the target functionality are investigated by means of efficiency coefficients. The results in terms of the time dependence of the post-event residual functionality highlight the need of a proper evaluation of the mutual interaction of seismic damage and lifetime deterioration in a perspective of risk mitigation.

Chapter 6 summarizes the results of the present Thesis, drawing conclusions as well as pointing out limitations and future developments in the research field of lifetime seismic performance and resilience of deteriorating concrete structures.

7. References

ACI-365 (2000). *Service-life Prediction*. State of the art report, American Concrete Institute, Committee 365.

Akiyama, M., & Frangopol, D.M. (2010). On life-cycle reliability under earthquake excitations of corroded reinforced concrete structures. *Proceedings of the Second International Symposium on Life-Cycle Civil Engineering (IALCCE2010)*, Taipei, Taiwan, October 27-31.

Akiyama, M., Frangopol, D.M., & Matsuzaki, H., (2011). Life-cycle reliability of RC bridge piers under seismic and airborne chloride hazards. *Earthquake Engineering and Structural Dynamics*, 40 (15), 1671–1687.

Alipour, A., Shafei, B., & Shinozuka, M.S. (2013). Capacity loss evaluation of reinforced concrete bridges located in extreme chloride-laden environments. *Structure and Infrastructure Engineering*, 9(1), 8–27.

Almusallam, A.A., Al-Gahtani, A.S., Aziz, A. R., Dakhil, F.H., & Rasheeduzzafar (1996). Effect of reinforcement corrosion on flexural behavior of concrete slabs. *Journal of Materials in Civil Engineering*, 8(3), 123-127.

Ang, A.H.-S. & Tang, W.H. (2007). *Probability Concepts in Engineering*. 2nd Edition, John Wiley & Sons, Hoboken, NJ, USA.

Apostolopoulos, C.A., & Papadakis, V.G. (2008). Consequences of steel corrosion on the ductility properties of reinforcement bar. *Construction and Building Materials*, 22(12), 2316–2324.

ASCE (2013). *Report card for America's Infrastructure*. American Society of Civil Engineers, Reston, VA. http://www.infrastructurereportcard.org/a/#p/bridges/overview

Berto, L., Vitaliani, R., Saetta, A., & Simioni, P., (2009). Seismic assessment of existing RC structures affected by degradation phenomena. *Structural Safety*, 31, 284–297.

Bertolini, L., Elsener, B. Pedeferri, P., & Polder R. (2004). *Corrosion of Steel in Concrete – Prevention, Diagnosis and Repair*. Wiley-VCH, Weinheim.

Biondini, F. (2000). *Strutture da Ponte Soggette ad azioni di Tipo Sismico – Modellazione ed Ottimizzazione*. PhD Dissertation, Department of Structural Engineering, Politecnico di Milano, Milan, Italy.

Biondini, F. (2004). A three-dimensional finite beam element for multiscale damage measure and seismic analysis of concrete structures. *Proceedings of the 13th World Conference on Earthquake Engineering (WCEE)*, August 1-6, Vancouver, BC, Canada: Paper No. 2963.

Biondini, F., Bontempi, F., Frangopol, D.M., & Malerba, P.G. (2004a). Cellular automata approach to durability analysis of concrete structures in aggressive environments. *Journal of Structural Engineering, ASCE*, 130(11), 1724–1737.

Biondini, F., Bontempi, F., Frangopol, D.M., & Malerba, P.G. (2004b). Reliability of material and geometrically non-linear reinforced and prestressed concrete structures. *Computers & structures*, 82(13), 1021–1031.

Biondini, F., Bontempi, F., Frangopol, D.M., & Malerba, P.G. (2006). Probabilistic service life assessment and maintenance planning of concrete structures, *Journal of Structural Engineering, ASCE*, 132(5), 810–825.

Biondini, F., Camnasio, E., & Palermo, A. (2012). Life-cycle performance of concrete bridges exposed to corrosion and seismic hazard. *Proceedings of the Structures Congress 2012 (ASCE2012)*, Chicago, IL, March 29-31.

Biondini, F., Camnasio, E., & Palermo, A. (2013). Lifetime Seismic Performance of Concrete Bridges Exposed to Corrosion. *Structure and Infrastructure Engineering*, ahead-of-print, doi:10.1080/15732479.2012.761248.

Biondini, F., & Frangopol, D.M. (2008a). Probabilistic limit analysis and lifetime prediction of concrete structures. *Structure and Infrastructure Engineering*, 4(5), 399–412.

Biondini, F., & Frangopol, D.M. (Eds.) (2008b). *Life-Cycle Civil Engineering*. CRC Press, Taylor & Francis Group.

Biondini, F., & Frangopol, D.M. (2009). Lifetime reliability-based optimization of reinforced concrete cross-sections under corrosion. *Structural Safety*, 31(6), 483–489.

Biondini, F., & Frangopol, D.M. (2010). Life-cycle performance of reinforced concrete structures exposed to aggressive agents: Design issues. *Proceedings of the SEI-ASCE Structures Congress 2010*.

Biondini, F., & Frangopol, D.M. (2011). *Life-Cycle of Civil Engineering Systems*. Special Issue of *Structure and Infrastructure Engineering*, 7(1-2), 1–196.

Biondini, F., Frangopol, D.M. & Malerba, P.G. (2008). Uncertainty Effects on Lifetime Structural Performance of Cable-Stayed Bridges, *Probabilistic Engineering Mechanics*, 23(4), 509–522.

Biondini, F., Frangopol, D.M., & Malerba, P.G. (2010). Structural geometry effects on the life-cycle performance of concrete bridge structures in aggressive environments. In *Bridge Maintenance, Safety Management, Health Monitoring and Informatics – IABMAS08: Proceedings of the Fourth International IABMAS Conference*, Seoul, Korea, July 13-17.

Biondini, F., Palermo, A., & Toniolo, G. (2011). Seismic performance of concrete structures exposed to corrosion: case studies of low-rise precast buildings. *Structure and Infrastructure Engineering*, 7(1-2), 109–119.

Biondini, F., & Vergani, M. (2012). Damage modeling and nonlinear analysis of concrete bridges under corrosion. *Proceedings of the Sixth International Conference on Bridge Maintenance, Safety and Management* (*IABMAS 2012*), Stresa, Lake Maggiore, Italy, July 8-12.

Bocchini, P., Decò, A., & Frangopol, D.M. (2012). Probabilistic functionality recovery model for resilience analysis. *Proceedings of the 6th International Conference on Bridge Maintenance, Safety and Management* (*IABMAS*), July 8-12, Stresa, Lake Maggiore, Italy.

Bocchini, P., & Frangopol, D.M. (2012b). Restoration of bridge networks after an earthquake: Multi-criteria intervention optimization. *Earthquake Spectra*, 28(2), 426–455.

Bontempi, F. (1992). Sulla costruzione dei domini di rottura di sezioni in C.A. e C.A.P. soggette a pressoflessione deviata. *Studi e Ricerche*, *Graduate School for Concrete Structures "F.lli Pesenti"*, Politecnico di Milano, Milan, Italy, 13, 261–277 (in Italian).

Bontempi, F., Malerba, P.G., & Romano, L. (1995). Formulazione diretta secante dell'analisi non lineare di telai in C.A./C.A.P.. *Studi e Ricerche*, *Graduate School for Concrete Structures "F.lli Pesenti"*, Politecnico di Milano, Milan, Italy, 16, 351–386 (in Italian).

Bruneau, M., Chang, S.E., Eguchi, R.T., Lee, G.C., O'Rourke, T.D., Reinhorn, A.M., Shinozuka, M., Tierney, K., Walace, W.A., & von Winterfeldt, D.V (2003). A framework to quantitatively assess and enhance the seismic resilience of communities. *Earthquake Spectra*, 19(4), 733–752.

Bruneau, M., & Reinhorn, A. (2004). Seismic resilience of communities-conceptualization and operationalization. *Proceedings of the International Workshop on Performance-based Seismic-Design, Bled, Slovenia*, June 28-July 1 (Vol. 1).

Bruneau, M., & Reinhorn, A. (2007). Exploring the concept of seismic resilience for acute care facilities. *Earthquake Spectra*, 23(1), 41–62.

CEB (1992). *Durable Concrete Structures – Design Guide*. Bulletin 183.

CEB (1997). *New Approach to Durability Design*. Committee Eurointernational du Beton, Bulletin, 283.

CEN-EN 1992-1-1 (2004). *Eurocode 2 – Design of concrete structures - Part 1-1: General rules and rules for buildings*. European Committee for Standardization, Brussels.

CEN-EN 1992-2 (2006). *Eurocode 2 – Design of concrete structures - Part 2: Concrete bridges – Design and detailing rules*. European Committee for Standardization, Brussels.

Ceravolo, R., De Stefano, A., & Pescatore, M. (2008a). Change in dynamic parameters and safety assessment of civil structures. *Mechanics of Time-Dependent Materials*, 12(4), 365–376.

Ceravolo, R., De Stefano, A., & Pescatore, M. (2008b). Including structural monitoring activities in safety probabilistic formulations: *Proceedings of the International Symposium on Life-Cycle Civil Engineering* (*IALCCE08*), June 11-14, Varenna, Lake Como, Italy.

Ceravolo, R., Pescatore, M., & De Stefano, A. (2009). Symptom-based reliability and generalized repairing cost in monitored bridges. *Reliability Engineering & System Safety*, 94(8), 1331–1339.

Chang, S.E., Pasion, C., Tatebe, K & Ahmad, R. (2008). *Linking Lifeline Infrastructure Performance and Community Disaster Resilience: Models and Multi-Stakeholder Processes*, Report MCEER-08-0004.

Chen, S-S, Frangopol, D.M. & Ang, A-H. S. (2010). *Life-Cycle of Civil Engineering Systems*, Taiwan Building Technology Center, DnE Information Service Net, Taipei, Taiwan, 2010.

Choe, D.E., Gardoni, P., Rosowsky, D., & Haukaas, T. (2008). Probabilistic capacity models and seismic fragility estimates for RC columns subject to corrosion. *Reliability Engineering & System Safety*, 93(3), 383–393.

Choe, D.E., Gardoni, P., Rosowsky, D., & Haukaas, T. (2009). Seismic fragility estimates for reinforced concrete bridges subject to corrosion. *Structural Safety*, 31, 275–283.

Cimellaro, G.P., Christovasilis, I.P., Reinhorn, A.M., DeStefano, A. & Kirova, T. (2010a). *L'Aquila Earthquake of April 6, 2009 in Italy: Rebuilding a Resilient City to Multiple Hazard*. Report MCEER-10-0010.

Cimellaro, G.P., Fumo, C., Reinhorn, A.M. & Bruneau, M. (2009) *Quantification of Disaster Resilience of Health Care Facilities*, Report MCEER-09-0009.

Cimellaro, G.P., Reinhorn, A.M., & Bruneau, M. (2006). Quantification of seismic resilience. *Proceedings of the 8th National Conference of Earthquake Engineering*, April 18-22, San Francisco, California, USA.

Cimellaro, G. P., Reinhorn, A. M., & Bruneau, M. (2010b). Framework for analytical quantification of disaster resilience. *Engineering Structures*, 32(11), 3639–3649.

Coronelli, D., & Gambarova, P. (2004). Structural assessment of corroded reinforced concrete beams: Modeling guidelines. *Journal of Structural Engineering*, 130(8), 1214–1224.

Decò, A., Bocchini, P., & Frangopol, D.M. (2013). A probabilistic approach for the prediction of seismic resilience of bridges. *Earthquake Engineering & Structural Dynamics*. doi: 10.1002/eque.2282.

Der Kiureghian, A., & Ditlevsen, O. (2009). Aleatory or epistemic? does it matter? *Structural Safety*, 31(2), 105–112.

DM 14 Gennaio 2008. *Norme tecniche per le costruzioni*. Gazzetta Ufficiale della Repubblica Italiana.

Duracrete (2000). *The European Union – Brite EuRam III, DuraCrete – Probabilistic Performance Based Durability Design of Concrete Structures*. Final Technical Report of Duracrete Project, Document BE95-1347/R17, CUR, Gouda (NL).

EN 206-1 (2001). *Concrete – Part 1. Specification, Performance, Production and Conformity*, European Committee for Standardization, 2001.

EN 1990 (2002). *Eurocode – Basis of Structural Design*, European Committee for Standardization.

ENV 13670-1 (2000). *Execution of Concrete Structures*, European Committee for Standardization.

Estes, A.C., & Frangopol, D.M. (2005). Life-cycle evaluation and condition assessment of structures. *Structural Engineering Handbook*, Chapter 36, 1–51.

FEMA (2000). *Planning for a Sustainable Future: The link between Hazard Mitigation and Livability*, Federal Emergency Management Agency, Washington, DC.

fib (2006). *Model Code for Service Life Design*. Bulletin, 34.

Frangopol, D.M. (2011). Life-cycle performance, management, and optimisation of structural systems under uncertainty: accomplishments and challenges 1. *Structure and Infrastructure Engineering*, 7(6), 389–413.

Frangopol, D.M., Bruhwiler, E. Faber, M.H, & Adey, B. (Eds.). (2004a). *Life-cycle performance of deteriorating structures: Assessment, design, and management*. American Society of Civil Engineers Reston, Virginia.

Frangopol, D.M. & Ellingwood, B.R. (2010). Life-Cycle Performance, Safety, Reliability and Risk of Structural Systems. Editorial, *Structure Magazine*, Joint Publication of NCSEA, CASE, SEI.

Frangopol, D.M., & Furuta, H. (Eds.). (2001). *Life-Cycle Cost Analysis and Design of Civil Infrastructure Systems*. American Society of Civil Engineers, ASCE, Reston, Virginia.

Frangopol, D.M., Kallen, M.J., & Noortwijk, J.M.V. (2004b). Probabilistic models for life-cycle performance of deteriorating structures: review and future directions. *Progress in Structural Engineering and Materials*, 6(4), 197–212.

Frangopol, D.M., Lin, K.Y., & Estes, A.C. (1997). Life-cycle cost design of deteriorating structures. *Journal of Structural Engineering*, 123(10), 1390–1401.

Frederiksen, J. M., Nilsson, L.O., Poulsen, E., Sandberg, P., Sorcnsen, H.E., & Klinghoffer, O. (1996). *HETEK - Chloride penetration into concrete - State of the art. Transport processes, corrosion initiation, test methods and prediction models*, The Road Directorate, Report (53), Copenhagen.

Ghosh, J., & Padgett, J.E. (2009). Multi-hazards considerations of seismic and aging threats to bridges. *Proceedings of the Structures Conference 2009 (ASCE2009)*, April 30 – May 2, Austin, TX, USA.

Ghosh, J., & Padgett, J.E. (2010). Aging considerations in the development of time-dependent seismic fragility curves. *Journal of Structural Engineering*, 136(12), 1497–1511.

Giberson, M.F. (1967). *The Response of Nonlinear Multi-story Structures Subjected to Earthquake Excitation*. PhD Dissertation, California Institute of Technology, Pasadena, CA.

Giberson, M.F. (1969). Two nonlinear beams with definitions of ductility. *Journal of the Structural Division*, 95(ST2),137–57.

Kafali, C. & M. Grigoriu, M. (2006) *System Performance Under a Multi-Hazard Environment*, Report MCEER-08-0006.

Kilareski, W.P. (1980). Corrosion induced deterioration of reinforced concrete – an overview, *Materials Performance*, NACE, 19(3), 48-50.

Kumar, R., Gardoni, P., & Sanchez-Silva, M. (2009). Effect of cumulative seismic damage and corrosion on the life cycle cost of reinforced concrete bridges. *Earthquake Engineering and Structural Dynamics*, 38, 887–905.

Kunnath, S.K, & Reinhorn, A.M. (1989). *Inelastic three-dimensional response analysis of reinforced concrete structures subjected to seismic loads*. Technical Report No. NCEER-88-0041, University at Buffalo, The State University of New York, NY, USA.

Malerba, P.G. (Ed.) (1998). *Limit and Nonlinear Analysis of Reinforced Concrete Structures*. International Centre for Mechanical Sciences (CISM), Udine, Italy (in Italian).

Malerba, P.G., & Bontempi, F. (1989). Analisi di telai in C.A. in presenza di non linearità meccaniche e geometriche. *Studi e Ricerche*, *Graduate School for Concrete Structures "F.lli Pesenti"*, Politecnico di Milano, Milan, Italy, 11, 209–224 (in Italian).

NCHRP (2006). *Manual on Service Life of Corrosion-Damaged Reinforced Concrete Bridge Superstructure Elements*. National Cooperative Highway Research Program, Report 558, Transportation Research Board, Washington, D.C., USA.

Nowak, A.S. & Frangopol, D.M. (Eds.) (2005). *Advances in Life-Cycle Analysis and Design of Civil Infrastructure Systems*. Lincoln, Nebraska.

Ou, Y.C., Tsai, L.L., & Chen, H.H. (2012). Cyclic performance of large-scale corroded reinforced concrete beams. *Earthquake Engineering & Structural Dynamics*, 41(4), 593–604.

Ouglova, A., Berthaud, Y., Foct, F., François, M., Ragueneau, F., & Petre-Lazar, I. (2008). The influence of corrosion on bond properties between concrete and reinforcement in concrete structures. *Materials and Structures*, 41(5), 969–980.

Oyado, M., Kanakubo, T., Sato, T., & Yamamoto, Y. (2011). Bending performance of reinforced concrete member deteriorated by corrosion. *Structure and Infrastructure Engineering*, 7(1-2), 121–130.

Renschler, C.S., Frazier, A.E., Arendt, L.A., Cimellaro, G.P., Reinhorn, A.M. & Bruneau, M. (2010). *A Framework for Defining and Measuring Resilience at the Community Scale: The PEOPLES Resilience Framework*, Report MCEER-10-0006.

Rodriguez, J., Ortega, L.M., & Casal, J. (1997). Load carrying capacity of concrete structures with corroded reinforcement. *Construction and Building Materials*, 11(4), 239–248.

Saetta, A.V. (2005). Deterioration of reinforced concrete structures due to chemical–physical phenomena: model-based simulation. *Journal of Materials in Civil Engineering*, 17(3), 313–319.

Sarja, A. (2000). Durability design of concrete structures – Committee report 130-CSL. *Materials and Structures*, 33(1), 14–20.

Sarja, A., & Vesikari, E. (Editors) (1996). *Durability Design of Concrete Structures*, Manuscript of RILEM Report of TC 130-CSL. RILEM Report Series 14. E&FN Spon, Chapman & Hall.

Schueller, G.I. & Pradlwarter, H.J. (2009). Uncertainty analysis of complex structural systems. *International Journal for Numerical Methods in Engineering*, 80(6-7), 881–913, 2009.

Spacone, E., & Limkatanyu, S. (2000). Responses of reinforced concrete members including bond-slip effects. *ACI Structural Journal*, 97(6), 831–839.

Strauss, A., Frangopol, D.M. & Bergmeister K. (2012). *Life-Cycle and Sustainability of Civil Infrastructure Systems*, CRC Press, Taylor & Francis Group plc., A. A. Balkema, Boca Raton, London, New York, Leiden.

Titi, A. (2012). *Lifetime Probabilistic Seismic Assessment of Multistory Precast Buildings*. PhD Thesis, Department of Structural Engineering, Politecnico di Milano, Milan, Italy.

Titi, A., & Biondini, F. (2012). Validation of diffusion models for life-cycle assessment of concrete structures. *Third International Symposium on Life-Cycle Civil Engineering* (*IALCCE 2012*), Vienna, Austria, October 3-6.

UNI 11104 (2004). *Concrete. Specification, performance, production and conformity - Additional provisions for the application of EN 206-1*. UNI, Ente Nazionale Italiano di Unificazione.

Val, D.V. & Melchers, R.E. (1997). Reliability of deteriorating rc slab bridges. *Journal of Structural Engineering*, 123(12), 1638–1644.

Wachtendorf, T., Connell, R., Tierney, K.J., & Kompanik, K. (2002). *Disaster Resistant Communities Initiative: Assessment Of The Pilot Phase – Year 3*. Disaster Research Center, University of Delaware, Newark, DE.

Wang, X., & Liu, X. (2004). Modeling bond strength of corroded reinforcement without stirrups. *Cement and Concrete Research*, 34(8), 1331–1339.

CHAPTER 2

CONCRETE DETERIORATION AND DIFFUSION PROCESSES

1. Transport phenomena in concrete

Concrete elements exposed to aggressive environments are subjected to aging and deterioration processes induced by chemical components, such as carbon dioxide, sulfates and chlorides. In fact, the cement paste can be penetrated through its pores by gases and liquid substances, driven by concentration gradients inside the material volume (Glicksman 2000). As a consequence, permeability is one of the key factors in determining the durability of concrete elements depending on the environmental aggressiveness.

Processes that allow the transport of water, carbon dioxide, oxygen, sulfate and chloride ions within concrete lead to the degradation of both concrete and steel. In fact, the material chemical composition is altered by the aggressive agents and the mechanical properties are modified as well. For example, in industrial environments sulfates contained in soil or water can contaminate the cement paste causing a progressive loss of concrete strength. Chlorides beyond a threshold value in carbonated concrete can lead to the corrosion of steel (Bertolini *et al.* 2004). Chlorides are critical in marine environments, where they diffuse into concrete as airborne chlorides and/or by direct contact with

seawater, especially in the tidal and splash zone. Chlorides can also come from the application of deicing salts on bridge decks (CEB 1992).

Four basics mechanisms determine the movements of fluids and ions through concrete (Bertolini *et al.* 2004, Bentur *et al.* 1997, Broomfield 1997, Collepardi, 2006, Pedeferri & Bertolini 2000):

- diffusion, which is due to a gradient of concentration: a substance moves through the pores of the region where the concentration is greater to where its concentration is lower;
- permeation, by which a fluid penetrates through the pores of the material because of a pressure gradient;
- capillary suction, when a watery solution is in contact with a porous material generating a surface tension;
- electrical migration, when electrical potential gradients cause the transport of ionic species.

Diffusion

Diffusion transport is driven by a concentration gradient. Substances such as oxygen, carbon dioxide, chlorides and sulfates move within concrete from the surface, where they are present in higher concentrations, to the internal zones where their concentration is lower. Under conditions of stationarity, the diffusive process is described by Fick's first law:

$$F = -D\frac{dC}{dx} \tag{2.1}$$

where F is the flux (kg/m^{2}s), C is the concentration (kg/m^3) of the diffusing species present at distance x from the surface and D is the diffusion coefficient (m^2/s), which depends on the diffusing species, on the characteristics of concrete and on the environmental conditions. This coefficient changes as a function of position and time, following variations in the pore structures, the external humidity and temperature, among others.

The complex nature of the transport processes in concrete and the difficulty in evaluating appropriate values of the relevant transport parameters have led to the adoption of the Fick's one dimensional diffusion law as an easy mathematical way to model the penetration profile of aggressive agents in concrete. This relationship was firstly proposed by Collepardi *et al.* (1972) to fit experimental penetration profiles of chlorides in concrete under diffusion conditions.

Actually, diffusion rarely reaches stationary conditions in concrete structures. Non stationary diffusion is governed by Fick's second law:

$$\frac{\partial C}{\partial t} = D\frac{\partial^2 C}{\partial x^2} \tag{2.2}$$

This equation is usually integrated under the assumption that the concentration of the diffusing species, measured at the surface of the concrete, is constant in time and is equal to C_s ($C = C_s$ for $x = 0$ and for any instant t). If the diffusion coefficient is considered constant in time and through the

thickness of concrete, i.e the concrete is homogeneous, and the initial chloride content is assumed null, the solution of Eqn. 2.2 is:

$$\frac{C(x,t)}{C_S} = 1 - \mathrm{erf}\left(\frac{x}{2\sqrt{Dt}}\right) \tag{2.3}$$

where:

$$\mathrm{erf(z)} = \frac{2}{\pi}\int_0^z e^{-t^2}\,dt \tag{2.4}$$

is the error function. This solution is generally used to estimate the chloride diffusion coefficient by fitting the theoretical profile of chloride concentration to non-steady-state laboratory tests or from structures exposed in the field.

In the diffusion process, it should be also considered that chemical species can bind to a certain degree with components of the cement matrix. The gradual consumption of these compounds modifies the conditions of diffusion, which can no longer be described by Fick's second law but requires a corrective term. The binding of diffusion species is important in experimentally determining the diffusion coefficient *D*. As long as the binding capacity of the concrete has not been exhausted, the net flux of material will appear to be less, thus underestimating the diffusion coefficient. However, it is difficult to estimate the corrective term, since it depends on both concrete properties and environmental variables. Therefore, the total concentration of the diffusing species is often taken into account and the effects of the chemical reactions in concrete are disregarded in the evaluation of the diffusion coefficient *D*.

Permeation

Permeation is due to a pressure gradient. The flux of a liquid through an element of section *A* and thickness *L* can be described by Darcy's law:

$$\frac{dq}{dt} = \frac{k\Delta PA}{L\mu} \tag{2.5}$$

where dq/dt is the flow (m^3/s), μ is the viscosity of the fluid (Ns/m^2), K is the intrinsic permeability of concrete (m^2) and ΔP is the pressure head applied (Pa).

The permeability of the cement paste to water and gases depends on the capillary porosity and the permeability coefficient decreases as the *w*/*c* ratio decreases and the hydration proceeds. With a *w*/*c* ratio of 0.75, the permeability coefficient of water in concrete is very high, usually 10-10m/s upon complete curing, while with a *w*/*c* ratio of 0.45 it can go below 10^{-12}-10^{-11}m/s (Bertolini *et al.* 2004).

Capillary suction

When water comes into contact with a porous material, it is absorbed by the underpressure in the pores by capillary action. This action increases as the size of the pores and the viscosity of the liquid decrease. On the other hand, the smaller the pores become, the slower the transport through concrete is, due to the increasing friction. Concrete is not hydrophobic, so the contact angle is small due to the presence of molecular attraction between the liquid and concrete surface, thus causing the capillary suction.

In general, capillary absorption is measured as mass or volume of liquid absorbed per unit of surface (g/m^2 for mass or m^3/m^2 for volume) in time t by a sorptivity test. The development of the absorption i as a function of time is expressed by the following equation:

$$i = S\sqrt{t} \tag{2.6}$$

where S ($g/m^2s^{0.5}$) is a constant that varies between $0.7 g/m^2s^{0.5}$ for high-strength concrete (low porosity) and $5 g/m^2s^{0.5}$ for normal strength concrete (higher porosity) (Bertolini *et al.* 2004).

Migration

Electrical fields in concrete can arise manly by pitting corrosion phenomena and by stray currents. The potential gradient of the electric field causes the transport of ions in solution. The velocity of ion movement is proportional to the strength of the electric field and the charge and size of the ion. The ion movement interacts with the diffusive process, which on the contrary tends to restore a uniform distribution of concentration.

The resistance opposed by the material to the electrical migration can be measured as:

$$R = \int_0^l \frac{\rho}{S} dl \tag{2.7}$$

where l (cm) is the thickness, S is the cross-sectional area (cm^2) and ρ (Ωcm) is the resistivity. Concrete resistivity depends on the degree of water saturation and on the ionic species present in the pore solution. Resistivity decreases greatly when the material humidity increases. It depends also on the type of cement and whether the concrete is carbonated or not. In particular, chloride ions increase the conductivity of the pore solution and carbonation decreases it. An increased resistivity is accompanied by a reduced corrosion rate (Polder *et al.* 2002). Moreover, the type of cement determine concrete microstructure, thus influencing the ion migration by the pore volume and pore-size distribution.

Among these processes, diffusion can be considered the main mechanism of transport in concrete, even if pure diffusion develops only in concrete completely and permanently saturated with water. Local environmental conditions on the surface, i.e. the microclimate, and their variations in time

influence the kinetics of diffusion. Moreover, the presence of cracks, the material porosity and the binding by the hydrated cement and the substances being transported, among the others, affect the development of concrete deterioration. Corrosion of the steel bars is the most significant deterioration process suffered by concrete structures. In particular, severe forms of corrosion are caused by chlorides, which interfere with the alkalinity of the cement paste and break the passivity film over steel bar surface.

In the following, the damage processes of aging concrete structures are reviewed, with focus on chloride induced corrosion. The diffusion mechanisms and the factors involved in the corrosion initiation and propagation are presented referring to the available literature. Basing on experimental tests, several numerical models have been proposed to describe the chloride diffusion in concrete. The validity of these models is then discussed. A simulation of the diffusion process according to a specific scenario is finally presented based on the Monte Carlo sampling technique.

2. Concrete damage

When subjected to extreme loading, weathering or the attack of aggressive agents, concrete deteriorates through a variety of physical and chemical processes. These processes may occur simultaneously, frequently giving rise to a synergistic action which leads to concrete cracking as a main consequence. Cracks in concrete generally interconnect flow paths and increase concrete permeability. Since the increased permeability in cracked concrete allows more water or aggressive chemical agents to penetrate into concrete, a link between cracking and corrosion phenomena can be established by a chain reaction of "deterioration-cracking-more permeable concrete-further deterioration" (Wang *et al.* 1997). It is therefore important to investigate the mutual interaction between concrete cracks, permeability and degradation of concrete, which can eventually result in destructive deterioration of concrete structures.

The processes of deterioration of concrete and corrosion of reinforcement are closely connected, since concrete cracking compromises its protective characteristics. On the other hand, the corrosion attack, produces concrete cracking and delamination and reduces its adhesion to the reinforcement, due to the expansive action of corrosion products. The severity of concrete deterioration induced by corrosion depends on several factors, among which:

- the environmental conditions, as the presence of carbon dioxide and aggressive agents such as sulfates and chlorides affects concrete structure causing degradation of concrete and corrosion of steel bars (Figure 2.1a);
- the microclimate i.e. the particular exposure of the surface of the element, since the presence of aggressive agents is not a sufficient condition for developing severe corrosion in concrete. For example, in marine environments the corrosion of a submerged structure is less severe than that in the tidal or splash zones because of the lack of oxygen (Figure 2.1b);
- the geometry of the structural element, since the concrete cover thickness is one of the key parameters determining the initiation time for corrosion, and the layout of the steel bars in the cross-section determines the characteristic of concrete cover spalling (scaling, delamination, border effects, Figure 2.1c);
- the chemical composition of the cement paste, which is related to the diffusion coefficient D of the material.

In the following, some the most common forms of physical and chemical deterioration of concrete will be mentioned. More details can be found in Biczok (1972) and Pedeferri & Bertolini (1996).

(a) (b) (c)

Figure 2.1 – Corroded steel bars of a concrete wall exposed to aggressive atmosphere; (b) Corrosion in the tidal zone; (c) Mechanisms of spalling: scaling, delamination and border effects.

2.1. Physical damage

Physical damage essentially depends on the temperature variations that can arise in the structure:

- hydrating heat that develops during concrete curing;
- freeze-thaw cycles;
- exceptional actions such as fire.

Hydrating heat

During concrete curing, the esothermal hydrating reactions provoke a significant temperature increase, that varies on the base of the chemical components in the cement paste. For example, the hydrating heat of different mix design of the Portland cement can range between 380 and 500KJ/kg. The temperature increase has effects especially in structural elements with great dimensions or thickness, since during the casting the temperature gradient between the surface and the core of the casting is significant. In fact, the surface cools and shrinkages being in contact with the air, while the core tends to expand. This causes tension stresses that can crack concrete surface if the temperature gradient exceeds 20-25°C, especially after some days from casting.

Freeze-thaw cycles

Whenever water contained in the pores freezes, its expansion causes tension stresses that can result in scaling, cracking and spalling of concrete and, eventually, in its complete disintegration. The freezing of pore water is usually a gradual process that moves from the surface to the inner part, from the pores of bigger size to the smaller ones. Freeze action is more significant in capillary pores, which saturate rapidly and where water pressure is higher. However, concrete has a low thermal conductivity and the presence of ions in the pore solution decreases the freeze temperature. Besides the microstructure of concrete, consequences of this type of deterioration also depend on environmental

conditions, on the degree of water saturation, on the number of freeze-thaw cycles, on the rate of freezing and on the minimum temperature reached.

In order to sustain the freeze and thaw attack, the w/c ratio should be low and the curing adequate to get a lower porosity. Moreover, the use of airing additives leads to the formation of air bubbles that are uniformly distributed and interconnected, thus allowing the water to expand without damaging concrete and not reducing concrete strength significantly (Collepardi 2006). The presence of deicing salts like calcium and sodium chloride on concrete surface helps in reducing the direct effect of the freeze and thaw attack but at the same time the high concentration of chlorides becomes a crucial factor for degradation of concrete and corrosion initiation.

Fire

Among the extreme events, fire may frequently affect concrete structures. The effects of fire are significant on concrete surface, while the core, and hence the steel bars, are protected from fire, due to the low thermal conductivity of concrete.

Concrete generally shows a good performance with respect to fire in structural terms. Nevertheless, the damage increases as the maximum reached temperature and the time of exposure to fire increase (Schneider 1988). Concrete cover spalling can occur due to the rapid shrinkage of concrete caused by water evaporation and decomposition of hydrating products. Moreover, if the inner pore water cannot reach the surface, the pressure of the water vapor can cause concrete cracking and explosive delamination of the concrete surface.

2.2. Chemical damage

Chemical damage occurs when concrete structures are in contact to aggressive environments containing chemical agents that interact with cement components causing degradation of the cement paste. Two of the main chemical damage phenomena are:

- sulfate attack;
- alkali-aggregates reaction.

Sulfate attack

Concrete often comes into contact with water or soil containing sulfates. Concentration of soluble sulfates in ground water of over several hundreds of mg/l should be considered potentially aggressive (Biczok 1972). These ions can penetrate the concrete and react with components of the cement matrix to cause expansive chemical reactions. The production of gypsum from the combination of concrete, calcium hydroxide and sulfates leads to a loss of mechanical strength. Moreover, the reaction between gypsum and alluminates leads to the formation of ettringite, which is an expansive reaction product.

The consequences are cracking and disgregation of concrete. In addition, part of the ettringite is commonly located in the interface between paste and aggregates, resulting in loss of bond. In particular cases, with high humidity levels (95%) and low temperatures (below 10°C), the formation of thaumasite can occur, which is incoherent and brittle. With regard to protection against sulfate attack, the quality of concrete is a crucial factor, since a low permeability effectively reduces the risk of this attack.

Alkali-aggregates reaction

Some types of aggregates can react with sodium (Na^+), potassium (K^+) and hydroxyl (OH^-) ions in the pore solution, giving rise to detrimental expansion, that causes irregular crack patterns and localized concrete spalling. Aggregates that contain amorphous or poorly crystalline silica cause alkali-silica reaction (ASR), which is the most important reaction of this kind. This reaction is favored by high relative humidity (80-90%) and by temperature increase. The alkali content in concrete can be reduced by adding pozzolanic material or fly ashes.

The significance of ASR for concrete structures is that, beyond concrete cracking due to the expansion of the reaction products, the tensile strength is reduced, which may have consequences on the structural capacity (den Uijl *et al.* 2002, Siemes *et al.* 2002).

3. Steel damage

In ordinary condition, reinforcing steel bars embedded in sound concrete are protected by a thin protective oxide film that prevents corrosion initiation. In fact, the alkaline solution contained in the pores of the hydrated cement paste promotes the passivation of steel (Arup 1983, Gouda 1970). However, corrosion can take place when the passive film is removed or locally damaged due to carbonation of concrete or to chloride penetration.

Based on that, the service life of reinforced concrete structures can be divided in two distinct phases (Figure 2.2). The first phase is the initiation of corrosion, in which the reinforcement is passive but carbonation and/or chloride penetration take place leading to the progressive loss of passivity. The second phase is propagation of corrosion, that begins when steel is depassivated and finishes when a limit state is reached beyond which consequences of corrosion cannot be further tolerated (Bažant 1979, Tuutti 1982).

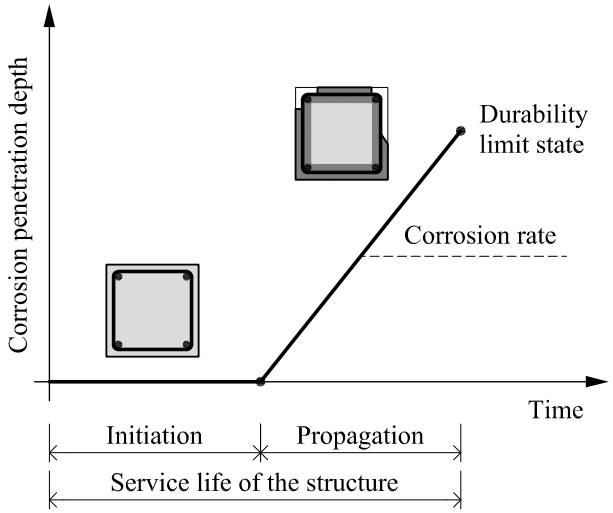

Figure 2.2 – Initiation and propagation periods for corrosion in a reinforced concrete structure (after Bertolini *et al.* 2004).

Initiation phase

During the initiation phase, aggressive substances that can depassivate steel penetrate from the surface into the inner layers of concrete. Carbonation begins at the surface of concrete and moves gradually towards the inner zones, neutralizing concrete alkalinity by the ingress of carbon dioxide from the atmosphere. As far as chloride attack, chloride ions can penetrate into concrete and reach the reinforcement, destroying the protective layer if their concentration on steel surface reaches a critical level.

The duration of the initiation phase depends mainly on the cover depth and the penetration rate of the aggressive agents as well as on the concentration necessary to depassivate the steel bars. Design

codes define cover depths according to the expected environmental class (EN 206-1 2001). The rate of ingress of the aggressive agents depends on concrete quality, i.e. porosity and permeability, and on the microclimate on concrete surface. Using protective measures that prolong the initiation phase is an effective way to improve concrete durability.

Propagation phase

When the steel protective layer is destroyed, corrosion starts if water and oxygen are present on the surface of the reinforcement. The corrosion rate greatly depends on temperature and humidity and determines the time it takes to reach the minimally acceptable state of the structure, i.e. the durability failure criterion. Corrosion induced by carbonation is generally uniform on steel surface, since carbonated concrete leads to complete dissolution of the protective layer (Figure 2.3a,b). In presence of high chlorides content, corrosion tends to be localized, with penetrated attacks of limited area (pits) surrounded by non-corroded areas. This is called pitting corrosion (Figure 2.3c). Sometimes, when very high levels of chlorides are present, the passive film is destroyed over wide areas, thus causing a generalized corrosion.

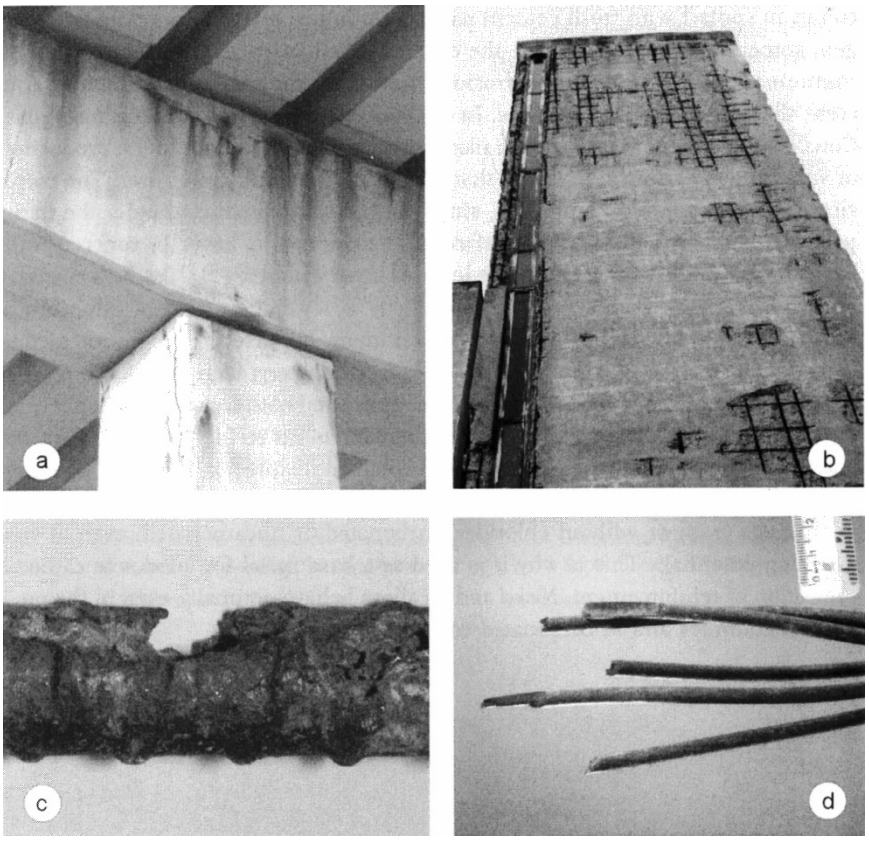

Figure 2.3 – Examples of consequences of corrosion of steel in concrete: (a) cracking of columns and cross beam; (b) spalling and delamination of the concrete cover; (c) reduction of cross-section of the rebar due to pitting corrosion; (d) brittle failures of prestressing tendons due to hydrogen embrittlement (Bertolini *et al.* 2004).

Other kinds of corrosion propagation can develop in particular conditions. If depassivation due to carbonation or chlorides occurs only in a part of the reinforcement, a macrocell can develop between corroding bars and those bars that are still passive. Stray currents can enter the reinforcement in some areas in structures of railway networks, such as bridges and tunnels (Pedeferri & Bertolini 2000). Moreover, hydrogen embrittlement can occur on high-strength steel used in prestressed concrete, under particular environmental, mechanical loading and electrochemical conditions, leading to the brittle failure of the material (Figure 2.3d, Nürnberger 2002).

3.1. Carbonate corrosion

In moist environments, carbon dioxide in the air forms an acid aqueous solution that reacts with the hydrated cement paste and neutralizes the concrete alkalinity. Concrete carbonation is provocked by the reaction between carbon dioxide (CO_2) and alkaline concrete components such as sodium and potassium hydroxides (NaOH, KOH) and solid hydration products ($Ca(OH)_2$). The reaction can be written schematically as follows:

$$CO_2 + Ca(OH)_2 \rightarrow CaCO_3 + H_2O \tag{2.8}$$

Carbonation makes the pH of the pore solution to drop down from alkalinity to values approaching neutrality. In humid carbonate concrete, steel corrodes as if it was in contact with water. If chlorides are present in the water solution, the corrosion scenario is even more aggressive (Alonso & Andrade 1994, Tuutti 1982).

The carbonation reaction starts at the external surface and penetrates into the concrete producing a low pH front. The rate of carbonation decreases in time, as carbon dioxide has to diffuse through the pores of the already carbonated layer. The penetration in time of carbonation can be described by the following equation:

$$d = Kt^{\frac{1}{n}} \tag{2.9}$$

where d is the depth of carbonation (mm) and t is the time (years). Often the exponent $1/n$ is approximately equal to 2, thus considering a parabolic trend (Figure 2.4a). The constant K (mm/years$^{0.5}$) depends on concrete quality and environmental conditions such as relative humidity and temperature (Parrott 1991, Alonso & Andrade 1994).

The transport of carbon dioxide occurs more easily in the pores filled with air, while the carbonation rate slows down in water-saturated concrete. However, the carbonation process needs humidity to occur. The maximum carbonation rate occurs in concrete with relative humidity around 60-80% (Figure 2.4b).

Carbonation depends also on the microclimate on the concrete surface. The rate of the process is influenced by the wet-and-dry cycles, the in-door/out-door exposure, the local CO_2 concentration and temperature. In real structures it is possible to measure carbonation depth in order to estimate the constant *K*. Values of *K* found for real structures exposed to the atmosphere but protected from rain vary from 2 to 15mm/year$^{0.5}$. Indicatively: $2<K<6$ for concrete of low porosity whose cement content is above 350kg/m^3; $6<K<9$ for concrete of medium porosity; $K>9$ for highly porous concrete with cement content below 250kg/m^3 (Bertolini *et al.* 2004).

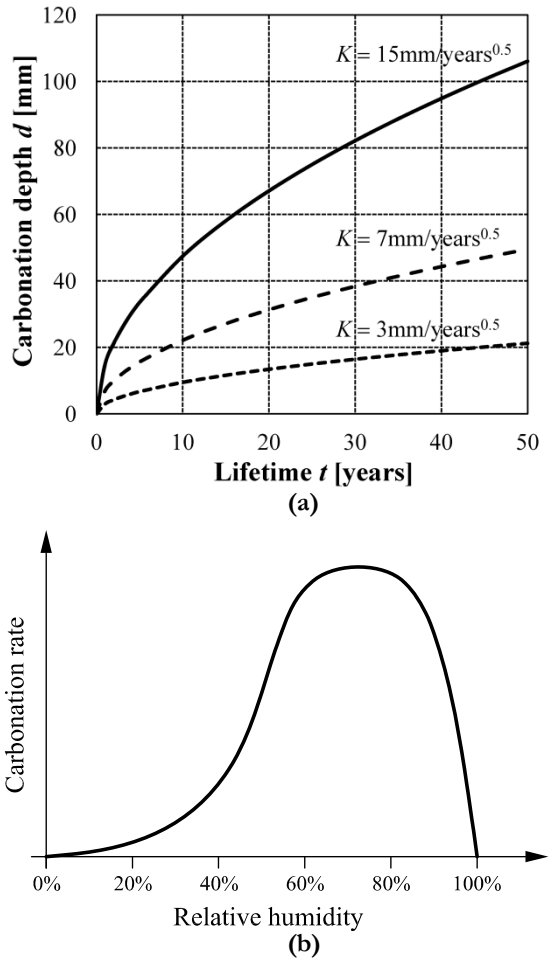

Figure 2.4 – (a) Depth of carbonation, calculated by the simplified function $s = K\sqrt{t}$, in relation to time and to *K* (constant relative humidity, no wetting of concrete); (b) Schematic representation of the rate of carbonation of concrete as a function of the relative humidity of the environment, under equilibrium conditions (after Tuutti 1982, adapted).

Some other empirical models have been proposed to take into direct account the effect of several parameters that influence the carbonation rate. Tuutti (1982) took into account the concentration of CO_2 in the air, the quantity of CO_2 that reacts with concrete and the diffusion coefficient. Bakker (1994) suggested a formula that takes into consideration the wetting-drying cycles on the hypothesis that the progress of carbonation is negligible during wetting. Parrott's formula (Parrott 1994)

correlates the depth of carbonation at time *t* to concrete permeability to air and the humidity of the environment.

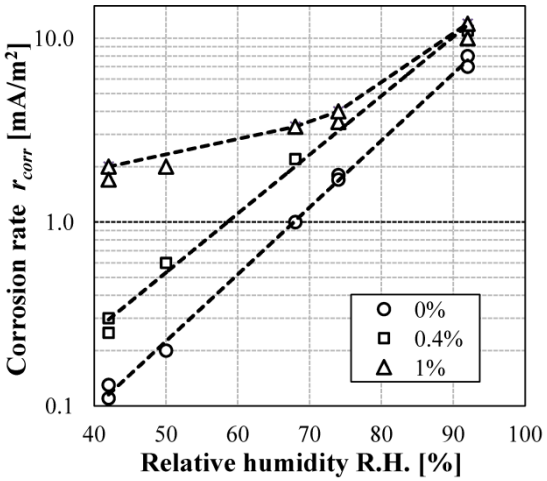

Figure 2.5 – Relationship between relative humidity and corrosion rate in carbonated mortar both without chlorides and in the presence of chlorides (after Glass *et al.* 1991, adapted).

Carbonation attack becomes more critical if chlorides are present in concrete, even if in such small quantities they would not usually give rise to corrosion. Figure 2.5 shows the corrosion rate of steel in artificially carbonated mortars in the absence and in the presence of chlorides. It can be seen that the corrosion rate is negligible only in conditions of external relative humidity below 75%, 60%, and even 40% as the chloride content increases from zero to 1% by cement mass.

3.2. Chloride corrosion

Chloride contamination of concrete is a frequent cause of corrosion of reinforcing steel. The main source of chloride in concrete is penetration from the environment. This occurs, for instance, in marine environments and in road structures, where chloride-bearing de-icing salts are used in wintertime. Chlorides lead to the local breakdown of the protective oxide film on the reinforcement in alkaline concrete, so that a subsequent localized corrosion attack takes place. The morphology of the attack is that typical of pitting in presence of high chlorides content.

Corrosion takes place when the chloride content over the steel bar surface reaches a threshold value. This threshold depends on several parameters, such as the electrochemical potential of the reinforcement, the presence of oxygen and the conditions of saturation (Alonso *et al.* 2001). The evaluation of the threshold value is affected by considerable scatter. In the field, statistical relationships have been established expressing the percentage of structures showing corrosion as a function of chloride content (Vassie 1984). In general, corrosion propagation actually starts in concrete that contains substantial moisture and oxygen when the corrosion rate is higher than

2mA/m² (Andrade 2002). Hence the chloride threshold can be defined as the chloride content required to reach this condition of corrosion.

The initiation time of corrosion depends on the rate of penetration of chloride ions through the concrete cover. The kinetics of penetration of chlorides is affected by several parameters related both to the concrete (type of cement, *w/c* ratio, moisture content) and the environment (chloride concentration, temperature). Chloride penetration from the environment produces a profile in concrete characterized by a high chloride content near the external surface and decreasing contents at greater depth. Measurements on real marine structures and road structures exposed to de-icing salts showed that these profile can generally be approximated by Eqn. 2.3 obtained from Fick's second law. However, only in concrete completely and permanently saturated with water chloride ions penetrate by pure diffusion. In most situations, other transport mechanisms contribute to chloride penetration (Bertolini *et al.* 2004, CEB 1992, Frederiksen 1996).

In the following, other aspects related to the chloride corrosion will be discussed in detail with respect to the numerical modeling of the process and the estimation of the parameters involved, such as the surface chloride content, the diffusion coefficient, and the critical chloride threshold.

4. Modeling of chloride diffusion

Starting from the 90s, several studies and experimental campaigns have been conducted in order to investigate the corrosion phenomena, regarding the effects on both the material properties and the structural behavior. Based on experimental results, several numerical models have been proposed to describe the diffusion process. The formulation of these models was aimed to provide useful design tools in order to get more durable structures (Duracrete 2000, *fib* 2006, Sarja & Vesikari 1996).

In particular, a full probabilistic design approach for the modeling of chloride induced corrosion in concrete has been proposed by the *Model Code for Service Life Design* (*fib* 2006). Since most observations indicate that the transport of chlorides in concrete is diffusion controlled (Bertolini *et al.* 2004), the modeling is based on the following limit state equation derived from the Fick's one-dimensional (1D) model:

$$C(x=c,t) = C_0 + (C_{S,\Delta x} - C_0)\left[1 - \operatorname{erf}\left(\frac{c-\Delta x}{2\sqrt{D_{app,C}\,t}}\right)\right] = C_{crit} \qquad (2.10)$$

where the actual chloride concentration $C(x = c, t)$ at the depth of cover concrete c and at time t is compared to the critical chloride concentration C_{crit} which defines the initiation of the corrosion process; C_0 is the initial chloride content in the cement paste; Δx is the depth of the convection zone, i.e. the concrete layer up to which the process of chloride penetration differs from Fick's model; $C_{S,\Delta x}$ is the chloride content at depth Δx and time t and $D_{app,C}$ is the apparent coefficient of chloride diffusion.

This model is based on several assumptions. Even if the transport of chlorides is mainly driven by diffusion, the surface of concrete elements is often exposed to a frequent change of wetting and subsequent evaporation that cannot be modeled by diffusion. Dry-periods and subsequent rewetting provoke a process of capillary suction. Compared to diffusion process, capillary action leads to a rapid transport of chlorides into the concrete up to a depth Δx where the chlorides can accumulate with time until they create a saturation concentration $C_{S,\Delta x} = C_{s,0}$, i.e. the environmental chloride concentration at concrete surface.

In order to still describe the penetration of chlorides using Fick's law of diffusion, the data of the convection zone, which may deviate considerably from ideal diffusion behavior, is neglected and Fick's law is applied starting at the depth Δx with a substitute surface concentration $C_{S,\Delta x}$. The depth of the convection zone depends on environmental conditions (marine environment, road environment) and exposure (saturation conditions, splash/spray conditions). With this simplification, the model yields a good approximation of chloride distribution at a depth $x \geq \Delta x$.

Although the substitute chloride concentration $C_{S,\Delta x}$ is theoretically a time-dependant variable, for simplification purposes it is considered time independent. $C_{S,\Delta x}$ may depend on the composition of concrete, the position of the structure, the orientation of its surface, the chloride concentration in

the environment and the general conditions of exposure with regard to rain and wind. For example, in marine structures the highest values of $C_{S,\Delta x}$ are normally found in the splash zone, where evaporation of water leads to an increase in the chloride content at the concrete surface. Therefore, the value of $C_{S,\Delta x}$ has to be determined taking into account the environmental aggressiveness and exposure, although discarding its evolution in time.

4.1. Apparent diffusion coefficient

The chloride migration coefficient $D_{RCM,0}$ is one of the governing parameters for the description of the material properties in the chloride induced corrosion model. It depends mainly on the material porosity, the concrete mix and on the w/c ratio. The type of cement has a considerable effect. In passing from concrete made with Portland cement to concrete made with the increasing addition of pozzolanic material or blast furnace slag, the diffusion coefficient can be drastically reduced. Several values for different types of cement and varying w/c ratio are proposed in literature (Figure 2.6a, Collepardi *et al.* 1970, Bamforth & Price 1996, Boulfiza *et al.* 2003, *fib* 2006, Hou & Zang 2004, Page *et al.* 1981, 1986). The chloride migration coefficient $D_{RCM,0}$ depends not just on the material properties in a strict sense, but also on environmental parameters, such as humidity and temperature, and the lifetime of the structure. This is the reason why it is more appropriate to talk about an "apparent" diffusion coefficient $D_{app,C}$.

Moreover, although the value of the diffusion coefficient D is assumed to be constant in the Fick's law (Eqn. 2.2), it is indeed time-variant parameter. Since porosity and the microcrack pattern in concrete evolve in time with the hydration process and aging, the diffusion coefficient $D_{app,c}$ has to be considered as a function of both time and exposure conditions (Figure 2.6b). In particular, it should be considered that it tends to reduce in time, especially for blended cement (Frederiksen *et al.* 1996, Bamforth & Chapman-Andrews 1994).

In the *fib* (2006) model, the evolution in time of the diffusion coefficient is accounted for by the following equation (*fib* 2006):

$$D_{app,C}(t) = D_{RCM,0}\, A(t) \tag{2.11}$$

where $D_{RCM,0}$ is the chloride migration coefficient and $A(t)$ is a function considering 'aging' (*fib* 2006):

$$A(t) = \left(\frac{t_0}{t}\right)^a \tag{2.12}$$

where t_0 = 28 days is the reference initial time. In this function, the functional relationship between exposure period and diffusion coefficient is taken into account by the aging coefficient a which has been experimentally evaluated for different cement types and environmental exposures.

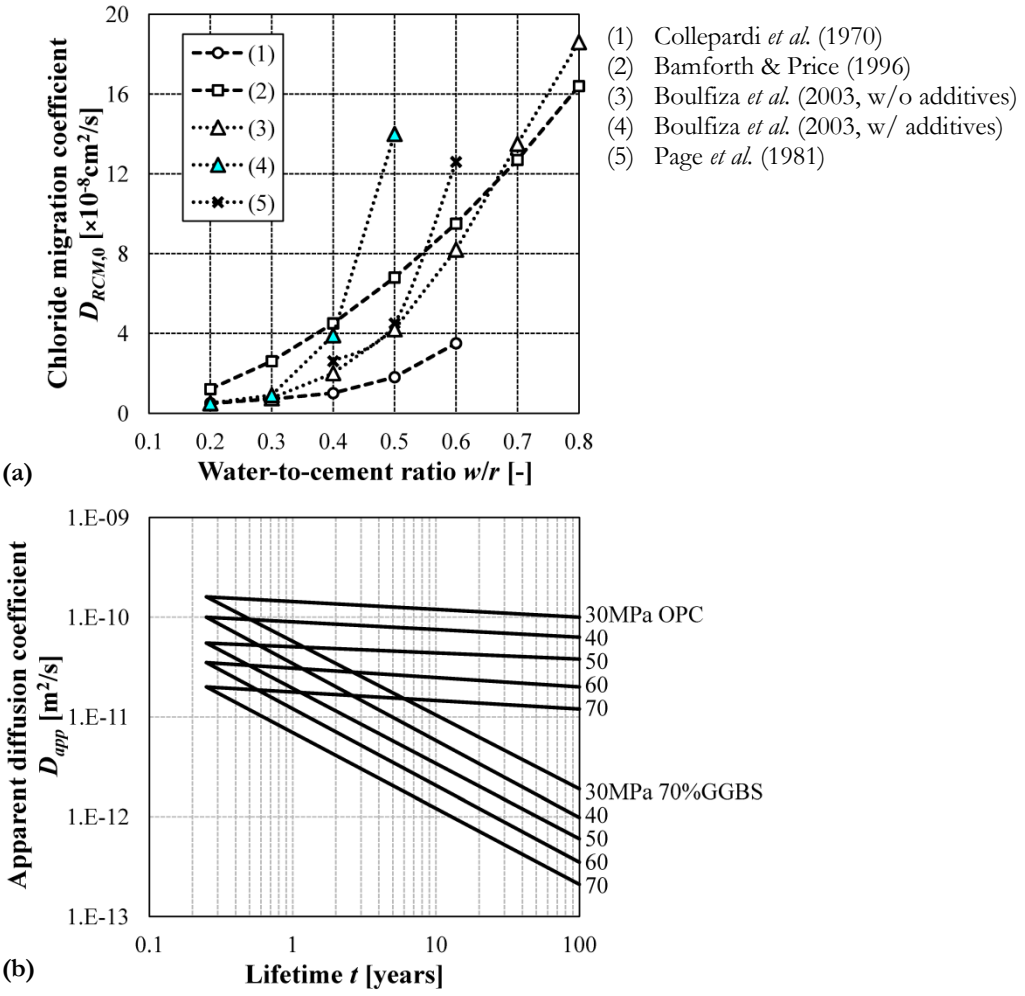

Figure 2.6 – (a) Dependency of the chloride diffusion coefficient on the *w/c* ratio (after Shafei *et al.* 2012, modified); (b) Dependency of the apparent diffusion coefficient on concrete strength, presence of admixtures and lifetime (OPC: Portland cement; GGBS: Granulated blast furnace slag; after Bamforth 1994, adapted).

Among the numerical models proposed to evaluate the apparent diffusion coefficient, one of the most comprehensive is the one proposed by Shafei *et al.* (2012).The diffusion coefficient $D_{app,C}$ is evaluated from an estimated value for a reference temperature and humidity $D_{Cl,ref}$ multiplied by a series of modification factors as below:

$$D_{app,C} = D_{Cl,ref} F_1(T) F_2(H) F_3(\Re) F_4(t_e) F_5(C_f) \tag{2.13}$$

where:

- $F_1(T)$ accounts for the dependence of chloride diffusion coefficient on the ambient temperature: as the external temperature rises up, the diffusion process increases;
- $F_2(H)$ represents the influence of relative humidity, since water is an essential component of numerous chemical reactions that may cause deterioration of concrete;

- $F_3(\boldsymbol{R})$ evaluates the effect of the carbonation process: from the reaction of carbon dioxide with calcium hydroxide in the hardened cement paste, the calcium carbonate is produced. The precipitation of calcium carbonate in the pores reduces the porosity of concrete, being insoluble;
- $F_4(t_e)$ denotes the influence of the concrete age, which causes a reduction in the chloride diffusion coefficient. The progress of hydration reactions with time slows down the diffusion process, especially during the initial life of the structure;
- $F_5(C_f)$ considers the effect of free chloride content on the chloride diffusion coefficient, as showed by Xi & Bazant (1999) and Kong *et al.* (2002).

4.2. Critical chloride threshold

The critical chloride concentration $C(x, t) = C_{crit}$ is the threshold value at which corrosion is assumed to start. The time to reach this concentration value represents the initiation time, while hereafter the propagation of corrosion of the steel bars occurs.

The relationship between chloride content and corrosion propagation is complex and affected by numerous factors including concrete grade, type and curing regime (Glass & Buenfeld 1997, Dhir *et al.* 1994). It was observed that the chloride threshold is related to the presence of hydroxyl ions (Hausmann 1967). Moreover, steel corrosion sometimes occurs at a relatively low chloride level while sometimes being absent at higher levels (Vassie 1984). In general, the threshold level tends to be higher in concretes with low permeability (Bakker *et al.* 1994, Thomas 1996). For example, the risk of corrosion in non-carbonated concrete obtained with Portland cement is considered low for chloride contents below 0.4% by mass of cement and high for levels above 1%.

The chloride threshold has also been found to be dependent on the presence of microscopic voids in the concrete near steel surface (Glass & Buenfeld 2000) In particular, Gowripalan *et al.* (2000) investigated the relationship between the chloride threshold level and the crack width/cover ratio. It is recognized that both crack width and cover thickness affect the initiation of steel corrosion in concrete. In fact, it occurs faster with increasing surface crack width when the cover is maintained and it occurs slower with increasing cover thickness when the surface crack width is maintained. Basing on the collected experimental data, it appears that the chloride threshold level is related to crack width/cover ratio by a hyperbolic relationship. If this relationship holds, the permissible crack width and the minimum concrete cover given in various Codes for design of concrete structures in seawater exposure would implicitly define the chloride threshold level (Table 2.1).

Table 2.1 – Crack width/cover ratio from various Codes (Gowripalan *et al.* 2000).

Codes	Allowable crack width w_{cr} [mm]	Minimum cover c_{min} [mm]	w_{cr}/c
CEB/FIP Model Code	0.3	40	0.0075
ACI Manual	0.15	50-60	0.0025-0.003
ENV 1991	0.3	40	0.0075
BS 8110	0.3	50	0.006
AS 3600	NA	40-50	-

NA: not available

It has to be noticed that both the critical chloride content and the presence of oxygen at steel bar surface are necessary conditions for corrosion propagation. In fact, in structures exposed to the atmosphere, oxygen can easily reach the steel surface through the air-filled pores, thus easily initiating corrosion. On the contrary, when reinforced concrete structures are submerged in water, or when the environmental conditions are close to saturation, the transport of oxygen to the steel is low. A lower risk of corrosion propagation and a much higher chloride threshold are then implied (Arup 1983). In fact, reinforcement corrosion has been reported to occur in the splash zone at a relatively lower chloride content than in the submerged zone (Sharp & Pullar-Strecker 1980).

4.3. Comparisons between chloride diffusion models

In conclusion, a comparison of the values of the different parameters involved in the chloride diffusion models found in literature is proposed (Table 2.2). The present review of the available models does not pretend to be exhaustive. However, the comparison highlights that a significant scatter affects the evaluation of the above mentioned parameters involved in the description of the diffusion process. This is mainly due to the different environmental exposure conditions considered in the definition of the models. Moreover, some values are determined on the basis of particular experimental data, others come from numerical models and reasonable assumptions.

In any case, the probabilistic approach is needed to take into account the uncertainties involved in the problem. The diffusion process is described in probabilistic terms by assuming the main parameters of the problem as random variables, for which distribution type, mean μ and standard deviation σ are defined.

Table 2.2 – Comparison between different chloride diffusion models: experimental data and/or random variables adopted for the chloride migration coefficient $D_{RCM,0}$, the chloride concentration at depth Δx $C_{s,\Delta x}$, the initial chloride concentration C_0 and the chloride threshold C_{crit}.

		$D_{RCM,0}$ [m²/s]	$C_{s,\Delta x}$ [wt.%/cem]	C_0 [kg/m³]	C_{crit} [wt.%/cem]	C_{crit} [kg/m³]
(1)		10^{-14} - 10^{-11}			0.75 - 2.5	
(2)					0.04 - 8.34	
(3)		10^{-14} - 10^{-11}				
(4)	Distribution type	Lognormal	Lognormal			Lognormal
	μ	4×10^{-14}	0.1			0.04
	σ	0.10μ	0.10μ			0.10μ
(5)	Distribution type	Normal	Normal		Beta	
	μ	4×10^{-12} - 20×10^{-12}	3		0.6	
	σ	0.20μ	0.30μ		0.15	
(6)	Atmosphere	8.3×10^{-13}	0.051			
	Soil	1.21×10^{-12}	0.033			
	Tidal zone	4.93×10^{-12}	0.542			
	Submerged zone	4.35×10^{-12}	0.570			
	Splash zone	4.83×10^{-12}	0.948			
(7)	Distribution type	Lognormal	Lognormal			Lognormal
	μ	1.62×10^{-12}	1.27			1.35
	σ	0.30μ	0.40μ			0.10μ
(8)	Distribution type	Lognormal	Lognormal		Lognormal	
	μ	10^{-12}	0.65		0.3	
	σ	0.15μ	0.06μ		0.16μ	
(9)	Distribution type	Lognormal		Lognormal		Lognormal
	μ	2×10^{-12}	0.972	3.5		0.9
	σ	0.75μ		0.5μ		0.19μ
(10)	Distribution type	Lognormal	Lognormal	Lognormal		Lognormal
	μ	2×10^{-12}	0.41 - 0.97	0.03 - 3.5		0.9
	σ	0.50μ - 0.75μ		0.14μ - 0.50μ		0.19μ

(1) Alonso *et al.* 2002
(2) Angst *et al.* 2009
(3) Bertolini *et al.* 2004
(4) Enright & Frangopol 1998
(5) *fib* 2006
(6) Ghods *et al.* 2005
(7) Lounis & Amleh 2004, Martin-Perez & Lounis 2003
(8) Sobhani & Ramezanianpour 2007
(9) Stewart & Rosowsky 1998
(10) Vu & Stewart 2000

4.4. Comparison between 1D and 2D diffusion

It has been assessed that the Fick's laws effectively describe the one-dimensional diffusion, so that the chloride concentration in concrete at a certain depth at different time instants can be evaluated analytically, depending on the environmental aggressiveness scenario. Monodimensional (1D) diffusion models are generally applied for durability analysis of concrete structures (*fib* 2006). However, the diffusion process in concrete structures is characterized by two- or three-dimensional patterns of concentration gradients. In order to assess the accuracy and the field of application of the 1D diffusion model, a comparison with more complex 2D models at cross-sectional level is needed. Among the numerical methods to solve the partial differential equations governing the diffusion process, cellular automata provide an alternative and general approach to the physical modeling of the phenomenon. Cellular automata were firstly introduced by Von Neumann and Ulam (Burks & Von Neumann 1966) and then developed and applied in many fields (Wolfram 1983). The method has been effectively applied in the solution of diffusion problems as well (Biondini *et al.* 2004). This approach allows to model more complex diffusion scenarios, being in general more reliable than simplified models.

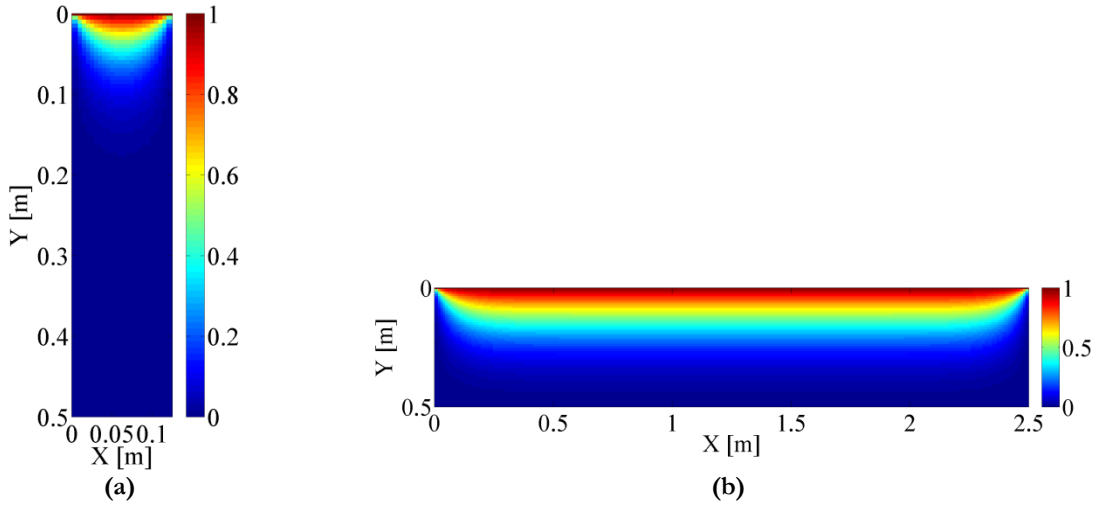

Figure 2.7 – Maps of chlorides concentration normalized with respect to the surface concentration at time instant t = 50 years for different shape factors: (a) β = 0.25; (b) β = 5 (Titi 2012).

Comparison between the 1D and 2D formulations in terms of concentration of the aggressive agents in a concrete cross-section has been carried out by means of parametric analyses (Titi 2012, Titi & Biondini 2012). The influence of the shape factor of the cross-section $\beta = B/H$ has been investigated by considering the diffusion flow perpendicular to B. Results showed that the geometric ratio between the dimensions of the section and the position where the differential equation is solved are key parameters in the comparison of the results. In fact, both approaches tend to the same results when the shape factor β increases, since the diffusion front tends to be uniform along the width of the

section and the boundary effects are negligible. On the contrary, if β decreases, the influence of the boundaries is significant (Figure 2.7).

However, if the concentration is evaluated in the position $x = B/2$, the results tend to converge even for low values of β. This is shown in Figure 2.8a, where the chloride concentration in a square concrete cross-section subjected to diffusion from one side is evaluated in $x = 0$m and $x = 0.25$m over a 50 year time interval. It can be noticed that the 1D approach overestimates the results in both cases, being though closer to the prediction of the 2D approach for $x = 0.25$m.

If the scenario of diffusion on four sides is considered (Figure 2.8b) is considered, the 1D approach underestimates the chloride concentration value estimated by the 2D approach. An approximate method for the 1D model which evaluates the concentration in a point of the cross-section as the sum of the concentration values deriving from the diffusion from each side is also considered (Figure 2.8b, continuous black line). In this case the results overestimate those of the 2D approach, thus being on the safe side.

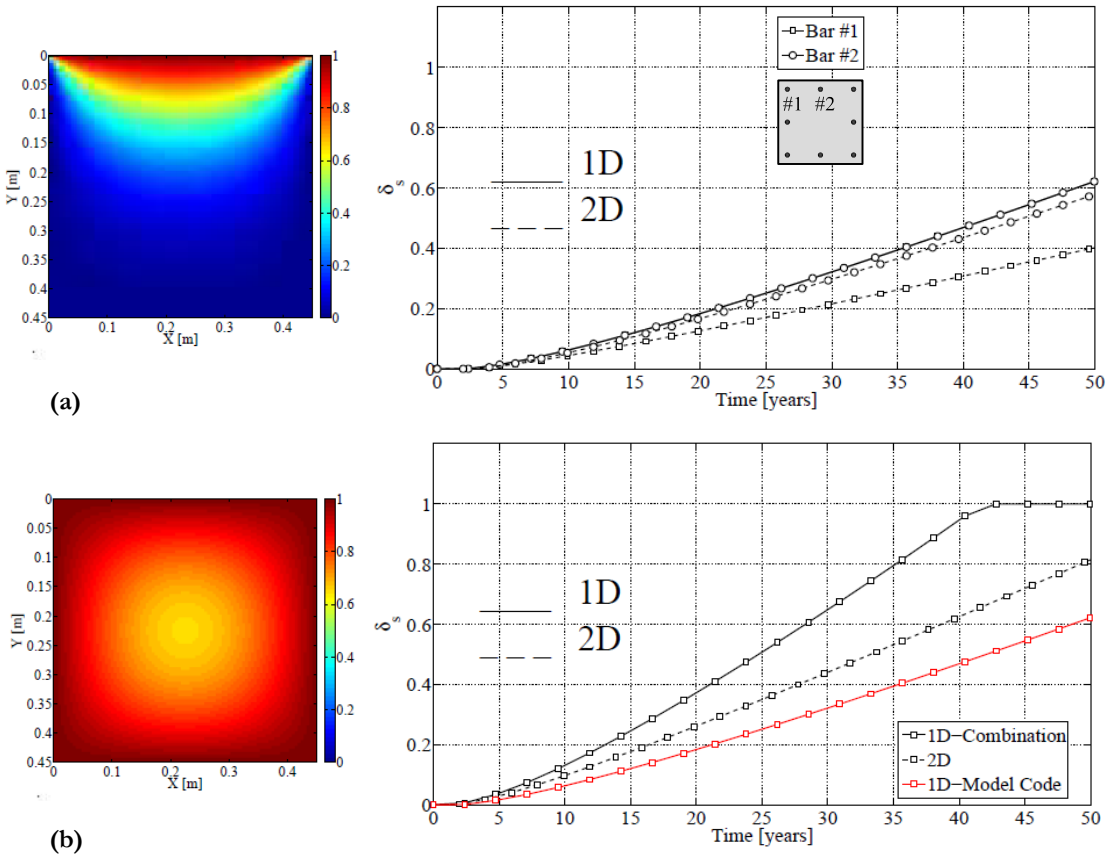

Figure 2.8 – Comparison between 1D and 2D diffusion models: diffusion from (a) one side and (b) four sides of a square concrete cross-section (Titi & Biondini 2012).

5. Application: modeling of chloride diffusion process

The probabilistic approach for 1D chloride diffusion modeling proposed by the *Model Code* (*fib* 2006) is herein presented as an application. The involved parameters are assumed as random variables with proper distribution type, mean μ and standard deviation σ, as listed in Table 2.3 (*fib* 2006). A severe scenario of environmental aggressiveness is considered, with $C_{s,\Delta x}$ = 3%.

Table 2.3 – Probability distributions and their parameters of the random variables involved in the diffusion process (*fib* 2006).

Random Variable	Distribution Type	μ	σ
Concrete cover c [mm]	Normal (*)	40	8
Aging coefficient a [-]	Beta (b_{min} = 0.0; b_{max} = 1.0) (#)	0.3	0.12
Depth of the convection zone Δx [mm]	Constant(^)	0	-
Chloride content at depth Δx $C_{s,\Delta x}$ [wt.%/cem]	Normal (*)	3	0.30μ
Chloride migration coefficient $D_{RCM,0}$ [m²/s]	Normal (*)	$15.8 \cdot 10^{-12}$	0.20μ
Critical chloride content C_{crit} [wt.%/cem]	Beta (b_{min} = 0.2; b_{max} = 2.0) (#)	0.6	0.15
Initial chloride content C_0 [wt.%/cem]	Uniform	0	-

(*) Truncated distributions with non negative outcomes.
(#) b_{min} = lower bound and b_{max} = upper bound of beta distributions.
(^) For spray conditions (spray road environment, spray marine environment).

The Probability Density Functions (PDFs) of chloride concentration obtained from a Monte Carlo Simulation (MCS) analysis with a sample size of 50,000 realizations are shown in Figure 2.9, with reference to a cover depth c = 40mm and time steps Δt = 10 years for a structural lifetime of 50 years (Biondini *et al.* 2013).

With reference to the Fick's one-dimensional model of diffusion, the initiation time t_i for propagation of steel bar corrosion can evaluated as follows by inverting the limit state Eqn. 2.10:

$$t_i = \frac{(c-\Delta x)^2}{4D_c}\left[erf^{-1}\left(\frac{C_{S,\Delta x}-C_{crit}}{C_{S,\Delta x}-C_0}\right)\right]^{-2} \tag{2.14}$$

where the approximation $D_c \cong D_{RCM,0}$ is assumed for short exposure time intervals.

Based on the assumed modeling of random variables, the PDF obtained for the corrosion initiation time t_i is shown in Figure 2.10. A lognormal distribution with mean μ = 1.19 years and standard deviation σ = 0.87 years appears to be a good estimate of the actual distribution for the corrosion

initiation time $t_i \leq 50$ years (Figure 2.10, continuous line). It is worth noting that the relatively short initiation time is related to the severe conditions assumed in this application for exposure, chloride content and diffusion coefficient of concrete.

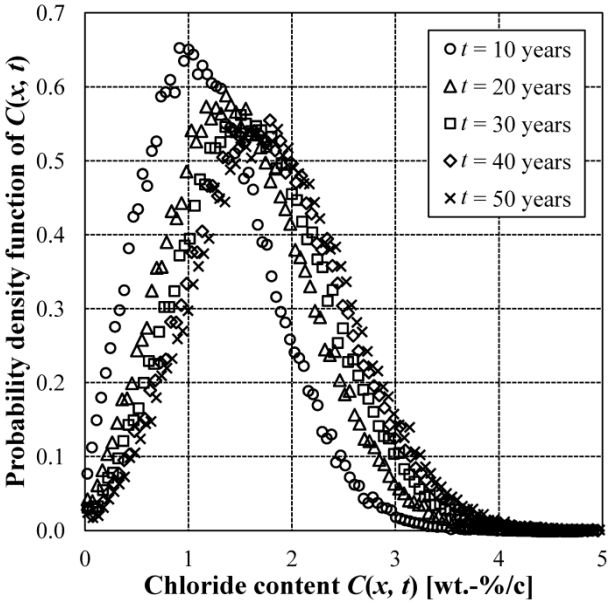

Figure 2.9 – PDFs of chloride concentration in concrete $C(x, t)$ at cover depth $x = c = 40$mm and time steps $\Delta t = 10$ years for a 50-year lifetime.

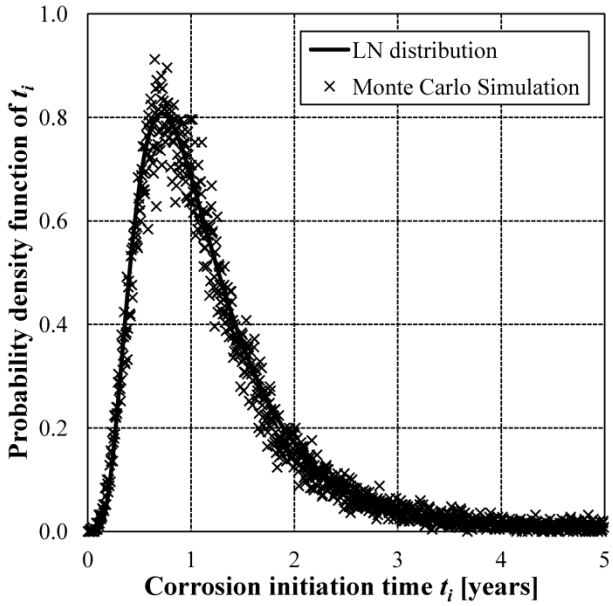

Figure 2.10 – PDF of corrosion initiation time t_i.

Different levels of surface chloride concentrations allow to simulate in the numerical model an increasing environmental aggressiveness. The chloride content $C_{s,\perp x}$ is set equal to $C = 1\%, 2\%, 3\%$ for illustrative purpose. Figure 2.11a shows the influence of the chloride concentration C on the PDFs of the chloride concentration in concrete $C(x, t)$ at cover depth $c = 40$mm at time steps $\Delta t =$

10 years and Δt = 50 years. It is observed that the increasing level of environmental severity leads to an increase of the chloride content in concrete and modifies the shape of the PDFs as well.

The distributions of the initiation time t_i evaluated for different environmental exposures change accordingly (Figure 2.11b). The lognormal distributions LN(8.03, 3.02), LN(2.07, 1.23), LN(1.19, 0.87) well approximate the initiation time results for a surface chloride concentration C = 1%, 2%, 3%, respectively.

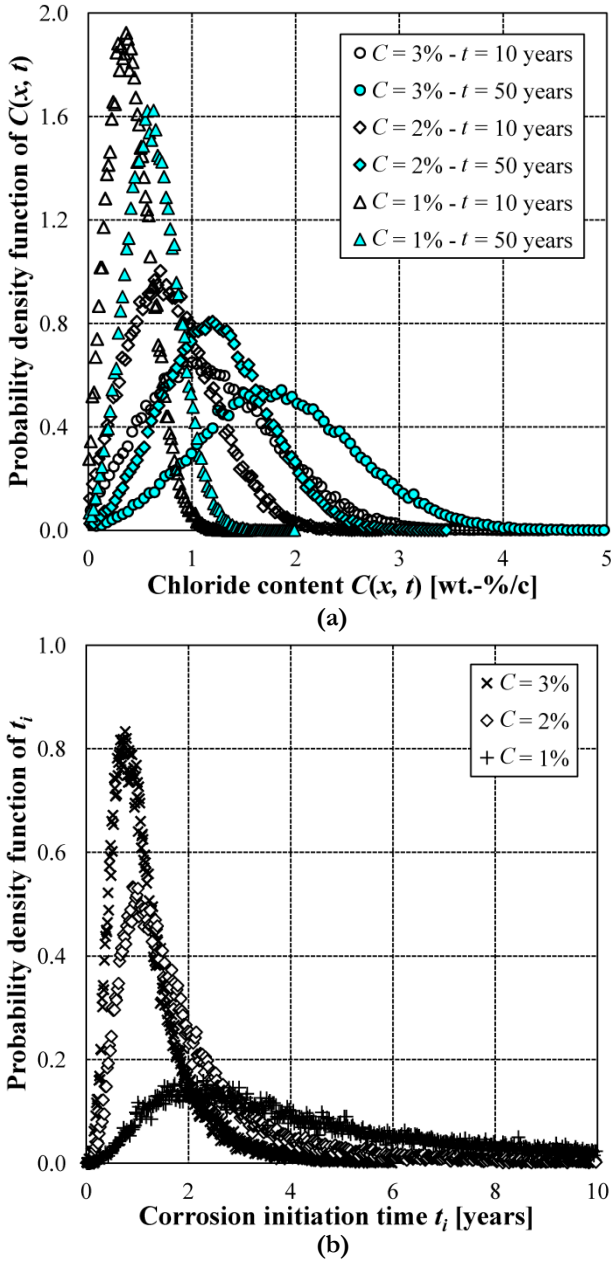

Figure 2.11 – Influence of the chloride concentration C = 1%, 2%, 3%. (a) Probability density functions of chloride concentration in concrete $C(x, t)$ at cover depth $x = c$ = 40mm and time steps Δt = 10 years and Δt = 50 years. (b) Probability density functions of corrosion initiation time t_i.

6. Conclusions

Deterioration processes in concrete structures exposed to aggressive environments have been presented. Transport phenomena affecting concrete elements have been reviewed starting from the theoretical aspects and focusing on the diffusion process. The effects of the environmental damage on both concrete and steel have been discussed, with particular attention on chloride induced corrosion, being one of the most severe form of deterioration of existing concrete structures. Factors influencing corrosion initiation and propagation have been considered, depending on both the environmental scenario and on the geometrical, mechanical and chemical properties of the concrete element. The surface chloride concentration and the coefficient of diffusion of concrete, among the others, are key parameters in the development of the diffusion process.

Available numerical models to describe the chloride diffusion in concrete have been presented, with particular attention on the Model Code approach (*fib* 2006). The validity of this model is then discussed. It has been assessed that the diffusion model based on 1D Fick's law can be effectively applied in most cases. The comparison with the results of a more refined 2D diffusion model showed the accuracy of the 1D formulation. The field of application and the possibility to overcome the limitations of the 1D diffusion model have been highlighted as well. In particular, 1D models are appropriate for cross-sections with high values of the aspect ratio with the longer edge exposed to the diffusion front and for cross-section composed by elongated rectangles, such as box cross-sections. In these practical applications, the 1D approach results then to be a convenient mathematical tool for evaluating the diffusion process, as suggested by current design codes.

The simulation of the diffusion process referring to a specific scenario has been finally presented according to the proposed model. A Monte Carlo simulation technique has been used to take into account the uncertainties related to both the environmental and material variables. The influence of the environmental aggressiveness on the initiation time and on the chloride concentration inside concrete has been investigated. In the next Chapter, the numerical models for evaluating the effects of corrosion damage on both concrete and steel under chloride diffusion will be presented.

7. References

Alonso, A., & Andrade, C. (1994). Life time of rebars in carbonated concrete, in *Progress in Understanding and Prevention of Corrosion*, J.M. Costa, A.D. Mercer (Eds.), *Institute of Materials, London*, 634–641.

Alonso, C., Castellote, M., & Andrade, C. (2001). Dependence of chloride threshold with the electrical potential of reinforcements. In *2nd Int. RILEM Workshop on Testing and Modeling the Chloride Ingress into Concrete*, PRO19, 415–425.

Alonso, C., Castellote, M., & Andrade, C. (2002). Chloride threshold dependence of pitting potential of reinforcements. *Electrochimica Acta*, 47(21), 3469–3481.

Andrade, C. (2002). Determination of chloride threshold in concrete. In *Proposal of the Monitoring, Group WG-B3-COST521, Final Report Workshop of COST-521*, Ed. R. Weydert, Luxembourg, 108–119.

Angst, U., Elsener, B., Larsen, C.K., & Vennesland, Ø. (2009). Critical chloride content in reinforced concrete – a review. *Cement and Concrete Research*, 39(12), 1122–1138.

Arup, H. (1983). The mechanisms of the protection of steel by concrete. *Society of Chemical Industry*, 151–157.

Bakker, R. (1994). Prediction of service life reinforcement in concrete under different climatic conditions at given cover. *International Conference on Corrosion and Protection of Steel in Concrete,* Sheffield, UK.

Bakker, R., Van der Wegen, G., & Bijen, J. (1994). Reinforced concrete: an assessment of the allowable chloride content. *Proceedings of CANMET/ACI International* Conference on Durability of Concrete, Nice.

Bamforth, P.B. (1994). Prediction of the onset of reinforcement corrosion due to chloride ingress. *Proceedings of International Conference on Concrete across Borders*.

Bamforth, P.B., & Chapman-Andrews, J.F. (1994). Long term performance of RC elements under UK coastal exposure conditions. *Proceedings of International Conference on Corrosion and corrosion protection of steel in concrete*, R.N. Swamy (Ed.), Sheffield Academic Press, 139–156.

Bamforth, P.B., & Price, W.F. (1996) An International Review of Chloride Ingress into Structural Concrete. *Rep. No. 1303/96/9092, Taywood Engineering Ltd., Technology division*, Middlesex, U.K.

Bažant, Z.P. (1979). Physical model for steel corrosion in concrete sea structures. *Journal of the Structural Division*, *ASCE*, 105(ST6), 1137–1166.

Bentur, A., Diamond, S., & Berke, N.S. (1997). *Steel Corrosion in Concrete, Fundamentals and Civil Engineering Practice*, E&FN Spon Press.

Bertolini, L. (2008). Steel corrosion and service life of reinforced concrete structures. *Structure and Infratructure Engineering*, 4(2), 123–137.

Bertolini, L., Elsener, B. Pedeferri, P., & Polder R. (2004). *Corrosion of Steel in Concrete – Prevention, Diagnosis and Repair*. Wiley-VCH, Weinheim.

Biczok, I. (1972). *Concrete Corrosion, Concrete Protection*. Akademiai Kiado, Budapest, Wiesbaden.

Biondini, F., Bontempi, F., Frangopol, D.M., & Malerba, P.G. (2004). Cellular automata approach to durability analysis of concrete structures in aggressive environments. *Journal of Structural Engineering, ASCE*, 130(11), 1724–1737.

Biondini, F., Camnasio, E., & Palermo, A. (2013). Lifetime Seismic Performance of Concrete Bridges Exposed to Corrosion. *Structure and Infrastructure Engineering*, ahead-of-print, doi:10.1080/15732479.2012.761248.

Boulfiza, M., Sakai, K., Banthia, N., & Yoshida, H. (2003). Prediction of chloride ions ingress in uncracked and cracked concrete, *ACI Materials Journal*, Title No.100-M5, 38–48.

Broomfield, J.P. (1997). *Corrosion of Steel in Concrete*, Spon Press.

Burks, A.W. & Von Neumann, J. (1966). *Theory of self-reproducing automata*. University of Illinois Press, 1966.

CEB (1992). *Durable Concrete Structures – Design Guide*. Committee Eurointernational du Beton, Bulletin, 183.

Collepardi, M. (2006). *The New Concrete*. Grafiche Tintoretto.

Collepardi, M., Marcialis, A., & Turriziani, R. (1970). Kinetic of penetration of chloride ions into concrete (in Italian). *Industria Italiana del Cemento* 4, 157–164

Collepardi, M., Marcialis, A., & Turriziani, R. (1972). Penetration of chlorides ions into cement paste and concretes. *Journal of American Ceramic Society*, 55, 534–535.

den Uijl, J.A., & Kaptijn, N. (2002). Structural consequences of ASR: an example on shear capacity. *Heron*, 47(2), 125–139.

Dhir, R.K., Jones, M.R., & McCarthy, M.J. (1987). PFA concrete: Chloride induced corrosion. *Magazine of Concrete Research*, 46(169), 269–277.

Duracrete (2000). The European Union – Brite EuRam III, DuraCrete – Probabilistic Performance Based Durability Design of Concrete Structures. Final Technical Report of Duracrete Project, Document BE95-1347/R17, CUR, Gouda (NL), 2000.

EN 206-1 (2001) *Concrete – Part 1. Specification, Performance, Production and Conformity*, European Committee for Standardization, 2001.

Enright, M.P., & Frangopol, D.M. (1998). Service-life prediction of deteriorating concrete bridges. *Journal of Structural Engineering*, 124(3), 309-317.

fib (2006). *Model Code for Service Life Design*. Bulletin, 34.

Frederiksen, J. M., Nilsson, L.O., Poulsen, E., Sandberg, P., Sorcnsen, H.E., & Klinghoffer, O. (1996). *HETEK - Chloride penetration into concrete - State of the art. Transport processes, corrosion initiation, test methods and prediction models*, The Road Directorate, Report (53), Copenhagen.

Ghods, P., Chini, M., Alizadeh, R., Hoseini, M., Shekarchi, M., & Ramezanianpour, A.A. (2005). The effect of different exposure conditions on the chloride diffusion into concrete in the Persian Gulf region. *Proceedings of the ConMAT Conference*.

Glass, G.K., & Buenfeld, N.R. (1997). The presentation of the chloride threshold level for corrosion of steel in concrete. *Corrosion Science*, 39(5), 1001–1013.

Glass, G.K., & Buenfeld, N.R. (2000). The inhibitive effects of electrochemical treatment applied to steel in concrete. *Corrosion Science*, 42(6), 923–927.

Glass, G.K., Page, C.L., & Short, N.R. (1991). Factors affecting the corrosion rate of steel in carbonated mortars. *Corrosion Science*, 32(12), 1283–1294.

Glicksman, M.E. (2000). Diffusion in solids. New York, NY: John Wiley & Sons.

Gouda, V.K. (1970). Corrosion and Corrosion Inhibition of Reinforcing Steel: I. Immersed in Alkaline Solutions. *British Corrosion Journal*, 5(5), 198–203.

Gowripalan, N., Sirivivatnanon, V., & Lim, C.C. (2000). Chloride diffusivity of concrete cracked in flexure. *Cement and Concrete Research*, 30, 725–730.

Hausmann, D.A. (1967). Steel corrosion in concrete - How does it occur?. *Materials Protection*, 11, 19–23.

Hou, H-b., & Zhang, G-z. (2004). Assessment on chloride contaminated resistance of concrete with non-steady-state migration method. *Journal of Wuhan University of Technology*, 19(4), 6–8.

Kong, J.S., Ababneh, A.N., Frangopol, D.M., & Xi, Y. (2002). Reliability analysis of chloride penetration in saturated concrete. *Journal of Probabilistic Engineering Mechanics*, 17(3), 302–315.

Lounis, Z., & Amleh, L. (2004). Reliability-based prediction of chloride ingress and reinforcement corrosion of aging concrete bridge decks. *Life cycle performance of deteriorating structures*, 113–222.

Martin-Perez, B., & Lounis, Z. (2003). Numerical modelling of service life of reinforced concrete structures. *In D.J. Naus (Ed.), Actas del 2nd International RILEM Workshop of Life Prediction and Aging Management of Concrete Structures*, 71–79.

Nürnberger, U. (2002). Corrosion induced failure mechanisms of prestressing steel. *Materials and Corrosion*, 53(8), 591–601.

Page, C.L., Short, N.R., & El Tarras, A. (1981). Diffusion of chloride ions in hardened cement paste. *Journal of Cement and Concrete Research*, 11(3) 395–406.

Page, C.L., Short, N.R., & Holden, W.R. (1986). The influence of different cements on chloride-induced corrosion of reinforcing steel. *Cement and Concrete Research*, 16(1), 79–86.

Parrott, L.J. (1991). Carbonation, moisture and empty pores. *Advances in Cement Research*, 4(15), 111–118.

Parrott, P.J. (1994). Design for avoiding damage due to carbonation-induced corrosion. *Proceedings of Canmet/ACI International Conference on Durability of Concrete*, Nice, 283.

Pedeferri, P., & Bertolini, L. (1996). *La Corrosione nel Calcestruzzo e negli Ambienti Naturali*, McGraw-Hill.

Pedeferri, P., & Bertolini, L. (2000). *Durability of Reinforced Concrete* (in Italian), McGrawHill Italia, Milan.

Polder, R.B., Peelen, W.H.A., Bertolini, L., & Guerrieri, M. (2002). Corrosion rate of rebars from linear polarization resistance and destructive analysis in blended cement concrete after chloride loading, *15th International Corrosion Congress,* September 22-27, 2002, Granada.

Sarja, A., & Vesikari, E. (Editors) (1996). *Durability Design of Concrete Structures*, Manuscript of RILEM Report of TC 130-CSL. RILEM Report Series 14. E&FN Spon, Chapman & Hall.

Schneider, U. (1988). Concrete at high temperatures - a general review. *Fire Safety Journal*, 13(1), 55–68.

Shafei, B., Alipour, A., & Shinozuka, M. (2012). Prediction of corrosion initiation in reinforced members subjected to environmental stressors: a finite-element framework. *Cement and Concrete Research*, 42, 365–376.

Sharp, J.V., & Pullar-Strecker, P. (1980). The United Kingdom concrete-in-the-ocean program. *International Conference on Performance of Concrete in Marine Environment*, ACI SP65, 397–417.

Siemes, T., Han, N., & Visser, J. (2002). Unexpectedly low tensile strength in concrete structures. *Heron*, 47(2), 111–124.

Sobhani, J., & Ramezanianpour, A.A. (2007). Chloride-induced corrosion of RC structures. *Asian Journal of Civil Engineering (Building and Housing)*, 8(5), 531–547.

Stewart, M.G., & Rosowsky, D.V. (1998). Time-dependent reliability of deteriorating reinforced concrete bridge decks. *Structural Safety*, 20(1), 91–109.

Thomas, M. (1996). Chloride thresholds in marine concrete. *Cement and Concrete Research*, 26(4), 513–519.

Titi, A. (2012). *Lifetime Probabilistic Seismic Assessment of Multistory Precast Buildings*. PhD Thesis, Department of Structural Engineering, Politecnico di Milano, Milan, Italy.

Titi, A., & Biondini, F. (2012). Validation of diffusion models for life-cycle assessment of concrete structures. *Third International Symposium on Life-Cycle Civil Engineering* (*IALCCE 2012*), Vienna, Austria, October 3-6.

Tuutti, K. (1982). *Corrosion of Steel in Concrete*, Swedish foundation for concrete research, Stockholm.

Vassie, P. (1984). Reinforcement corrosion and the durability of concrete bridges. *Proceedings of the Institution of Civil Engineers – Part I*, 76, 713–723.

Vu, K.A.T., & Stewart, M.G. (2000). Structural reliability of concrete bridges including improved chloride-induced corrosion models. *Structural Safety*, 22(4), 313–333.

Wang, K., Jansen, D.C., Shah, S.P., & Karr, A.F. (1997). Permeability study of cracked concrete. *Cement and Concrete Research*, 27(3), 381-393.

Wolfram, S. (1983). Statistical mechanics of cellular automata. *Reviews of Modern Physics*, 55(3).

Xi, Y., & Bazant, Z.P. (1999). Modeling of chloride penetration in saturated concrete. *Journal of Materials in Civil Engineering*, 11(1), 58–65.

CHAPTER 3

MODELING OF CORROSION DAMAGE

1. Effects of corrosion on concrete and reinforcing steel

Among the deterioration processes affecting concrete elements in aggressive environments, corrosion of steel bars results the most critical issue for huge stocks of the existing structures. In particular, the diffusion of chlorides in marine environments represents, in general, the most severe attack for concrete structures. The structural performance of concrete structures should hence be considered time-dependent due to environmental damage affecting the structures over the service life. In fact, after the initiation period, which extends depending on the quality of the materials and on the environmental exposure, corrosion inevitably occurs.

Therefore, proper damage models are needed for a reliable lifetime structural analysis. Available experimental data is generally not sufficient for a detailed modeling capable to reproduce the variety of the damaging processes. In fact, the deterioration in concrete structures undergoing diffusion is, in general, very complex. However, in most cases simplified degradation models can be successfully adopted. Models for uniform and localized (pitting) corrosion should account for the reduction of cross-sectional area of corroded bars, the reduction of ductility of reinforcing steel, the deterioration of concrete strength due to the development of longitudinal cracks induced by the corrosion

products, and the spalling of concrete cover. Over the last decades, several models have been formulated and their accuracy has been validated with reference to experimental tests carried out on beams subjected to accelerated and natural corrosion (Al-Harty *et al.* 2011, Almusallam 2001, Apostolopoulos & Papadakis 2008, Biondini &Vergani 2012, Cabrera 1996, Oyado *et al.* 2011). The comparison between numerical and experimental results demonstrated the accuracy and capability of the models to reproduce the effects of local corrosion damage on the structural response at element level.

Structural damage can be viewed as a degradation of the mechanical properties which makes the structural system less able to withstand the applied actions. The effects of corrosion damage can be described in the structural model through damage indices and corrosion can selectively be applied to damaged structural elements with a different level of penetration in each reinforcing bar and a different deterioration for concrete parts, in order to consider prescribed damage patterns and corrosion levels.

In general terms, degradation laws can be adopted to model concrete and steel damage according to the functions $A_c(t)$ and $A_s(t)$ respectively (Biondini *et al.* 2004):

$$\begin{aligned} A_c(t) &= [1-\delta_c(t)]A_{c0} \\ A_s(t) &= [1-\delta_s(t)]A_{s0} \end{aligned} \tag{3.1}$$

where the symbol "0" denotes the undamaged state at the initial time $t = t_0$, and the dimensionless functions $\delta_c = \delta_c(t)$, $\delta_s = \delta_s(t)$ represent damage indices which give a direct measure of the damage level within the range [0; 1] depending on the environmental exposure (Figure 3.1a).

Such indices can be correlated to the diffusion process by assuming a linear relationship between the rate of damage and the concentration of the aggressive agent after the reaching of a concentration threshold, as shown in Figure 3.1b:

$$\begin{aligned} \frac{\partial \delta_c(t)}{\partial t} &= \frac{C(t)}{C_c \Delta t_c} = \rho_c C(t) \\ \frac{\partial \delta_s(t)}{\partial t} &= \frac{C(t)}{C_s \Delta t_s} = \rho_s C(t) \end{aligned} \tag{3.2}$$

where C_c and C_s represent the values of constant concentration $C(x, t)$, in a certain position and at a specified time instant, which lead to a complete damage of the materials after the time periods Δt_c and Δt_s, respectively. In particular, the values of C_{cr}, ϱ_c and ϱ_s depend on the type of material and considered damage process (Biondini *et al.* 2004). It will be shown that this linear approximation results to be a reasonable assumption in most cases, despite the complexity of the corrosion process.

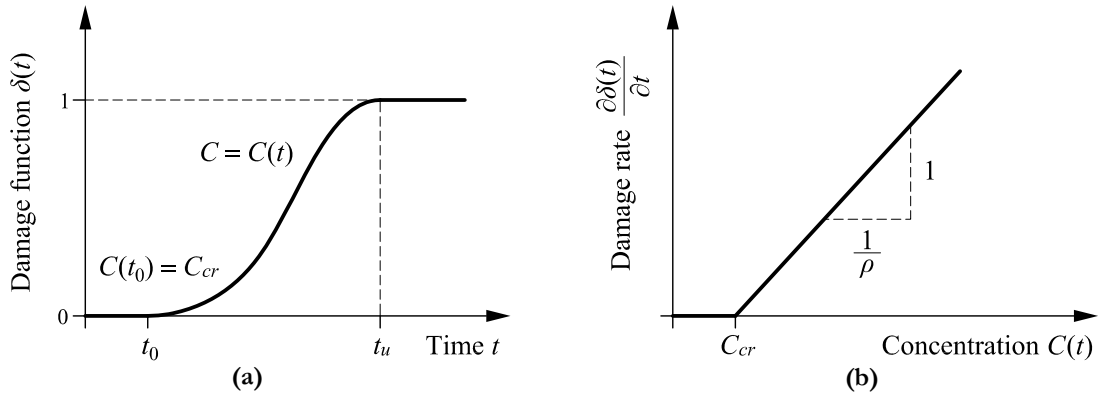

Figure 3.1 – Modeling of mechanical damage: (a) time evolution of damage indices during diffusion process; (b) linear relationship between rate of damage and concentration of aggressive agent.

In the following, the modeling of corrosion damage is discussed, with particular emphasis on chloride-induced corrosion. The effects of corrosion on concrete and steel are illustrated, in order to highlight how the mechanical properties of the materials can vary during lifetime. The effectiveness of the damage models is validated by comparing the numerical results with experimental data available in literature. Finally, an application of the adopted damage model is proposed, accounting for uniform corrosion of steel bars and deterioration of concrete under a specified corrosion scenario.

2. Steel damage modeling

The corrosion process induced by chloride diffusion into concrete members leads to the reduction in the area of steel reinforcing bars. The corrosion penetration $x(t)$ can be evaluated over time as follows:

$$x(t) = \int_{t_i}^{t_i+t_p} r_{corr} dt \tag{3.3}$$

where r_{corr} (mm/year) is the steel corrosion rate, t_i is the initiation time and $t_p = (t - t_i)$ is the propagation time. By this equation, the loss of steel due to the corrosion process can be estimated. A dimensionless penetration index $\delta \in [0; 1]$ can be expressed as:

$$\delta = \frac{x(t)}{\Phi_0} \tag{3.4}$$

where $\Phi_0 = \Phi(0)$ is the uncorroded steel bar diameter at time $t = 0$. The definition of the penetration index depends on the type of the corrosion attack, which can be uniform, localized (pitting attack) or a combination of the two.

The severity of the steel damage depends also on the corrosion rate, which determines the rapidity with which the structure may reach a specified limit state. While the dependency of the corrosion initiation time on different parameters, such as concrete cover thickness or quality and type of cement, has been widely researched and modeled (Browne *et al.* 1983, Hamada, 1968), the evaluation of the propagation time is affected by greater uncertainties. In fact, the corrosion rate can hardly be assessed reliably, since it depends on several parameters related to both environmental conditions and characteristics of concrete. For this reason, the few available experimental data cannot be representative of a wide range of corrosion scenarios.

Available models for uniform and pitting corrosion are presented in the following, as well as a model to estimate steel corrosion rate. Other consequences of the corrosion process, such as steel ductility reduction and steel strength loss are discussed.

2.1. Uniform corrosion

In carbonated concrete and/or in presence of low chlorides content over the steel surface, the corrosion process leads to a uniform reduction of the reinforcing bar diameter (Figure 3.2a). The reduction in the diameter $\Phi(t)$ of a corroding reinforcing bar at time t can be estimated as follows (Berto *et al.* 2009):

$$\Phi(t) = \Phi_0 - nx(t) \tag{3.5}$$

where the coefficient n allows to take into account the possibility of a one-side or two-side attack of corrosion (Saetta *et al.* 1999). By introducing the dimensionless penetration index $\delta = nx(t)/\Phi_0$, the Eqn. 3.5 can be expressed as:

$$\Phi(t) = \Phi_0(1-\delta) \tag{3.6}$$

The area A_s of a corroded steel bar can be represented as a function of the corrosion index as follows (Biondini *et al.* 2004):

$$A_s(\delta) = [1-\delta_s(\delta)]\,A_{s0} \tag{3.7}$$

where $A_{s0} = \pi\Phi_0^2/4$ is the area of the undamaged steel bar and $\delta_s = \delta_s(\delta)$ is a dimensionless damage function which provides a measure of cross-section reduction in the range [0; 1], from no damage to complete damage. In case of uniform corrosion, the damage function δ_s is evaluated as follows (Biondini 2011, Biondini & Vergani 2012):

$$\delta_s = \delta(2-\delta) \tag{3.8}$$

2.2. Localized corrosion

In presence of high chloride content, the corrosion tends to be localized. The severity of the attack is related to the depth of the pits developing along the steel bars. The reduction in the steel bar cross-section should hence account for the maximum depth of the pit attack, which can be estimated by knowing the corrosion rate expressed as the current intensity. The ratio between the mean and the maximum pit depth can be measured experimentally as the pitting factor R:

$$R = \frac{x(t)_{\max}}{x(t)_{\text{mean}}} \tag{3.9}$$

Different values of the pitting factor R have been measured for corrosion in natural environment in the range of 4-8, with maximum pit depth of 0.5mm, and for accelerated corrosion in the range of 5-13 (Gonzalez *et al.* 1995). Stewart (2009) carried out experimental tests on steel bars with varying diameters, measuring pitting factors from 5 to 7. Moreover, the pits develop randomly over the steel surface along the length of the steel bar, in particular in correspondence of defects at the interface between steel and concrete (Zhang *et al.* 2009).

Stewart (2009) proposed a model to estimate the cross-sectional reduction of the steel bars, by considering that the pit starts to develop from the point A and progressively expands following the shape profile of a circle of radius $p(t)$ (Figure 3.2b). The maximum depth of the pit $p(t)$ is evaluated as follows:

$$p(t) = x(t)_{\text{mean}} R \tag{3.10}$$

The width of the pit b and the angles θ_1 and θ_2 can be evaluated as follow:

$$b(t) = 2p(t)\sqrt{1-\left(\frac{p(t)}{\Phi_0}\right)^2} \tag{3.11}$$

$$\theta_1(t) = 2\arcsin\left(\frac{b(t)}{\Phi_0}\right) \qquad \theta_2(t) = 2\arcsin\left(\frac{b(t)}{2p(t)}\right) \tag{3.12}$$

The pit area A_{pit} can finally be evaluated as:

$$\begin{cases} A_{pit}(t) = A_1 + A_2 & p(t) \le \Phi_0/\sqrt{2} \\ A_{pit}(t) = A_0 - A_1 + A_2 \quad \text{if} & \Phi_0/\sqrt{2} \le p(t) \le \Phi_0 \\ A_{pit}(t) = A_0 & p(t) \ge \Phi_0 \end{cases} \tag{3.13}$$

where:

$$A_1 = 0.5\left[\theta_1\left(\frac{\Phi_0}{2}\right)^2 - b\left|\frac{\Phi_0}{2} - \frac{p(t)^2}{2}\right|\right] \tag{3.14}$$

$$A_2 = 0.5\left[\theta_1 p(t)^2 - b\frac{p(t)^2}{\Phi_0}\right] \tag{3.15}$$

$$A_0 = \frac{\pi\Phi_0^2}{4} \tag{3.16}$$

The reduction of the steel bar cross-section is usually evaluated in percentage as:

$$\alpha_{pit} = \frac{A_{pit}}{A_0} \tag{3.17}$$

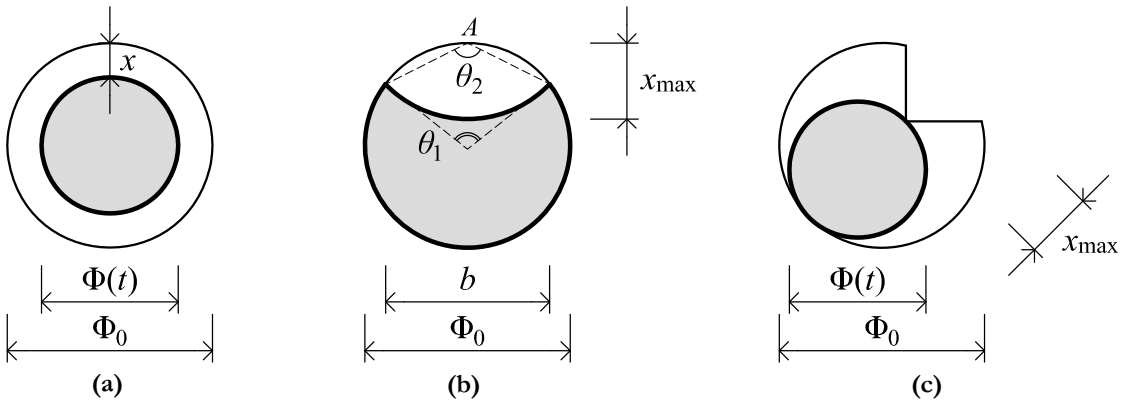

Figure 3.2 – Reduction of the steel bar cross-section due to (a) uniform corrosion, (b) pitting corrosion based on Val-Melchers (1998) model and (c) pitting corrosion based on Rodriguez (1997) model.

Rodriguez (1997) proposed a model that takes into account both uniform and pitting corrosion, as usually occur in accelerated corrosion tests (Figure 3.2c). The loss of the steel area ΔA_s can be evaluated as follow by assuming $R = 2$:

$$\Delta A_s = \frac{\pi}{4}(2p(t)\Phi_0 - p(t)^2) \tag{3.18}$$

2.3. Steel corrosion rate

The corrosion propagation is affected by great uncertainties, mainly due to the numerous set of conditions influencing the corrosion rate. The rate of corrosion depends on temperature and humidity, being higher when both temperature and humidity increase (Andrade 2002). It also depends on concrete resistivity which is lower when relative humidity is higher (Gjørv 2009, Andrade & Alonso 2001) and which is related to the corrosion rate by a linear relationship (Gulikers 2005).

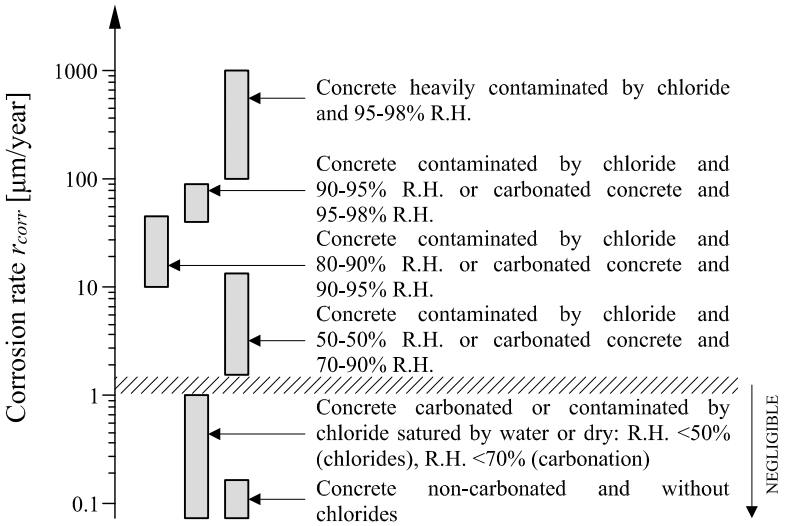

Figure 3.3 –Schematic representation of corrosion rate of steel in different concretes and exposure conditions (after Andrade *et al.* 1990, modified).

On structures exposed to the atmosphere, the corrosion rate can vary from several tens of µm/year to localized values of 1mm/year as the relative humidity rises from 70 to 95% and the chloride content increases from 1% by mass of cement to higher values. The corrosion rate is usually expressed as the penetration rate and is measured in µm/year. The corrosion rate can be considered negligible if it is below 2µm/year, low between 2-5µm/year, moderate between 10-50µm/year and very high for values above 100µm/year (Figure 3.3).

Once the attack begins in chloride-contaminated structures, a high corrosion rate can lead in a relatively short time to an unacceptable reduction in the cross-section of the reinforcement. In presence of high chloride contents, even for relative humidities the corrosion rate can be up to 2

μm/year. These corrosion rates have been observed in particular on heavily chloride containing structures such as bridge decks (Vassie 1984).

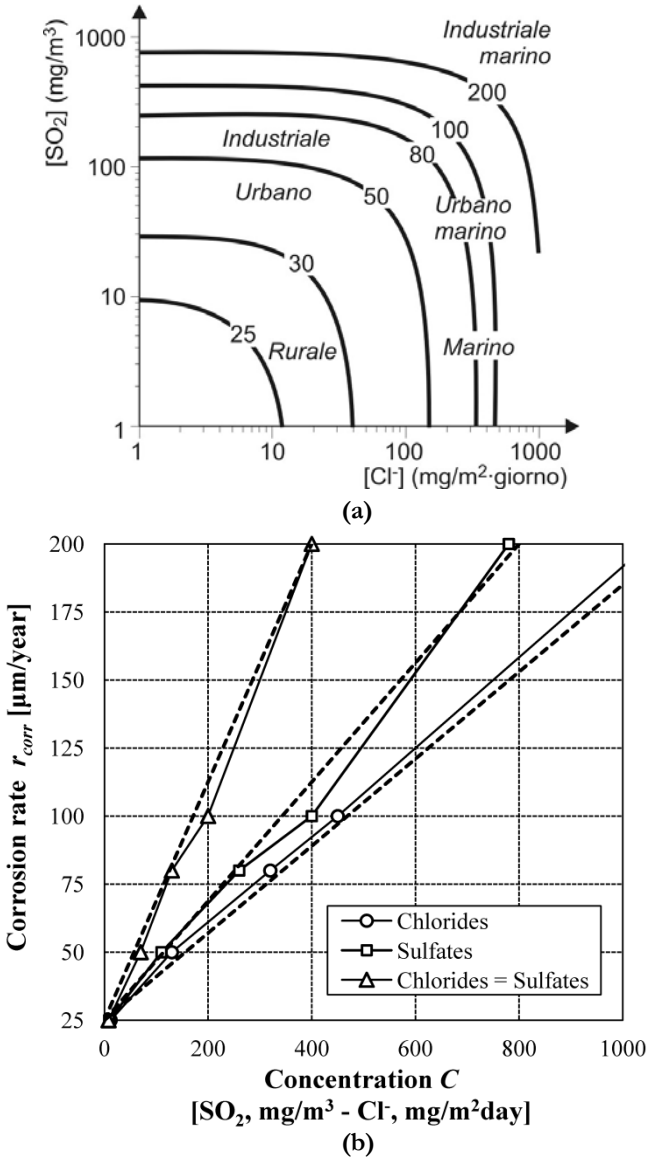

Figure 3.4 – (a) Relationship between sulfate concentration, chloride accumulation rate on the surface and steel corrosion rate (μm/year), with indication of typical exposures (Pedeferri & Bertolini 1996); (b) Linear relationship between the concentration of the aggressive agents and the rate of corrosion.

On the basis of correlations between chloride content and corrosion current density in concrete (Bertolini *et al.*, 2004; Liu & Weyers, 1998; Pastore & Pedeferri, 1994; Thoft-Christensen, 1998), a linear relationship between rate of corrosion r_{corr} and chloride content C can be assumed for structures exposed to severe environmental conditions. This is assessed by the experimental measures of the corrosion rate of steel exposed to different environments containing sulfates and chlorides (Figure 3.4a). The same relationship is here assumed for reinforcing steel as well (Biondini *et al.* 2004, 2006). It is observed that the rate of corrosion increases as the concentration of both sulfates and chlorides

increases. In industrial and marine environments, where the concentration of both the aggressive agents is high, the corrosion rate can be higher than 100μm/year. If the corrosion rate is plotted as a function of chloride concentration, sulfate concentration or a combination of them, it can be noticed that a linear dependency can be assumed (Figure 3.4b).

Moreover, the rate of corrosion should be considered a time-dependent parameter. In fact, it is expected that the formation of rust products on the steel surface may progressively reduce the steel degradation rate over time. In particular, the corrosion rate will reduces with time rapidly during the first few years after initiation but then more slowly as it approaches a nearly uniform level (Andrade *et al.* 2002, Liu & Weyers 1998, Tuutti 1982, Yalsin & Ergun 1996). However, since there is lack of explicit data for time-dependent corrosion rate modeling, the mean value of the rate of corrosion can be considered constant in time and its variability can be taken into account in probabilistic terms (Akgül & Frangopol 2004, Frangopol *et al.* 1997, Ghosh & Padgett 2010, Val *et al.* 2000).

2.4. Steel ductility reduction

Steel corrosion results not just in the reduction of the cross section of the steel bars, but also in a reduction of the steel ductility. Experimental results showed that the steel ultimate strain reduces even for relatively low percentages of steel mass loss, leading to a shift from ductile to brittle behavior for higher levels of corrosions (Almusallam 2001, Apostolopoulos & Papadakis 2008, Figure 3.5).

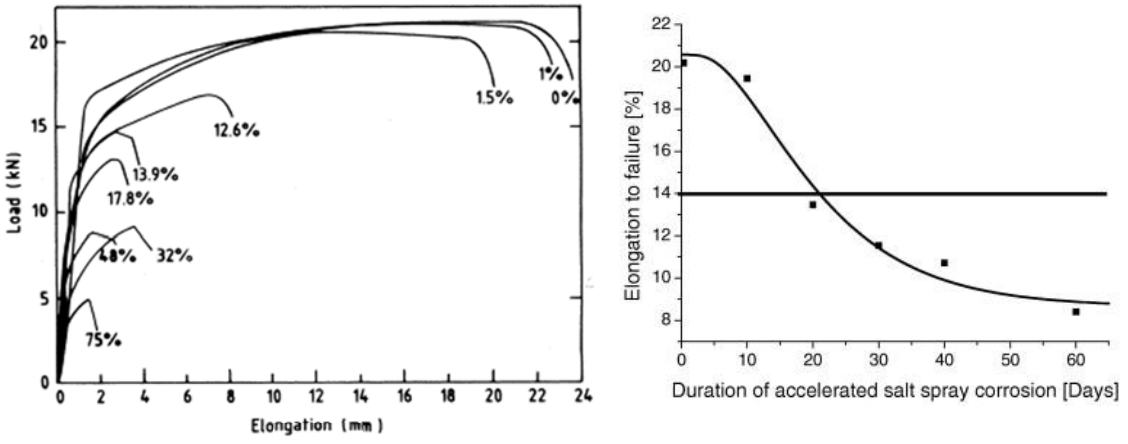

(a) **(b)**

Figure 3.5 – (a) Elongation vs. load curves for steel bars with different corrosion levels (% in mass, Almusallam 2001); (b) Corrosion effect on steel ultimate strain (Apostolopoulos & Papadakis 2008).

On the basis of experimental results, Kobayashi (2006) proposed a numerical relationship between the residual ultimate strain and the initial one:

$$\frac{\varepsilon'_{su}}{\varepsilon_{su}}\% = 100 - 18.1x \tag{3.19}$$

where x (%) represents steel cross-sectional reduction. This relationship has been derived basing on experimental data on tensile tests carried out on corroded bars with low percentage of mass loss. Therefore the equation holds for levels of corrosion up to 3-4%.

Coronelli & Gambarova (2004) proposed the following relationship for the evaluation of the reduction of steel ultimate strain from the value $\varepsilon'_{su} = \varepsilon_{su}$ to the value $\varepsilon'_{su} = \varepsilon_{sy}$ indicating the complete loss of ductility:

$$\varepsilon'_{su} = \varepsilon_{sy} + (\varepsilon_{su} - \varepsilon_{sy})\left(1 - \frac{\alpha_{pit}}{\alpha_{pit,\max}}\right) \qquad \text{if} \quad \alpha_{pit} \le \alpha_{pit,\max} \tag{3.20}$$

where ε_{sy} is the steel strain at yielding, a_{pit} and $a_{pit,max}$ are the depth and maximum depth of the pitting attack, respectively. Based on experimental studies, the parameter $a_{pit,max}$ ranges between 0.1-0.5.

In Stewart (2009), an abrupt shift from a ductile to a brittle behavior is considered to occur for a corrosion value of 20%, evaluating the corroded area of the steel bar A_{pit} as in Eqn. 3.13.

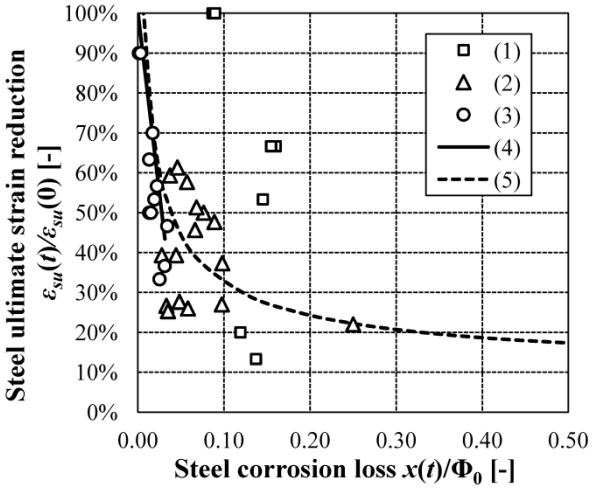

(6) Apostolopoulos & Papadakis (2008, marine environment)
(7) Apostolopoulos & Papadakis (2008, industrial environment)
(8) Kobayashi (2006)
(9) Kobayashi model (2006)
(10) Biondini & Vergani model (2011)

Figure 3.6 – Comparison between different models and experimental data related to the evaluation of steel ultimate strain reduction $\varepsilon'_{su}/\varepsilon_{su}$ versus corrosion steel loss x.

Biondini & Vergani (2011, 2012) related the steel ductility reduction to a function of the section loss based on the experimental results by Apostolopoulos & Papadakis (2008). According to this model, the lifetime steel ultimate strain $\varepsilon_{su}(t)$ depends on the damage function as follows:

$$\varepsilon_{su}(t) = \begin{cases} \varepsilon_{su0} & 0 \le \delta_s \le 0.016 \\ 0.1521\delta_s^{-0.4583}\varepsilon_{su0} & 0.016 < \delta_s \le 1 \end{cases} \tag{3.21}$$

where ε_{su0} is the ultimate strain for uncorroded steel. Figure 3.6 shows a comparison between the above mentioned models and experimental data collected for the evaluation of steel ultimate strain reduction $\varepsilon'_{su}/\varepsilon_{su}$ versus normalized corrosion steel loss x.

2.5. Steel strength reduction

Experimental tests showed that a linear decrease of both yielding and ultimate strength $f(t)$ occurs at the increase of the corrosion level (Du *et al.* 2005):

$$f(t) = [1 - \beta Q_{corr}(t)] f_0 \tag{3.22}$$

where f_0 if the strength of the non-corroded bars, $Q_{corr}(t)(\%)$ is the level of corrosion and β is a coefficient depending on the type of corrosion. However, the steel strength reduction is limited (Figure 3.7). It has been observed that the steel strength reduction is mainly due to the localized corrosion. Stewart (2009) proposed to evaluate Q_{corr} as the maximum pitting depth ratio (Eqn. 3.9).

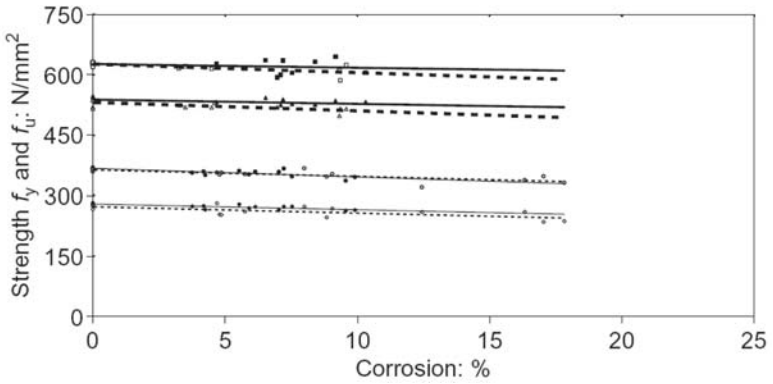

Figure 3.7 – Reduction of yielding and ultimate strength of corroded steel bars (Cairns *et al.* 2005)

3. Concrete damage modeling

Although the main effect of corrosion on reinforced concrete elements is the reduction of the steel-bar cross-section, in case of uniform corrosion the degradation of concrete may become significant. Corrosion products on steel bar surface provoke tension stresses in the surrounding concrete, leading to the cracking and delamination of the concrete cover. The spalling becomes not just a durability but also a safety issue when significant portions of the concrete cover detach from slabs, roof girders and bridge decks (Broomfield 1997). Other effects of concrete deterioration are the reduction of concrete strength and the loss of bond between concrete and steel.

The presence of cracks and spalling gives evidence of the corrosion process. On the other hand, deterioration of the concrete protective cover makes the ingress of the aggressive agents more severe, accelerating the corrosion process. Experimental studies investigated the relationship between the width of cracks on concrete surface with the corrosion level (Vidal *et al.* 2004, Zhang *et al.* 2009). The time between corrosion initiation and corrosion induced concrete cracking has been investigated as well (Maaddawy & Soudki 2007, Pantazopoulou *et al.* 2001). A numerical modeling of the cracking phenomena induced by the expansion of the corrosion products was proposed by Li *et al.* (2007).

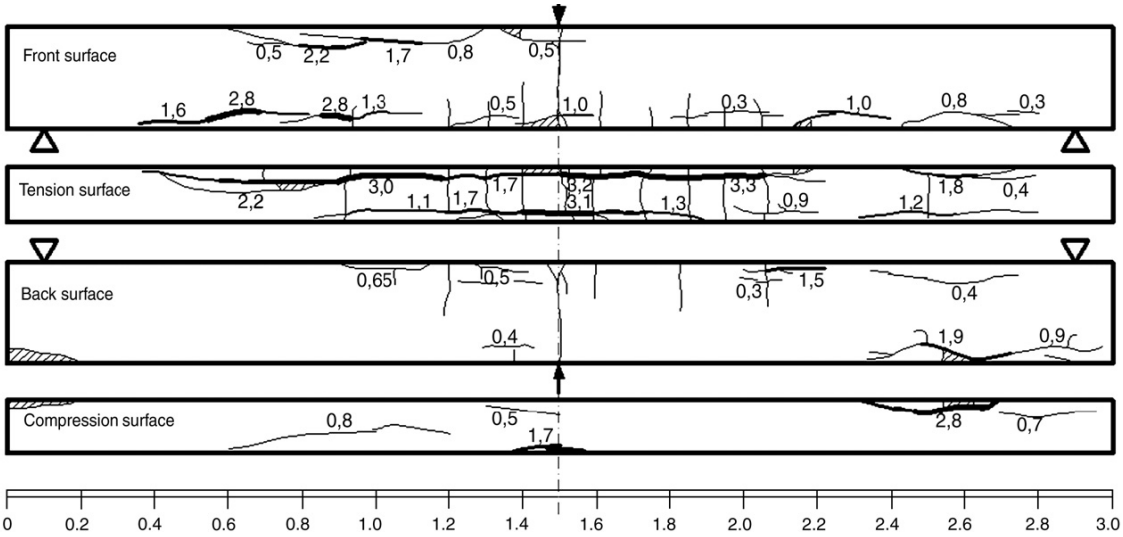

Figure 3.8 – Crack patterns of a deteriorating concrete beam subjected to natural corrosion after 23 years (Zhang *et al.* 2009)

Corrosion cracks usually develop along the longitudinal steel bars, forming a 90° angle with the flexural cracks (Zhang *et al.* 2009, Figure 3.8). The arrangement of the reinforcing bars in the cross-section and the geometry of the concrete element strongly influence the crack pattern and the mechanisms of failure of the concrete cover (Bažant 1979). Concrete cover can fail along fracture planes inclined of 45° or parallel to the steel bar (Figure 3.9a, b). Border effect may emphasize the phenomenon (Figure 3.9c). Factors influencing concrete cracking are the ratio between concrete cover thickness c and the distance between the steel bars d, and concrete quality. For low c/d ratios,

corrosion products will crack the concrete sooner than for high c/d ratios. Moreover, concrete high porosity, corresponding to high w/c ratios, allows the corrosion products to expand in the pores, thus reducing cracking.

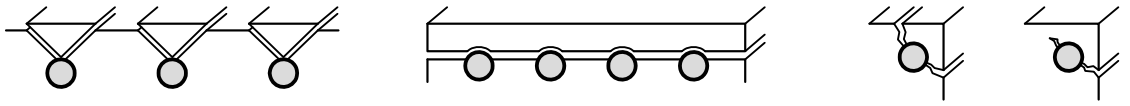

(a) (b) (c)

Figure 3.9 – (a) Scaling, (b) delamination and (c) border effects of corrosion induced cracking of concrete cover.

Several experimental studies have been carried out to investigate the relationship between the c/d ratio and the corrosion level necessary to start concrete cracking (Alonso *et al.* 1998, Cabrera 1996, Rasheeduzzafar *et al.* 1990, Figure 3.10). By fitting the experimental data by Alonso *et al.* (1998), a linear relationship between the corrosion penetration attack x_0 at a certain crack width and the c/d ratio can be estimated as follows:

$$x_0 = 7.53 + 9.32\frac{c}{d} \tag{3.23}$$

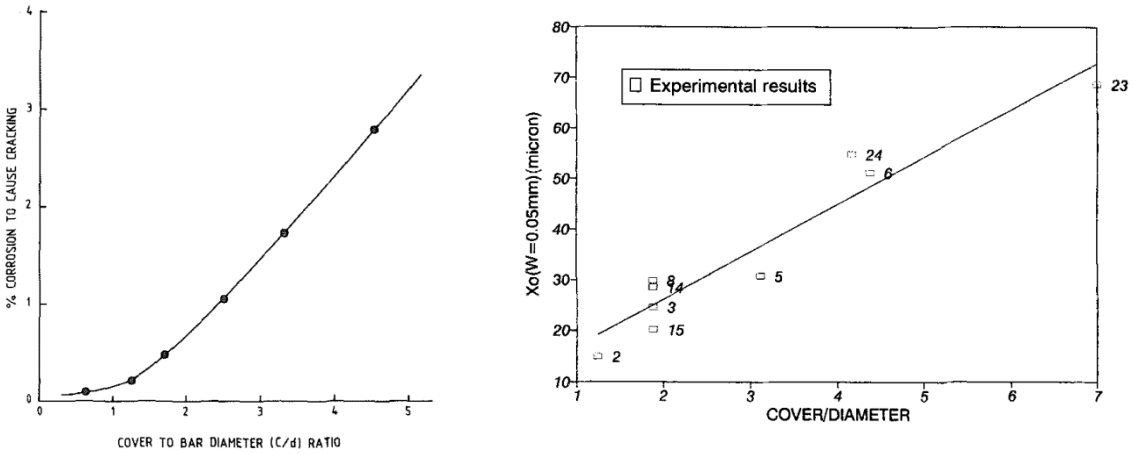

(a) (b)

Figure 3.10 – (a) Relationship between c/d ratio and corrosion level causing cracking (Rasheeduzzafar *et al.* 1990); (b) Relationship between c/d ratio and corrosion penetration attack x_0 causing cracking (Alonso *et al.* 1998).

3.1. Concrete strength reduction

The increase of the transversal strain due to the crack opening is accounted for by a reduction of concrete strength. Coronelli & Gambarova (2004) proposed a model to evaluate the reduced concrete strength over time a follows:

$$f_c(t) = \frac{f_{c0}}{1 + \kappa \dfrac{\varepsilon_{\perp}(t)}{\varepsilon_{c0}}} \tag{3.24}$$

where $\varkappa$ is a coefficient related to bar diameter and roughness ($\varkappa = 0.1$ for medium-diameter ribbed bars), ε_{c0} is the strain at peak stress in compression and $\varepsilon_{\perp}(t)$ is a transversal strain at time t. The evaluation of the transversal strain $\varepsilon_{\perp}(t)$ is based on the following relationship:

$$\varepsilon_{\perp}(t) = \frac{n_{bars} w}{b_i} \tag{3.25}$$

where b_i is the width of the undamaged cross-section, n_{bars} is the number of steel bars and w is the mean crack opening for each bar.

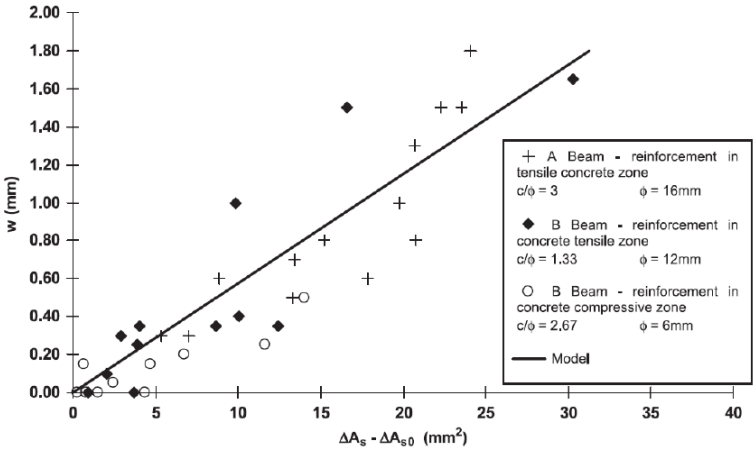

Figure 3.11 – Crack width evolution with steel bar cross-section reduction (Vidal *et al.* 2004).

In order to estimate the mean crack opening w, a linear relationship can be established between the amount of corroded steel and the crack width according to Vidal *et al.* (2004) (Figure 3.11):

$$w = \kappa_w (\delta_s - \delta_{s0}) A_{s0} \tag{3.26}$$

where $\varkappa_w = 0.0575\text{mm}^{-1}$, δ_s is the damage function and δ_{s0} is the amount of steel damage necessary for cracking initiation. For uniform corrosion, the damage threshold δ_{s0} is evaluated as follows (Biondini & Vergani 2012, Vidal *et al.* 2004):

$$\delta_{s0} = 1 - \left[1 - \frac{1}{\Phi_0} \left(7.53 + 9.32 \frac{c}{\Phi_0} \right) \times 10^{-3} \right]^2 \tag{3.27}$$

where $\Phi_0 = \Phi(0)$ and c is the concrete cover. The reduction of concrete strength is generally applied to the entire concrete cover. Since the longitudinal crack pattern strongly depends on the arrangements of the reinforcing bars, the propagation of corrosion induced cracking should be therefore limited to the zone adjacent to the reinforcing bars to model the damage phenomena

properly (Biondini & Vergani 2011, 2012, Vergani 2010). For example, Figure 3.12 shows the identification of the damaged concrete elements in the numerical model of a rectangular concrete cross-section according to different reinforcement layouts. When the steel bars are located at the corners, damage is assumed to be concentrated mainly around the steel bars (Figure 3.12a), otherwise damaged is assumed to develop along the edges of the cross-section (Figure 3.12b).

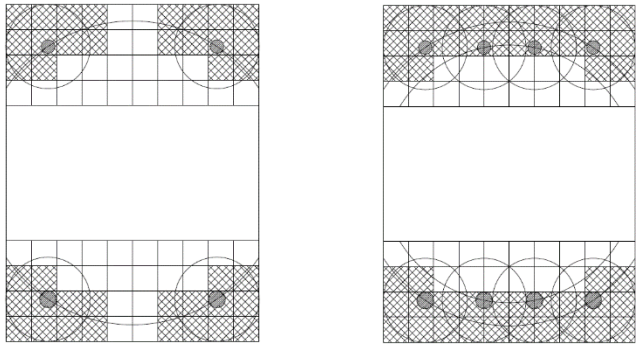

(a) **(b)**

Figure 3.12 – Identification of damaged concrete elements (hatched area) in a numerical model according to different reinforcement layouts (Vergani 2010, Biondini & Vergani 2012).

3.2. Corrosion effects on bond

In sound concrete, bond performance is primarily dependent on concrete compressive strength, confinement and surface of the bar (deformed or round). During lifetime, loss of bond between concrete and steel can occur due to the formation corrosion products over the steel surface inducing radial pressures on the surrounding concrete. The presence of concrete cracks and the progressive smoothing of the ribbed bars due to corrosion worsen the phenomena (Bhargava *et al.* 2007).

Experimental research focused on bond performance found that low levels of corrosion (<~5% reduction in bar cross-section) have a beneficial effect on bond in deformed bars (Almusallam *et al.* 2001, Cabrera 1996). At corrosion levels above this, the bond capacity drops off significantly with a change in the failure mode from splitting of concrete to continuous slippage of the bar (Fang *et al.* 2006).

In literature, several correlations have been proposed for the corrosion level and the ultimate bond strength τ_{bu}, depending on the test (pull-out or flexure test), on the material and on the characteristics of the specimen (Stanish *et al.* 1999, Lee *et al.* 2002).

3.3. Corrosion effects on confinement

The confinement of a concrete cross-section may vary over lifetime due to corrosion of transversal reinforcement. Several studies investigated the uniaxial compression behavior of confined specimens subjected to corrosion in order to get time-variant material stress-strain curves. Yamamoto *et al.* (2006) investigated the relationship between the elastic modulus and the width of the corrosion crack width, comparing the corrosion pattern of confined and non-confined specimens. Yuya *et al.* (2007) estimated the relationship between axial stresses and hoops rate at prescribed axial strains and compared the results for different corrosion methods (accelerated or mechanical).

In particular, corrosion of transversal reinforcement can have significant effects when considering the structural behavior of concrete elements subjected to transversal actions, such the seismic loading, as reported in Yamamoto *et al.* (2006), Saito *et al.* (2007), Ou *et al.* (2012) and Biondini *et al.* (2012).

4. Validation of the damage model

The experimental tests carried out by Rodriguez *et al.* (1997) are herein presented in order to validate the proposed damage models regarding the effects of chloride induced corrosion on steel bars and concrete. The tests were carried out within the Brite/Euram project BE-4062 started in 1992 and some models were developed for the assessment of concrete structures affected by steel corrosion and other deterioration mechanisms. Numerical results of nonlinear analyses are compared with the experimental results to prove the accuracy of the damage models adopted in this study thus performing a reliable structural analysis of deteriorating concrete elements. Reduction of steel bar area due to uniform and pitting corrosion, reduction of steel ultimate strain and degradation of concrete are taken into account in the numerical model.

The tested beams shown in Figure 3.13 have been cast adding calcium chloride to the mixing water, subjected to an accelerated corrosion process with a current density of 100μA/cm², and loaded up to failure by using a four points bending test. Two types of beams with different reinforcement ratios were tested. The beams with lower reinforcement ratio (Type 11, ρ_s = 0.85%) showed a flexural failure of the tensile bars. For beams with higher reinforcement ratio (ρ_s = 2.18%), a crushing failure of concrete in compression occurred. For sake of brevity, only beams Type 11 will be considered. The mechanical properties of concrete and steel are listed in Table 3.1 and Table 3.2.

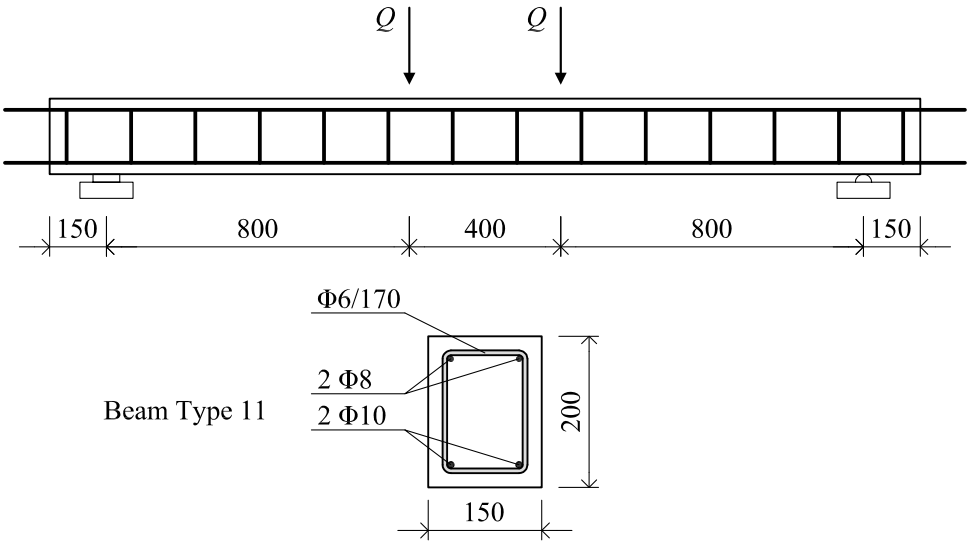

Figure 3.13 – Geometrical dimensions of the concrete beams [mm], characteristic of the cross-section and testing scheme.

For these members the mean and maximum values of corrosion penetration depth measured during the tests are listed in Table 3.3. It is worth nothing that maximum values of penetration are in some cases three times the mean value. As a consequence, failure of the steel bars reasonably occurs in the section with higher reduction. Moreover, the effects of corrosion are significant on the stirrups, due

to their small diameter. The analyses account for the different levels of corrosion of tensile and compressive bars.

Table 3.1 – Concrete mechanical properties.

	Beam 111	Beams 114-116
f_c [MPa]	50	34
f_{ct} [MPa]	4.1	3.1
E_c [GPa]	37.3	33.8

Table 3.2 – Steel mechanical properties.

	Bars Φ6	Bars Φ8	Bars Φ10
f_{sy} [MPa]	626	615	575
f_{su}[MPa]	760	673	655
E_s [GPa]	210	210	210

Table 3.3 – Measured corrosion penetration [mm]. Mean values (maximum values).

Beams	Tensile bars	Compressive bars	Stirrups
114	0.45 (1.1)	0.52	0.39 (1.1)
115	0.36 (1.0)	0.26	0.37 (3.0)
116	0.71 (2.1)	0.48	0.66 (5.0)

Nonlinear analyses are performed by using OpenSees (Mazzoni *et al.* 2005). The beams are subdivided into 6 finite elements due to symmetry. Two different types of modeling are developed and compared:

- distributed plasticity (DP) modeling: the member cross-section is modeled by fibers or isoparametric domains by discretizing the concrete area and modeling each longitudinal steel bar (Bontempi 1992, Malerba 1998, Malerba & Bontempi 1989, Spacone *et al.* 1996). Cover concrete fibers are distinguished from the core, where the Mander model is adopted in order to take into account the confinement effect of stirrups (Mander *et al.* 1988). Proper stress-strain relationships are assigned to the fibers to model the mechanical properties of the materials in undamaged and/or damaged conditions. The beam is modeled following a displacement-based approach (Zienkiewicz & Taylor 2000).
- lumped plasticity (LP) modeling: the flexural behavior of the beam is evaluated by means of moment-curvature relationships based on the properties of the uncorroded and/or corroded materials. These relationships are then linearized by using a four stepwise curve. Each beam

segment is modeled by a Giberson element (Sharpe 1974) where plasticity is concentrated at the ends while the central part remains elastic. The nonlinear behavior of the plastic hinges is defined according to the linearized moment-curvature relationship. In this model, plasticity is assumed to develop mainly in the central part of the beam between the loads Q. The length of the plastic hinges of the elements next to the central part is calibrated on the non-corroded Beam 111 and assumed equal to 15cm.

For concrete, a Saenz's law is adopted in compression with strain at maximum strength $\varepsilon_{c0} = 0.20\%$, while a bilinear law is chosen in tension. For steel, a bilinear model with hardening after yielding is used. The failure is associated with the reaching of the strain limits $\varepsilon_{cu} = 0.35\%$ and $\varepsilon_{su0} = 5.00\%$ for concrete and steel respectively. Steel ultimate strain $\varepsilon_{su}(t)$ is assumed to vary over time according to Eqn. 3.21 based on the actual steel cross-section reduction.

All the analyses are performed considering a displacement control strategy, where each step Δx is set to 0.025mm in order to have continuous curves. The comparison between experimental tests and numerical simulation results with both distributed and concentrated plasticity is provided in the following. Results are shown in terms of force-displacement curve. The displacement Δ is referred to the deflection of middle section, while the force P is the sum of the applied loads Q.

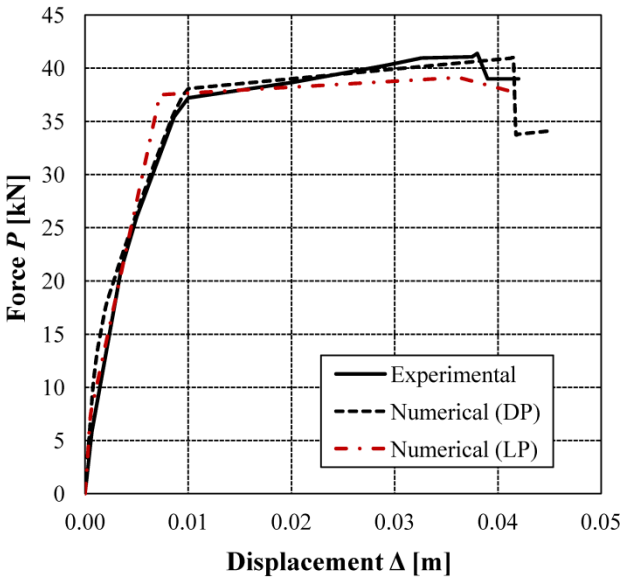

Figure 3.14 – Force-displacement curves for the undamaged Beam 111: comparison between numerical and experimental results.

Figure 3.14 shows the results of the undamaged Beam 111. Both the numerical models well predict the failure point in terms of ultimate displacement and approximates the yielding and ultimate strength of the concrete member with good accuracy. However, differences can be seen in the initial branch. The distributed plasticity model slightly over-estimates the pre-cracking stiffness, as observed also by other numerical validations (Vergani 2010), while it well approximates the yielding point. On the contrary, the lumped plasticity modeling better suits the initial stiffness and under-estimates the

yielding point in terms of displacement. Moreover, the lumped plasticity modeling slightly underestimates the maximum strength of the element.

The case of Beam 114 is now considered. The beam is subjected to severe corrosion due to a longer exposure period. The comparison between numerical and experimental results is illustrated in Figure 3.15. A uniform corrosion is considered as a first assumption by reducing the steel bar area (Figure 3.15a). With respect to the undamaged situation, a decrease in the ultimate strength is observed. A significant reduction of the deflection of the middle section is evident, which is probably due to the loss of ductility of longitudinal bars. Both the numerical models bring to similar results, overestimating the strength and ultimate displacement of the element, thus the hypothesis of uniform corrosion is not satisfying.

The analysis is then repeated by adding the effect of pitting corrosion to the uniform reduction of steel bar area, by considering the Rodriguez model (Eqn. 3.18) and the maximum observed depth of the pit (Table 3.3). Figure 3.15b shows the corresponding force-displacement diagram. The numerical models still overestimate the strength, even if the estimated values are closer to the actual ones. On the contrary, the ductility of the element is estimated with better accuracy. This is due to the further reduction of the steel ultimate strain accounted for by the model, since the presence of pits is considered in the evaluation of steel corrosion loss.

Numerical results referring to a complete damage model are shown in Figure 3.15c. The nonlinear analysis also considers the concrete damage of the concrete in terms of a reduction of strength in tension and in compression and a reduction of stiffness (Table 3.1). Good accuracy is reached with both models both in the prediction of the failure point and of the initial stiffness. However, it can be noticed that the lumped plasticity modeling still underestimates the yielding displacement and overestimates the ultimate displacement. This can be due to the estimation of the length of the plastic hinge, which reasonably may vary in a corroded element with respect to the undamaged condition.

The case of Beam 115, which is subjected to a lower level of corrosion, is now considered. By adopting a uniform corrosion model, the strength is overestimated by both the numerical models (Figure 3.16a). However, the initial stiffness is better approximated than the case of Beam 114, in particular in the case of lumped plasticity. This is reasonable since the uniform corrosion model is more appropriate in simulating moderate corrosion scenarios.

By introducing the modeling of concrete degradation, the comparison between experimental and numerical results shows a good accuracy in the case of steel uniform corrosion (Figure 3.16b). In particular, the distributed plasticity modeling well approximates the strength of the element, while the lumped plasticity modeling catches the ultimate displacement.

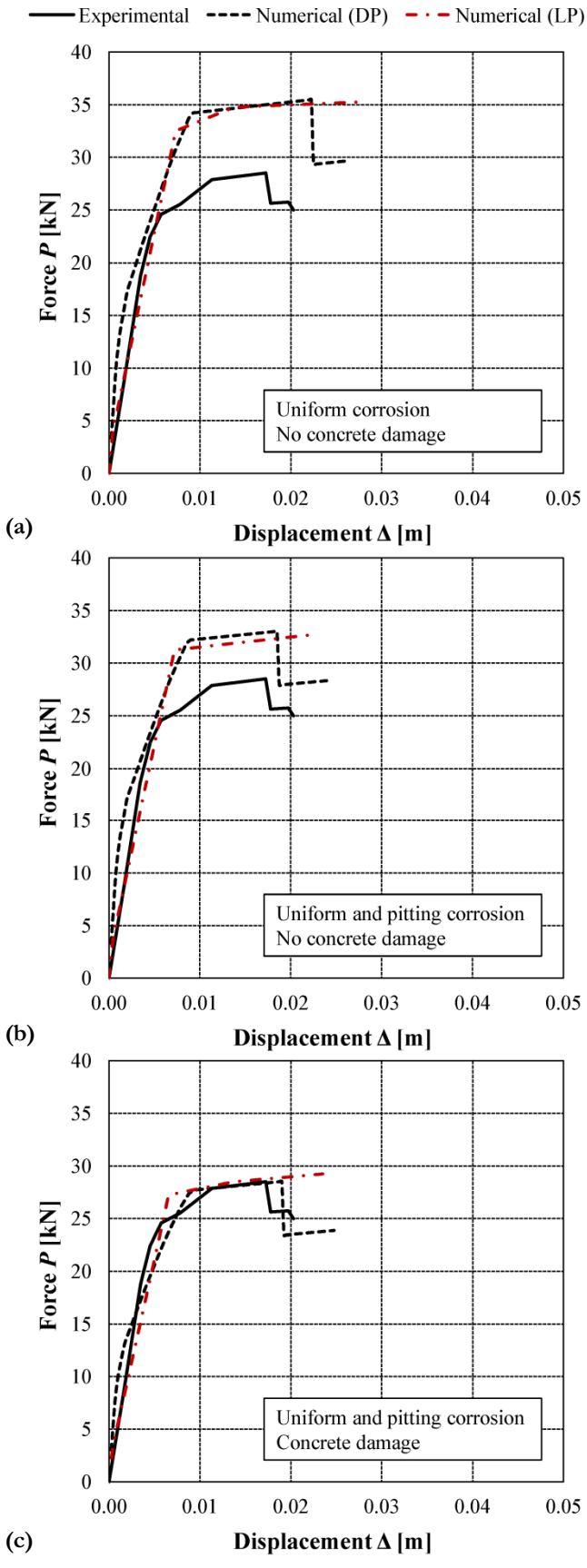

Figure 3.15 – Force-displacement curves for Beam 114 (severe corrosion).

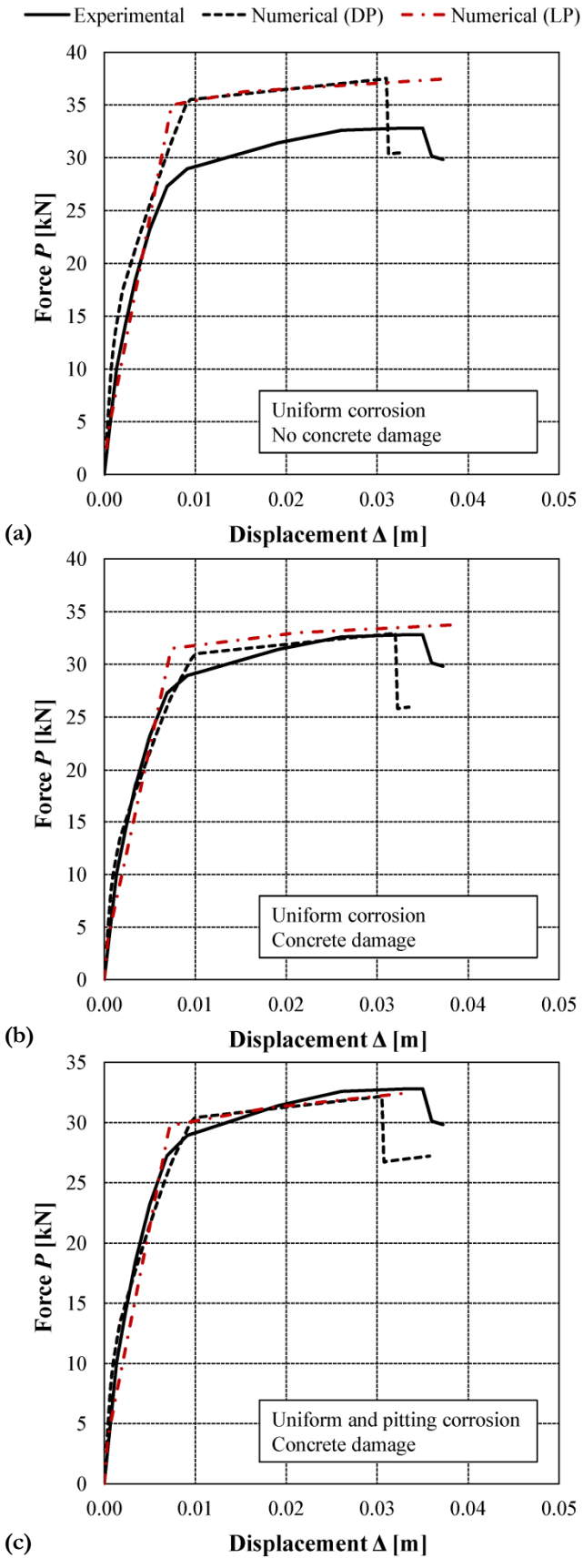

Figure 3.16 – Force-displacement curves for Beam 115 (moderate corrosion).

If the case of pitting corrosion is considered for Beam 115, the strength and stiffness of the corroded element are well approximated by both the numerical models (Figure 3.16b). However, the ultimate displacement is a bit underestimated. This is due to the reduced strength of concrete, in the models, which leads the steel bars to higher tension levels for lower deflections.

The case of Beam 116 is finally considered. The beam is subjected to the highest level of corrosion, with a pitting factor $R = 3$ for the tensile bars. Figure 3.17 shows the comparison between experimental and numerical results considering mixed corrosion and concrete damage. In order to better estimate the stiffness, concrete cover strength in tension is neglected, thus modeling the severe spalling of concrete cover due to the corrosion of tensile bars.

In case of distributed plasticity modeling, the numerical results well approximate the strength of the element, while slightly overestimating the yielding displacement and underestimating the ultimate displacement. The lumped plasticity model well estimates the stiffness, the strength the yielding and ultimate displacement. Nevertheless, it has to be noticed that this beams showed experimental displacements greater than those observed for Beams 114 and 115 with lower levels of corrosion, thus not being in compliance with the adopted model.

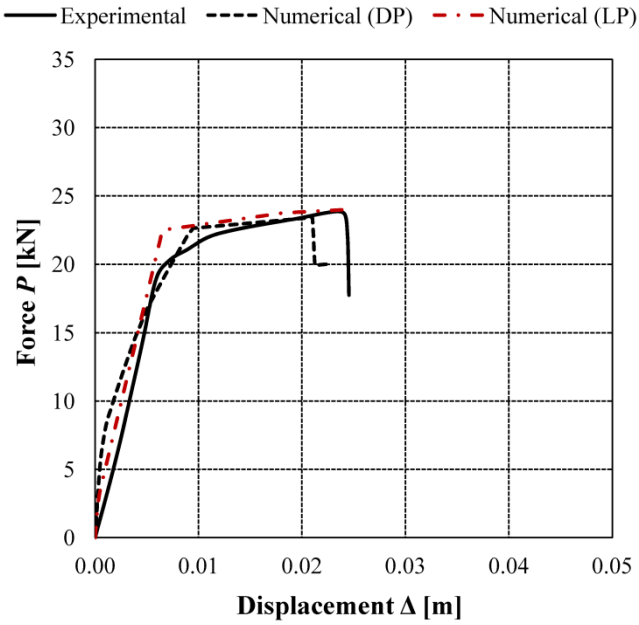

Figure 3.17 – Force-displacement curves for Beam 116 (very severe corrosion).

In the comparison of the numerical and experimental results, it should be considered that numerous uncertainties are related to the actual corrosion of the steel bars and to the mechanical properties of the materials. However, basing on these results, the adopted damage model results to catch with good accuracy the effects of corrosion on the flexural behavior of deteriorating concrete beams, in particular with respect to the loss of strength due to the reduced steel bar area and to the reduction

of steel ultimate strain mainly due to the pitting attack. Moreover, good accuracy can be achieved by the damage model by using both distributed or lumped plasticity models for the structural analysis.

5. Application: modeling of corrosion damage

The time evolution of the steel bar diameter, steel ultimate strain and concrete strength is here evaluated in probabilistic terms under a prescribed environmental scenario in the hypothesis of uniform corrosion conditions according to the above presented damage models (Biondini *et al.* 2013). According to the probability distribution of the random variables affecting the diffusion process (Chapter 2, Table 2.3) and considering the corrosion initiation time shown in Chapter 2, Figure 2.10, the reduction of the steel bar diameters Φ_{nom} = 16mm and Φ_{nom} = 26mm is evaluated over a lifetime of 50 years with Δt = 10 years. The nominal dimensions of the steel bars are considered as random variables, with a truncated normal distribution with $\mu = \Phi_{nom}$ and $\sigma = 0.10\mu$. The different nominal dimensions of the steel bars allow a comparison of the effects that the size of the diameter has on both steel and concrete mechanical properties.

On the basis of correlations between chloride content and corrosion current density in concrete (Bertolini *et al.*, 2004; Liu & Weyers, 1998; Pastore & Pedeferri, 1994; Thoft-Christensen, 1998), a linear relationship between rate of corrosion r_{corr}, in the range 0-200 μm/year, and chloride content C, in the range 0-3%, is approximately assumed for structures exposed to severe environmental conditions (Biondini *et al.*, 2004, 2006).

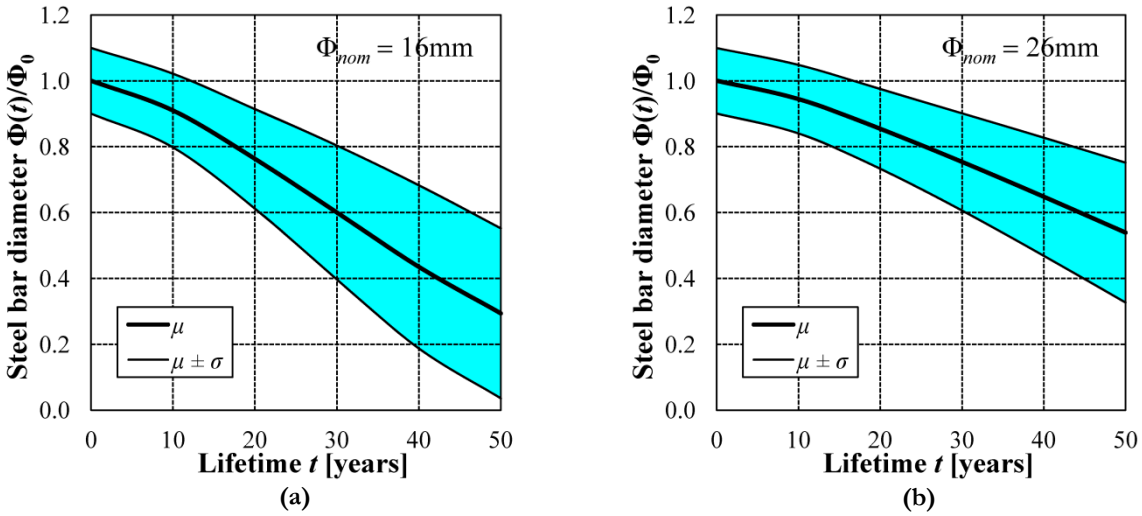

Figure 3.18 – Time evolution of steel bar diameter $\Phi(t)$ for (a) Φ_{nom} = 16mm and (b) Φ_{nom} = 26mm (mean μ and standard deviation σ from the mean).

According to this scenario, the time-variant mean values μ of steel bar diameter ratio $\Phi(t)/\Phi_0$ and the corresponding standard deviations σ are shown in Figure 3.18. The scatter around the mean increases during lifetime due to the increasing effects of the uncertainties related to the degradation phenomena, which are added to the material and geometrical inherent variability. It is noted that the effects of steel reinforcement corrosion are more significant for small bar diameters, as expected, since the percentage of bar diameter loss is greater. Consequently, in a corroding structure few large

diameter bars are apparently safer than a higher number of small diameter bars as far as steel corrosion loss (Andrade *et al.* 1990).

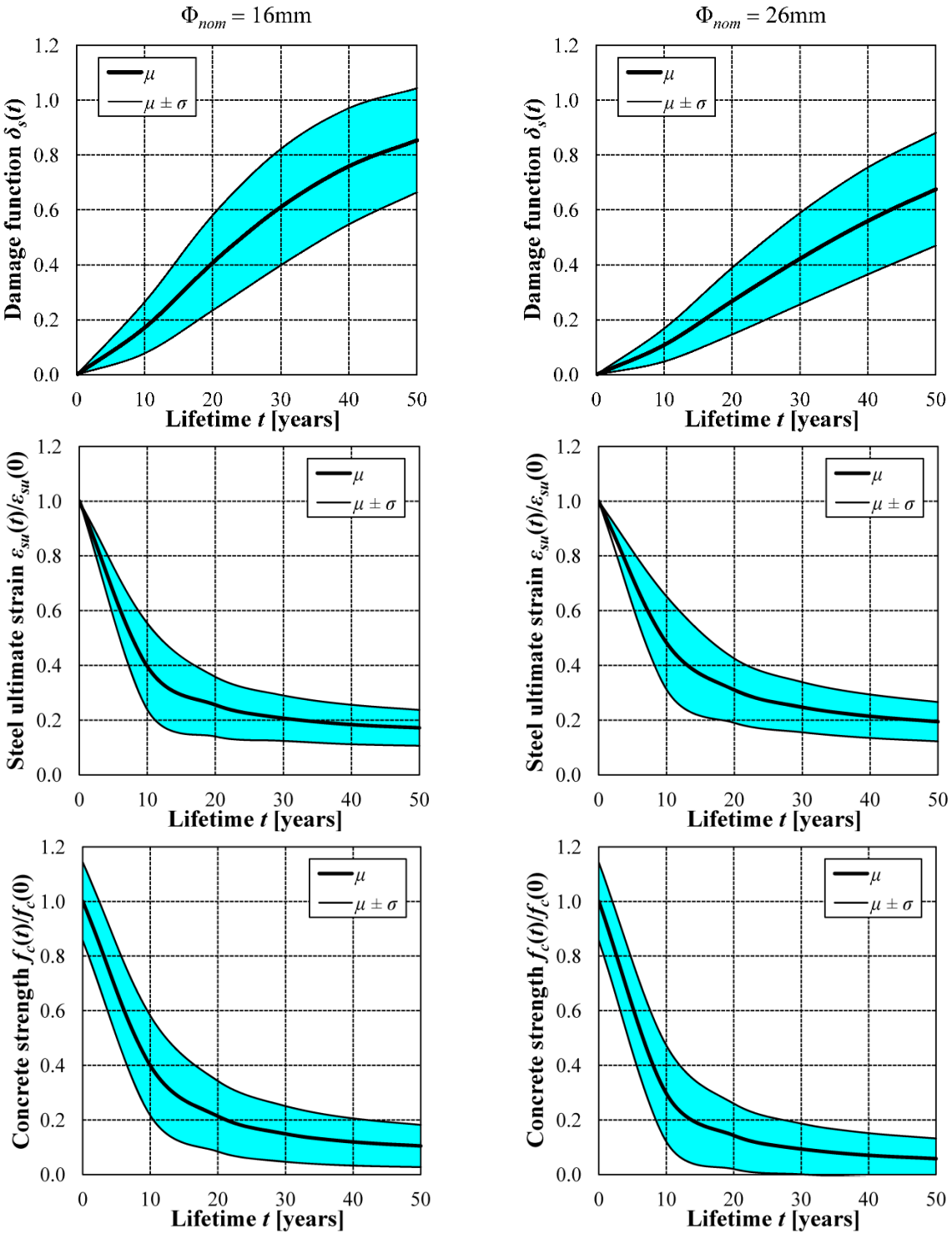

Figure 3.19 – Time evolution of the damage function $\delta_s(t)$, steel ultimate strain $\varepsilon_{su}(t)$ and concrete strength $f_c(t)$ for (a) Φ_{nom} = 16mm and (b) Φ_{nom} = 26mm (mean μ and standard deviation σ from the mean).

The evolution of the damage function $\delta_s(t)$, which has a direct dependency on the reduction of the bar diameter, allows to evaluate the ultimate deformation of steel $\varepsilon_{su}(t)$ and the strength of concrete cover $f_c(t)$ during lifetime. In fact, the time evolution of the ultimate deformation of steel $\varepsilon_{su}(t)$, which can be considered as an indicator of the material ductility, results to be dependent on the size of the diameter through the dimensionless corrosion penetration index δ (Eqn. 3.4). However, the influence of the size of steel bars on the lifetime reduction of steel ultimate strain is less significant than the one on the steel loss ratio (Figure 3.19). On the contrary, a greater reduction of concrete cover strength is observed in the case of Φ_{nom} = 26mm, as shown in Figure 3.19, since the width of cracks increases with larger diameters (Eqn. 3.26). Smaller bars seem therefore preferable than larger bars, in order to avoid significant cracks and spalling of concrete, since these phenomena can worsen the consequences of the ingress of the aggressive agents into concrete.

The validity of the MC simulation results with respect to the sample size n = 50,000 is highlighted in Figure 3.20, with reference to the evolution of the steel bar diameter for both Φ_{nom} = 16mm and Φ_{nom} = 26mm. The evolution of both mean μ and standard deviation σ towards stable values after n = 50,000 realizations proves the accuracy of the simulation process.

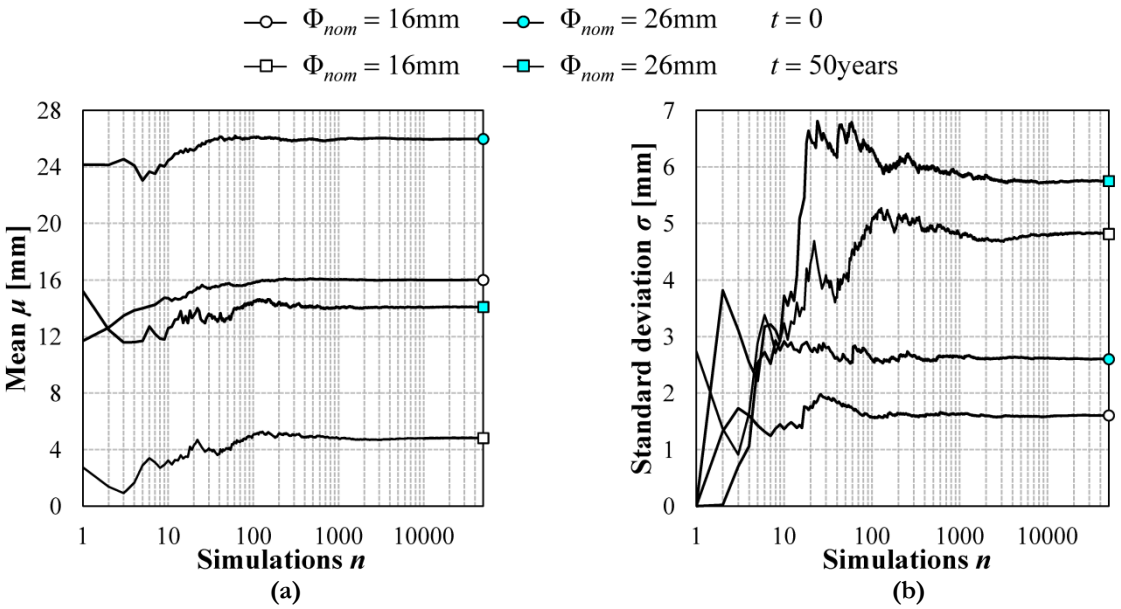

Figure 3.20 – Evolution during the simulation process of (a) mean μ and (b) standard deviation σ of steel bar diameter Φ_{nom} = 16mm and Φ_{nom} = 26mm at time t = 0 and t = 50 years.

6. Conclusions

A reliable lifetime structural analysis needs models capable to estimate the evolution of mechanical properties of deteriorating concrete members over the service life. First, the effects of corrosion processes on both reinforcing steel and concrete have been discussed. Among the damage processes affecting concrete structures in aggressive environments, the attention has been focused on chloride-induced corrosion, being one of the most severe forms of attack. The reduction of reinforcing steel cross-section area, depending on the type of corrosion (uniform, pitting or a combined process), the reduction of steel ultimate strain and strength have been considered. Concrete damage is accounted for by a reduction of concrete strength depending on the increase of transversal strain due to the corrosion crack opening.

Available models for taking into account the local damage effects on the properties of the materials have then been reviewed. The effectiveness of the proposed models has been validated by simulating experimental tests carried out on corroded concrete beams. The comparison between numerical and experimental results showed good accuracy in modeling the effects of corrosion, in particular with respect to the loss of strength due to the reduced steel bar area and to the reduction of steel ultimate strain, which is mainly due to the pitting attack. Moreover, these models lead to accurate results by using both distributed or lumped plasticity models for the structural analysis.

Finally, an application of the adopted damage model has been proposed, accounting for uniform corrosion of steel bars and deterioration of concrete under a specified corrosion scenario. Based on the modeling of the local damage, the effects on the overall performance of concrete structures will be discussed in the next Chapter.

7. References

Al-Harthy, A.S., Stewart, M.G., & Mullard, J. (2011). Concrete cover cracking caused by steel reinforcement corrosion. *Magazine of Concrete Research*, 63(9), 655–667.

Akgül, F., & Frangopol, D.M. (2004). Lifetime performance analysis of existing prestressed concrete bridge superstructures. *Journal of Structural Engineering*, 130(12), 1889–1903.

Almusallam, A. (2001). Effect of degree of corrosion on the properties of reinforcing steel bars. *Construction and Building Materials*, 15, 361–368.

Alonso, C., Andrade, J., Rodriguez, J., & Diez, J.M. (1998). Factors controlling cracking of concrete affected by reinforcement corrosion. *Materials and Structures*, 31, 435–441.

Andrade, C. (2002). Determination of chloride threshold in concrete. In *Proposal of the Monitoring, Group WG-B3-COST521, Final Report Workshop of COST-521*, Ed. R. Weydert, Luxembourg, 108–119.

Andrade, C., & Alonso, C. (2001). On-site measurements of corrosion rate of reinforcements, *Construction and Building Materials*, 15, 141–145.

Andrade, C., Alonso, M.C., & Gonzalez, J.A. (1990). An initial effort to use the corrosion rate measurement for estimating rebar durability. *Corrosion Rates of Steel in Concrete*, *ASTM STP 1065*, N.S. Berke, V. Chaker and D. Whinting Eds., American Society for Testing and Materials, Philadelphia, 29–37.

Andrade, C., Alonso, C., & Sarrìa, J., (2002). Corrosion rate evolution in concrete structures exposed to the atmosphere, *Cement & Concrete Composites*, 24, 55–64.

Apostolopoulos, C.A., & Papadakis, V.G. (2008). Consequences of steel corrosion on the ductility properties of reinforcement bar. *Construction and Building Materials*, 22, 2316–2324.

Bažant, Z.P. (1979). Physical model for steel corrosion in concrete sea structures - theory. *Journal of Structural Division*, 105(6), 1137–l 153.

Berto, L., Vitaliani, R., Saetta, A., & Simioni, P. (2009). Seismic assessment of existing RC structures affected by degradation phenomena. *Structural Safety*, 31, 284–297.

Bertolini, L., Elsener, B. Pedeferri, P., & Polder R. (2004). *Corrosion of Steel in Concrete – Prevention, Diagnosis and Repair*. Wiley-VCH, Weinheim.

Bhargava, K., Ghosh, A.K., Mori, Y., & Ramanujam, S. (2007). Corrosion-induced bond strength degradation in reinforced concrete -Analytical and empirical models. *Nuclear Engineering and Design*, 237(11), 1140–1157.

Biondini, F. (2011). Cellular automata simulation of damage processes in concrete structures. In: *Soft Computing Methods for Civil and Structural Engineering*, Y. Tsompanakis and B.H.V. Topping, (Editors), Saxe-Coburg Publications, Stirlingshire, Scotland, Chapter 10, 229–264.

Biondini, F., Bontempi, F., Frangopol, D.M., & Malerba, P.G. (2004). Cellular automata approach to durability analysis of concrete structures in aggressive environments. *Journal of Structural Engineering, ASCE*, 130(11), 1724–1737.

Biondini, F., Bontempi, F., Frangopol, D.M., & Malerba, P.G. (2006). Probabilistic service life assessment and maintenance planning of concrete structures, *Journal of Structural Engineering, ASCE*, 132(5), 810–825.

Biondini, F., Camnasio, E., & Palermo, A. (2012). Life-cycle performance of concrete bridges exposed to corrosion and seismic hazard. *Proceedings of the Structures Congress 2012 (ASCE2012)*, Chicago, IL, March 29-31.

Biondini, F., Camnasio, E., & Palermo, A. (2013). Lifetime Seismic Performance of Concrete Bridges Exposed to Corrosion. *Structure and Infrastructure Engineering*, ahead-of-print, doi:10.1080/15732479.2012.761248.

Biondini, F., & Vergani, M. (2011). Modellazione del degrado di strutture in calcestruzzo armato soggette a corrosione (in Italian). *Giornate AICAP 2011*, Padua, May 19–21.

Biondini, F., & Vergani, M. (2012). Damage modeling and nonlinear analysis of concrete bridges under corrosion. *Proceedings of the Sixth International Conference on Bridge Maintenance, Safety and Management* (*IABMAS 2012*), Stresa, Lake Maggiore, Italy, July 8-12.

Bontempi, F. (1992). Sulla costruzione dei domini di rottura di sezioni in C.A. e C.A.P. soggette a pressoflessione deviata. *Studi e Ricerche*, *Graduate School for Concrete Structures "F.lli Pesenti"*, Politecnico di Milano, Milan, Italy, 13, 261–277 (in Italian).

Broomfield, J.P. (1997). *Corrosion of steel in concrete*, Spon Press.

Browne, R.D., Geoghegan, M.P., & Baker, A.F. (1983). *Corrosion of Reinforcements in Concrete Construction.* A.P Crane Ed., Ellis Hordwood Ltd, London, 193–222.

Cabrera, J.G. (1996). Deterioration of concrete due to reinforcement steel corrosion. *Cement & Concrete Composites*, 18, 47–59.

Cairns, J., Plizzari, G.A., Du, Y., Law, D.W., & Franzoni, C. (2005). Mechanical properties of corrosion-damaged reinforcement. *ACI Materials Journal*, 102(4).

Coronelli, D., & Gambarova, P. (2004). Structural assessment of corroded reinforced concrete beams: modeling guidelines. *Journal of Structural Engineering, ASCE*, 130(8), 1214–1224.

Du, Y.G., Clark, L.A., & Chan, A.H.C. (2005). Effect of corrosion on ductility of reinforcing bars. *Magazine of Concrete Research*, 57(7), 407–419.

Fang, C., Gylltoft, K., Lundgren, K., & Plos, M. (2006). Effect of corrosion on bond in reinforced concrete under cyclic loading. *Cement and Concrete Research*, 36(3), 548–555.

Frangopol, D.M., Lin, K.-Y., & Estes, A. (1997). Reliability of reinforced concrete girders under corrosion attack. *Journal of Structural Engineering*,123(3), 286–297.

Ghosh, J., & Padgett, J.E. (2010). Aging considerations in the development of time-dependent seismic fragility curves. *Journal of Structural Engineering*, 136(12), 1497–1511.

Gjørv, O.E. (2009). *Durability Design of Concrete Structures in Severe Environments*, Taylor and Francis.

Gonzalez, J.A., Andrade, C., Alonso, C., & Feliu, S. (1995). Comparison of rates of general corrosion and maximum pitting penetration on concrete embedded steel reinforcement. *Cement and Concrete Research*, 25(2), 257–264.

Gulikers, J. (2005). Theoretical considerations on the supposed linear relationship between concrete resistivity and corrosion rate of steel reinforcement. *Materials and Corrosion*, 56(6), 393–403.

Hamada, M. (1968). *Proceedings of the Fifth International Symposium of the Chemistry of Cement*, Tokyo, Session III-3, Principal paper, 343–409.

Kobayashi, K. (2006). The seismic behavior of RC members suffering from chloride-induced corrosion. *Proceedings of the 2nd International* fib *Congress*.

Lee, H.S., Noguchi, T., & Tomosawa, F. (2002). Evaluation of the bond properties between concrete and reinforcement as a function of the degree of reinforcement corrosion. Cement and Concrete Research, 32 (8), 1313–1318.

Li, C.Q., Zheng, J.J., Lawanwisut, W., Melchers, R.E. (2007). Concrete delamination caused by steel reinforcement corrosion, *ASCE Journal of Materials in Civil Engineering*, 19(7), 591–600.

Liu, T., & Weyers, R.W. (1998). Modeling the dynamic corrosion process in chloride contaminated structures. *Cement and Concrete Research*, 28 (3), 365–379.

Maaddawy, T.E., & Soudki, K. (2007) A model for prediction of time from corrosion initiation to corrosion cracking. *Cement & Concrete Composites*, 29, 168–175.

Malerba, P.G. (Ed.) (1998). *Limit and Nonlinear Analysis of Reinforced Concrete Structures*. International Centre for Mechanical Sciences (CISM), Udine, Italy (in Italian).

Malerba, P.G., & Bontempi, F. (1989). Analisi di telai in C.A. in presenza di non linearità meccaniche e geometriche. *Studi e Ricerche*, *Graduate School for Concrete Structures "F.lli Pesenti"*, Politecnico di Milano, Milan, Italy, 11, 209–224 (in Italian).

Mander, J.B., Priestley, M.J.N & Park. R. (1988). Theoretical stress-strain model for confined concrete. *Journal of Structural Engineering*, 114(8), 1804–1826.

Mazzoni, S., McKenna, F. & Fenves, G.L. (2005). *OpenSees command language manual*. Pacific Earthquake Engineering Research (PEER) Center.

Ou, Y.-C., Tsai, L.L., & Chen, H.H. (2012). Cyclic performance of large-scale corroded reinforced concrete beams. *Earthquake Engineering & Structural Dynamics*, 41(4), 593–604.

Oyado, M., Kanakubo, T., Sato, T., & Yamamoto, Y. (2011). Bending performance of reinforced concrete member deteriorated by corrosion. *Structure and Infrastructure Engineering*, 7(1-2), 121–130.

Pantazopoulou, S.J., & Papoulia, K.D. (2001). Modeling cover-cracking due to reinforcement corrosion in RC structures. *Journal of Engineering Mechanics*, 127(4), 342–351.

Pastore, T., & Pedeferri, P., (1994). *La Corrosione e la Protezione delle Opere Metalliche Esposte all'Atmosfera* (In Italian). L'edilizia, December, 75–92.

Pedeferri, P., & Bertolini, L. (1996). *La Corrosione nel Calcestruzzo e negli Ambienti Naturali*, McGraw-Hill, 1996.

Rasheeduzzafar, Al-Saadoun, S.S., & Al-Gahtani, A.S. (1992). Corrosion cracking in relation to bar diameter, cover, and concrete quality. *Journal of Materials in Civil Engineering*, 4(4), 327–342.

Rodriguez, J., Ortega, L.M., & Casal, J. (1997). Load carrying capacity of concrete structures with corroded reinforcement. *Construction and Building Materials*, 11(4), 239–248.

Saetta, A., Scotta, R., & Vitaliani, R. (1999). Coupled environmental-mechanical damage model of rc structures. *Journal of Engineering Mechanics*, 125(8), 930–940.

Saito, Y., Oyado, M., Kanakubo, T., & Yamamoto, Y. (2007). Structural performance of corroded RC column under uniaxial compression load. *First International Workshop on Performance, Protection & Strengthening of Structures under Extreme Loading*, Whistler, Canada.

Sharpe, R.D. (1974). *The Seismic Response of Inelastic Structures*. PhD Thesis, Department of Civil Engineering, University of Canterbury, Christchurch, New Zealand.

Spacone E., Filippou F.C., & Taucer F.F. (1996). Fibre beam-column element for nonlinear analysis of R/C frames. Part I: Formulation. *Earthquake Engineering and Structural Dynamics*, 25, 711–725.

Stanish, K., Hooton, R. D., & Pantazopoulou, S. J. (1999). Corrosion effects on bond strength in reinforced concrete. *ACI Structural Journal*, 96(6).

Stewart, M.G. (2009). Mechanical behaviour of pitting corrosion of flexural and shear reinforcement and its effect on structural reliability of corroding RC beams. *Structural Safety*, 31, 19–30.

Thoft-Christensen, P. (1998). Assessment of the reliability profiles for concrete bridges. *Engineering Structures*, 20(11), 1004–1009.

Tuutti, K. (1982). *Corrosion of Steel in Concrete*, Swedish foundation for concrete research, Stockholm.

Val, D.V., Stewart, M.G., & Melchers, R.E. (1998). Effect of reinforcement corrosion on reliability of highway bridges. *Engineering Structures*, 20(11), 1010-1019.

Val, D.V., Stewart, M., & Melchers, R.E. (2000). Life-cycle performance of RC bridges: Probabilistic approach. *Computer Aided Civil Infrastructure Engineering*, 15(1), 14–25.

Vassie, P. (1984). Reinforcement corrosion and the durability of concrete bridges. *Proceedings of the Institution of Civil Engineers – Part I*, 76, 713–723.

Vergani, M. (2010). *Modellazione del Degrado di Strutture in Calcestruzzo Armato Soggette a Corrosione* (in Italian). Master Degree Thesis, Politecnico di Milano, Italy.

Vidal, T., Castel, A., & Francois, R. (2004). Analyzing crack width to predict corrosion in reinforced concrete. *Cement and Concrete Research*, 34, 165–174.

Yalsyn H., & Ergun M. (1996). The prediction of corrosion rates of reinforcing steels in concrete. *Cement and Concrete Research*, 26(10),1593–1599.

Yamamoto, T., Hattori, A., & Miyagawa, T. (2006). Uniaxial compression behavior of confined concrete deteriorated by corrosion of reinforcing steel. *Journal of the Society of Material Science*, 55 (10), 911–916 (in Japanese).

Yuya, S., Oyado, M., Kanakubo, T., & Yamamoto, Y. (2007). Structural Performance of Corroded RC Column under Uniaxial Compression Load. http://rcs.kz.tsukuba.ac.jp/protect2007s.pdf

Zhang, R., Castel, A., & François, R. (2009). Concrete cover cracking with reinforcement corrosion of RC beams during chloride-induced corrosion process, *Cement and Concrete Research*, 40(3), 415–425.

Zienkiewicz, O.C., & Taylor R.L. (2000) *The Finite Element Method, Volume 1: The Basis*. Butterworth-Heinemann.

CHAPTER 4

SEISMIC PERFORMANCE OF CONCRETE STRUCTURES EXPOSED TO CORROSION

1. Time-variant structural analysis of corroded concrete cross-sections

A time-variant structural analysis that accounts for the evolution of both material and mechanical properties of the concrete elements is needed to properly investigate the effects that the deterioration phenomena have on the lifetime performance of concrete structures. The analysis of such structures has to take into account both mechanical nonlinearity, related to the constitutive properties of concrete and steel, and geometrical nonlinearity, due to the second order effects.

Nonlinear three-dimensional elements have been formulated considering nonlinear material properties and the effects that the displacements have on equilibrium (Biondini 2000, Biondini *et al.* 2004b, Bontempi *et al.* 1995, Malerba 1998). The cross-sectional and structural analyses can be effectively carried out by the use of finite element method and numerical integration (Bontempi 1992, Bontempi & Malerba 1997, Bontempi *et al.* 1995, Malerba & Bontempi 1989). Based on this approach, the effects of corrosion damage on both concrete and steel have been implemented in the formulation of three-dimensional deteriorating beam elements by using time-variant element stiffness matrix

(Biondini *et al.* 2004a, Biondini 2011, Biondini & Vergani 2012). Such elements allow to model the structural behavior of corroded concrete members with good accuracy by distributed plasticity.

In a multiscale damage evaluation, the structural effects of environmental deterioration can be assessed at material, sectional, element and structural level progressively by defining proper damage indices (Biondini 2004). In fact, the lifetime analysis of concrete structures is based on the evaluation of the corrosion-induced material damage in terms of reducing steel bar diameter, ultimate steel strain and concrete strength, among others, by means of proper damage functions, as discussed in Chapter 3. A time-variant cross-sectional analysis is then needed to investigate the evolution of both moment-curvature relationships and resistance domains. In fact, the mechanical properties of the cross-section evolve over lifetime in terms of strength and ductility depending on the environmental aggressiveness and exposure conditions (Biondini *et al.* 2010b).

Finally, a structural modeling based on the time-variant properties of the deteriorating concrete elements allows to investigate the effects of the deterioration process on the overall structural performance. A general methodology for the lifetime assessment of concrete structures has been proposed in Biondini *et al.* (2004a, 2006) and in Biondini & Frangopol (2008a), and it has been extended to account for seismic performance in Biondini *et al.* (2011).

In the following, the finite element method for the time-variant analysis of a generic reinforced concrete cross-section is proposed. The formulation of the stiffness matrix, expressed as a sum of the contributions of both concrete and reinforcing steel bars, highlights the role of mechanical nonlinearity as well as of material deterioration. Lumped plasticity models have been selected to perform the structural analysis. Plasticity is assumed to be concentrated at beam ends, which rotations are derived by integration over the plastic hinge length of the cross-sectional curvature (Giberson 1967, 1969, Kunnath & Reinhorn 1989). This model is generally less computationally expensive, which makes it preferable in case of probabilistic analysis. The accuracy of this modeling has been validated in Chapter 3, §4. Measures and indices for the evaluation of seismic damage are then reviewed in order to identify suitable performance indicators of the structural behavior of concrete structures over lifetime. Moreover, the need of limit states based on both seismic intensity and environmental aggressiveness is highlighted.

The probabilistic approach to predict the lifetime seismic performance of concrete structures exposed to aggressive environments is then applied to the case studies of a 2D multistory frame and a 3D continuous bridge. The seismic capacity of the structures is evaluated in probabilistic terms by considering the uncertainties involved in the problem. The aim is to investigate the effects of corrosion damage on the seismic deteriorating structural systems and to point out the importance of a life-cycle oriented performance-based design which accounts for both the seismic and environmental hazards.

1.1. Problem statement

A unit reinforced concrete beam segment with generic cross-section, local reference system (x, y, z) and sign conventions shown in Figure 4.1 is considered. The cross-section is reinforced with steel bars with area A_{si} and prestressing tendons A_{pk}. The stress resultants $\mathbf{r} = \mathbf{r}(t)$, the kinematic field $\mathbf{w} = \mathbf{w}(t)$ and the global strains $\mathbf{e} = \mathbf{e}(t)$ referring to the center of gravity of the cross-section can be collected in the following vectors, respectively:

$$\mathbf{r} = \mathbf{r}(t) = [N \quad M_z \quad M_y]^T \tag{4.1}$$

where N is the axial force, M_z and M_y are the bending moments with respect to the z and y axes;

$$\mathbf{w} = \mathbf{w}(t) = [w_0 \quad \varphi_z \quad \varphi_y]^T \tag{4.2}$$

where w_0 is the displacement along the x axis, φ_z and φ_y are the rotations around the z and y axes;

$$\mathbf{e} = \mathbf{e}(t) = [\varepsilon_0 \quad \chi_z \quad \chi_y]^T \tag{4.3}$$

where ε_0 is the axial elongation, χ_z and χ_y are the bending curvatures around the z and y axes. These quantities are assumed positive according to the sign conventions of the local reference system.
The linearity of concrete strain field is assumed while the bond-slip of reinforcement and the shear deformation are neglected. Under these hypotheses, the displacements of a generic point $P(z, y)$ $\mathbf{s}(z, y, t)$ are completely defined by the displacement of the center of gravity and the coordinates of the point $P(z, y)$ as follows:

$$\mathbf{s}(z, y, t) = [1 \quad y \quad -z] \begin{bmatrix} w_0 \\ \varphi_z \\ \varphi_y \end{bmatrix} = \mathbf{l}(z, y)\mathbf{w}(t) \tag{4.4}$$

where $\mathbf{l}(z, y)$ is a transformation vector.
The global strains at point $P(z, y)$ can hence be expressed as:

$$\boldsymbol{\varepsilon}(z, y, t) = \frac{\partial \mathbf{w}(z, y, t)}{\partial x} = [1 \quad y \quad -z] \begin{bmatrix} \varepsilon_0 \\ \chi_z \\ \chi_y \end{bmatrix} = \mathbf{l}(z, y)\mathbf{e}(t) \tag{4.5}$$

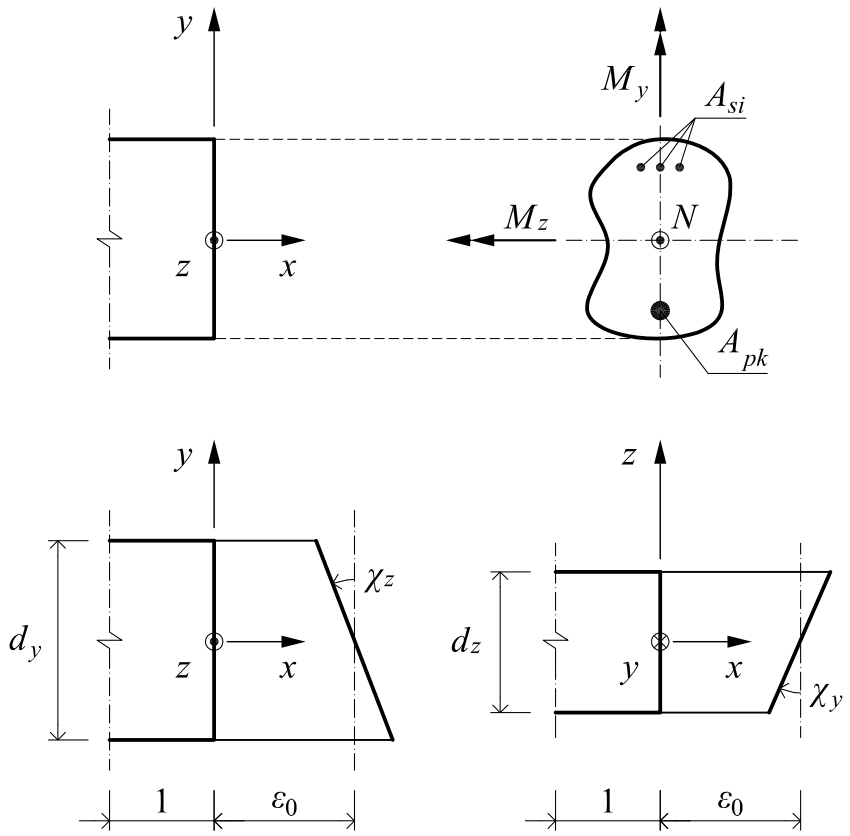

Figure 4.1 – Generic reinforced concrete beam cross-section: definition of the local reference system and sign conventions for stress resultants and global strains.

In order to describe the material behavior, mono-dimensional constitutive laws are adopted as follows:

- $\sigma_{c,x} = f(\varepsilon_c, x, t)$ for the concrete matrix;
- $\sigma_{s,x} = f(\varepsilon_s, x, t)$ for the reinforcing steel bars;
- $\sigma_{sp,x} = f(\varepsilon_{sp}, x, t)$ for prestressing tendons, if present.

The nonlinear function between stresses and strains depends on the material properties and on the adopted formulation (i.e. secant or tangent). The constitutive law can be generalized as follows:

$$\boldsymbol{\sigma}(z,y,t) = E(\boldsymbol{\varepsilon})\boldsymbol{\varepsilon}(z,y,t) = E(\boldsymbol{\varepsilon})\mathbf{l}(z,y)\mathbf{e}(t) \tag{4.6}$$

1.2. Equilibrium equations

The equilibrium equations are derived from the virtual work principle by equating the work of the static field of an equilibrated system to the work of the kinematic field of a virtual compatible system:

$$\delta L_e = \delta L_i \tag{4.7}$$

where:

$$\delta L_e = \delta \mathbf{e}^T(t)\mathbf{r}(t) = [\delta\varepsilon_0 \quad \delta\chi_z \quad \delta\chi_y]\begin{bmatrix} N \\ M_z \\ M_y \end{bmatrix} \tag{4.8}$$

$$\delta L_i = \int_A \delta\boldsymbol{\varepsilon}(z,y,t)\boldsymbol{\sigma}(z,y,t)dA = \int_A \delta\mathbf{e}^T(t)\mathbf{l}^T(z,y)\boldsymbol{\sigma}(z,y,t)dA \tag{4.9}$$

By equating internal and external work, given an arbitrary variation of virtual displacement, the following equilibrium equation is given:

$$\int_A \mathbf{l}^T\boldsymbol{\sigma}(z,y,t)dA = \mathbf{r}(t) \tag{4.10}$$

Based on Eqn. 4.1, Eqn. 4.3 and Eqn 4.6, the Eqn. 4.10 can be developed as follows:

$$\int_A E(\boldsymbol{\varepsilon})\begin{bmatrix} 1 & y & -z \\ y & y^2 & -yz \\ -z & -zy & z^2 \end{bmatrix} dA \begin{bmatrix} \varepsilon_0 \\ \chi_z \\ \chi_y \end{bmatrix} = \begin{bmatrix} N \\ M_z \\ M_y \end{bmatrix} \tag{4.11}$$

By defining the element stiffness matrix $\mathbf{H}(t)$ as:

$$\mathbf{H}(t) = \int_A \mathbf{h}(z,y)dA = \int_A E(\boldsymbol{\varepsilon})\begin{bmatrix} 1 & y & -z \\ y & y^2 & -yz \\ -z & -zy & z^2 \end{bmatrix} dA \tag{4.12}$$

the equilibrium equation can be expressed as follows:

$$\mathbf{H}(\boldsymbol{\varepsilon},t)\mathbf{e}(t) = \mathbf{r}(t) \tag{4.13}$$

The stiffness matrix $\mathbf{H}(t) = \mathbf{H}_c(t) + \mathbf{H}_s(t) + \mathbf{H}_{sp}(t)$ is derived at each time instant by integration over the area of the damaged cross-section by assembling the contributions of concrete $\mathbf{H}_c = \mathbf{H}_c(t)$, reinforcing steel $\mathbf{H}_s = \mathbf{H}_s(t)$ and prestressing tendons $\mathbf{H}_{sp} = \mathbf{H}_{sp}(t)$. In particular, by analyzing the different contributions separately and considering that $\varepsilon_{cls} = \varepsilon_s = \varepsilon$ (no bond-slip of reinforcement) and $\varepsilon_{sp} = \varepsilon + \varepsilon_i$ (ε_i initial deformation of prestressing tendons), the different contributions can be expressed as follows:

- concrete matrix:

$$\begin{aligned} &\int_{A_{cls}} \mathbf{l}^T(z,y)E_{cls}(\boldsymbol{\varepsilon})\boldsymbol{\varepsilon}(z,y,t)dA_{cls} = \\ &= \left[\int_{A_{cls}} \mathbf{l}^T(z,y)E_{cls}(\boldsymbol{\varepsilon})\mathbf{l}(z,y)dA_{cls}\right]\mathbf{e}(t) = \\ &= \mathbf{H}_c(t)\mathbf{e}(t) \end{aligned} \tag{4.14}$$

- reinforcing steel bars:

$$\begin{aligned}&\int_{A_s} \mathbf{l}^T(z,y)E_s(\boldsymbol{\varepsilon})\boldsymbol{\varepsilon}(z,y,t)dA_s = \\ &= \left[\sum_{i=1}^{nA_s} \mathbf{l}^T(z,y)E_s(\boldsymbol{\varepsilon})\mathbf{l}(z,y)A_{si}\right]\mathbf{e}(t) = \\ &= \mathbf{H}_s(t)\mathbf{e}(t)\end{aligned} \tag{4.15}$$

- prestressing tendons:

$$\begin{aligned}&\int_{A_{sp}} \mathbf{l}^T(z,y)E_{sp}(\boldsymbol{\varepsilon})\boldsymbol{\varepsilon}_{sp}(z,y,t)dA_{sp} = \\ &= \left[\sum_{i=1}^{nA_p} \mathbf{l}^T(z,y)E_{sp}(\boldsymbol{\varepsilon})\mathbf{l}(z,y)A_{spi}\right]\mathbf{e}(t) + \sum_{i=1}^{nA_p} \mathbf{l}^T(z,y)E_{sp}(\boldsymbol{\varepsilon})\varepsilon_i A_{spi} = \\ &= \mathbf{H}_{sp}(t)\mathbf{e}(t) + \mathbf{r}_{sp}(\varepsilon_i, \mathbf{e}(t))\end{aligned} \tag{4.16}$$

The resolving system at each time instant t can be finally expressed as:

$$[\mathbf{H}_c(t) + \mathbf{H}_s(t) + \mathbf{H}_{sp}(t)]\mathbf{e}(t) = \mathbf{r}(t) - \mathbf{r}_{sp}(\varepsilon_i, t) \tag{4.17}$$

Eqn. 4.17 allows to solve the following cross-sectional problems:

- given the vector of the stress resultants $\mathbf{r}(t)$ verify if it belongs or not to the resistance domain of the cross-section;
- given the vector of the global strains $\mathbf{e}(t)$ verify if a vector of the stress resultants $\mathbf{r}(t)$ exists in order to satisfy the equilibrium of the cross-section.

The solution of the first problem implies solution of a nonlinear system with unknown $\mathbf{e}(t)$. In fact, both the stiffness matrix and the constant term in Eqn. 4.17 depend on the unknown vector $\mathbf{e}(t)$, which represents the deformed shape of the cross-section. The solution is admissible if the corresponding strains $\boldsymbol{\varepsilon}(z, y, t)$ for all the points $P(z, y)$ are lower than the material strain limits. The evaluation of lifetime resistance domains can hence be performed.

On the contrary, the solution of the second problem implies just a matrix product to get the vector $\mathbf{r}(t)$ that verifies the equilibrium of the cross-section. Lifetime moment-curvature relationships can be obtained by imposing increasing global strains $\mathbf{e}(t)$ from zero up to failure and evaluating the corresponding stress resultants $\mathbf{r}(t)$ under a prescribed axial force N.

1.3. Numerical integration

Both of the above mentioned cross-sectional problems imply the evaluation of the stiffness matrix $\mathbf{H}(t)$ based on the kinematic field of the cross-section at each time instant. This can be effectively carried out by the use of finite element method (Zienkiewicz & Taylor 2000) and numerical integration (Bontempi 1992, Bontempi & Malerba 1997, Bontempi *et al.* 1995, Malerba & Bontempi

1989). The area of a generic cross-section can be subdivided in isoparametric sub-domains, for example in four-node isoparametric elements (ISOP4). Each sub-domain is replaced by a grid of points which location depends on the adopted integration rule (Bontempi *et al.* 1995). In particular, the Gauss-Legendre and the Gauss-Lobatto schemes can be selected depending on the function to be integrated and the geometry of the problem (Figure 4.2). By a biunique mapping between the actual sub-domain and the parent element, the integrating function is evaluated in the natural coordinates (ζ, η) and then numerically integrated by using Gauss polynomials. The procedure can be expressed as follows:

$$\begin{aligned} I &= \int_D f(z,y)dzdy = \\ &= \int_{-1}^{1}\int_{-1}^{1} f(\zeta,\eta)\,\det\mathbf{J}(\zeta,\eta)d\zeta d\eta = \\ &\cong \sum_{i=1}^{l}\sum_{j=1}^{m} w_i w_j f(\zeta_i,\eta_j)\det\mathbf{J}(\zeta_i,\eta_j) \end{aligned} \tag{4.18}$$

where $f = f(z, y)$ is the integrating function over the sub-domain D, $\det\mathbf{J}(\zeta, \eta)$ is the determinant of the Jacobian of the mapping, w_i, w_j are the weights depending on the selected interpolating functions and integration rule, l and m define a $l \times m$ integration grid over the cross-section lying in the z-y plane.

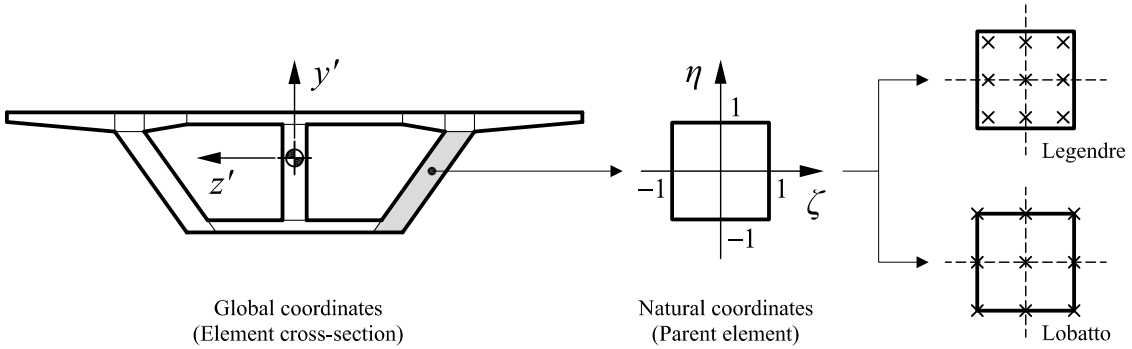

Figure 4.2 – Subdivision of the element cross-section in sub-domains and locations of the Gauss integration points according to the Legendre and Lobatto rules.

1.4. Constitutive laws

In order to define the behavior of concrete and steel, appropriate constitutive laws have to be defined. If concrete and steel are subjected to material deterioration, stress-strains relationships are time-variant. In particular, concrete strength $f_c = f_c(t)$ evolves over lifetime according to concrete deterioration (Chapter 2, §2) and concrete ultimate strain $\varepsilon_{cu} = \varepsilon_{cu}(t)$ may depend on corrosion of the transversal reinforcement. On the other side, steel ultimate strain $\varepsilon_{su} = \varepsilon_{su}(t)$ is affected by steel ductility reduction due to steel corrosion (Chapter 2, §3). The constitutive laws implemented in the developed numerical code are herein presented.

Concrete

Three different constitutive models are available for concrete behavior in compression (Figure 4.3):

- linear model:

$$\sigma_c(t) = \begin{cases} \dfrac{f_c(t)}{\varepsilon_{cu}(t)} & 0 \geq \varepsilon > \varepsilon_{cu} \\ 0 & \varepsilon \leq \varepsilon_{cu} \end{cases} \tag{4.19}$$

- parabolic model:

$$\sigma_c(t) = \begin{cases} \dfrac{f_c(t)}{\varepsilon_{c0}}\left(2 + \dfrac{\varepsilon}{\varepsilon_{c0}}\right)\varepsilon & 0 \geq \varepsilon > \varepsilon_{c0} \\ f_c(t) & \varepsilon_{c0} \geq \varepsilon > \varepsilon_{cu} \\ 0 & \varepsilon \leq \varepsilon_{cu} \end{cases} \tag{4.20}$$

- Saenz's curve:

$$\sigma^* = E_0 \varepsilon_{c0} \qquad k_c = \frac{\sigma^*}{f_c(t)} \qquad \eta_c = \frac{\varepsilon(t)}{\varepsilon_{c0}} \tag{4.21}$$

$$\sigma_c(t) = \begin{cases} \dfrac{k_c \eta_c - \eta_c^2}{1 + (k_c - 2)k_c} f_c(t) & 0 \geq \varepsilon > \varepsilon_{cu} \\ 0 & \varepsilon \leq \varepsilon_{cu} \end{cases} \tag{4.22}$$

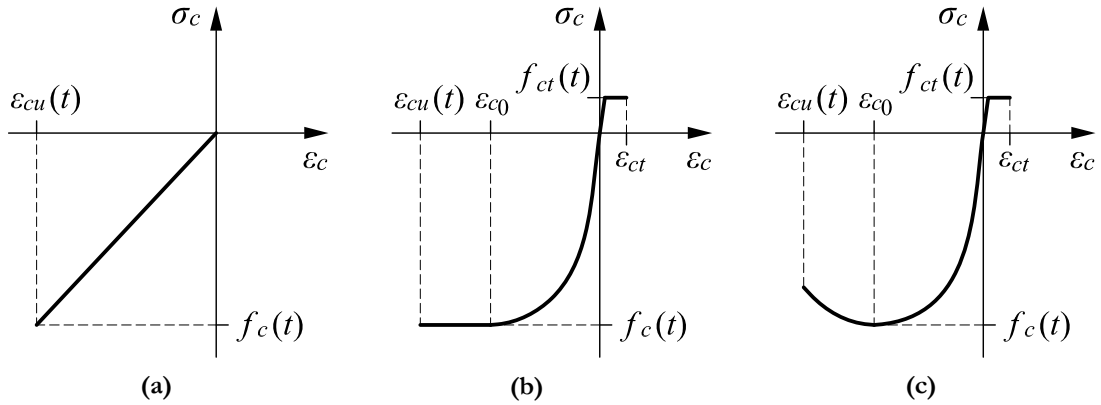

Figure 4.3 – Selected constitutive laws for concrete: (a) linear, (b) parabolic curve and (c) Saenz's curve in compression, elastic-perfectly plastic behavior in tension.

Concrete strength in tension can be neglected or assumed as elastic-perfectly plastic:

$$\sigma_c(t) = \begin{cases} E_0 \varepsilon & 0 \le \varepsilon < \dfrac{f_{ct}}{E_0} \\ f_{ct} & \varepsilon \ge \dfrac{f_{ct}}{E_0} \end{cases} \tag{4.23}$$

Steel

For steel of reinforcing bars and prestressing tendons, an elastic-plastic with hardening model is generally assumed both in tension and in compression (Figure 4.4):

$$\sigma_s(t) = \begin{cases} E_0 \varepsilon & |\varepsilon| < |\varepsilon_y| \\ f_y + \dfrac{f_{su}(t) - f_y}{\varepsilon_{su}(t) - \varepsilon_y}(\varepsilon - \varepsilon_y) & |\varepsilon_y| < |\varepsilon| < |\varepsilon_{su}(t)| \\ 0 & |\varepsilon| > |\varepsilon_{su}(t)| \end{cases} \tag{4.24}$$

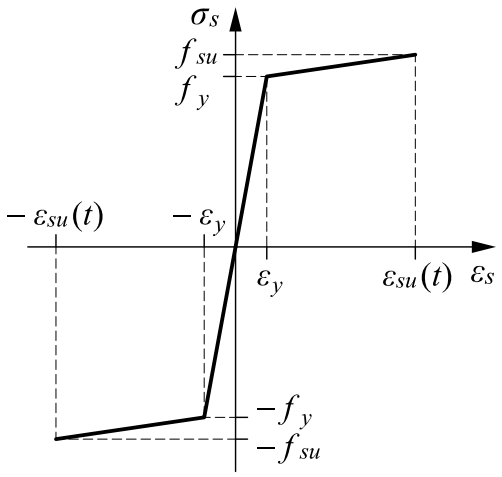

Figure 4.4 – Elastic-plastic with hardening constitutive law for steel.

2. Seismic assessment of deteriorating structures

The evaluation of the long time performance of concrete structures becomes critical when the structure is subjected to extreme events such as natural hazards and man-made disasters (Frangopol 2011, Frangopol & Liu 2007). Among others, earthquakes still represent a dominant hazard to our society. The probabilistic assessment of structures under seismic hazard developed recently (Cornell *et al.* 2002, Lupoi *et al.* 2003) as well as the investigation on the mutual effects of seismic and environmental hazards (Akiyama & Frangopol 2010, Akiyama *et al.* 2011a, Akiyama *et al.* 2012, Alipour *et al.* 2011, Berto *et al.* 2009, Biondini *et al.* 2010a, 2011, 2013, Choe *et al.* 2008, 2009, Ghosh & Padgett 2009, 2010, Kumar *et al.* 2009, Titi 2012).

The safety and serviceability assessment of deteriorating concrete frames highlighted that the increasing deterioration of concrete as well as the progressive corrosion of reinforcing bars may usually lead to significant changes in the safety coefficients, with respect to both ultimate and service limit states (Biondini & Frangopol 2008a, Biondini *et al.* 2011). The load carrying capacity as well as the ductility properties of concrete frames decrease as the level of rebar corrosion increases. Such effects become of great concern especially for structures located in earthquake-prone regions, where the ductility characteristics and the actual collapse mechanisms are main issues in the safety assessment.

The capability of a structure to withstand a specific earthquake action with an adequate level of safety, according to a certain level of ductility and resistance, may not be preserved over time. In fact, the response to seismic loading depends on the actual structural damage due to the deterioration processes over time. In particular, the dissipative capacity of the critical zones where plastic hinges are expected to develop when a strong earthquake occurs is affected by the lifetime reduction of both strength and displacement ductility. For example, corrosion of stirrups can become critical in those zones where confinement is required for a proper performance of the concrete element, such as the bottom and/or the top of columns (Oyado *et al.* 2007). As a consequence, a shift of the failure mechanism from ductile to brittle type may occur, with an abrupt change in the displacement ductility capacity.

Current seismic design philosophies rely on the dissipative capacity of these critical zones, which is actually time-variant. Moreover, the design of concrete frame systems requires a collapse mechanism involving the maximum number of stories to optimize the seismic performance, according to capacity design criteria (Biondini *et al.* 2010c, CEN-EN 1998-1 2004, Priestley & Paulay 1992). These criteria no longer hold if the hierarchy of resistance in the structural system is affected by the deterioration of the load carrying elements. While the strength reduction of concrete members suffering corrosion can be directly related to the reduction of the steel bars area, the impacts on stiffness and ductility of the overall structure are associated with more complex mechanisms, ranging from the lack of

confinement due to corrosion of transversal reinforcement (Oyado *et al.* 2007) to bond deterioration between reinforcing steel and surrounding concrete (Ou *et al.* 2012).

In general, damage scenarios are more critical for bridges than for buildings, since usually the entire structure is directly exposed to the aggressive atmosphere without any kind of protection. Bridge decks are also exposed to the application of deicing salts, which speed up the corrosion process (CEB 1992). Moreover, bridges represent strategic structures in the road network and their integrity has to be preserved especially after a seismic event. Therefore, the assessment of bridge systems over lifetime results to be a critical issue (Akiyama *et al.* 2011b), also considering the poor condition rating of existing bridges and infrastructure network (ASCE 2013, Sohanghpurwala 2006).

The influence of corrosion on the traffic load capacity of bridge systems has been widely studied (Val *et al.* 1998, Estes & Frangopol 2001, Biondini & Frangopol 2008a, 2008b), showing that the deterioration of performance resulting from reinforcement corrosion could have a significant effect on both serviceability and ultimate limit states. Fragility curves as computational methods for estimating the seismic performance of bridges with respect to different damage states have been widely used (Nielson & DesRoches 2007a, 2007b, Padgett & DesRoches 2007b, 2008).

These studies showed that the effects of corrosion are relevant for bridge structures subjected to seismic loading, since the transversal load-carrying capacity is significantly affected by corrosion of both longitudinal and transversal reinforcement. Moreover, the situation can be further complicated if different geometrical parameters, as distribution of bridge pier heights and deck stiffness are considered, since these aspects can considerably affect the overall seismic performance of bridge systems (Palermo & Pampanin 2008).

The understanding of failure mechanisms of corroded concrete elements is essential in the assessment of the seismic behavior of deteriorating structural systems. The definition proper performance indicators and damage measures is needed at both cross-sectional and global structural level to evaluate the seismic structural response over lifetime. These aspects are reviewed in the following.

2.1. Failure mechanisms of corroded concrete elements

Concrete structures can exhibit different failure modes, ranging from flexural failure (crushing of concrete or buckling of compressive steel after spalling of concrete cover in compression and fracture of steel in tension), shear failure (web-shear failure and stirrup yielding), bond failure (bar pull-out from concrete) and a combination of them (Priestley *et al.* 1996). The corrosion-induced deterioration processes affecting concrete and steel over lifetime may cause a shift in the failure mechanisms of concrete elements and may increase the vulnerability of the structural systems to seismic hazard.

Experimental studies have been recently carried out on corroded columns subjected to cyclic loading. In general, deteriorated concrete members showed reduced deformation capacity due to corrosion

of the longitudinal bars (Saito *et al.* 2007, Yamamoto & Kobayashi 2006) and degradation of bond stress versus slip relationships (Fang *et al.* 2006). Kobayashi (2006) showed that under cycling loading reinforced concrete beams suffered severe spalling of the concrete cover caused by the steel corrosion and corrosion cracks that led to debonding between the concrete cover and reinforcing bars. As the amount of corrosion of the longitudinal bars increases, the displacement ductility and flexural capacities decrease. Moreover, the failure mode may change from flexure failure, due to buckling of the longitudinal reinforcement (Akiyama *et al.* 2011a, Berry & Eberhard 2005, Dhakal & Maekawa 2002, Naito *et al.* 2011, Papia *et al.* 1988), to flexural-shear failure, which is mainly due to fracturing of the shear reinforcement (Ou *et al.* 2012).

Material deterioration affects the hysteretic behavior of concrete members as well. Moment versus curvature relationships of the plastic hinges evolve over lifetime due to the reduction of the cross-section of the steel bars, the cracking of concrete cover due to the expansion of corrosion products and bond degradation. This generally results in reduced resistance and displacement ductility dissipative capacity of concrete members, which complete models for analyzing corroded reinforced concrete members should account for (Akiyama *et al.* 2011b, Frangopol & Akiyama 2011).

2.2. Damage measures and damage indices

In order to assess the structural performance of concrete elements, it is necessary to relate the demand in terms of deformation and seismic load to proper damage measures. Damage measures in Earthquake Engineering proposed in scientific literature are numerous and various (Cosenza & Manfredi 2000, Williams & Sexsmith 1995, CEB 1998). The damage measures can be classified into different categories according to different criteria:

- the level at which damage is evaluated: local indicators can describe the damage referring to the material strain level, to a cross-section or a single element while global indicators refer to the performance of a subassemblage of the structure or to the structure as a whole;
- the type of procedure considered in the damage representation, i.e demand versus capacity or state evolution; the second one is the most adequate to reflect the evolution of the structural degradation during the seismic loading (cumulative indices);
- the level of discretization, which can be refined or simplified: damage measure are usually based on simplified assumptions, compatible with the hypothesis considered in the structural modeling.

The choice of appropriate damage parameters, defined from the structural response characteristics, and the use of empirical coefficients, which need to be validated through experimental evidence, are key points in the evaluation of the damage scenario. The most commonly used parameters for the

evaluation of structural damage are the ductility in terms of rotation, curvature or displacement and the plastic energy dissipation.

Considering ductility as a damage measure means to assume collapse at the reaching of maximum plastic rotation θ_u, curvature χ_u or displacement δ_u. The ductility is evaluated with respect to the yield values θ_y, χ_u and δ_y respectively (Banon *et al.* 1981, Park 1986, Penzien 1993):

$$\mu_\theta = \frac{\theta_u}{\theta_y} \qquad \mu_\chi = \frac{\chi_u}{\chi_y} \qquad \mu_\Delta = \frac{\Delta_u}{\Delta_y} \tag{4.25}$$

When the dissipated energy criterion is adopted, collapse is considered to occur when the amount of energy a structure can dissipate is reached during cyclic loading. Energy-based measures allow to account for both stiffness and strength degradation of damaged members (Gosain *et al.* 1977, Kratzig 1989, Park *et al.* 1987b). However, the assessment of structural energy is hard to obtain. The combination of both ductility and energy can be considered as well.

As descriptor of a physical property, these damage parameters indicate the performance of the structure under specific load conditions and allow to define the damage state of the structure, identifying the corresponding point on the force-displacement diagram of the structure. Based on these measures, damage indices can be defined as normalized damage indicators for which zero corresponds to a virgin state and one to the achievement of the assumed failure criterion. In a generalized form, the relationship between a damage index D and a damage parameter d may be expressed by the following relationship (Powell & Allahabadi 1988):

$$D = \left(\frac{d - d_t}{d_u - d_t} \right)^m \tag{4.26}$$

where d_t is a threshold value below which there is no degradation, where d_u is the ultimate value expressing the maximum allowable value of the property in question and m is a parameter affecting the shape of the function $D = D(d)$ (Figure 4.5).

This formulation can be extended to the combination of more damage parameters, weighting each contribution by proper coefficients (Biondini 2004):

$$D = \frac{\sum_{i=1}^{q} w_r \left(\frac{d - d_t}{d_u - d_t} \right)^m}{\sum_{i=1}^{q} w_r} = \sum_{i=1}^{q} \beta_r \left(\frac{d - d_t}{d_u - d_t} \right)^m \tag{4.27}$$

One of the most used combined damage index was proposed by Park & Ang (1985), which consists in a linear combination of normalized deformation and plastic energy dissipation as follows:

$$D_{PA} = \frac{\Delta_{\max}}{\Delta_u} + \beta_e \frac{\int dE}{F_y \Delta_u} \tag{4.28}$$

where Δ_{max} is the maximum displacement reached during loading, Δ_u is the displacement capacity of the structure, E is the energy dissipation, $F_y\Delta_u$ is the maximum allowable plastic energy dissipation and β_e is a free deterioration parameter that characterizes the structural elements. This index has been widely applied in Seismic Engineering and experimentally validated. Several proposals have been done for the value of coefficient β_e (Biondini 2000, 2004, Cosenza *et al.* 1993).

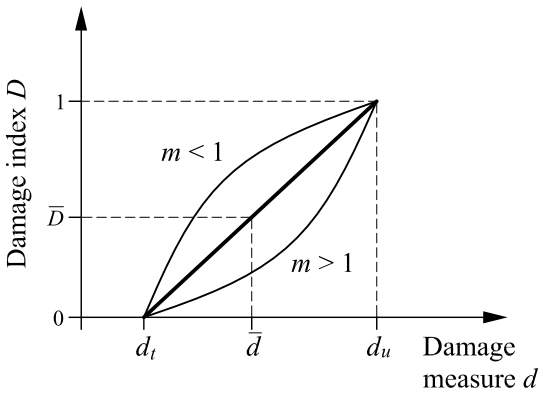

Figure 4.5 – Qualitative relationship between a damage index *D* and a damage measure *d*.

The above mentioned measures of the seismic damage should be integrated with the damage indices that account for the environmental deterioration, as described in Chapter 3, in order to consider the coupled effect of mechanical and environmental stressors in a life-cycle seismic assessment of concrete structures exposed to corrosion.

2.3. Damage levels and design limit states

Once a proper damage measure has been chosen for evaluating the performance of a structure quantitatively, engineering judgment should be used to set damage levels by which each range of the damage index is associated to a physical damage of the structure. For example, numerical investigations and the damage suffered by concrete structures during seismic events led Park *et al.* (1987a) to classify damage as reported in Table 4.1.

Different damage states can be specifically established for each structural typology (FEMA 2009). Except for brittle systems, damage is primarily a function of displacement, rather than force. In the inelastic range, increasingly larger damage would result from increased displacement although lateral force would remain constant or decrease. Hence, reliable prediction of earthquake damage requires the definition of damage states based on displacement limits. In this sense, two classical damage measures are the inter-story drift θ and the displacement ductility μ_Δ.

Table 4.1 – Damage levels classifications based on structural damage index (Park *et al.* 1987a).

Damage index *D*	Damage level	Physical damage	
$D < 0.1$	No damage	Localized minor cracking	
$0.1 \leq D < 0.25$	Minor damage	Light cracking throughout	
$0.25 \leq D < 0.4$	Moderate damage	Severe cracking, localized spalling	↑ repairable
$0.4 \leq D < 1.0$	Severe damage	Crushing of concrete, reinforcement exposed	↓ not repairable
$D \geq 1.0$	Collapse	Total or partial collapse	

The inter-story drift θ_i represents the relative horizontal displacement of the two adjacent floors i+1 and i in a building and can also be expressed as a percentage of the story height $h_{i+1,i}$ separating the two adjacent floors:

$$\theta_i = \frac{\Delta_{i+1} - \Delta_i}{h_{i+1,i}} \tag{4.29}$$

Table 4.2 – Structural performance levels and damage for concrete vertical elements (FEMA 2000).

Type	Collapse Prevention	Life Safety	Immediate Occupancy
Primary	Extensive cracking and hinge formation in ductile elements. Limited cracking and/or splice failure in some nonductile columns. Severe damage in short columns.	Extensive damage to beams. Spalling of cover and shear cracking (<1/8" width) for ductile columns. Minor spalling in nonductile columns. Joint cracks <1/8" wide.	Minor hairline cracking. Limited yielding possible at a few locations. No crushing (strains below 0.003).
Secondary	Extensive spalling in columns (limited shortening) and beams. Severe joint damage. Some reinforcing buckled.	Extensive cracking and hinge formation in ductile elements. Limited cracking and/or splice failure in some nonductile columns. Severe damage in short columns.	Minor spalling in a few places in ductile columns and beams. Flexural cracking in beams and columns. Shear cracking in joints <1/16" width.
Drift	4% transient or permanent	2% transient; 1% permanent	1% transient; negligible permanent

Table 4.3 – Limitation of interstory drift (CEN-EN 1998-1 2004).

Type of Building	Interstory Drift θ
Buildings having non-structural elements of brittle materials attached to the structure.	≤1%
Buildings having ductile non-structural elements.	≤1.5%
Buildings having non-structural elements fixed in a way so as not to interfere with structural deformations, or without non-structural elements.	≤2%

For concrete frames, the damage levels listed in Table 4.2 based on drift limits can be identified (FEMA 2000). A qualitative classification based on primary or secondary damage is also given.

European standards (CEN-EN 1998-1 2004) prescribe the checking of drift limits in the design process for damage limitations. The limits listed in Table 4.3 may be adopted.

For bridges the classification of the seismic damage mainly accounts for the performance of columns and abutments (Table 4.4). The most used damage measure for bridges is the displacement ductility demand μ_Δ placed on columns and/or bearings, according to the following formula:

$$\mu_\Delta = \frac{\Delta_{\max}}{\Delta_y} \tag{4.30}$$

where Δ_{max} is the maximum horizontal displacement of a target point (for example the top of the pier) during the earthquake excitation and Δ_y is the horizontal displacement of the same point at reinforcing steel yielding in the base cross-section of the pier. Choi *et al.* (2004) proposed ranges of the ductility damage measures in accordance to the damage level classification in FEMA (2009) for different bridge components. The damage states (DS) related to bridge piers are listed in Table 4.5.

Table 4.4 – Possible consequences of earthquakes on bridges (FEMA 2009).

		Damage State Description
DS-1	None	No damage
DS-2	Minor	Minor cracking and spalling to the abutment, cracks in shear keys at abutments, minor spalling and cracks at hinges, minor spalling at the column (damage requires no more than cosmetic repair) or minor cracking to the deck.
DS-3	Moderate	Any column experiencing moderate cracking and spalling (column structurally still sound), any connection having cracked shear keys or bent bolts, or moderate settlement of the approach.
DS-4	Extensive	Any column degrading without collapse (column structurally unsafe), any connection losing some bearing support, or major settlement of the approach.
DS-5	Complete	Any column collapsing and connection losing all bearing support, which may lead to imminent deck collapse.

Table 4.5 – Definition of damage states based on ductility base pier section (Choi *et al.* 2004).

Damage States	Minor	Moderate	Extensive	Complete
Piers	$1 \le \mu_\Delta < 2$	$2 \le \mu_\Delta < 4$	$4 \le \mu_\Delta < 7$	$\mu_\Delta \ge 7$

Limit states can be defined in terms of arbitrary lateral drift limits for bridges as well, as prescribed by several design codes (Table 4.6). Analogous definitions of damage states for bridges have been defined in the assessment of the performance of the structures by means of fragility curve analysis (Hwang *et al.* 2000, Mander & Basoz 1999, Mander *et al.* 2007, Nielson & DesRoches 2007a, 2007b, Padgett & DesRoches 2008, Shinozuka 2000a, 2000b). The linking between damage states and the residual functionality of the bridge is fundamental in assessing the performance of both the structure and the road network after a seismic event. These relationships may be developed through both

numerical analysis and assimilation of empirical data from past earthquake relying on expert opinion (Padgett & DesRoches 2007a).

Table 4.6 – Drift limits according to different Codes (after Mander *et al.* 2007, adapted).

Damage State	Drift Limits		
	NZ	Japan	Caltrans
DS-1	-	-	-
DS-2	0.62	0.53	0.53
DS-3	2.30	1.60	1.90
DS-4	4.40	4.60	5.10
DS-5	5.64	5.66	6.16

Performance levels can be effectively defined for bridges with respect to the inelastic displacement demand ratio similarly to what has been developed for buildings (SEAOC 1995). Based on this approach, Biondini *et al.* (2013) proposed to classify the performance levels with reference to the yielding displacement Δ_y of the bridge, i.e. the displacement at which a pier reaches its yielding, and the plastic displacement $\Delta_p = \Delta_u - \Delta_y$, being Δ_u the displacement at which a pier reaches its ultimate capacity (Table 4.7). If the structure remains elastic, the bridge does not suffer any damage, and it can be declared "fully operational" as soon after the seismic event. If the elastic limit is exceeded, then an increasing inelastic demand is placed to the structure as far as the maximum displacement of the structure increases until collapse. As a consequence, the bridge undergoes increasing damage with the increase in the plastic demand. Different structural performance (SP) levels can be qualitatively identified as "operational", with limitation to traffic, "lifesafe", "near collapse" and "collapse", with evidence of their meaning, in order to classify the reduced post-earthquake performance of the structure.

Table 4.7 – System displacement limits considering different damage states.

Structural Performance	Qualitative Description	System Displacement Limit	Limit State
SP-1	Fully Operational	Δ_y	↑ minimization of damage
SP-2	Operational	$\Delta_y + 0.3\Delta_p$	
SP-3	Life Safe	$\Delta_y + 0.6\Delta_p$	
SP-4	Near Collapse	$\Delta_y + 0.8\Delta_p$	↑ no collapse
SP-5	Collapse	$\Delta_y + \Delta_p$	↓ collapse

With respect to a given probability of occurrence of a seismic event over the estimated service life, current design codes allow that the structure might suffer damage within specified limit states, so that the structural integrity and life safety is always preserved. According to CEN-EN 1998-1(2004) the following limit states are given:

- no collapse (ultimate limit state): after a seismic event with low probability of occurrence over the service life, the structure shall retain its structural integrity and adequate residual resistance, although at some parts of the bridge considerable damage may occur. Flexural yielding of specific sections (i.e. the formation of plastic hinges) is allowed to occur in the piers. However, the load carrying capacity of the structural elements has to be preserved;
- minimization of damage (serviceability limit state): a seismic action with a high probability of occurrence may cause only minor damage to secondary components and to those parts of the structure intended to contribute to energy dissipation. All other parts of the structure should remain undamaged, with no need of repair interventions.

However, for deteriorating structures, the design criteria and the definition of limit states should be revised since the performance of ageing structures reduces over time (Biondini *et al.* 2013). New generation performance-based design procedures should be developed by using a performance matrix in which the structural behavior, evaluated in terms of maximum allowable drift or displacement ductility, is related not only to the seismic intensity level but also to the environmental hazard, taking into account increasing levels of aggressiveness. Based on that, a proper calibration of the design objectives should also be planned in order to ensure a structural lifetime with suitable levels of performance, from fully operational to collapse.

3. Application: 2D three-story concrete frame

Current seismic design codes of concrete frames rely on capacity design criteria where the failure mechanism of "strong columns-weaks beams" may be selected (CEN-EN 1998-1 2004). These criteria were first developed for typical reinforced concrete cast-in-place frames. Recent research investigations showed that the capacity design criteria hold for precast structures as well, under condition of a proper design of connections (Biondini & Toniolo 2009). Nevertheless, this approach is time-invariant and does not account for the interaction with environmental aggressiveness. Environmental deterioration can significantly reduce local strength and ductility, thus modifying the failure mechanism selected during the design phases. As a consequence, capacity design criteria may no longer hold in presence of lifetime deterioration of the structural elements.

The three-story concrete frame shown in Figure 4.6 is considered as a case study (Biondini *et al.* 2011). The columns have inter-story height h = 4.0m and a square cross-section with side b = 70cm. The beams have a span of l = 8.0m and a rectangular cross-section 0.5×0.8m. An axial load N = 250kN is applied to the columns at each story level, considering both dead and live loads. The structure is considered exposed to the aggressive atmosphere containing chlorides along the external perimeter. Lifetime material degradation is assumed to affect the columns only. The related structural effects are investigated over a 50-year lifetime.

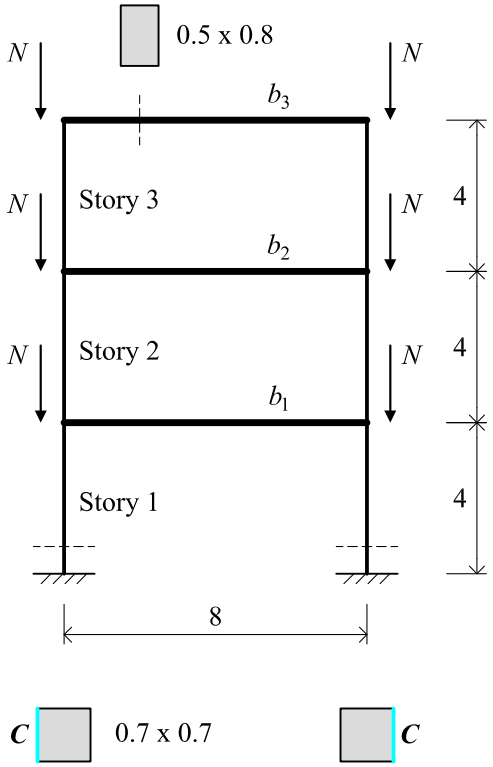

Figure 4.6 – Three-story concrete frame. Geometrical data [m] and environmental exposure scenario.

The time-variant structural performance of the critical cross-sections at the base of the columns, where plastic hinges are expected to develop during a seismic event, is investigated in probabilistic terms. The inherent randomness of the diffusion process, as well as the material and geometrical uncertainties, which affect the structural response, are taken into account by means of Monte Carlo simulation over a sample size n = 50,000 in order to assure the convergence of the process. First, the time-variant cross-sectional analysis of the columns aims to investigate the time evolution of both resisting moment and curvature ductility. The resisting moment of the columns is then compared to that of the beams in order to evaluate the time-evolution of the over-strength factor. Finally, nonlinear static analysis are carried out over a 50-year lifetime in order to assess the global structural performance in terms of total base-shear and displacement ductility.

3.1. Lifetime performance of the column cross-section

The concrete cross-section is reinforced with 8 steel bars having nominal diameters Φ_{nom} = 22mm, with a concrete cover c = 40mm. The concrete core is confined by stirrups Φ8/75 (Figure 4.7a). The lifetime flexural behavior of the columns of the frame is investigated by assuming the structural model shown in Figure 4.7b. The concrete cross-section is subdivided in 4-node isoparametric domains and a numerical integration is performed in each domain by using a 5×5 Gauss-Lobatto integration scheme.

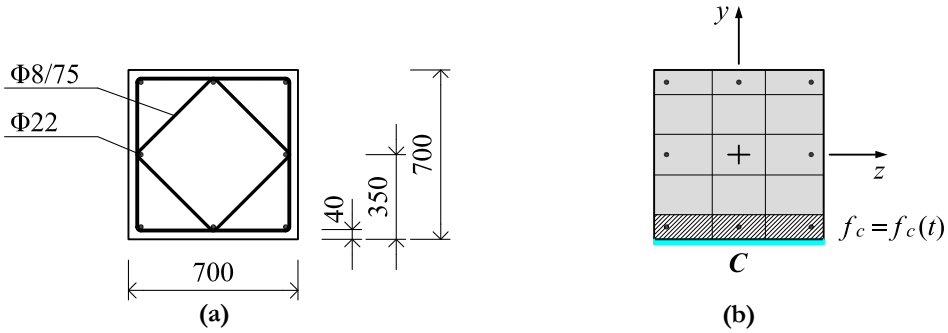

Figure 4.7 – Column cross-section. (a) Geometry and reinforcement layout [mm]; (b) Structural model and location of the aggressive agent.

For concrete, a Saenz's law in compression and an elastic perfectly plastic model in tension are assumed, by considering nominal compressive strength f_c = 35MPa, tension strength $f_{ct} = 0.25 f_c^{2/3}$, initial modulus $E_{c0} = 9500 f_c^{1/3}$ (CEN-EN 1992-1-1 2004). Strain values at peak ε_{c0} = 0.22% and at failure point ε_{cu} = 0.35% in compression and $\varepsilon_{ctu} = 2 f_{ct}/E_{c0}$ in tension are considered. The effects of confinement are also taken into account by assuming the confined strain in compression ε_{cu}* as a function of the stirrup mechanical ratio ω_w as follows (CEB 1985):

$$\varepsilon_{cu}^{*} \cong \varepsilon_{cu} + 0.05\omega_{w} \tag{4.31}$$

For steel, the stress-strain diagram is described by an elastic perfectly plastic model in both tension and compression, with nominal yielding strength f_{sy} = 430MPa and elastic modulus E_s = 206GPa. The ultimate strain limit ε_{su0} = 6.00% is also assumed. The failure of the cross-section is associated with the reaching of the ultimate strains of both concrete and steel.

The modeling of the chloride diffusion is carried out in fully probabilistic terms by assuming the parameters listed in Chapter 2, Table 2.3. The nominal dimensions of the steel bars are considered as random variables as well, with a truncated normal distribution with $\mu = \Phi_{nom}$ and $\sigma = 0.10\mu$. The cross-section is considered exposed along one side to the atmosphere with surface chloride concentration $C_{s,\Delta x} = C$. Based on the proposed damage model (Chapter 3, §2.3), a linear approximation of the dependency between rate of corrosion r_{corr}, and chloride content C is assumed (Biondini *et al.*, 2004, 2006). The chloride content varies from 0 to 3%, while the ranges 0-200 μm/year and 0-75 μm/year are assumed for evaluating steel corrosion loss of longitudinal bars and stirrups respectively. Corrosion of stirrups is assumed to define concrete damage function, in order to account for the time evolution of concrete ultimate strain (Eqn. 4.31). Such values reproduce a deterioration process with significant damage of the materials exposed to severe environmental conditions.

The material deterioration is evaluated in terms of reduction of the steel bar diameter $\Phi(t)$ and of the concrete strength $f_c(t)$. The reduction of the concrete strength is applied to the subdomains of the cross-section in contact with the aggressive agents, as indicated in Figure 4.7b by the hatched area. The ultimate strain of concrete ε_{cu}^{*} is assumed to be a time-variant parameter because of the variation of the stirrup mechanical ratio ω_w. In fact, the edge of the stirrups closer to the exposed surface is subjected to corrosion as well as the longitudinal steel bars.

The results of the probabilistic analysis are shown in Figure 4.8 in terms of lifetime evolution of steel and concrete damage functions $\delta_s(t)$ and $\delta_c(t)$, according to the adopted damage rates. Based on the damage functions, the time evolution of the steel bar diameter $\Phi(t)$ (Figure 4.9), the concrete strength $f_c(t)$ and ultimate concrete strain $\varepsilon^{*}_{cu}(t)$ (Figure 4.10) are evaluated. Mean values μ and standard deviations σ are indicated.

It can be noticed that a reduction of about 40% of the steel bar diameter is obtained after 50 years in terms of mean values. The steel bars subjected to such reduction are those closer to the surface exposed to the aggressive agent, while the reduction for the other steel bars is negligible. As far as the standard deviation, an increasing scatter around the mean is observed over time due to the combined effect of inherent mechanical uncertainties and randomness related to the corrosion process.

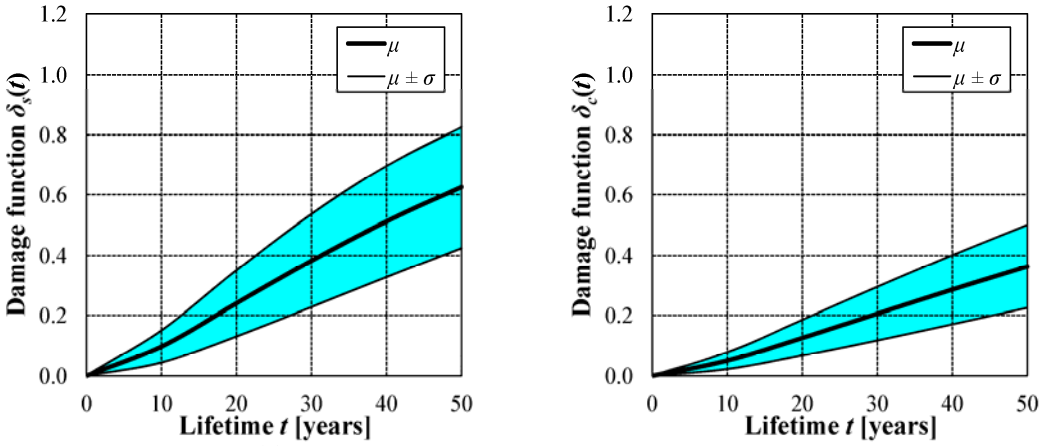

Figure 4.8 – Time evolution of the considered damage functions: (a) steel damage function $\delta_s(t)$; (b) concrete damage function $\delta_c(t)$ (mean μ and standard deviation σ from the mean).

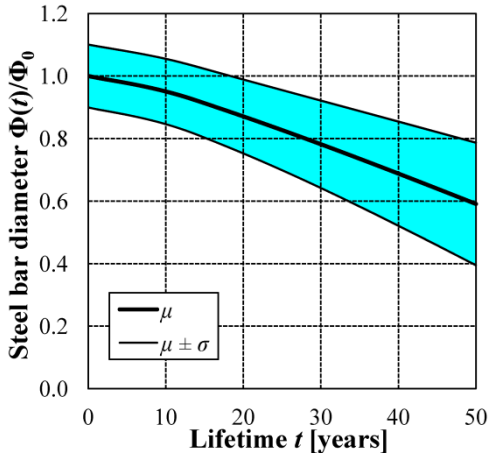

Figure 4.9 – Time evolution of the steel bar diameter $\Phi(t)$ (mean μ and standard deviation σ from the mean).

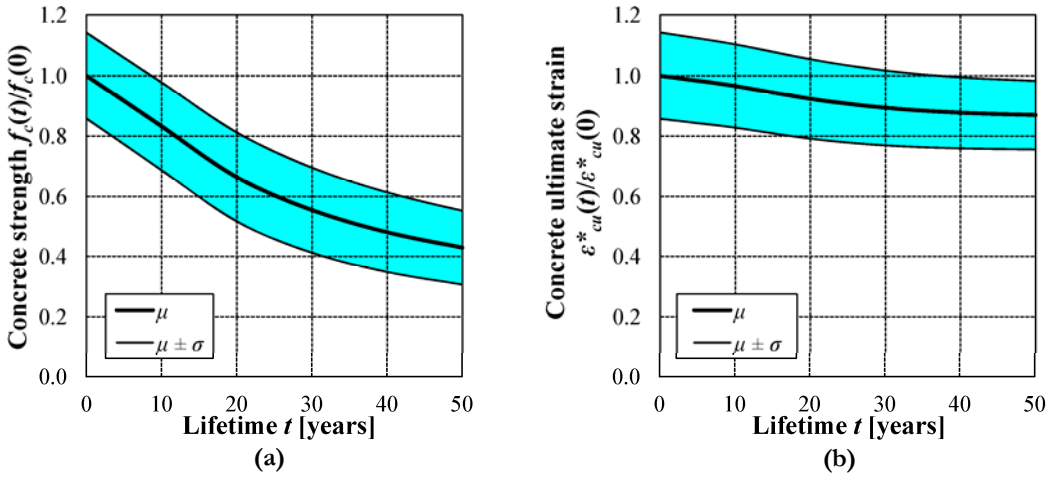

Figure 4.10 – Time evolution of (a) concrete strength $f_c(t)$ and (b) ultimate concrete strain $\varepsilon^*_{cu}(t)$ (mean μ and standard deviation σ from the mean).

Concrete suffers a less severe deterioration due to the lower damage rate considered. Both concrete strength $f_c(t)$ and ultimate strain $\varepsilon^*_{cu}(t)$ reduce over lifetime, thus indicating a loss of compressive strength and ductility resources of the deteriorated cross-section.

Based on the results of the simulation of the corrosion process, the lifetime behavior of the column cross-section is evaluated in terms of bending moment M_z versus curvature χ_z. The cross-sectional analysis is carried out in fully probabilistic terms by considering as random variables the geometrical coordinates of the cross-sections and the strength values of the materials (Table 4.8)

Table 4.8 – Material and geometrical random variables. Probability distributions and their parameters.

Random Variable	Distribution Type	μ	σ
Concrete strength, f_c [MPa]	Lognormal	$f_{c,nom}$	5
Steel strength, f_{sy} [MPa]	Lognormal	$f_{sy,nom}$	30
Coordinates of the nodal points, (y_i,z_i) [mm]	Normal	$(y_i,z_i)_{nom}$	5
Coordinates of the steel bars, (y_m,z_m) [mm]	Normal	$(y_m,z_m)_{nom}$	5

Figure 4.11 shows the obtained bending moment-curvature relationships evaluated according to sample mean values referring to the first 50 years of lifetime with time step Δt = 10 years. The diagrams refer to the columns of the second story of the frame subjected to an axial force N = 500kN.

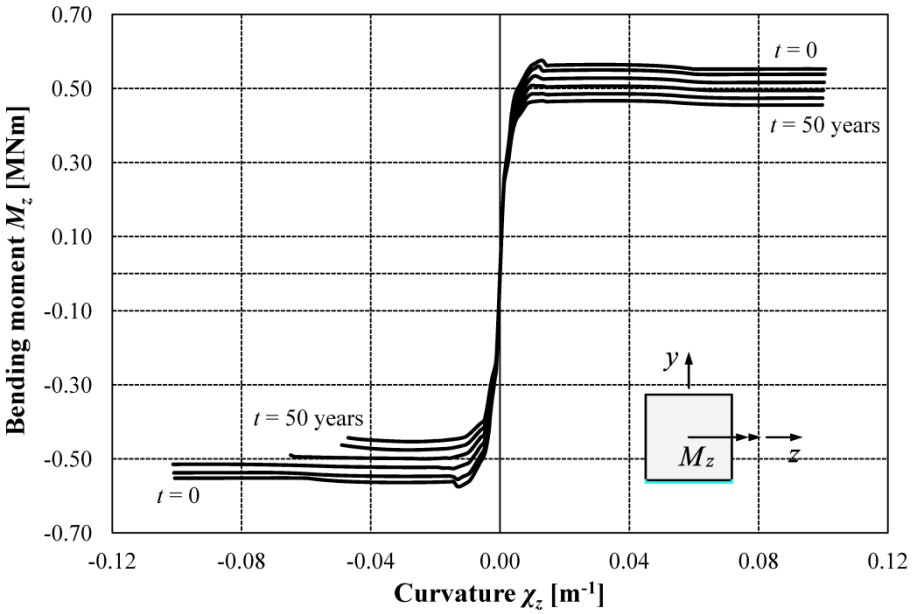

Figure 4.11 – Column cross-section undergoing corrosion damage: bending moment-curvature diagrams during the first 50 years of lifetime (N= 500kN) according to sample mean values.

Since the cross-section exposure to the aggressive agent is not symmetric with respect to the z-axis, the bending moment-curvature relationships show a different behavior over lifetime for $M_z > 0$ and $M_z < 0$. A similar reduction of strength is observed for both positive and negative bending moments,

due to the corrosion of the steel bars in tension and to the deterioration of concrete in compression. For the ultimate curvature at collapse, a significant non-symmetric behavior is observed. In fact, for $M_z < 0$ the ultimate curvature is drastically reduced over lifetime since the failure is governed by the concrete crashing of the compressive zone in the most exposed part.

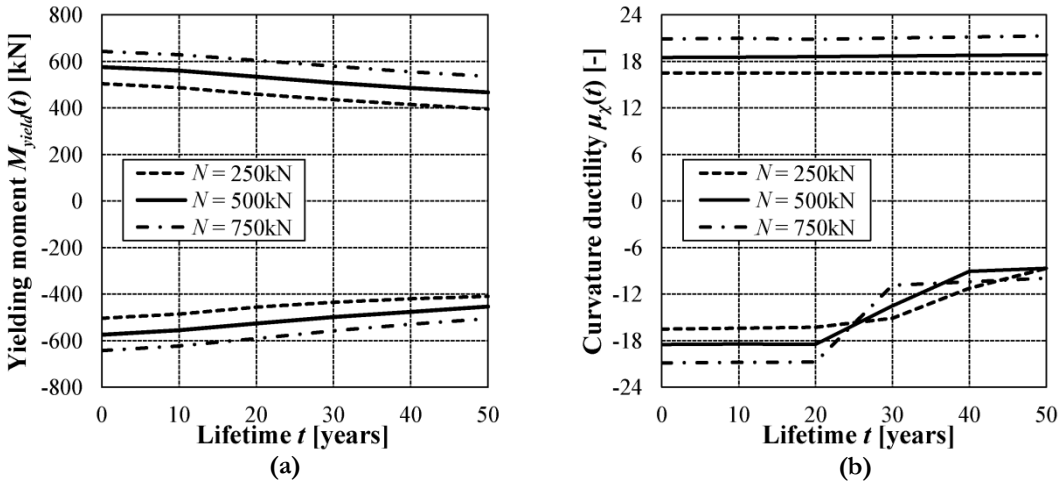

Figure 4.12 – Time evolution of (a) yielding moment $M_{yield}(t)$ and (b) curvature ductility $\mu_\chi(t)$ during the first 50 years of lifetime for different values of axial force N (mean values μ).

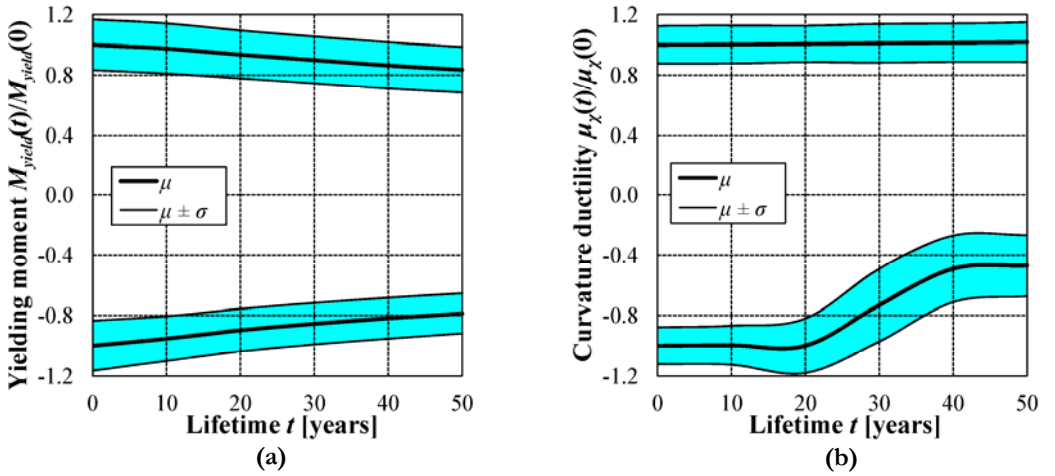

Figure 4.13 – Time evolution of the structural performance of the column cross-section in terms of (a) yielding moment $M_{yield}(t)$ and (b) curvature ductility $\mu_\chi(t)$ during the first 50 years of lifetime (N = 500kN, mean μ and standard deviation σ from the mean).

These aspects are highlighted in Figure 4.12 which shows the time evolution of the yielding moment $M_{yield}(t)$, which in this case corresponds to the maximum bending strength of the cross-section, and curvature ductility $\mu_\chi(t)$ given by the ratio of curvatures at collapse and yielding, for the three values of the axial force N = 250, 500, 750kN at each story. In particular, the lifetime reduction of the yielding moment $M_{yield}(t)$ is gradual, while the curvature ductility $\mu_\chi(t)$ shows an abrupt reduction after 20 years. These means that the bending behavior of the cross-section shifts from ductile to brittle, which is mainly due to the reduction of concrete strength and ultimate strain.

The probability distribution of strength and ductility of the columns of the second story are shown in Figure 4.13. The results are scaled with respect to the mean values of the indicators at time $t = 0$. It can be noticed that the scatter around the mean is almost constant over lifetime for both yielding moment and positive curvature ductility while it increases for the negative curvature ductility. This indicates that in this case the randomness related to the degradation processes of concrete mainly affects the distribution of the probabilistic results.

The results of the probabilistic cross-sectional analysis can be compared with the deterministic ones found in Biondini *et al.* (2011) where the time-variant performance of the column is investigated by means of the more general 2D diffusion modeling based on cellular automata (Biondini *et al.* 2004a, 2006). The comparison shows good accuracy between the two models in terms of both bending strength and curvature ductility, thus validating the adopted 1D diffusion modeling in case of exposure along one side of the cross-section.

3.2. Lifetime over-strength factor

The design of the frame herein investigated relies on cast-in-place moment resisting beam-to-column connections, which emulate the structural behavior of monolithic frames. The capacity design criteria of "strong columns-weak beams" is selected by assuming for beams a suitable over-strength ratio γ_c in terms of resistant bending moment M_{Rd}:

$$\gamma_c = \frac{\left| M_{Rd}^{columns} \right|}{\left| M_{Rd}^{beams} \right|} \tag{4.32}$$

For columns, the resistant bending moment $M_{Rd} = M_{yield}(t)$ is assumed at each time instant, thus implying the time dependence of the over-strength factor $\gamma_c = \gamma_c(t)$. The cases of a low ductility class frame and a high ductility class frame are considered by assuming $\gamma_c(0) = 1.1$ and $\gamma_c(0) = 1.3$, respectively, as suggested by CEN-EN 1998-1 (2004).

Table 4.9 – Mean resistant bending moments of the beams for the low and high ductility frames.

	M_{b1} [kNm]	M_{b2} [kNm]	M_{b3} [kNm]
Low ductility	1127.9	985.6	457.1
High ductility	954.4	834.0	386.8

Based on the mean value of the resistant bending moments of the undamaged cross-sections of the columns (Figure 4.13a), the resistant bending moments of the beams at each story M_{b1}, M_{b2} and M_{b3} are evaluated and assumed as random variables with mean μ listed in Table 4.9 and standard deviation $\sigma = 0.15\mu$. The value of the standard deviation σ is selected according to the standard deviation of the

resistant bending moment of the undamaged cross-sections of the columns at time $t = 0$ obtained from the simulation process (Figure 4.13a).

The corresponding time evolution of the over-strength factor $\gamma_c(t)$ associated to each story is shown in Figure 4.14 in terms of mean values for both the low ductility and high ductility frames. It can be noticed that the lifetime trend of the over-strength factor γ_c reflects the time evolution of the resistant bending moments of the columns. Moreover, the higher is the axial load in the column cross-sections, the greater is the reduction of the overstrength factor $\gamma_c(t)$. This means that the flexural behavior of columns with high axial load is less affected by the degradation of the materials over lifetime.

Moreover, for the case of low ductility frame a change of collapse mechanism may occur for $\gamma_c(t) < 1$, since the capacity design criterion of "strong columns-weak beams" no longer holds. This means that after about 20 years of lifetime the collapse mechanism may shift from the proper "beam-sway" to an undesired "column-sway" (Figure 4.14a). This reflects the structural behavior at cross-sectional level in terms of ductility shown in Figure 4.12. This does not occur for the case of high ductility frame in terms of mean values. However, the uncertainties involved in the evaluation of the strength of both columns and beams may lead the high ductility class frame under the limit state condition $\gamma_c(t) = 1$ as well (Figure 4.14b), since a standard deviation $\sigma \approx \pm 0.2\mu$ almost constant over lifetime is observed for the both the ductility classes.

This shows the importance of selecting the most appropriate ductility class in the design phases, according to both the desired seismic performance and the environmental exposure in order to assure a satisfying safety level over the structural lifetime.

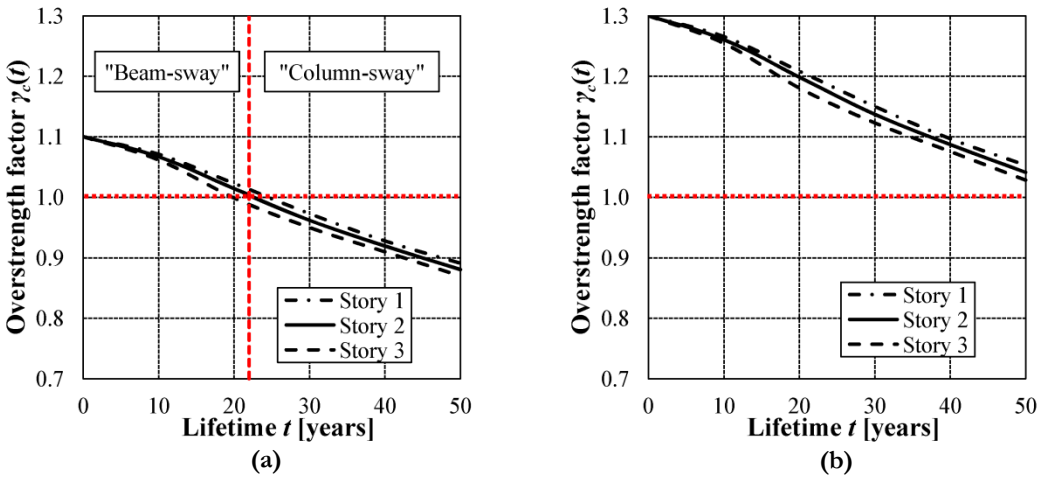

Figure 4.14 – Time evolution of the over-strength factor $\gamma_c(t)$ for (a) low ductility and (b) high ductility frames at different story levels.

3.3. Structural modeling

The frame is modeled by assuming lumped plasticity at the ends of both columns and beams, as schematically shown in Figure 4.15. The model is developed by using the numerical code Ruaumoko2D (Carr 2008). Elastic beam-type elements with lumped inelastic rotational springs are used for both columns and beams to simulate the nonlinear behavior of the connections due to the formation of plastic hinges. The cyclic behavior of the plastic hinge is defined by the relationship between moment and rotation achieved by means of integration of the bending-moment-curvature rule. The integration is developed by assuming a parabolic distribution of the curvature along a fixed length region. The parabola is defined by the curvature values at the ends of the plastic hinge segment and by a zero value of the first derivative at the extremity with a lower value of curvature. The length of the plastic hinge L_p is evaluated as follows (Priestley & Paulay 1992):

$$L_p(t) = 0.08L_e + 0.022f_y\Phi(t) \tag{4.33}$$

where L_e is the length of the element, f_y and $\Phi(t)$ are the strength and the diameter of the steel longitudinal bars, respectively. By adopting this formulation, the length of the plastic hinge results to be a time-variant parameter depending on the steel bars diameter $\Phi(t)$. This means that in corroded elements the contribution to the plastic hinge length of the second term in Eqn. 4.33 reduces over time. However, it is observed that the main contribution is given by the first term, which depends on the length of the element.

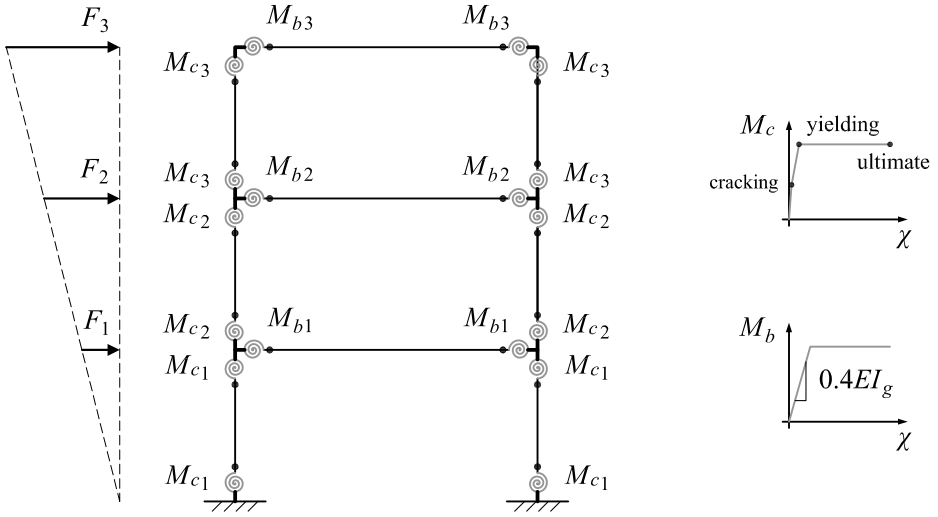

Figure 4.15 – Structural modeling of the concrete frame.

Before implementation, the bending moment-curvature relationships of the columns are linearized at each time instant by a trilinear curve (Figure 4.16), by evaluating the cracking moment M_{cr}, the yielding moment M_{yield} and the ultimate curvature χ_{ult}. The cracking moment M_{cr} corresponds to the

stress level that leads the concrete to crack. The ultimate curvature χ_{ult} correspond to the reaching of failure in terms of ultimate strain of the materials. The yielding curvature χ_{yield} is evaluated as the abscissa of the intersection between the tangent to the post-cracking branch of the curve and the value M_{yield}. In the numerical model, the cyclic behavior of the plastic hinge is defined based on the Fukada hysteresis rule (Fukada 1969). The post-elastic behavior of beam ends is modeled by an elastic perfectly plastic moment-curvature relationship, where the cracked second moment of area $I = 0.4I_g$ (I_g gross inertia moment) is considered to evaluate the initial stiffness.

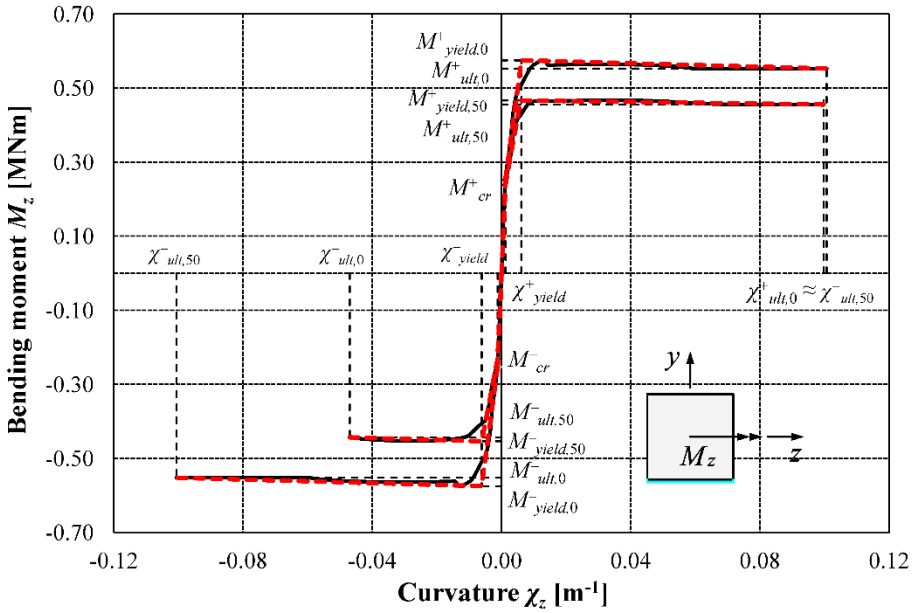

Figure 4.16 – Stepwise linearization of the bending moment-curvature M_z-χ_z diagrams at time $t = 0$ and $t = 50$ years.

3.4. Lifetime seismic capacity

To investigate the time evolution of the collapse mechanism of the concrete frame, nonlinear static analyses are carried out. For sake of brevity only the case of the low ductility frame is considered. Time-variant push-over analyses with a linear distribution of applied forces, as shown in Figure 4.15 are carried out by monotonically increasing the intensity of the horizontal forces up to failure. The second order geometrical effects are neglected.

The results are shown in Figure 4.17 in terms of total base shear $F_{base}(t)$ versus top displacement $\Delta_t(t)$. These push-over curves refer to the analyses carried out by using the mean properties of the structure at each time instant t. A gradual reduction of the total base shear is observed over a 50-year lifetime, thus reflecting the time evolution of the bending resistance at cross-sectional level. On the contrary, an abrupt reduction of the ultimate displacement and hence of the displacement ductility $\mu_\Delta(t)$ is observed after about 20 years of lifetime. In fact, as expected from the time evolution of the over-strength factor, a change of collapse mechanism occurs shifting from a controlled "beam-sway" to

an undesired "column-sway". In particular, at time instant $t = 20$ years the situation is intermediate, since $\gamma_c(t) \approx 1$. This means that depending on the variability related to the strength of both beams and columns the structure may show one of the two failure mechanisms.

This shows that the same structure may exhibit a different seismic performance depending on the environmental exposure. In fact, the deterioration of the columns due to corrosion leads to a redistribution of strength within the structure. As a consequence, at the occurrence of a seismic event after 20 years of lifetime, the overall dissipation capacity results to be lumped at the bottom of the columns, with all the beams in the elastic range and with a limited displacement ductility of the structure.

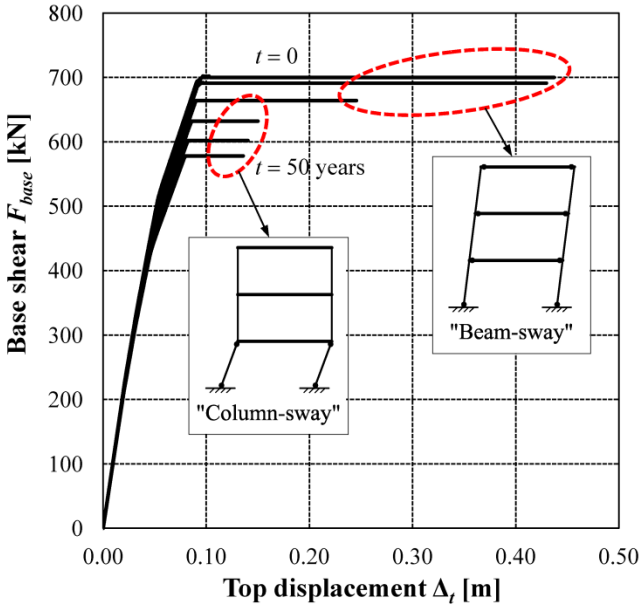

Figure 4.17 – Time evolution of the total base shear $F_{base}(t)$ versus top displacement $\Delta_t(t)$ for the low ductility frame during the first 50 years of lifetime ($\Delta t = 10$ years).

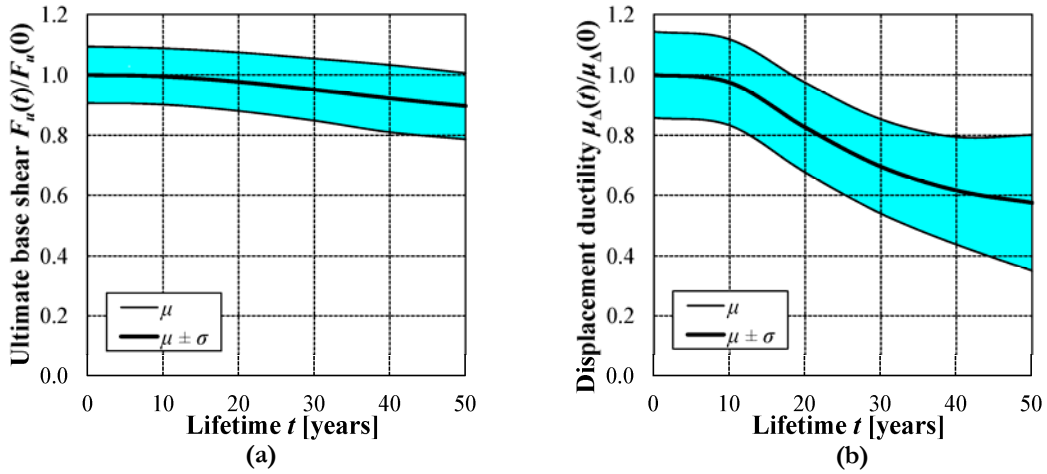

Figure 4.18 – Time evolution of the structural performance of the low ductility frame in terms of (a) total base shear $F_{base}(t)$ and (b) displacement ductility $\mu_\Delta(t)$ during the first 50 years of lifetime (N= 500kN, mean μ and standard deviation σ from the mean).

The probabilistic results of the analyses are shown in Figure 4.18 in terms of normalized total base shear at ultimate point $F_u(t)$ and displacement ductility $\mu_\Delta(t) = \Delta_u(t)/\Delta_y(t)$. The mean values at time $t = 0$ are $F_u(0) = 643$kN and $\mu_\Delta(0) = 5.4$. It can be noticed that the scatter around the mean of the total base shear reflects the trend of the standard deviations of the bending resistance of the column cross-section (Figure 4.13a). On the contrary, the distribution of the results in terms of curvature ductility varies over lifetime, since it depends on both the positive and negative curvature ductility of the corroded columns (Figure 4.13b).

4. Application: 3D continuous concrete bridge

The case study of a 3D continuous concrete bridge is herein investigated to assess the lifetime performance under environmental and seismic hazard (Biondini *et al.* 2013). Lifetime bending moment versus curvature relationships of the cross-sections at the base of the piers are evaluated in probabilistic terms accounting for both the degradation of concrete and steel under a prescribed exposure scenario. Time-variant performance indicators such as bending resistance and curvature ductility are then evaluated.

The lifetime probabilistic seismic performance of the bridge structural system is therefore obtained by time-variant nonlinear static analyses. The comparison between the seismic capacity of the bridge structure and the seismic demand aims to define design target levels which are related to the actual lifetime evolution of the seismic performance within a life-cycle oriented performance-based design approach. Moreover, in order to investigate the effects of damage on the seismic behavior of the deteriorated bridge and to clarify the interaction between seismic and environmental hazards, nonlinear dynamic analyses under prescribed ground motions are carried out over the structural lifetime.

The four-span geometrically regular continuous bridge shown in Figure 4.19a is considered. Similar bridge structural schemes with irregular geometry have been investigated in Biondini *et al.* (2010). The total length of the bridge is 200m, with spans of 50m. The bridge deck is a two-box girder, as shown in Figure 4.19b. The bridge is assumed to be exposed to chloride diffusion over a 50 year lifetime. Material deterioration due to chloride-induced corrosion is considered to affect the bridge piers along the four sides and over the whole height.

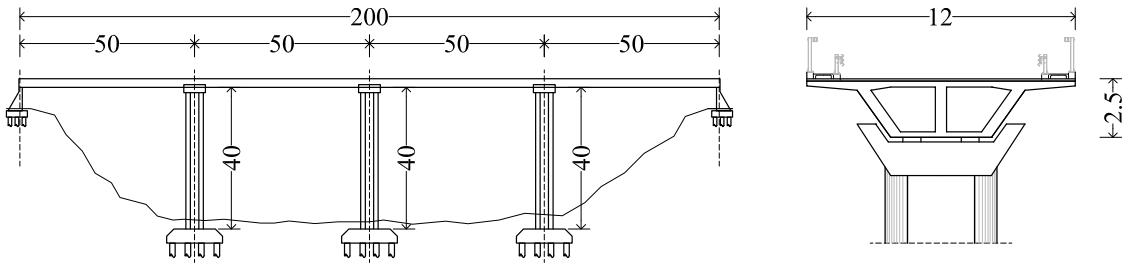

Figure 4.19 – Bridge structure: (a) overall dimensions [m] and (b) deck cross-section at midspan.

4.1. Lifetime performance of the pier cross-section

The bridge pier has a box cross-section (Figure 4.20a), which is typically adopted for medium/high bridge piers. The pier cross-section has main nominal dimensions $d_y = d_z = 5.00$m and it is reinforced with 80 + 156 = 236 steel bars having nominal diameters Φ_{nom} = 16mm and Φ_{nom} = 26mm,

respectively, with a concrete cover c = 40mm (Figure 4.20b). A nominal compression strength of the concrete f_c = 30MPa and a nominal yielding strength of the steel f_{sy} = 500 MPa are assumed. Strain values ε_{c0} = 0.22% and ε_{c0} = 0.35% for concrete in compression and ε_{su0} = 5.00% for steel are also assumed.

The pier cross-section is considered exposed to the diffusive attack of chlorides along both the external and internal perimeters with surface chloride concentration $C_{s,\Delta x}(t) = C$ (Figure 4.20c). The hollow core is exposed to the atmosphere as the external surface since this type of piers is not hermetically closed over the whole height, having openings particularly in the top part. The one-dimensional Fick's law of diffusion is applied in the normal direction to each side of the cross-section boundary. The parameters describing the exposure scenario are listed are listed in Chapter 2, Table 2.3 in terms of random variables assumed in the chloride diffusion model. The interaction of the diffusion process from more than one side of the cross-section is neglected, since the effects of two-dimensional patterns of diffusion are here relevant only for the few steel bars placed close to the corners of the cross-section. Moreover, the shape and the dimensions make the one-dimensional diffusion model accurate enough for such a cross-section (Chapter 2, §4.4).

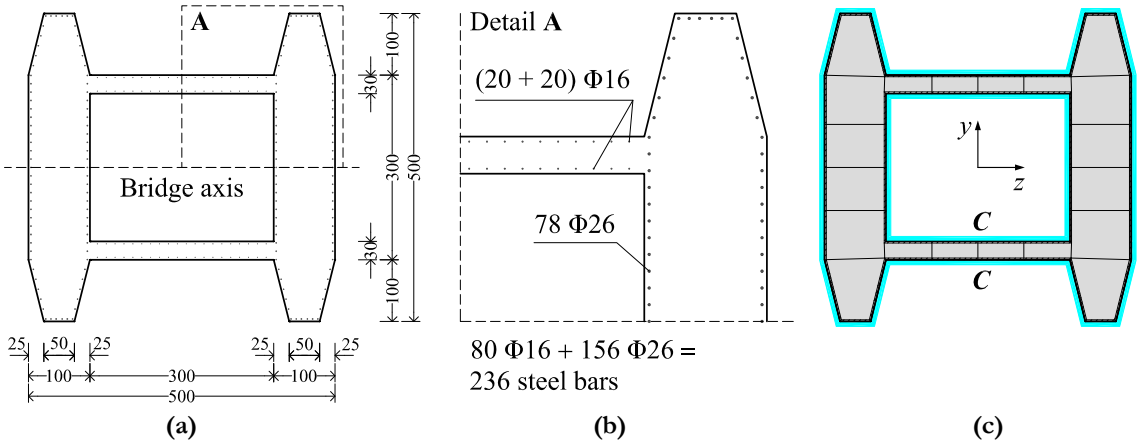

Figure 4.20 –Pier cross-section: (a) geometrical dimensions [cm] and (b) detail of reinforcement layout [mm]; (c) discretization of the section and location of the aggressive agent.

The deterioration over lifetime of the box cross-section of the bridge piers is evaluated according to the damage models described in Chapter 3 and applied in Chapter 3, §5. In particular, the corrosion of the longitudinal steel bars is evaluated according to the uniform corrosion model. The time evolution of both steel ultimate strain and concrete strength are considered as well, based on the adopted steel damage function. The reduction of strength in concrete is applied to the entire concrete cover. In this study, the effect of corrosion of the shear reinforcement is not taken into account, since the variation of the low transversal steel ratio should not affect significantly the bending performance of such a section.

A time-variant structural analysis is carried out in terms of lifetime of bending moment-curvature diagram M_z-χ_z computed by considering an axial load of N = 25MN and M_y = 0. The limit state of

failure of the cross-section is associated to the reaching of the strain limits of the materials according to the adopted constitutive rules. For concrete, the stress-strain diagram is described by the Saenz's law in compression and by an elastic perfectly plastic model in tension, with the following parameters (CEN-EN 1992-1-1 2004): compression strength f_c, tension strength $f_{ct} = 0.25 f_c^{2/3}$ MPa; initial modulus $E_{c0} = 9500 f_c^{1/3}$MPa; strain limit in tension $\varepsilon_{ctu} = 2 f_{ct} / E_{c0}$. For steel, the stress-strain diagram is described by an elastic perfectly plastic model in both tension and compression with steel strength f_{sy} and elastic modulus E_s = 210GPa.

The cross-sectional performance is investigated in fully probabilistic terms with respect to both the diffusion and deterioration model. As far as the structural modeling, material and geometrical randomness are considered as well, as indicated in Table 4.8.

The time evolution of the flexural behavior of the pier is shown in Figure 4.21a over a lifetime of 50 years with time step Δt = 10 years. The results shown in the plot refer to bending moment and curvature evaluated considering the sample mean values $\Phi(t) = \mu(t)$ of the steel bar diameters at each time step (Chapter 3, Figure 3.18) and the mean geometrical and mechanical properties of the cross-section. It can be noticed that the bending capacity of the pier significantly decreases over lifetime, while the curvature capacity shows a different trend. In fact, the ultimate curvature varies depending on the amount of steel in the section, which reduction can actually lead to a more ductile behavior, as shown after 30 and 40 years of lifetime.

The comparison with the results found in literature validate the 1D diffusion modeling approach for such a cross-section. In fact, the lifetime evolution of both bending strength and curvature ductility well agrees with the results reported by Biondini *et al.* (2010a), which are obtained by means of a more general 2D diffusion modeling based on cellular automata (Biondini *et al.* 2004a, 2006).

Figure 4.21b also shows a four side stepwise linearization of the moment-curvature diagram (dotted lines) at time t = 0. The values of bending moment M_{cr} and curvature χ_{cr} at first cracking of concrete have been reduced with respect to the actual value in order to fit properly the post-cracking stiffness, as shown in Figure 4.21b. In this way, also the post-yielding stiffness is estimated more accurately. The yielding curvature χ_{yield} is evaluated as follows (Park & Paulay 1975):

$$\chi_{yield} = \frac{M_{ult}}{M'_y} \chi'_y \tag{4.34}$$

where M_{ult} is the moment at failure, M'_y and χ'_y are respectively the bending moment and the corresponding curvature evaluated at the first yield of the longitudinal steel bars. The yielding moment of the section M_{yield} is then calculated as the value corresponding to χ_{yield} by linearly interpolating the cracking point and the first yielding point. These latter values define the nominal yielding point (point 3, Figure 4.21b). The maximum bending moment M_{max} and the corresponding curvature χ_{max} are evaluated as the maximum ordinate and corresponding abscissa of the curve. The

ultimate properties of the section, i.e. M_{ult} and χ_{ult}, correspond to the achievement of strain limits of concrete or steel.

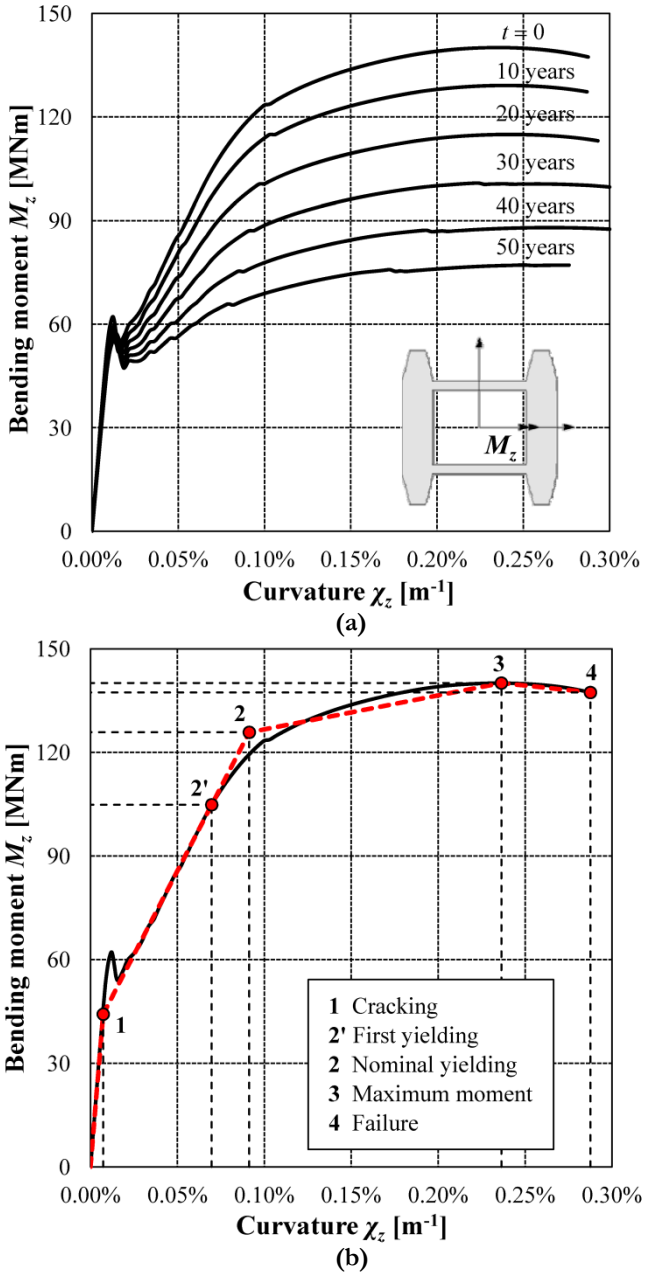

Figure 4.21 – Pier cross-section undergoing corrosion damage: (a) bending moment-curvature diagrams during the first 50 years of lifetime (N = 25MN) according to sample mean values; (b) stepwise linearization of the bending moment-curvature diagram at time t = 0.

4.2. Lifetime structural performance indicators

Figure 4.22 and Figure 4.23 show the time evolution of the bending moments and curvatures associated with the nominal yielding (point 2, Figure 4.21b) and the failure (point 4, Figure 4.21b) of the box cross-section bridge pier. The probabilistic results are obtained by a Monte Carlo simulation

based on a sample of 50,000 realizations. The results are scaled with respect to the mean values of the indicators at time $t = 0$. It can be noticed that, since different uncertainties are associated with each parameter, not only the evolution of the mean μ but also the scatter around the mean is different during 50 years of lifetime.

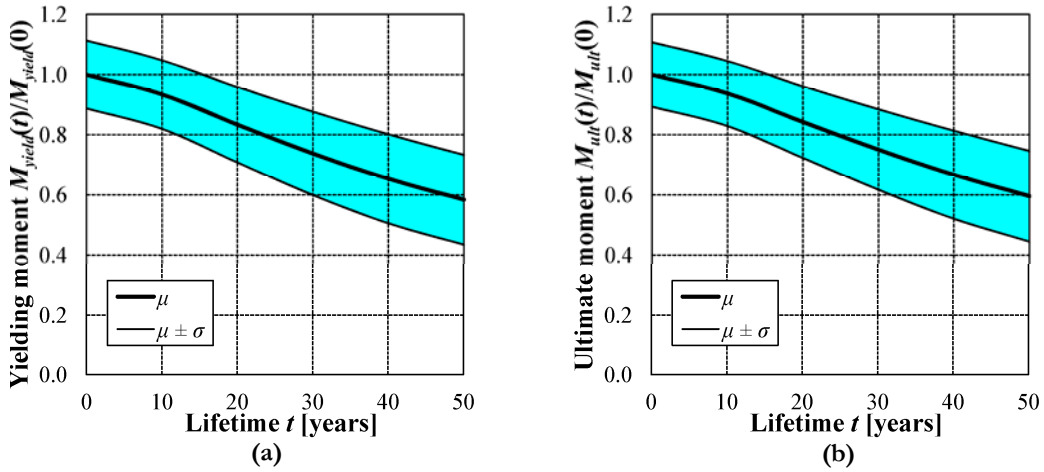

Figure 4.22 – Time evolution of the structural performance of the pier cross-section in terms of (a) yielding moment $M_{yield}(t)$ and (b) ultimate moment $M_{ult}(t)$ (mean μ and standard deviation σ from the mean).

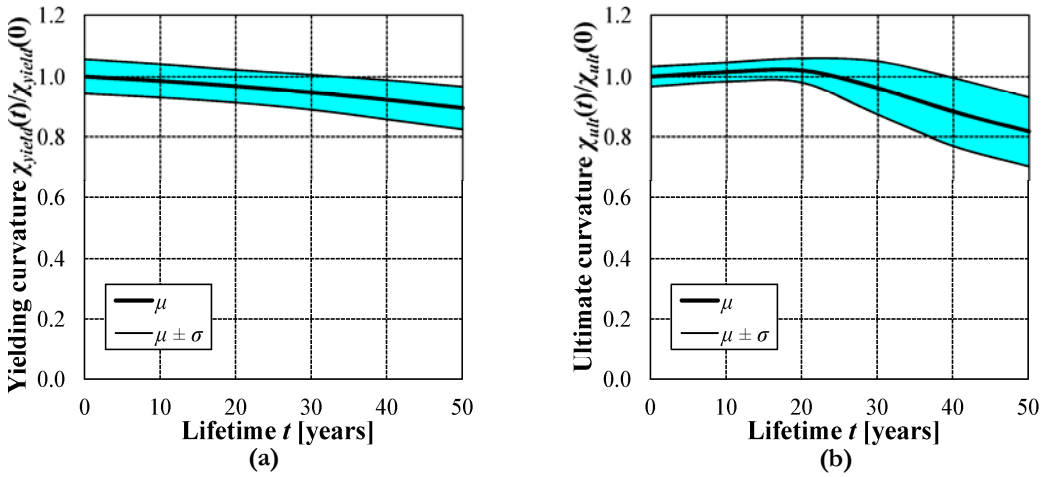

Figure 4.23 – Time evolution of the structural performance of the pier cross-section in terms of (a) yielding curvature $\chi_{yield}(t)$ and (b) ultimate curvature $\chi_{ult}(t)$ (mean μ and standard deviation σ from the mean).

The ultimate bending moment $M_{ult}(t)$ (Figure 4.22b) and the curvature ductility $\mu_\chi(t) = \chi_{ult}(t)/\chi_{yield}(t)$ (Figure 4.24) can be assumed as suitable indicators of the seismic performance of the bridge pier. The bending strength and curvature ductility decrease over a lifetime of 50 years of about 40% and 10%, respectively, from the initial values $M_{ult}(0) = 140$MNm and $\mu_\chi(0) = 3.10$. The bending strength undergoes a monotonic decrease, while the curvature ductility shows a different trend according to the evolution of both the yielding curvature and the ultimate curvature (Figure 4.23). While the yielding curvature reduces over 50 years of lifetime, the ultimate curvature increases during the first

20 years of lifetime. This is due to the slight decrease of the amount of steel in the concrete cross-section, which leads to a more ductile behavior. When the steel loss becomes more significant, then the ultimate curvature starts decreasing. This variation in the ultimate curvature trend is hence reflected in the curvature ductility as well.

It should also be noticed that while the standard deviation of the results of the yielding curvature remains substantially the same throughout the lifetime, greater uncertainties affect the estimation of the ultimate curvature of a corroded section, as shown in Figure 4.23. This indicates that the failure mechanism of the section may depend with large uncertainty on the degradation of both concrete and steel properties.

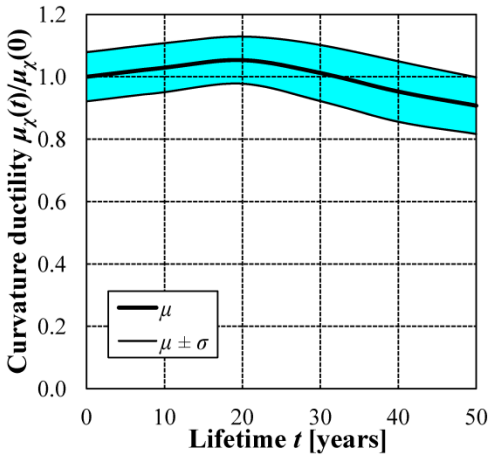

Figure 4.24 – Time evolution of the structural performance of the pier cross-section in terms of curvature ductility $\mu_\chi(t)$ (mean μ and standard deviation σ from the mean).

4.3. Structural modeling

The bridge is modeled by using the numerical code Ruaumoko3D (Carr 2008) according to the model shown in Figure 4.25. Connections of the deck with both piers and abutments are monolithic. The structure is considered fully fixed at the abutments and at the base of the piers. The seismic analysis is carried out by assuming a uniform gravity load p = 300kN/m, including self weight, dead loads and a 20% of live loads applied on the deck. The deck is modeled by elastic beam elements, since under transversal loading the nonlinear behavior is expected to develop only in the piers (Priestley *et al.* 2007).

The piers are modeled by using Giberson beam elements (Sharpe 1974), with plastic hinges that can develop at top and bottom of the piers. Shear failures are excluded based on a proper capacity design. The flexural behavior of the plastic hinges, which are modeled as rotational inelastic springs, is defined by moment-rotation relationships achieved by integration of the bending moment-curvature hysteresis rules. The integration is developed by assuming a parabolic distribution of the curvature

along a fixed length region of the plastic hinge L_p. Before implementation, the bending moment-curvature relationships have been linearized, as shown in Figure 4.21b. The main parameters of the model are the time-variant values of bending moment and curvature at cracking (M_{cr}, χ_{cr}), yielding (M_{yield}, χ_{yield}), peak (M_{max}, χ_{max}) and failure (M_{ult}, χ_{ult}). The cyclic behavior of the plastic hinges is defined based on the Schoettler-Restrepo hysteresis rule (Carr 2008).

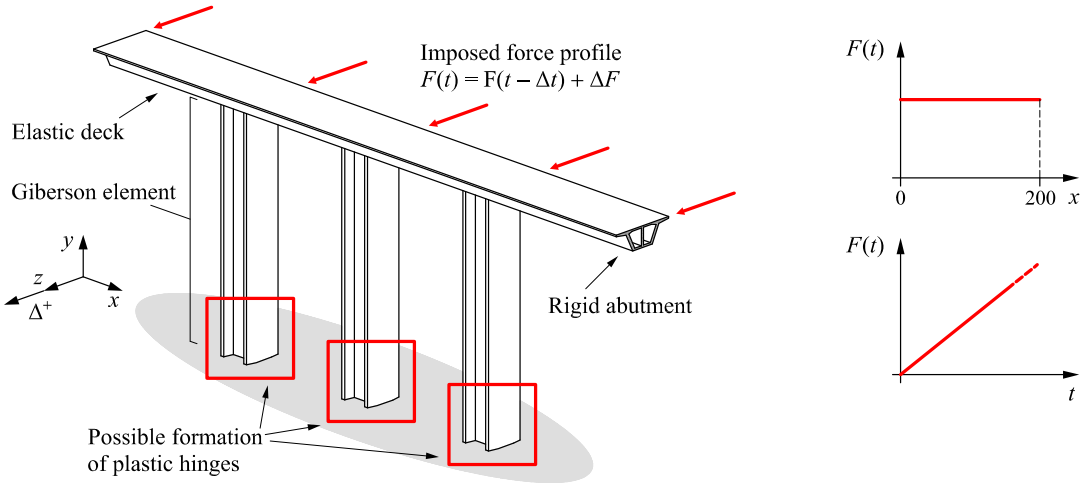

Figure 4.25 – Structural modeling of the bridge structure with indication of the applied push-over forces.

4.4. Lifetime nonlinear static analyses

A probabilistic lifetime nonlinear static (push-over) analysis of the bridge is carried out by applying a uniform distribution of monotonically increasing horizontal forces at deck level, as suggested in CEN-EN 1998-1 (2004) due to the regular scheme of the bridge. Nonlinear geometrical *P*-Δ effects are not considered. Results of the lifetime push-over analyses assuming the mean properties of the bridge piers (Figure 4.21a) are shown in Figure 4.26 in terms of total base shear force F_{base} versus top displacement of the central pier Δ_c. These diagrams show a significant decrease in the total base shear capacity of the bridge, which reduces to about 50% of the original value after 50 years of lifetime.

The points corresponding to the formation of the plastic hinges at the base of the central pier are highlighted on the push-over curves in Figure 4.26. As it can be noticed, in deteriorating structures the plastic hinging occurs for lower levels of displacement, which is mainly due to the reduced steel reinforcement area in concrete members.

The points corresponding to increasing displacement levels are also indicated on the push-over curves shown in Figure 4.26. As listed in Table 4.7, different seismic performance levels can be established according to the maximum displacement that the structure undergoes during an earthquake and with respect to the inelastic displacement demand ratio.

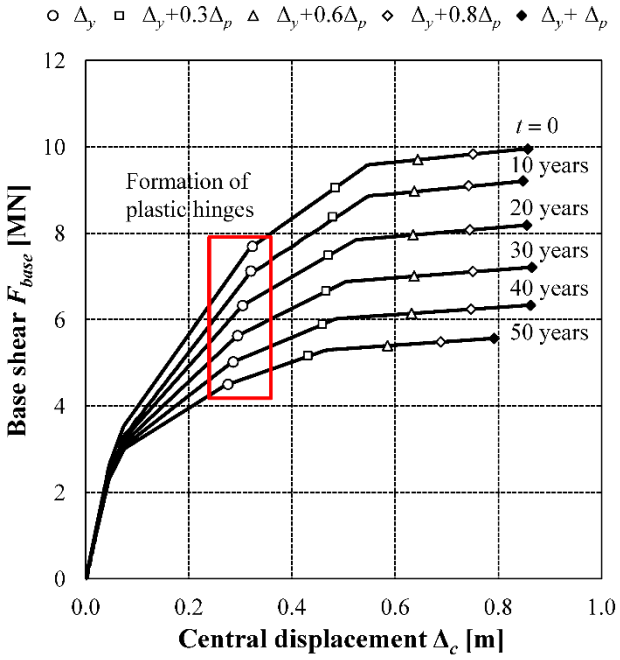

Figure 4.26 – Push-over analyses based on the lifetime properties of the piers. Time evolution of total base shear force F_{base} versus top displacement of the central pier Δ_c during the first 50 years of lifetime with indication of increasing levels of displacement according to Table 4.7.

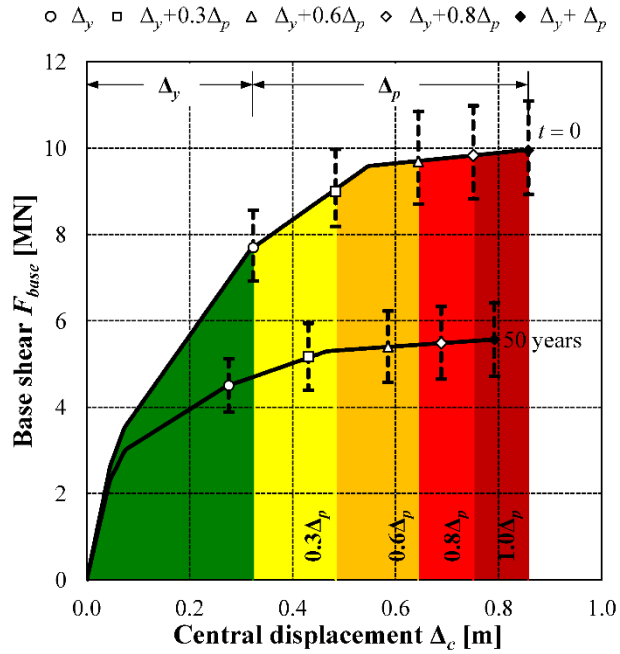

Figure 4.27 – Push-over analyses. Total base shear force F_{base} versus top displacement of the central pier Δ_c at time $t = 0$ and $t = 50$ years with indication of the yielding Δ_y and plastic Δ_p displacement according to different levels of performance.

For a prescribed displacement level, the push-over curve provides the total resisting force of the bridge piers and hence the maximum peak ground acceleration sustainable by the structure within a specified performance level. As it can be noticed from Figure 4.26, for each performance level, a

progressive decrease in the strength capacity of the structure occurs as the corrosion of concrete members becomes more severe, which implies that after 50 years the structure could not sustain an earthquake event of the same magnitude it was designed for. This is evident in Figure 4.27, where the push-over curves at the beginning of lifetime and after 50 years are compared.

Table 4.10 – System displacement limits considering different structural performance levels.

SPL	F_{base}		Lifetime					
			0	10 years	20 years	30 years	40 years	50 years
SP-1	$F_y(t) / F_y(0)$	μ	1	0.939	0.847	0.760	0.684	0.624
		σ	0.106	0.107	0.117	0.128	0.134	0.136
SP-2	$F_{OP}(t) / F_{OP}(0)$	μ	1	0.936	0.839	0.744	0.659	0.590
		σ	0.109	0.111	0.124	0.138	0.149	0.153
SP-3	$F_{LS}(t) / F_{LS}(0)$	μ	1	0.935	0.837	0.742	0.657	0.588
		σ	0.110	0.112	0.125	0.139	0.149	0.152
SP-4	$F_{NC}(t) / F_{NC}(0)$	μ	1	0.942	0.850	0.753	0.666	0.596
		σ	0.098	0.101	0.118	0.138	0.148	0.150
SP-5	$F_{ult}(t) / F_{ult}(0)$	μ	1	0.936	0.840	0.746	0.661	0.591
		σ	0.108	0.110	0.123	0.137	0.149	0.153

Since a shift of both yielding and ultimate displacements occurs in time, the seismic performance of a deteriorating bridge, evaluated in terms of displacements on the basis of the initial properties of the structure, may not comply with the prescribed target performance levels over the expected lifetime. Moreover, the uncertainties associated with each performance level in terms of total base shear are different, as shown by the dotted lines in Figure 4.27, which represent the dispersion of the results around the mean shear value. Results of the probabilistic analyses are listed in Table 4.10, in terms of normalized mean values and standard deviations of the total base shear throughout the lifetime. It can be noticed that the dispersion of the results around the mean becomes greater not only as the age of the structure increases, but also, in general, considering increasing levels of performance.

Figure 4.28a shows the lifetime evolution of the total base shear $F_{base}(t)$ at different structural performance levels. For example, the total base shear $F_{base}(t)$ at ultimate displacement Δ_u of the structure decreases of about 40% during a 50-year lifetime. Base shear forces at intermediate displacement levels from yielding displacement up to collapse decrease as well proportionately. The displacement ductility of the structural system $\mu_\Delta(t) = \Delta_u(t)/\Delta_y(t)$ may change as well, as shown in Figure 4.28b, since the reduction in steel area and the degradation of concrete strength in the corroded members vary the distribution of stiffness in the structure. As a consequence, a change in the global collapse mechanism and a performance decay of the bridge may occur.

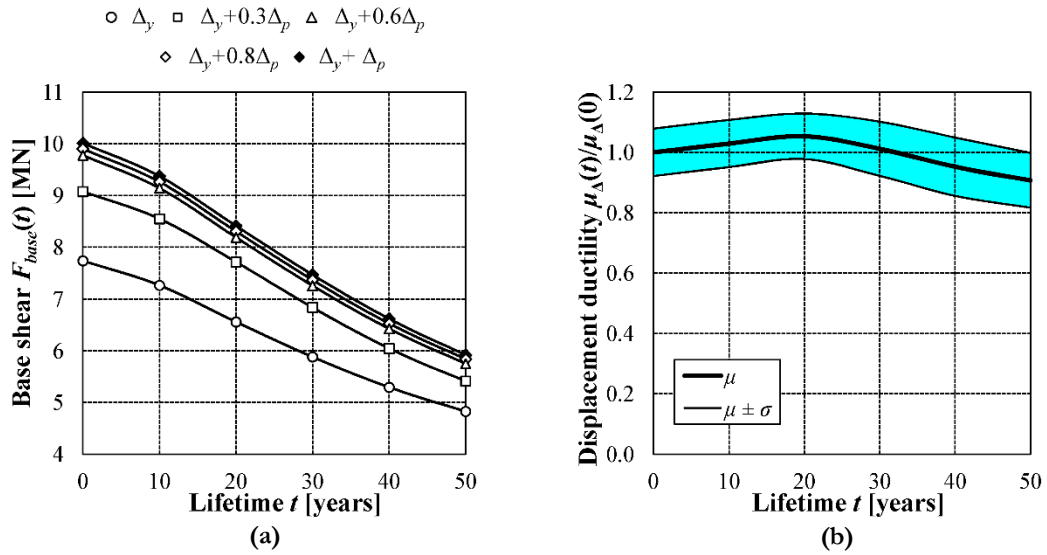

Figure 4.28 – Push-over analyses of the bridge. Time evolution of (a) mean total base shear force F_{base} with reference to different levels of displacement (see Table 4.7) and (b) displacement ductility μ_Δ (mean values μ and standard deviation σ from the mean).

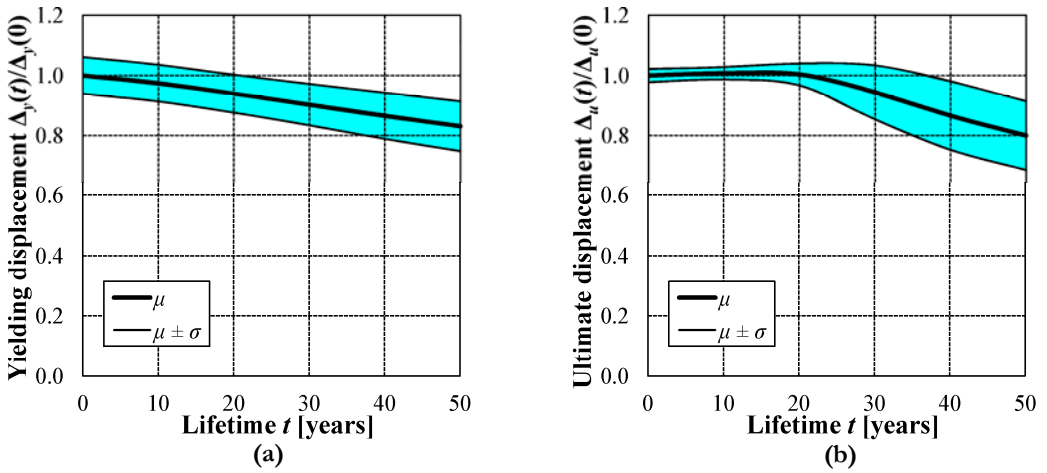

Figure 4.29 – Push-over analyses. Time evolution of (a) yielding displacement Δ_y and (b) ultimate displacement Δ_u of the central pier (mean μ and standard deviation σ from the mean).

The time-variant trend of both mean and standard deviation of displacement ductility results from the combination of the variability of both yielding and ultimate displacement, as shown in Figure 4.29. In fact, while the yielding displacement $\Delta_y(t)$ decreases monotonically, the trend of the ultimate displacement $\Delta_u(t)$ is similar to that of the ultimate curvature $\chi_{ult}(t)$ (Figure 4.23). Moreover, larger uncertainties affect the behavior of the bridge at collapse, especially after 25 years of lifetime, while the transition from elastic to plastic field is mainly related to the properties of the reinforcing steel bars only. This result confirms that at the design stage higher safety factors should be applied to check the ultimate deformation capacity of the bridge with respect to the safety factors used to check the reaching of the yielding displacement.

4.5. Lifetime nonlinear dynamic analyses

Time-history nonlinear dynamic analyses are carried out with reference to the ensemble of ten earthquake records listed in Table 4.11 (Pampanin *et al.* 2002). These records were selected to match the Eurocode 8 design response spectrum for soil class B and peak ground acceleration PGA = 0.54*g* (CEN-EN 1998-1 2004), as shown in Figure 4.30.

Table 4.11 – Characteristics of the seismic records (Pampanin *et al.* 2002).

Earthquake record	Year	Station	Soil Type	Scaling Factor	Scaled PGA [*g*]
EQ1 - Loma Prieta	1989	Hollister Diff. Array	D	2.0	0.54
EQ2 - Loma Prieta	1989	Gilroy Array #7	D	3.0	0.68
EQ3 - Landers	1992	Desert Hot Springs	C	4.1	0.62
EQ4 - Landers	1992	Yermo Fire Station	D	3.3	0.50
EQ5 - Cape Mendocino	1992	Rio Dell Overpass-FF	C	1.8	0.69
EQ6 - Superstition Hills	1987	Plaster City	D	3.3	0.61
EQ7 - Northridge	1994	Canoga Park-Topanga Can	D	1.8	0.64
EQ8 - Northridge	1994	Beverly Hills 14145 Mulhol	C	1.4	0.56
EQ9 - Northridge	1994	N Holliwood-Coldwater Can	C	2.6	0.69
EQ10 - Northridge	1994	Sunland-Mt. Gleason Ave	C	3.3	0.52

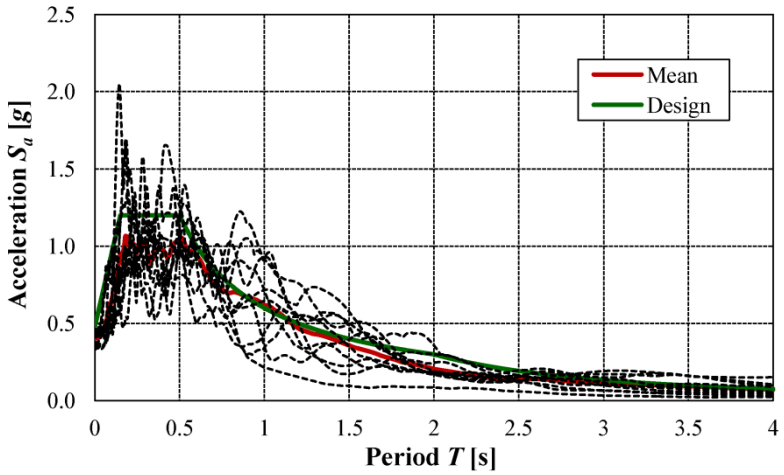

Figure 4.30 – Comparison between the design response spectrum (soil class B, PGA = 0.54*g* CEN-EN 1998-1 2004) and the mean spectrum of the considered earthquakes (Table 4.11).

In this study, the records are scaled to prescribed seismic intensity levels, corresponding to frequent, occasional, rare and maximum considered ground motions, as listed in Table 4.12 (SEAOC 1995). These ground motions have increasing mean return periods, ranging from a 25-year to a 2500-year return period, thus corresponding to an increasing seismic hazard. The investigation is therefore focused on the effects of increasing seismicity on corroded structures under the same environmental

exposure. Further analyses should be required to combine different levels of environmental aggressiveness and seismic hazard (Biondini *et al.* 2012).

Table 4.12 – Recommended design ground motions for use in high seismic regions, with indication of PGAs (in units of *g*'s) for sites not located in near source zones, soil type B (SEAOC 1995).

Earthquake	Description	Probability of Exceedance	Mean Return Period	PGA
EQ-I	Frequent	87% / 50years	25years	0.11
EQ-II	Occasional	50% / 50years	72years	0.17
EQ-III	Rare	--	250 to 800 years	0.40
EQ-IV	Maximum Considered	--	800 to 2500 years	0.60

The dynamic analyses are carried out on the bridge model considering the mean values of the bending moment-curvature diagrams of the box cross-section bridge pier. Results are reported in terms of mean and absolute maxima/minima values of total base shear F_{base} (Figure 4.31) and top displacement of the central pier Δ_c (Figure 4.32).

As expected based on the results of the push-over analyses, these parameters vary depending not only on the seismic intensity level but also on the age of the structure. The influence of the ageing phenomena in concrete is more evident with the increase in the peak ground acceleration in terms of both base shear force and displacement demand. Since the concrete members become less stiff over lifetime, the total shear at the base of the bridge piers decreases, while the displacement demand at deck level increases.

This trend is clearly indicated by the mean values of forces and displacements shown in Figure 4.31 and Figure 4.32, respectively. The curves related to the maxima/minima values are less smooth than the curves of the mean values due to the inherent randomness of the considered seismic excitations acting on the structure.

Moreover, it has been observed that the maximum/minimum displacement at the beginning of the lifetime is generally due to the ground motions with higher peak ground acceleration (e.g. EQ7). On the contrary, at the end of the lifetime, the observed major displacements are reached for the seismic events with longer durations (e.g. EQ2 and EQ3). This can be due to the developing of the degradation phenomena, since the structure becomes less stiff and more ductile between 10 and 30 years of lifetime (Figure 4.28b).

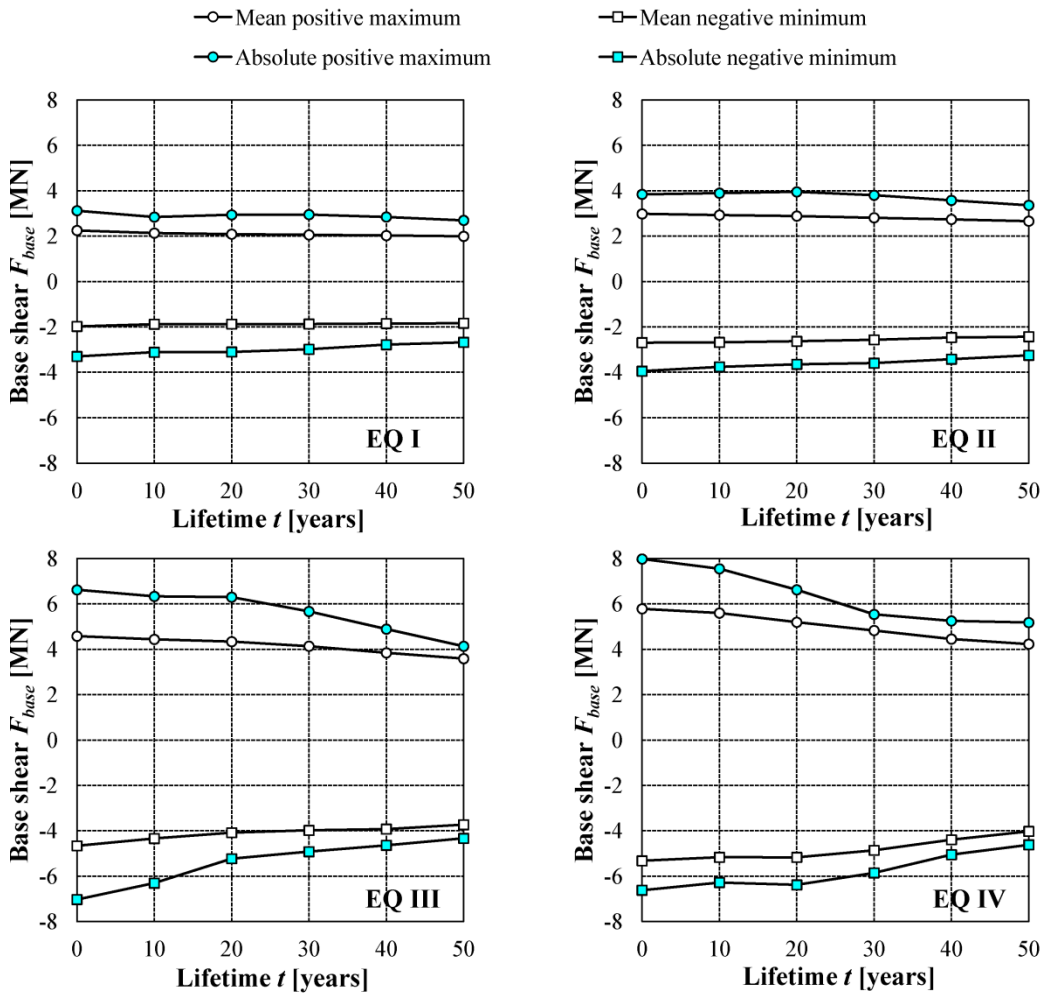

Figure 4.31 – Time-history analyses. Time evolution of total base shear force F_{base} based on the properties of the piers shown in Figure 4.21 considering increasing levels of PGA (Table 4.12).

According to the results of the time-histories analyses, the trend shown by the push-over analyses is confirmed. In fact, considering the major seismic intensity "Level IV", at time $t = 0$ the maximum base force is about 7MN, while the maximum displacement is between 0.2 and 0.4m. This indicates an elastic response of the structure, which is expected to remain operational after the earthquake. On the contrary, after 50 years of lifetime the most severe seismic input places a demand of 5MN of base shear and of 0.6m of maximum displacement. These data correspond to a point in the "near collapse" zone on the push-over curve at $t = 50$ years in Figure 4.27.

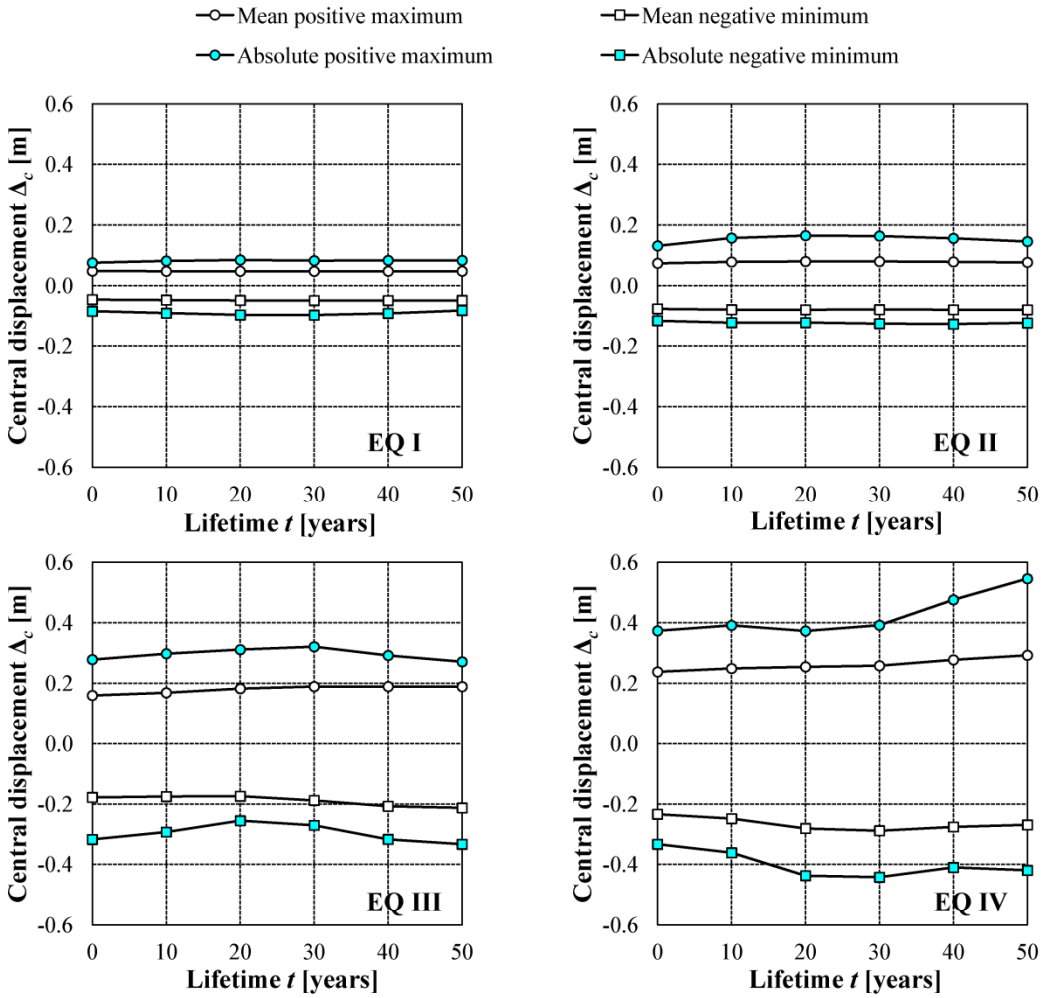

Figure 4.32 – Time-history analyses. Time evolution of central pier top displacement Δ_c based on the properties of the piers shown in Figure 4.21 considering increasing levels of PGA (Table 4.12).

Finally, time histories of total base shear F_{base} and top displacement of the central pier Δ_c are shown in Figure 4.33 and Figure 4.34, respectively, for three of the earthquakes listed in Table 4.11 (EQ2, EQ3 and EQ7). These results refer to time instants $t = 0$ and $t = 50$ years. It can be noticed that over the lifetime the overall strength of the bridge decreases and the displacement demand increases, due to the reduced stiffness of the corroded concrete piers. This could cause an unsatisfactory structural performance of a bridge that was designed to respect prescribed performance levels at the beginning of its lifetime.

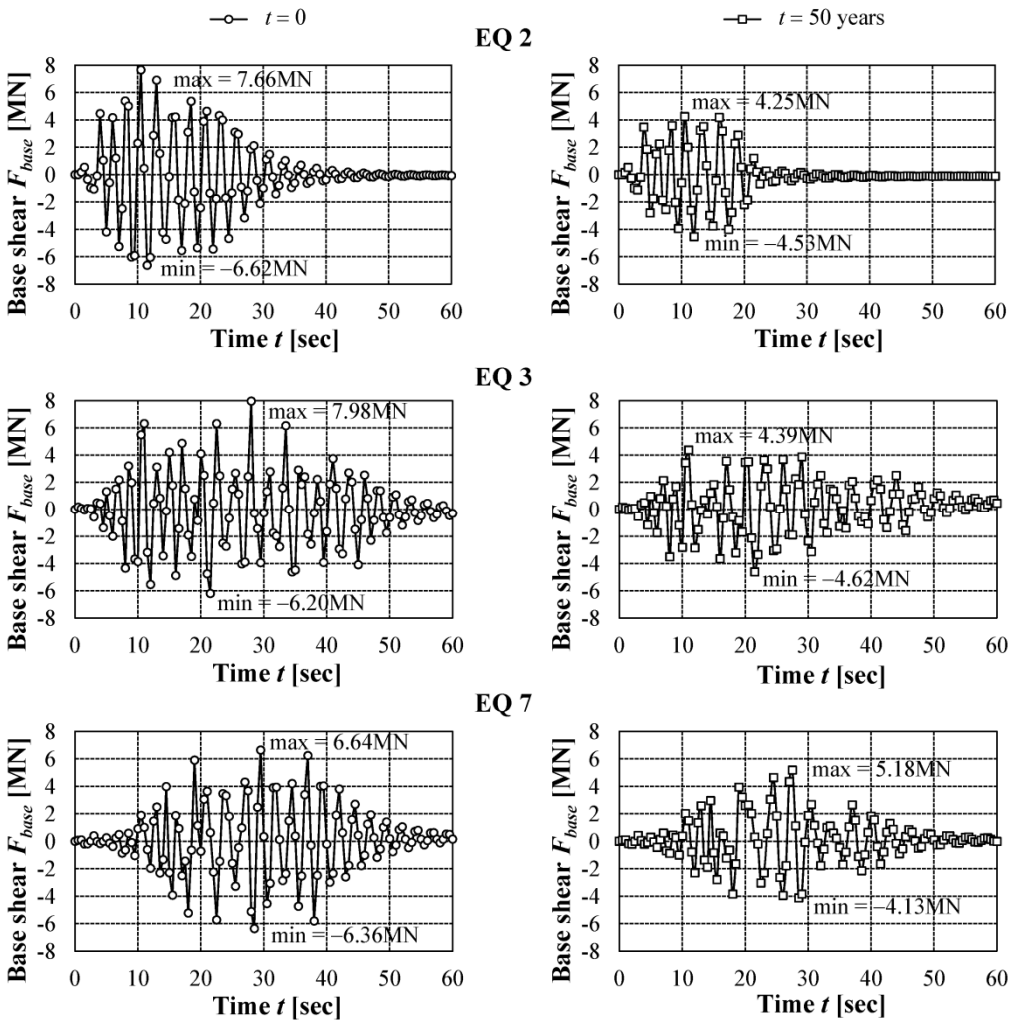

Figure 4.33 – Time-history analyses. Time histories of total base shear F_{base} at time $t = 0$ and $t = 50$ years for three of the earthquakes listed in Table 4.11.

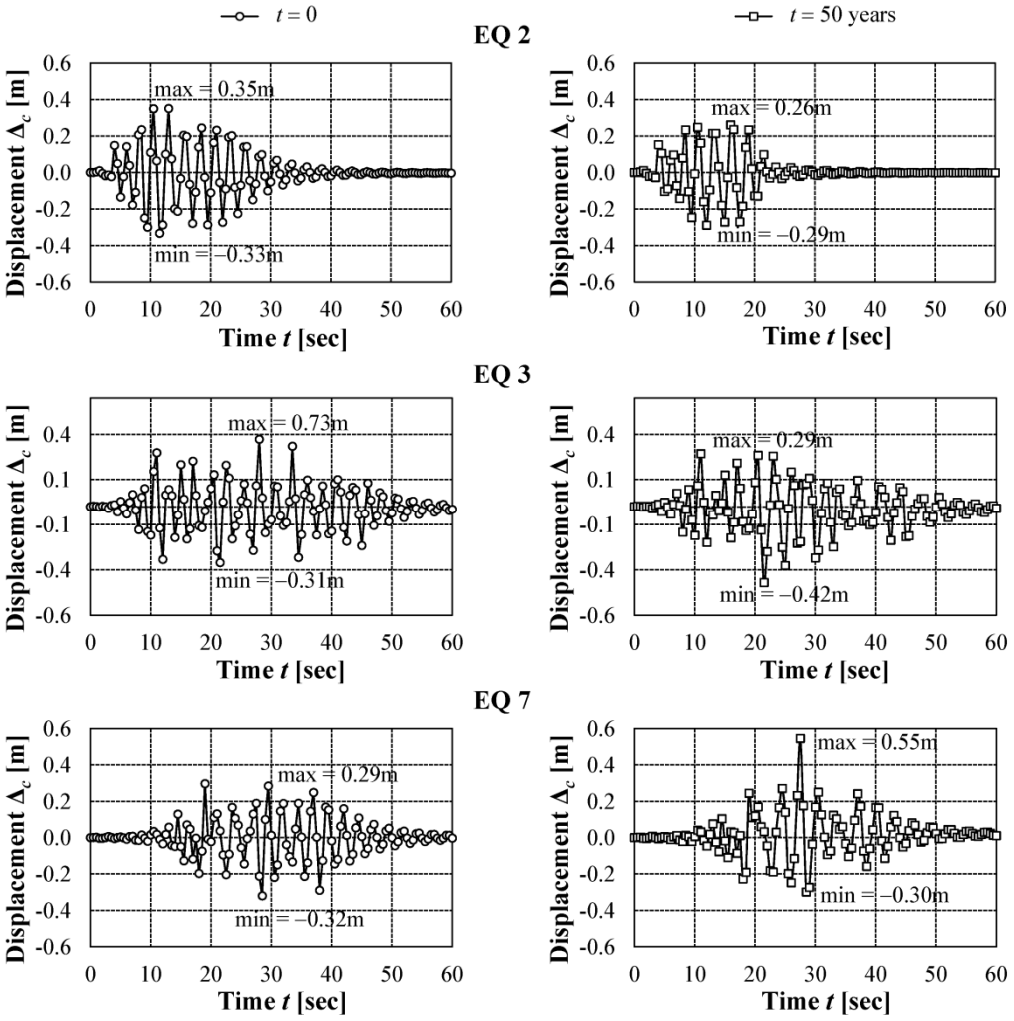

Figure 4.34 – Time-history analyses. Time histories of central pier top displacement Δ_c at time $t = 0$ and $t = 50$ years for three of the earthquakes listed in Table 4.11.

5. Conclusions

The structural effects of local damage induced by corrosion of steel reinforcement and degradation of concrete in structures exposed to the diffusive attacks of aggressive agents have been investigated. Based on proper damage models, the proposed probabilistic procedure allowed to model the degradation process into concrete members at cross-sectional level and hence to evaluate their lifetime performance in terms of both bending moment resistance and curvature ductility. In fact, the definition of proper performance indicators and damage measures is needed at both cross-sectional and global structural level to assess the actual behavior of deteriorating structural system over lifetime.

In particular, the effects of material deterioration on the overall seismic performance have been highlighted. The mutual interaction between seismic hazard and environmental aggressiveness becomes crucial in the lifetime assessment of concrete structures. This has been shown by the case studies of a multistory frame and a continuous bridge. The proposed general framework for the assessment of the lifetime performance of the structures has been applied and nonlinear static and dynamic analyses have been carried out.

The results obtained for the multistory concrete frame showed a significant reduction of both shear strength and displacement ductility. This causes an alteration of the resisting hierarchy in the structure, which leads to a redistribution of internal forces and to a shift in the energy-dissipating failure mode. In fact, under seismic excitation an undesirable mechanism of collapse may occur due to the variation of the stiffness of the corroded concrete members, especially if the deterioration process is localized in certain parts of the structure.

As far as the concrete bridge, the results showed the time evolution of the cross-sectional behavior of the plastic hinge zones at the bottom of the piers is reflected at global structural level by a significant reduction of the base shear strength and a variation of the displacement ductility. In fact, the seismic performance of integral bridges strictly depends on the capacity of the piers. As a consequence, a design targeted to satisfy certain performance levels in terms of forces or displacements, as stated by recent performance-based design codes, could become unsatisfactory throughout the lifetime of the structure whether considering the residual capacity of concrete members.

The investigation demonstrated the importance of taking the severity of the environmental exposure and the required structural lifetime into account in both the seismic assessment of existing structures and the seismic design of new structures. The design criteria should be revised since force reducing factors at global level and over-strength factors at local level are expected to vary over time due to the aging of the structure. In this regard, new generation performance-based design procedures should be developed by using a performance matrix in which the structural behavior is related to both the seismic intensity level and the environmental hazard, taking into account increasing levels

of aggressiveness. A proper calibration of the design objectives and limit states should also be planned in order to ensure a structural lifetime with suitable levels of performance and safety.

To this aim, further investigation about the interaction between seismic and corrosion hazards is needed. Different exposure condition should be considered in order to investigate the effects of increasing environmental aggressiveness and/or localized exposure. In this study severe exposure conditions have been used in order to emphasize the influence of corrosion damage over time. However, a proper calibration of the deterioration model based on experimental data is recommended. Moreover, different structural typologies of frames and bridges should be considered by applying the general lifetime assessment methodology herein proposed. Other aspects related to the seismic hazard, such as the recurrence of seismic events and multiple ground excitation, should be also taken into account in order to properly define a life cycle-oriented performance-based design approach and to plan seismic assessment strategies.

6. References

Akiyama, M., & Frangopol, D.M. (2010). On life-cycle reliability under earthquake excitations of corroded reinforced concrete structures. *Proceedings of the Second International Symposium on Life-Cycle Civil Engineering (IALCCE2010)*, Taipei, Taiwan, October 27-31.

Akiyama, M., Frangopol, D.M., & Matsuzaki, H., (2011a). Life-cycle reliability of RC bridge piers under seismic and airborne chloride hazards. *Earthquake Engineering and Structural Dynamics*, 40 (15), 1671–1687.

Akiyama, M., Frangopol, D.M., & Suzuki, M. (2011b). Integration of the effects of airborne chlorides into reliability-based durability design of reinforced concrete structures in a marine environment. *Structure and Infrastructure Engineering*, 8(2), 125–134.

Akiyama, M., Matsuzaki, H., Dang, H.T., & Suzuki, M. (2012). Reliability-based capacity design for reinforced concrete bridge structures. *Structure and Infrastructure Engineering*, 8(12), 1096–1107.

Alipour, A., Shafei, B., & Shinozuka, M.S. (2013). Capacity loss evaluation of reinforced concrete bridges located in extreme chloride-laden environments. *Structure and Infrastructure Engineering*, 9(1), 8–27.

ASCE (2013). *Report card for America's Infrastructure*. American Society of Civil Engineers, Reston, VA. http://www.infrastructurereportcard.org/a/#p/bridges/overview.

Banon, H., Irvine, H.M., & Biggs, J.M. (1981). Seismic damage in reinforced concrete frames. *Journal of the Structural Division*, 107(9), 1713–1729.

Berry, M.P., & Eberhard, M.O. (2005). Practical performance model for bar buckling. *Journal of Structural Engineering*, 131(7), 1060–1070.

Berto, L., Vitaliani, R., Saetta, A., & Simioni, P. (2009). Seismic assessment of existing RC structures affected by degradation phenomena. *Structural Safety*, 31, 284–297.

Biondini, F. (2000). *Strutture da Ponte Soggette ad azioni di Tipo Sismico – Modellazione ed Ottimizzazione*. PhD Dissertation, Department of Structural Engineering, Politecnico di Milano, Milan, Italy.

Biondini, F. (2004). A three-dimensional finite beam element for multiscale damage measure and seismic analysis of concrete structures. *Proceedings of the 13th World Conference on Earthquake Engineering (WCEE)*, August 1-6, Vancouver, BC, Canada: Paper No. 2963.

Biondini, F. (2011). Cellular Automata Simulation of Damage Processes in Concrete Structures. *In: Soft Computing Methods for Civil and Structural Engineering*, Y. Tsompanakis and B.H.V. Topping, (Eds.), Saxe-Coburg Publications, Stirlingshire, Scotland, Chapter 10, 229–264.

Biondini, F., Bontempi, F., Frangopol, D.M., & Malerba, P.G. (2004a). Cellular automata approach to durability analysis of concrete structures in aggressive environments. *Journal of Structural Engineering*, 130(11), 1724–1737.

Biondini, F., Bontempi, F., Frangopol, D.M., & Malerba, P.G. (2004b). Reliability of material and geometrically non-linear reinforced and prestressed concrete structures. *Computers & structures*, 82(13), 1021–1031.

Biondini, F., Bontempi, F., Frangopol, D.M., & Malerba, P.G. (2006). Probabilistic service life assessment and maintenance planning of concrete structures. *Journal of Structural Engineering*, 132(5), 810–825.

Biondini, F., Camnasio, E., & Palermo, A. (2010a). Lifetime seismic performance of concrete bridges. *Proceedings of the Fifth International Conference on Bridge Maintenance, Safety, and Management* (*IABMAS2010*), July 11-15, Philadelphia, PA.

Biondini, F., Camnasio, E., & Palermo, A. (2012). Life-cycle performance of concrete bridges exposed to corrosion and seismic hazard. *Proceedings of the Structures Congress 2012* (*ASCE2012*), Chicago, IL, March 29-31.

Biondini, F., Camnasio, E., & Palermo, A. (2013). Lifetime Seismic Performance of Concrete Bridges Exposed to Corrosion. *Structure and Infrastructure Engineering*, ahead-of-print, doi:10.1080/15732479.2012.761248.

Biondini, F., & Frangopol, D.M. (2008a). Probabilistic limit analysis and lifetime prediction of concrete structures. *Structure and Infrastructure Engineering*, 4(5), 399–412.

Biondini, F., & Frangopol, D.M. (Eds.) (2008b). *Life-Cycle Civil Engineering*. CRC Press, Taylor & Francis Group.

Biondini, F., Frangopol, D.M., & Malerba, P. G. (2010b). Structural geometry effects on the life-cycle performance of concrete bridge structures in aggressive environments. In *Bridge Maintenance, Safety Management, Health Monitoring and Informatics – IABMAS08: Proceedings of the Fourth International IABMAS Conference*, Seoul, Korea, July 13-17, Taylor & Francis.

Biondini, F., Palermo, A. & Toniolo, G. (2011). Seismic performance of concrete structures exposed to corrosion: Case studies of low-rise precast buildings. *Structure and Infrastructure Engineering*, 7(1–2), 109–119.

Biondini, F., & Toniolo, G. (2009). Probabilistic calibration and experimental validation of the seismic design criteria for one-story concrete frames. *Journal of Earthquake Engineering*, 13(4), 426–462.

Biondini, F., Toniolo, G., & Tsionis, G. (2010c). Capacity design and seismic performance of multi-storey precast structures. *European Journal of Environmental and Civil Engineering*, 14(1), 11-28.

Biondini, F., & Vergani, M. (2012). Damage modeling and nonlinear analysis of concrete bridges under corrosion. *Proceedings of the 6th International Conference on Bridge Maintenance, Safety and Management (IABMAS 2012)*, July 8-12, Stresa, Italy.

Bontempi, F. (1992). Sulla costruzione dei domini di rottura di sezioni in C.A. e C.A.P. soggette a pressoflessione deviata. *Studi e Ricerche*, *Graduate School for Concrete Structures "F.lli Pesenti"*, Politecnico di Milano, Milan, Italy, 13, 261–277 (in Italian).

Bontempi, F., & Malerba, P.G. (1997). The role of softening in the numerical analysis of RC framed structures. *Structural Engineering and Mechanics*, 5(6), 785–801.

Bontempi, F., Malerba, P.G., & Romano, L. (1995). Formulazione diretta secante dell'analisi non lineare di telai in C.A./C.A.P.. *Studi e Ricerche*, *Graduate School for Concrete Structures "F.lli Pesenti"*, Politecnico di Milano, Milan, Italy, 16, 351–386 (in Italian).

Carr, A.J. (2008). *RUAUMOKO Program for Inelastic Dynamic Analysis*. Department of Civil Engineering, University of Canterbury, Christchurch, New Zealand.

CEB (1985). *Model Code for Seismic Design of Concrete Structures*. Bulletin 165.

CEB (1992). *Durable Concrete Structures – Design Guide*. Bulletin 183.

CEB (1998). *Seismic Design of Reinforced Concrete Structures for controlled Inelastic Response*. Bulletin 240.

CEN-EN 1992-1-1 (2004). *Eurocode 2 – Design of concrete structures – Part 1-1: General rules and rules for buildings*. European Committee for Standardization, Brussels.

CEN-EN 1998-1 (2004). *Eurocode 8: Design of Structures for Earthquake Resistance. Part 1: General rules, seismic actions and rules for buildings*. European Committee for Standardization, Brussels.

Choe, D.E., Gardoni, P., Rosowsky, D., & Haukaas, T. (2008). Probabilistic capacity models and seismic fragility estimates for RC columns subject to corrosion. *Reliability Engineering & System Safety*, 93(3), 383–393.

Choe, D., Gardoni, P., Rosowsky, D., & Haukaas, T. (2009). Seismic fragility estimates for reinforced concrete bridges subject to corrosion. *Structural Safety*, 31, 275–283.

Choi, E., DesRoches, R., & Nielson, B. (2004). Seismic fragility of typical bridges in moderate seismic zones. *Engineering Structures*, 26(2), 187–199.

Cornell, C.A., Jalayer, F., Hamburger, R. O., & Foutch, D.A. (2002). Probabilistic basis for 2000 SAC Federal Emergency Management Agency steel moment frame guidelines. *Journal of Structural Engineering*, 128(4), 526–533.

Cosenza, E., & Manfredi, G. (2000). Damage indices and damage measures. *Progress in Structural Engineering and Materials*, 2(1), 50–59.

Cosenza, E., Manfredi, G., & Ramasco, R. (1993). The use of damage functionals in earthquake engineering: a comparison between different methods. *Earthquake Engineering & Structural Dynamics*, 22(10), 855–868.

Dhakal, R.P., & Maekawa, K. (2002). Reinforcement stability and fracture of cover concrete in reinforced concrete members. *Journal of Structural Engineering*, 128(10), 1253–1262.

Estes, A.C., & Frangopol, D.M. (2001). Bridge lifetime system reliability under multiple limit states. *Journal of Bridge Engineering*, 6 (6), 523–528.

Fang, C., Gylltoft, K., Lundgren, K., & Plos, M. (2006). Effect of corrosion on bond in reinforced concrete under cyclic loading. *Cement and Concrete Research*, 36(3), 548–555.

FEMA (2000). *Prestandard and commentary for the seismic rehabilitation of buildings*. Report FEMA-356, Department of Homeland Security, Federal Emergency Management Agency, Washington, DC.

FEMA (2009). *HAZUS-MH MR4 Earthquake Model User Manual*. Department of Homeland Security, Federal Emergency Management Agency, Washington, D.C., US.

Frangopol, D.M. (2011). Life-cycle performance, management, and optimisation of structural systems under uncertainty: accomplishments and challenges 1. *Structure and Infrastructure Engineering*, 7(6), 389–413.

Frangopol, D.M., & Akiyama, M. (2011). Lifetime seismic reliability analysis of corroded reinforced concrete bridge piers. In *Computational Methods in Earthquake Engineering*, Springer Netherlands, 527–537.

Frangopol, D.M., & Liu, M. (2007). Maintenance and management of civil infrastructure based on condition, safety, optimization, and life-cycle cost. *Structure and Infrastructure Engineering*, 3(1), 29–41.

Fukada, Y. (1969). Study on the restoring force characteristics of reinforced concrete buildings. *Proceedings of the Kanto District Symposium*, Tokyo, Japan, Architectural Institute of Japan, 40 (in Japanese).

Ghosh, J., & Padgett, J.E. (2009). Multi-hazards considerations of seismic and aging threats to bridges. *Proceedings of the Structures Conference 2009 (ASCE2009*), April 30 – May 2, Austin, TX, USA.

Ghosh, J., & Padgett, J.E. (2010). Aging considerations in the development of time-dependent seismic fragility curves. *ASCE Journal of Structural Engineering*, 136(12), 1497–1511.

Giberson, M.F. (1967). *The Response of Nonlinear Multi-story Structures Subjected to Earthquake Excitation*. PhD Dissertation, California Institute of Technology, Pasadena, CA.

Giberson, M.F. (1969). Two nonlinear beams with definitions of ductility. *Journal of the Structural Division*, 95(ST2),137–57.

Gosain, N.K., Jirsa, J.O., & Brown, R.H. (1977). Shear requirements for load reversals on RC members. *Journal of the Structural Division*, 103(7), 1461–1476.

Hwang, H., Liu, J.B., & Chiu, Y.H. (2000). *Seismic fragility analysis of highway bridges*. Technical Report No. MAEC RR-4, Mid-America Earthquake Center, Urbana, IL.

Kobayashi, K. (2006). The seismic behavior of RC members suffering from chloride-induced corrosion. *Proceedings of the Second International Congress*, *fib*, June 2006.

Krätzig, W.B., Meyer, I.F., & Meskouris, K. (1989). Damage evolution in reinforced concrete members under cyclic loading. *Proceedings of the 5th International Conference on Structural Safety and Reliability (ICOSSAR89)*, San Francisco, CA, 2, 795–804.

Kumar, R., Gardoni, P., & Sanchez-Silva, M. (2009). Effect of cumulative seismic damage and corrosion on the life cycle cost of reinforced concrete bridges. *Earthquake Engineering and Structural Dynamics*, 38, 887–905.

Kunnath, S.K, & Reinhorn, A.M. (1989). *Inelastic three-dimensional response analysis of reinforced concrete structures subjected to seismic loads*. Technical Report No. NCEER-88-0041, University at Buffalo, The State University of New York, NY, USA.

Lupoi, A., Franchin, P., & Schotanus, M. (2003). Seismic risk evaluation of RC bridge structures. *Earthquake Engineering & Structural Dynamics*, 32(8), 1275–1290.

Malerba, P.G. (Ed.) (1998). *Limit and Nonlinear Analysis of Reinforced Concrete Structures*. International Centre for Mechanical Sciences (CISM), Udine, Italy (in Italian).

Malerba, P.G., & Bontempi, F. (1989). Analisi di telai in C.A. in presenza di non linearità meccaniche e geometriche. *Studi e Ricerche*, *Graduate School for Concrete Structures "F.lli Pesenti"*, Politecnico di Milano, Milan, Italy, 11, 209–224 (in Italian).

Mander, J.B., & Basoz, N. (1999). Seismic fragility curve theory for highway bridges in transportation lifeline loss estimation. *Optimizing post-earthquake lifeline system reliability*, TCLEE monograph no. 16 (Vol. 59) (pp. 315–338). Reston, VA: American Society of Civil Engineering and Design 1980.

Mander, J.B., Dhakal, R.P., Mashiko, N., & Solberg, K.M. (2007). Incremental dynamic analysis applied to seismic financial risk assessment of bridges. *Engineering Structures*, 29(10), 2662–2672.

Naito, H., Akiyama, M., & Suzuki, M. (2010). Ductility evaluation of concrete-encased steel bridge piers subjected to lateral cyclic loading. *Journal of Bridge Engineering*, 16(1), 72–81.

Nielson, B.G., & DesRoches, R. (2007a). Seismic fragility methodology for highway bridges using a component level approach. *Earthquake Engineering & Structural Dynamics*, 36(6), 823–839.

Nielson, B.G., & DesRoches, R. (2007b). Analytical seismic fragility curves for typical bridges in the central and southeastern United States. *Earthquake Spectra*, 23(3), 615-633.

Ou, Y.-C., Tsai, L.L., & Chen, H.H. (2012). Cyclic performance of large-scale corroded reinforced concrete beams. *Earthquake Engineering & Structural Dynamics*, 41(4), 593–604.

Ou, Y.-C., Wang, P.-H., Tsai, M.-S., Chang, K-C., & Lee, G.C. (2010). Large-scale experimental study of precast segmental unbonded post-tensioned concrete bridge columns for seismic regions. *Journal of Structural Engineering*, ASCE, 136(3), 255–264.

Oyado, M., Saito, Y., Yasojima, A., Kanakubo, T., & Yamamoto, Y. (2007). Structural performance of corroded RC column under seismic load. *Proceedings of the First International Workshop on Performance, Protection and Strengthening of Structures under Extreme Loading*, Whistler, Canada, August 20–22.

Padgett, J.E., & DesRoches, R. (2007a). Bridge functionality relationships for improved seismic risk assessment of transportation networks. *Earthquake Spectra*, 23(1), 115–130.

Padgett, J.E., & DesRoches, R. (2007b). Sensitivity of seismic response and fragility to parameter uncertainty. *Journal of Structural Engineering*, 133(12), 1710–1718.

Padgett, J.E., & DesRoches, R. (2008). Methodology for the development of analytical fragility curves for retrofitted bridges. *Earthquake Engineering & Structural Dynamics*, 37(8), 1157–1174.

Palermo, A., & Pampanin, S. (2008). Enhanced seismic performance of hybrid bridge systems: comparison with traditional monolithic solutions. *Journal of Earthquake Engineering*, 12(8), 1267–1295.

Pampanin, S., Christopoulos, C., & Priestley, M.J.N. (2002). *Residual Deformations in the Performance-Based Seismic Assessment of Frame Structures*. IUSS Press, Pavia, Italy.

Papia, M., Russo, G., & Zingone, G. (1988). Instability of longitudinal bars in RC columns. *Journal of Structural Engineering*, ASCE, 114(2), 445–461.

Park, R. (1986). Ductile design approach for reinforced concrete frames. *Earthquake Spectra*, 2(3), 565–619.

Park, Y.J., & Ang, A.H.S. (1985). Mechanistic seismic damage model for reinforced concrete. *Journal of Structural Engineering*, 111(4), 722–739.

Park, Y.J., Ang, A.H. S., & Wen, Y.K. (1987a). Damage-limiting aseismic design of buildings. *Earthquake Spectra*, 3(1), 1–26.

Park, R., & Paulay, T. (1975). *Reinforced concrete structures*. New York: John Wiley & Sons.

Park, Y.J., Reinhorn, A.M., & Kunnath, S.K. (1987b). IDARC: Inelastic damage analysis of reinforced concrete frame-shear-wall structures. *Technical Report NCEER-87-0008*, National Center for Earthquake Engineering Research, State University of New York, Buffalo, NY.

Penzien, J. (1993). Seismic design criteria for transporation structures. *Structural Engineering in Natural Hazards Mitigation: Proceedings of the ASCE Structures Congress 1993*, Irvine, CA, 1, 4–36.

Priestley, M.J.N., & Paulay, T. (1992). *Seismic Design of Reinforced Concrete and Masonry Buildings*. New York ,NY, USA, John Wiley & Sons.

Powell, G.H., & Allahabadi, R. (1988). Seismic damage prediction by deterministic methods: concepts and procedures. *Earthquake engineering & structural dynamics*, 16(5), 719–734.

Priestley, M.J.N., Calvi, G.M., & Kowalsky, M.J. (2007). *Displacement-Based Seismic Design of Structures*. Pavia: IUSS Press.

Priestley, M.N.J., Seible. F., & Calvi, G.M. (1996). *Seismic Design and Retrofit of Bridges*. John Wiley & Sons, New York, NY.

Saito, Y., Oyado, M., Kanakubo, T., & Yamamoto, Y. (2007). Structural performance of corroded RC column under uniaxial compression load. *First International Workshop on Performance, Protection & Strengthening of Structures under Extreme Loading*, Whistler, Canada.

SEAOC Vision 2000 Committee (1995). *Performance Based Seismic Engineering*. Sacramento, California: Structural Engineers Associate of California.

Sharpe, R.D. (1974). *The Seismic Response of Inelastic Structures*. PhD Thesis, Department of Civil Engineering, University of Canterbury, Christchurch, New Zealand.

Shinozuka, M., Feng, M.Q., Kim, H.K., & Kim, S.H. (2000a). Nonlinear static procedure for fragility curve development. *Journal of Engineering Mechanics*,126(12), 1287–1295.

Shinozuka, M., Feng, M.Q., Lee, J., & Naganuma, T. (2000b). Statistical analysis of fragility curves. *Journal of Engineering Mechanics*, 126(12), 1224–1231.

Sohanghpurwala, A.A. (2006). *Manual on Service Life of Corrosion-damaged Reinforced Concrete Bridge Superstructure Elements* (Vol. 558). National Cooperative Highway Research Program, Transportation Research Board National Research, Washington, DC, US.

Titi, A. (2012). *Lifetime Probabilistic Seismic Assessment of Multistory Precast Buildings*. PhD Thesis, Department of Structural Engineering, Politecnico di Milano, Milan, Italy.

Val, D.V., Stewart, M.G., & Melchers, R.E. (1998). Effect of reinforcement corrosion on reliability of highway bridges. *Engineering Structures*, 20, 1010–1019.

Williams, M.S., & Sexsmith, R.G. (1995). Seismic damage indices for concrete structures: a state-of-the-art review. *Earthquake Spectra*, 11(2), 319–349.

Yamamoto, T., & Kobayashi, K. (2006). Report of research project on structural performance of deteriorated concrete structures by JSCE 331-review of experimental study. *Proceedings of the International Workshop on Life Cycle Management of Coastal Concrete Structures*, Nagoake, Japan, 171-180.

Zienkiewicz, O.C., & Taylor R.L. (2000) *The Finite Element Method, Volume 1: The Basis*. Butterworth-Heinemann.

CHAPTER 5

SEISMIC RESILIENCE OF DETERIORATING STRUCTURES

1. The concept of resilience

In the last decade, resilience has become an emerging research topic in Civil Engineering, as the capacity of structures, infrastructure systems and entire communities to withstand and recover efficiently from extreme events (Bruneau *et al.* 2003). In general terms, resilience is the ability to reduce the chances of a shock, to absorb a shock if it occurs causing an abrupt reduction of performance and to recover quickly re-establishing normal performance. The concept of resilience has recently gained attention recognizing the fact that threats and disasters such as earthquakes, floods, hurricanes or terroristic attack cannot be averted. Even if every risk cannot be prevented, societies can enhance their resilience against various type of attacks minimizing the losses in terms of human lives, disruption and costs.

To this aim, the concept of resilience can be applied to both preventive assessment (Cimellaro *et al.* 2010b, 2010c Decò *et al.* 2013) and disaster management (Bocchini *et al.* 2012, Bocchini & Frangopol 2012a). In the first case, the resilience assessment of existing structures allows the formulation of preventive strategies and the planning of maintenance interventions. In fact, risk mitigation is based on the evaluation of the functionality of a system and its vulnerability with respect to natural extreme

events, such as earthquakes, or disasters like explosions. Based on the information available, this is usually performed in a probabilistic context (Chang & Shinozuka 2004), in order to satisfy the need of the modern society which is increasingly less disposed to suffer disruptions and more demanding in limiting losses and costs related to a catastrophic event. On the other hand, extreme events still occur. The small amount of information usually available soon after and the need for quick effective tools that assist the decision making process have led to the development of resilience analysis characterized by a deterministic approach (Bocchini & Frangopol 2012b).

The concept of resilience has been also recognized by the Authorities as a crucial factor in the protection and defense of a community. The *United Nations International Strategy for Disaster Reduction* (UN/ISDR) defined the resilience as *"the ability of a system, community or society exposed to hazards to resist, absorb, accommodate to and recover from the effects of a hazard in a timely and efficient manner, including through the preservation and restoration of its essential basic structures and functions."* (UN/ISDR 2009). Resilience is hence strictly connected to the concept of system functionality. Different structures and systems can have their functionality defined in different ways. Even for the same system, multiple parameters can be taken as indicators of system functionality.

Another issue is related to the quantification of the functionality. In particular, the concept of resilience, which is suitable for describing the behavior of a community functionality of a network system, has not yet been defined completely for assessing the performance of a structure subjected to an extreme event. Several studies have been carried out recently in order to investigate which parameters are the most appropriate to quantify the structural resilience. Particular attention has been reserved to seismic resilience, being the earthquakes one of the major risks our communities have to face. The quantitative measure of resilience became one of the main themes at the Multidisciplinary Center for Earthquake Engineering Research (MCEER). The framework proposed by MCEER aims to improve the resilience of infrastructure systems, hospitals and communities in general in terms of reduced probability of system failure, reduced consequences due to failure and reduced time to system restoration (Chang *et al.* 2008, Cimellaro *et al.* 2009, 2010a, Kafali & Grigoriu 2008, Renschler *et al.* 2010).

The quantification of resilience is mainly related to two aspects: the estimation of the losses and the definition of the functionality recovery. The estimation of the losses associated to an extreme event requires first of all the definition of damage descriptors. These can be different for every specific scenario considered, but considering all the possible cases some common parameters can be identified. Losses can be distinguished in structural and non-structural losses. Both of them determine the functionality decrease of a system. Moreover, the estimation of the cost associated to each loss allows to translate the damage in monetary terms. On the other hand, the recovery of functionality depends on multiple factors related to system and/or society response. The importance of the system, the availability of resources and the organization of the community are some of the factors affecting the rapidity of the recovery process and the way how a systems recovers its functionality target.

The various definitions of resilience given for network systems, critical facilities and structures and the corresponding evaluation of the losses are presented in the following. Available recovery models are reviewed as well. The investigation is then focused on the evaluation of the structural functionality and resilience of deteriorating systems (Titi & Biondini 2013). In fact, deterioration processes affect progressively the lifetime functionality of the structures, which can be evaluated in terms of seismic capacity. As a consequence, a deteriorated structure may exhibit a reduced resilience at the occurrence of an earthquake event. The proposed approach for the lifetime assessment of seismic resilience is then applied to the case study of the concrete bridge presented in Chapter 4.

1.1. Quantifying resilience

Resilience can be defined as the ability of communities or systems to mitigate hazards, contain the effects of disasters when they occur, and carry out recovery activities in order to minimize disruption. In particular, the seismic resilience is the ability of a community's infrastructure (lifelines, road network, structures) to perform during and after an earthquake. Emergency response and strategies that cope with the event and contain the losses enable the community to return to levels of predisaster functioning, or other acceptable levels as rapidly as possible (Bruneau *et al.* 2003).

In the definition of resilience, it is logical to start analyzing resilience of organizations whose functions are essential for communities after an extreme event, such as water and power lifelines, hospitals and organizations that have the responsibility for emergency management. For example, hospital functionality is essential to provide emergency care for injured victims. Water is an essential lifeline service that must be provided continuously even in emergency conditions. The first studies related to resilience have been focused on the definition of functionality of these systems, which are critical in the emergency response to an extreme event. Moreover, the resilience of a community should be enhanced by preventive interventions, when the extreme event has not occurred yet.

A resilient system shows:

- reduced failure probabilities of the critical components and infrastructures;
- reduced consequences from failures, in terms of lives lost, damage and negative economic and social consequences;
- reduced time to recovery to a pre-event or target level of performance.

This approach is based on the monitoring of a measure $Q(t)$ which is assumed to be the indicator of the "quality" of a community or infrastructure functionality (Figure 5.1). This performance level can range from 0% to 100%, where 100% means no degradation in service and 0% means complete disruption. If an extreme event occurs at time t_0, the performance of the system suffers an abrupt reduction. However, the system can still show a residual functionality Q_r. Restoration of the system

is expected to occur over time, until time t_h, which is the investigated time horizon. By the time t_h, the system can recover its full functionality or have reach a functionality target Q_t.

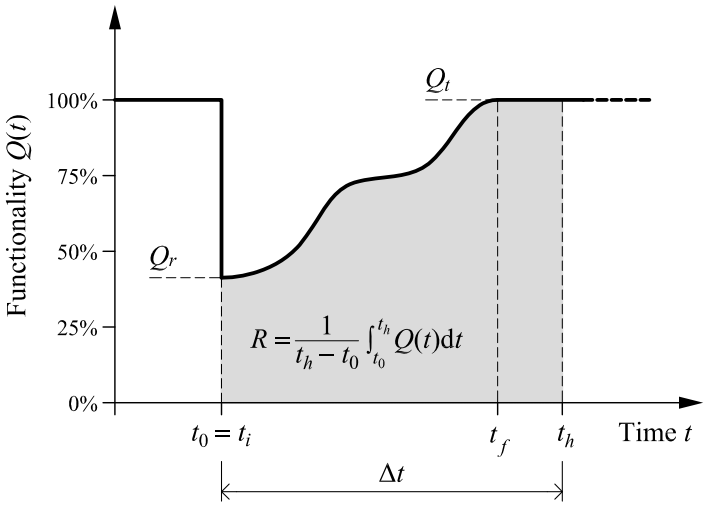

Figure 5.1 – Conceptual definition of resilience.

Resilience R can be computed as (Bocchini *et al.* 2012, Figure 5.1):

$$R = \frac{1}{t_h - t_0} \int_{t_0}^{t_h} Q(t)dt \tag{5.1}$$

by considering resilience as the area underlying the functionality profile, normalized over the interval period between t_0 and t_h. Resilience depends entirely on the residual functionality of the system after the occurrence of an extreme event and on the functionality recover over time.

Therefore, in quantitative terms, resilience is defined as a normalized function indicating the capability to sustain a level of functionality or performance for a given structure, infrastructure or community over a period of time including disruption and recovery after an extreme event (Cimellaro *et al.* 2005).

1.2. Dimensions of resilience

The resilience of a system can be declined in the following four properties that can be assumed as the parameters to measure resilience:

- robustness;
- resourcefulness;
- redundancy;
- rapidity.

Robustness

Robustness is the strength or ability of elements and systems to withstand a given level of stress or demand, without suffering disproportioned degradation or loss of function. The robustness of a system determines the residual functionality after an extreme event. In fact, under the same conditions, a more robust system will show a higher residual functionality than a less robust system (Figure 5.2). The robustness r can be expressed as (Cimellaro *et al.* 2010b):

$$r = 1 - L(\mu_L + \alpha\sigma_L) \tag{5.2}$$

where L is a random variable representing the total losses and expressed as a function of the corresponding mean μ_L and standard deviation σ_L and α is a multiplier corresponding to a specific level of losses. In this definition, robustness is therefore also the capacity of keeping the variability of the losses within a narrow band.

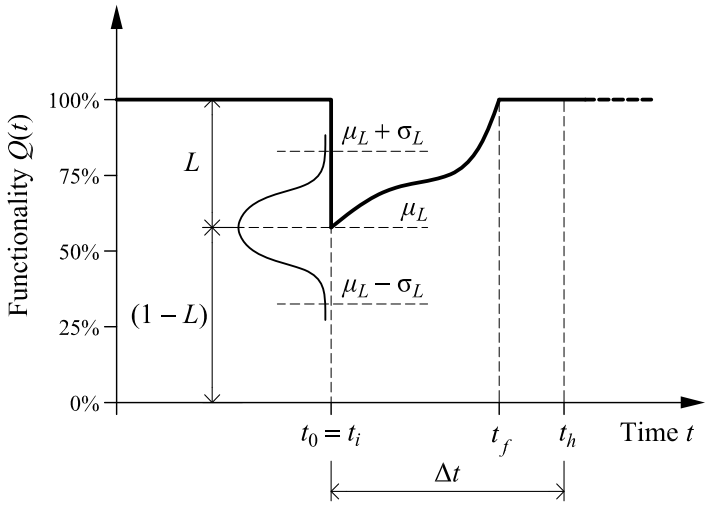

Figure 5.2 – Influence of robustness on the resilience of a system (after Cimellaro *et al.* 2010b, adapted).

Resourcefulness

Resourcefulness is the capacity to identify problems, establish priorities and mobilize resources when conditions threaten to disrupt some elements. In other terms, resourcefulness is the ability to apply material (monetary, physical, technological and informational) and human resources in the process of recovery of system functionality. This concept is better clarified in Figure 5.3. The resilience is expanded in the third dimension illustrating that added resources can be used to reduce time to recovery. In theory, if infinite resources were available, time to recovery would asymptotically approach zero. However, even in the presence of enormous financial and labor capabilities, practical limitation will impose a minimum time to recovery. On the contrary, where resources are scarce, time to recovery lengthens, approaching infinity in the absence of any resources. It has to be observed that

even in a resourceful society, the time to recover may become longer due to inadequate planning, organizational failures or ineffective policies (Bruneau & Reinhorn 2007).

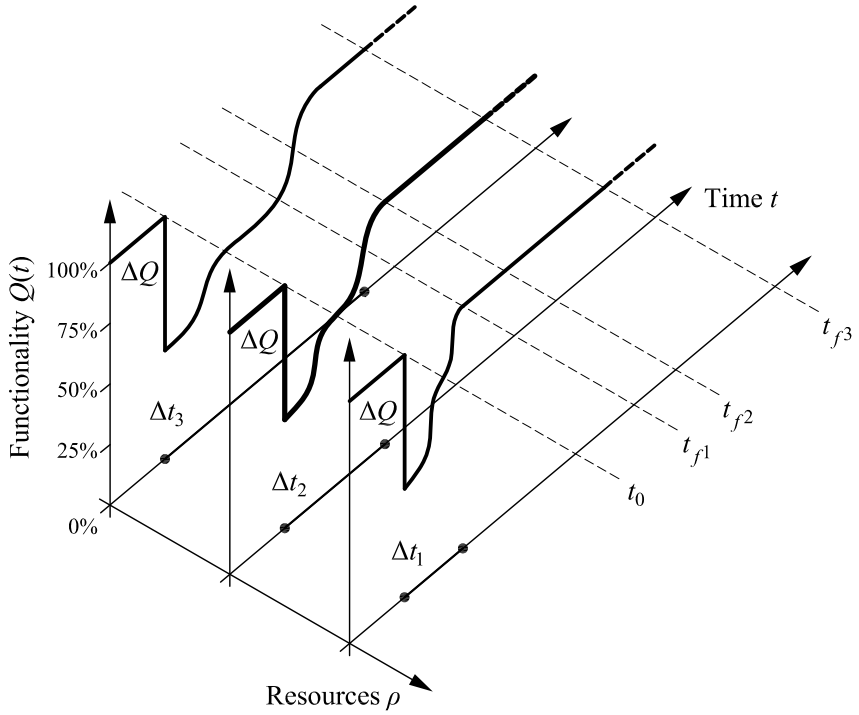

Figure 5.3 – Expansion of resilience in the resourcefulness dimension (after Bruneau & Reinhorn 2007, adapted).

Redundancy

Redundancy is the extent to which alternative elements or systems exist being substitutable. In the case of disruption, degradation or loss of functionality, other elements or components of a system allow to keep functional requirements satisfied. According to the Earthquake Engineering field, for example, redundancy is the quality of having alternative paths in the structure by which lateral forces can be transferred, which allows the structure to remain stable following the failure of any single element (FEMA 356 2000). In other words, it describes the availability of alternative resources in the recovery process of a system.

As for resourcefulness, this concept can be better clarified graphically by grouping multiple plots of the type shown in Figure 5.3. While each individual 3D resilience space could represent, for example, a single hospital, the collection of those (Figure 5.4) represents the resilience of all acute care facilities over a geographical area. Another example could be the one of a road network, where critical and strategic parts such as bridges are interconnected each other. The availability of multiple interconnections that allow the functionality of the system, even if with detouring, represent the redundancy of the road network. By the property of redundancy, resilience can be defined in a fourth dimension.

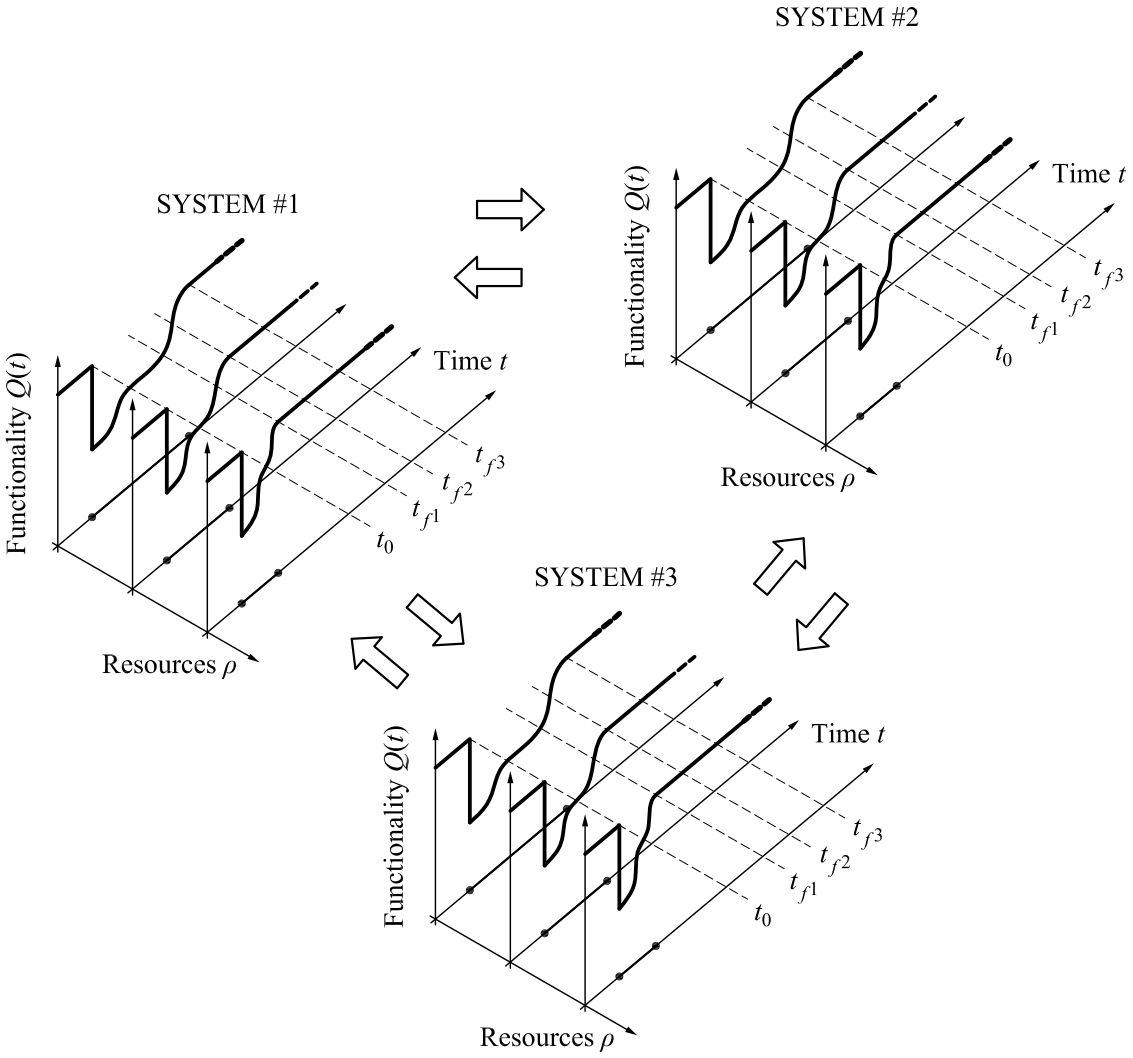

Figure 5.4 – Expansion of resilience in the redundancy dimension (after Bruneau & Reinhorn 2007, adapted).

Rapidity

Rapidity is the capacity to meet priorities and achieve goals in a timely manner in order to contain losses, recover functionality and avoid future disruption. It is graphically represented by the slope of the functionality during the recovery curve during the recovery time (Figure 5.5) and can be expressed as follows:

$$v = \frac{dQ(t)}{dt} \qquad \text{for} \quad t_i \le t \le t_f \tag{5.3}$$

An average value of the rapidity can be estimated by knowing the total losses L and the total recovery time to restore full functionality:

$$v = \frac{L}{t_f - t_0} \qquad \text{for} \quad t_i \le t \le t_f \tag{5.4}$$

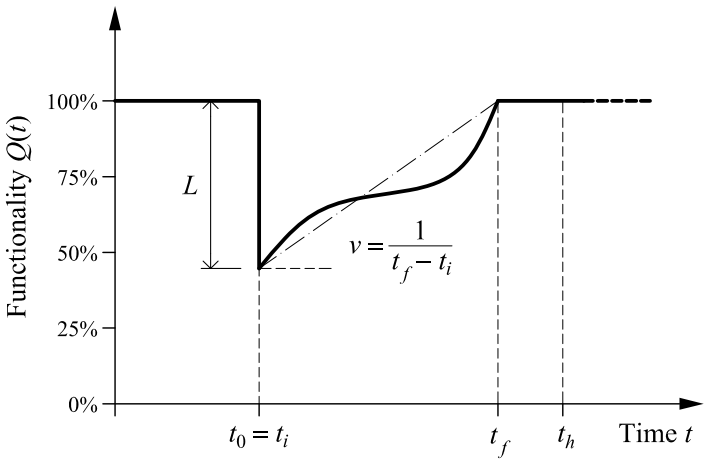

Figure 5.5 – Influence of rapidity on the resilience of a system (after Cimellaro *et al.* 2010b, adapted).

It is through redundancy and resourcefulness, which are the means of resilience, that rapidity and robustness, which are the ends of resilience, can be improved in a system. In particular, resourcefulness and redundancy are strongly coupled depending both on human factors and available resources. Resilience results to be a function of these four quantities, but while the influence of robustness and rapidity is clear, the influence of resourcefulness and redundancy is more complex.

Beyond robustness, resourcefulness, redundancy and rapidity, resilience can be characterized by considering the following four dimensions:

- *T*echnical;
- *O*rganizational;
- *S*ocial;
- *E*conomic.

These four dimensions of resilience are usually indicated by the acronym *TOSE*. The technical dimension of resilience refers to the ability of physical systems to perform with acceptable levels when subjected to an extreme event. The organizational dimension of resilience refers to the capacity of organizations that are responsible of managing the emergency to make decisions and take effective actions. The social dimension of resilience consists of measures oriented to reduce the loss of critical services after the occurrence of an extreme event. Similarly, the economic dimension of resilience refers to the capacity to reduce both direct and indirect economic losses resulting from earthquakes (Bruneau & Reinhorn 2007). Of these four dimensions, the technical and organizational dimensions are the most pertinent to the performance and resilience of critical structural and infrastructural systems. The social and the economic dimensions are related to the performance and resilience of the community as a whole. Each resilience dimension can be declined considering the performance criteria of robustness, redundancy resourcefulness and rapidity, as indicated by Bruneau *et al.* 2003 (Table 5.1).

Table 5.1 – Resilience performance measures and criteria (Bruneau *et al.* 2003).

PERFORMANCE MEASURES	PERFORMANCE CRITERIA			
	Robustness	**Redundancy**	**Resourcefulness**	**Rapidity**
TECHNICAL	Damage avoidance and continued service provision	Backup/duplicate systems, equipment and supplies	Diagnostic and damage detection methodologies and technologies	Optimizing time to return to pre-event functional levels
ORGANIZATIONAL	Continued ability to carry out designated functions	Backup resources to sustain operations	Plans and resources to cope with damage and disruption	Minimize time needed to restore services and perform key response tasks
SOCIAL	Avoidance of casualties and disruption in the community	Alternative means of providing for community needs	Plans and resources to meet community needs	Optimizing time to return to pre-event functional levels
ECONOMIC	Avoidance of direct and indirect economic losses	Untapped or excess economic capacity	Stabilizing measures	Optimizing time to return to pre-event functional levels

In conclusion, Renschler *et al.* (2010) identified seven dimensions of community resilience represented by the acronym *PEOPLES*: *P*opulation and Demographics, *E*nvironmental/Ecosystem, *O*rganized Governmental Services, *P*hysical Infrastructure, *L*ifestyle and Community Competence, *E*conomic Development, and *S*ocial-Cultural Capital. This nomenclature highlights that both the physical and environmental assets as well as the socio-economic-political/organizational aspects influence the resilience of a community. *PEOPLES* Resilience Framework represents one of the most ongoing research that links the resilience properties (robustness, resourcefulness, redundancy and rapidity) and the resilience dimensions (technical, organizational, societal and economic) in order to measure the disaster resilience of communities.

1.3. Resilience time dependence

An important aspect that should be taken into account in the resilience framework is the time dependence of system functionality. This is evident for reinforced concrete structures, which performance is affected by the deterioration processes over lifetime, as assessed in the previous Chapters. Aging and environmental aggressiveness progressively modify the functionality of the structures and consequently the resilience of the structural system. While in the case of an extreme event the loss of functionality is abrupt, the damage caused by deterioration arises progressively in time. Therefore, the pre-event functionality of the system should be considered time-variant (Titi & Biondini 2013), while up to now it has been considered constant both before the occurrence of the extreme event and after the completion of the restoration process.

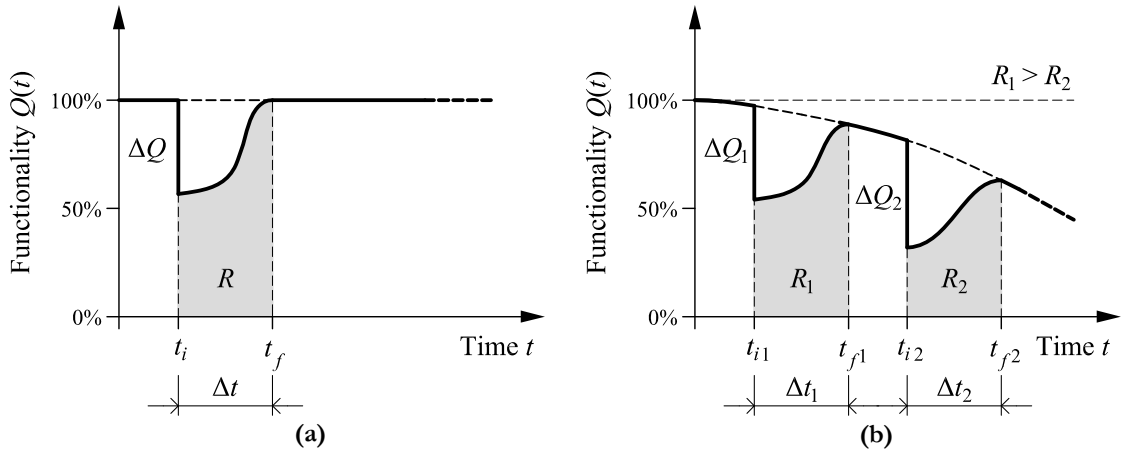

Figure 5.6 – (a) Functionality of a non-deteriorating system with occurrence of the extreme event at time t_0 and recovery over the time interval Δt; (b) Functionality of a deteriorating system with occurrence of the extreme events at time t_{0k} and recovery over the time interval Δt_k, $k = 1, 2, \ldots$.

Figure 5.6 shows the difference in the time evolution of system functionality for non-deteriorating and deteriorating systems. For non deteriorating systems (Figure 5.6a) the resilience results to be dependent only on the recovery profile of the functionality function $Q(t)$ over the time interval between t_0 (the occurrence of the event) and t_h (the completion of the restoration process or the investigated time horizon). However, the effects of damage due to aging and environmental aggressiveness could reduce over time the system functionality. As a consequence, for deteriorating systems the time of occurrence of the extreme event plays a crucial role in the evaluation of the resilience.

Based on that, several parameters in the definition of system resilience are affected by the time-dependence of the functionality. First, the initial functionality at the occurrence of the event is time-variant, since in general the functionality decreases over time. The later in lifetime the event will occur, the lower the initial functionality $Q(t_0)$ will be. Second, the loss of functionality $\Delta Q(t_0)$ results to be a time-function as well.

In fact, since it is dependent on the initial properties of the systems at time t_0, the losses will be proportional not just on the magnitude of the event but also on the time-variant functionality of the system (Figure 5.6b). In fact, recent studies showed that the coupling between the environmental deterioration and the seismic damage has to be taken into account in a resilience assessment (Titi & Biondini 2013). Finally, the functionality $Q_f(t)$ depends on time since the target of post-recovery interventions can be chosen to restore the full functionality of the original state or the pre-event functionality considering the aging of the structure.

Therefore, the following aspects should be taken into account for deteriorating systems:

- effects of environmental aggressiveness;
- effects of post-recovery interventions;
- effects of maintenance interventions.

Effects of environmental aggressiveness

Environmental aggressiveness affects the structural performance over the lifetime. Increasing the severity of the environmental exposure, which is mainly related to the concentration of the aggressive agents in the atmosphere, the structural system suffers a more significant decay of its performance. The functionality and resilience of the system will vary accordingly, being lower as the severity of the exposure increases. This is shown in Figure 5.7 considering the same loss of functionality ΔQ.

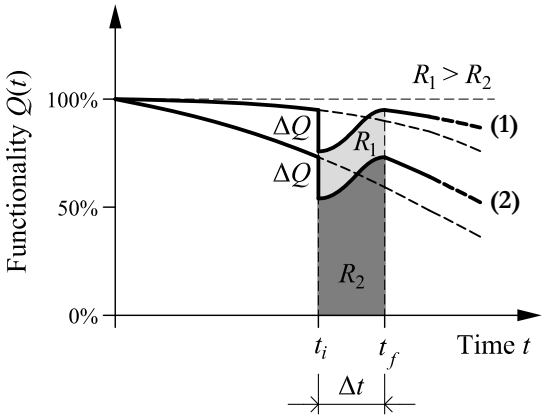

Figure 5.7 – Effects of the environmental aggressiveness in the resilience evaluation: (1) slight/moderate exposure; (2) severe exposure.

Effects of maintenance interventions

Over lifetime, the system could be subjected to maintenance programs aimed to improve its functionality, preserve its serviceability and extend its lifetime. The effect of these interventions is represented by a sudden increase of the functionality ΔQ_m. Consequently, systems under a maintenance program will show a greater resilience at the occurrence of an extreme event, as shown in Figure 5.8.

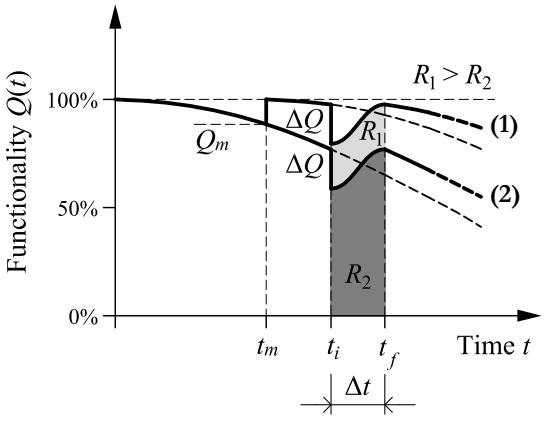

Figure 5.8 – Effects of maintenance actions in the resilience evaluation: (1) with intervention; (2) without intervention.

Effects of post-recovery interventions

The functionality $Q(t)$ targeted by post-event interventions is a decisional parameter that may depend on the importance of the structure, on the resources available and on time limitations. If the structure plays a strategic role, it is preferable to restore the full functionality. However, there could be restrains due to the availability of resources, implying a partial restoring of the functionality. Moreover, limitation in time in order to minimize disruption could lead to an initial partial restoring rather than a longer full restore of functionality.

Figure 5.9 shows the effectiveness of post-recovery actions, ranging from the restoring of the full functionality and the restoring of the pre-event functionality taking into account the evolution of system degradation. These two limit conditions will be indicated in the following as total recovery and partial recovery.

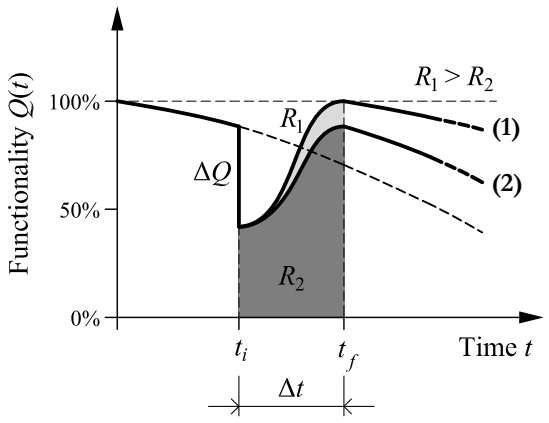

Figure 5.9 – Effects of the post-recovery interventions in the resilience evaluation: (1) total restoring of the initial functionality; (2) partial restoring of the pre-event functionality.

2. The definition of functionality

In order to quantify the resilience of a system, a measure of functionality $Q(t)$ and its evolution in time have to be defined. The functionality $Q(t)$ has been defined as a parameter ranging between 0% and 100% representing the quality of network systems, infrastructures and communities (Bruneau *et al.* 2003, Bruneau & Reinhorn 2004). Hence, the resilience with respect to a specific event can be measured by the size of the expected degradation in quality, which is the probability of failure of the system over the recovery time.

Chang & Shinozuka (2004) defined the functionality over time as the probability of a system or a community of meeting both robustness and rapidity standards in an emergency scenario. The disaster resilience of a community can be measured with respect to the network physical condition, the water service, the population still living at home and the economic activity. In this sense, the functionality of a system is declined in the technical, organizational, social and economic performance measure of resilience.

Functionality is measured as a non-dimensional quantity and mathematically defined as a non stochastic process (Bruneau & Reinhorn 2007, Cimellaro *et al.* 2006). Cimellaro *et al.* (2010b) provided the following definition of functionality $Q(t)$ as a function of time:

$$Q(t) = 1 - L(I, \Delta t)[H(t - t_0) - H(t - (t_0 + \Delta t))] f_{rec}(t, t_0, \Delta t) \qquad (5.5)$$

where I is the intensity measure of the event, $L(I, \Delta t)$ is the loss function, H is the Heaviside step function, Δt is the recovery time of the event occurring a t time t_0 and f_{rec} is the recovery function.

Though being clarifying about the concept of resilience, these approaches are more conceptual than practical in the quantification of the functionality of a system. Since functionality cannot be defined univocally due to the different parameters characterizing each system, the functionality of network systems, critical facilities and structures has to be investigated separately in order to clarify its quantitative evaluation.

2.1. Functionality of network systems

For geographically distributed systems designated to provide a service, such as a power grid or a water distribution network, the quantification of functionality after an event is rather simple, being kilowatts, liters or households provided with service quantifiable values. The definition of the functionality of electric, hydraulic and road network system has been investigated by recent studies and the proposed models have been applied to several case studies.

Çağnan *et al.* (2006) applied a restoration model to the post-earthquake electric power recovery in Los Angeles after the 1994 Northridge earthquake by considering the number of customers restored

over time under different scenarios. Shinozuka (2009) proposed a model to simulate the robustness and resilience of a water and power system under a set of scenario earthquakes consistent with the seismic hazard of Los Angeles area. The model is able to evaluate the performance of the systems under different network damage scenarios in technical terms (power supplied in each service area), societal (rate of customers without power supply), organizational (repair and restoration efficiency) and economic (regional output or employment loss). The optimal post-earthquake restoration is the one that minimizes the average time each customer is without power supply (Xu *et al.* 2006) or that provides differential rationing of the available electricity in order to minimize total economic losses (Rose *et al.* 1997).

Rose (2004) evaluated the economic resilience of the water system of Portland (Oregon, US) by simulating the water input disruption for alternative combinations of earthquake types and mitigation options. The role of water system as a critical infrastructure service supporting the urban economy has been investigated also by Chang *et al.* (2002). In this approach, the severity of the water delivery system disruption is evaluated in terms of consequent business closure, thus already taking into account the economic losses.

For a road network, bridges are usually the key elements that assure the functionality of the system after an extreme event. Therefore, resilience can be measured by the ability to recover the serviceability of the bridges in a fast an efficient way in order to keep the connectivity between the points of the network (Bocchini & Frangopol 2012a, 2012b). Depending on the bridge damage levels and the bridge restoration activities in progress, the traffic flows on the network segments can be assessed for a specific scenario and the network performance indicator is estimated as follows:

$$\Gamma(t) = \frac{1}{\gamma_T TTT(t) + \gamma_D TTD(t)} \tag{5.6}$$

where $TTT(t)$ is the total travel time, i.e. the sum of the time spent by all the users of the network to reach their destination, $TTD(t)$ is the total travel distance, γ_T is a balancing factor associated with the time spent by the network users and γ_T is a similar factor associated with the distance traveled. The total travel time depends on the time needed to cover each segment of the network, while the total travel distance is related to the connectivity between the nodes of the network and the eventual detouring. Eqn. 5.6 can be used to assess the performance of the network ranging between Γ^{100} where all the bridges are in service and Γ^{0} where all are out of service. With these two limit cases, the functionality of the road network $Q(t)$ is computed as:

$$Q(t) = \frac{\Gamma(t) - \Gamma^0}{\Gamma^{100} - \Gamma^0} \tag{5.7}$$

The functionality $Q(t)$ ranges between 0% and 100% as customary in literature and takes simultaneously into account all the traffic flows of any complex network.

The allowable traffic carrying capacity due to closure decisions and repair procedures is investigated in Padgett & DesRoches (2007) basing on the data collected by a survey of US Department of Transportation bridge inspectors and officials. This data is utilized to assess the probability of meeting various damage states. The recovery of the functionality is then defined in the form of probability matrices where the probability of the bridge closure for a certain time depends on the severity of the damage suffered by each component of the bridge (damage at the approaches, at the expansion joints, to columns…).

2.2. Functionality of critical facilities

The serviceability of critical facilities, such as hospitals or ports, in the aftermath of an extreme event would significantly contribute to enhancing the seismic resilience of communities. However, the definition of functionality is less immediate since there is no engineering unit to measure the functionality of these facilities.

Several proposals have been formulated to this regard (Bruneau & Reinhorn 2004, 2007, Cimellaro *et al.* 2010b). A first option is to quantify the functionality of the hospital system of a region by the percentage of healthy population after an extreme event, normalized with respect to the total healthy population before that event. A drop in population health would occur when individuals are killed during an extreme event or deaths can occur after the event due to insufficient health care capacity. A second option focuses on relating the resilience of facilities to the number of patients per day as a measure of the treatment capacity of the health care facilities. As an alternative option, Cimellaro *et al.* (2010b) defined the functionality of a single hospital as normalized waiting time distinguishing between the waiting time before and after the critical condition, which corresponds to the maximum capacity of the hospital.

Ports could have an important role in the community resilience as well. Chang (2000) investigated the impact of the 1995 Kobe earthquake on the Port. The functionality of the Port is estimated by the international container traffic, showing a decrease after the event in comparison with other ports, thus implying significant economic losses for the city of Kobe.

2.3. Functionality of structures

A first attempt in the definition of the functionality of structural systems is proposed by Bruneau & Reinhorn (2004, 2007), distinguishing between structural and non-structural components. Since great uncertainties are inherent to the field of Structural Engineering and in particular of Seismic Engineering, the quantification of seismic resilience has to be carried out in probabilistic terms (Figure 5.10). Different limit states can be defined according to the loss in the structural integrity. A

serviceability level is defined as a small loss of integrity, while the collapse level is defined as the maximum loss prior to collapse. Moreover, a proportional coupling often exists between the time to recovery and the initial loss of structural integrity. Every definition of the limit states is a random variable, represented by the bell-curves in Figure 5.10.

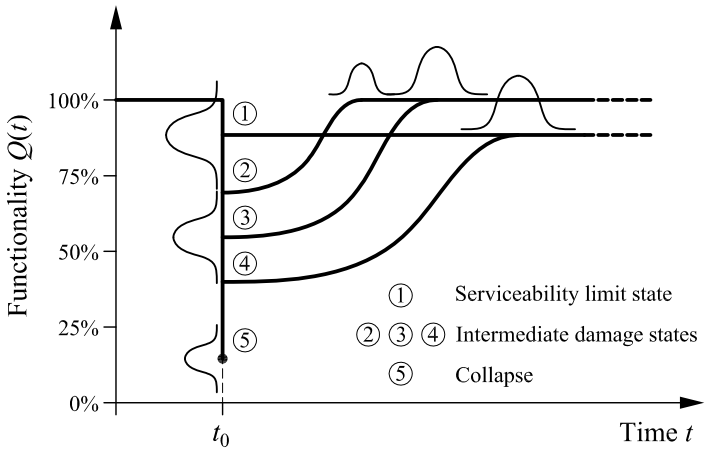

Figure 5.10 – Probabilistic aspect of seismic resilience (after Bruneau & Reinhorn 2004, adapted).

In this approach, the functionality of the structure is evaluated in terms of "investment value" in the structural/non structural systems. Even in the case of no structural loss, non-structural damage may occur. The probable non-structural loss can be expresses by the product of the probability of exceeding the performance limit state and of the value of replacing the damaged component versus the initial investment. The drop of the resilience curve at time t_0 can hence be evaluated, as well as the time to recovery to pre-earthquake conditions depending on the severity of the damage. Similar considerations can be done in the case of both structural and non-structural damage.

Moreover, Bruneau & Reinhorn (2007) observed that the financial investment needed to restore the pre-event functionality correspond to the cost required to shift the fragility curve to lower probabilities of failure. On the contrary, the lack of recovery actions could lead to increased probabilities of failure of the system.

In this work, the system functionality Q of structure under seismic hazard is related to the seismic capacity in terms of peak ground acceleration a_g:

$$Q = Q(a_g) \tag{5.8}$$

As a first assumption, a linear relationship can be assumed between structural functionality and seismic capacity, considering the dualism "greater seismic capacity-greater structural functionality" (Figure 5.11a). A minimum $a_{g,\min}$ and a maximum $a_{g,\max}$ corresponding to 0 and full functionality respectively define the range of the functionality function $Q(a_g)$:

$$Q = \frac{a_g - a_{g,\min}}{a_{g,\max} - a_{g,\min}} \tag{5.9}$$

Another approach could be based on the definition of a stepwise relationship related to seismic capacity thresholds and discrete functionality limit states (Figure 5.11b). This approach can be used in post-earthquake assessments where the qualitative evaluation of the structure functionality is performed identifying damage states by visual inspection. In this case, a drop in the functionality function corresponds to a reduction of the seismic capacity of the damaged structure.

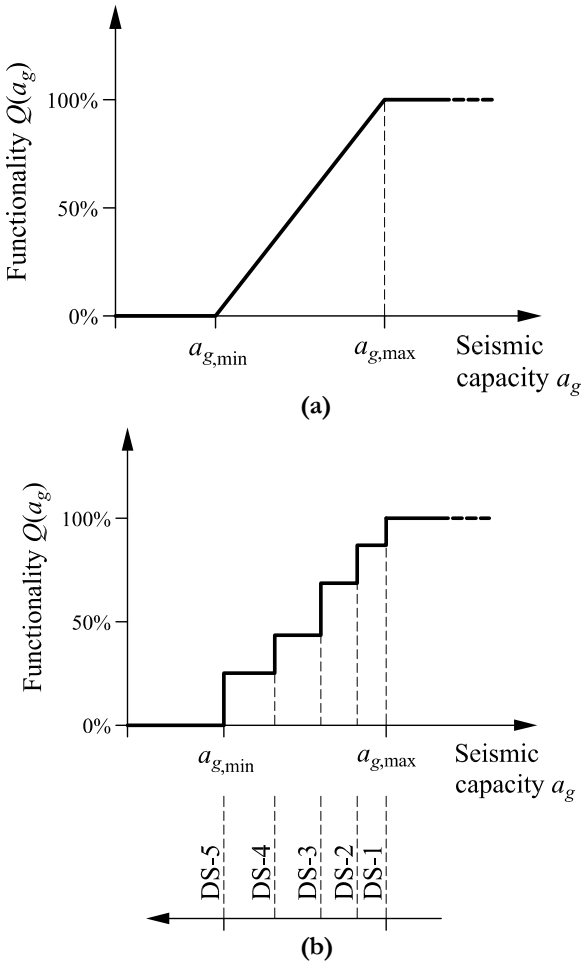

Figure 5.11 – (a) Linear relationship between system functionality and seismic capacity in the range $a_{g,\min}$ and $a_{g,\max}$; (b) Definition of discrete functionality limit states.

Further aspects have to be taken into account if the functionality of deteriorating systems is considered. In fact, the seismic capacity $a_g = a_g(t)$ is expected to vary over time due to deterioration processes. The time evolution of the seismic capacity may be nonlinear (Figure 5.12a). Moreover, it is possible to identify a range of peak ground accelerations between a minimum $a_{g,\min}$ and a maximum $a_{g,\max}$ value that correspond to the minimum and maximum level of performance of the structure respectively.

In fact, the structural functionality is expected to vary over time as well depending on environmental aggressiveness. The time evolution of the system functionality depends on the structural typology and in general it is assumed to show a decrease as the seismic capacity reduces due to deterioration processes. In this way, structures showing a seismic capacity higher than $a_{g,\max}$ are assumed to satisfy a prescribed limit state, while deteriorated structures with a seismic capacity lower than $a_{g,\min}$ do not assure the structural safety anymore (Figure 5.12b).

If the minimum seismic capacity corresponds to the maximum allowable functionality loss $a_{g,\min} = 0$ and the maximum seismic capacity is set equal to the nominal capacity of the uncorroded structure $a_{g,\max} = a_{g0,nom}$, the time-variant functionality can be expressed as the ratio between the actual and original capacity. The peak ground acceleration $a_g(t)$ is then assumed as time-variant functionality indicator as follows:

$$Q(t) = \frac{a_g(t)}{a_{g0,nom}} \tag{5.10}$$

where $a_g = a_g(t)$ is the seismic capacity of the deteriorating system at time t and $a_{g0,nom}$ is the nominal seismic capacity of the undamaged system at time $t = 0$. Peak ground acceleration values $a_g(t)$ associated to the reaching of prescribed limit states, from damage limitation up to collapse, can be considered in the definition of the lifetime functionality $Q(t)$ (Titi & Biondini 2013).

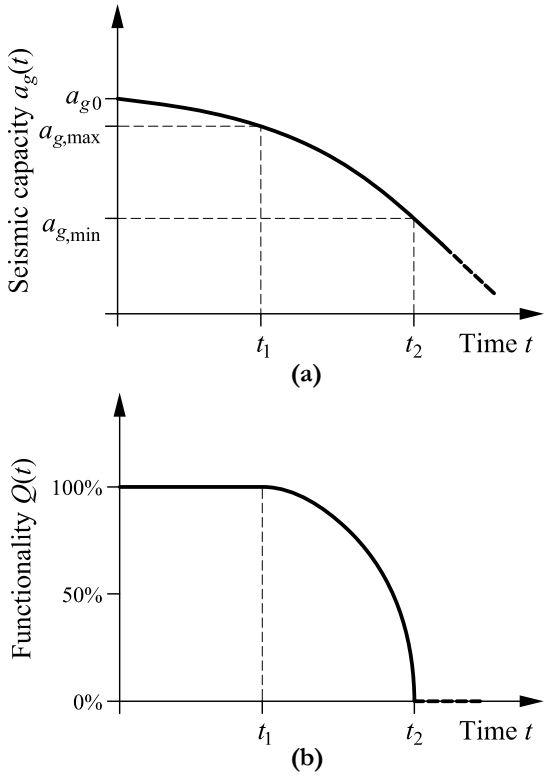

Figure 5.12 – (a) Qualitative time evolution of the seismic capacity of deteriorating structures and (b) corresponding system functionality.

Since the seismic capacity a_g is proportional to the resisting base shear of a structure, in nonlinear static analyses the functionality can be expressed as the ratio between the total base shear $F_{base}(t)$ at different time instants and the nominal base shear capacity at the beginning of lifetime $F_{base,nom,0}$:

$$Q(t) = \frac{F_{base}(t)}{F_{base,nom,0}} \tag{5.11}$$

3. The estimation of the losses

The evaluation of the losses is a key point in the definition of the resilience of a system. Losses are evaluated by the difference between the initial (pre-event) functionality and the residual (post-event) functionality. As for the functionality, losses depend on the type of system considered.
For an electric power plant, the losses correspond to electricity outage at the production site (Rose *et al.* 1997) or to the damage to the transmission substations (Çağnan *et al.* 2006). For a water system, losses are represented by the water outage pattern and by the consequences of the economic activities due to the disruption of the service (Chang & Shinozuka 2004, Chang *et al.* 2002).
In any case, the quantification of the drop of functionality implies a certain uncertainty, thus losses are considered as random variables in a probabilistic approach (Cimellaro *et al.* 2010b). In fact, the estimation of the losses is related to the probabilities of damage and/or failure of the system, which depend on the hazard considered. The risk analysis is usually carried out by the use of fragility curves, which evaluate the probability of exceeding a certain damage limit state with respect to the intensity measure chosen to characterize the extreme event. A methodology for loss estimation is proposed in FEMA (2009), where the probability of damage is estimated for different structural typologies based on post-event collected data. For bridges, the losses are measured by the reduced traffic capacity related to the damage sustained by each bridge component, which is estimated on the basis of survey results in the form of damage state probability matrices (Padgett & DesRoches 2007).
The evaluation of the damage suffered by the system implies the estimation of the repair costs and of the economic losses (Alesch *et al.* 2003, Shinozuka 2009). The costs depend on the post-recovery target functionality as well (Bocchini & Frangopol 2012a, 2012b). Bruneau & Reinhorn (2007) proposed to measure the loss function as the ratio of the actual loss $L_{LS}(t_0)$ (monetary, physical, technological, informational) at an expected performance limit state in regard to the cost of maintaining the full performance measure *FP* expressed in the same units of the loss, expressed as:

$$L(t_0) = \sum_j [L_{LS,j}(t_0)/FP] P_{LS,j} R_j \geq LS_j \tag{5.12}$$

where $P_{LS}(R \geq LS)$ is the probability that the expectation R will exceed the performance limit state LS, i.e. $P_{LS}(R \geq LS)$ is the fragility function of a system damage state.
In order to get more detailed information about the functionality of the system, the losses should be divided in structural losses L_S and non-structural losses L_{NS} (Cimellaro *et al.* 2005, 2006, 2010b). The physical structural losses are expressed as ratio of building repair and replacement costs, taking into account the depreciation annual rate in the time interval between the initial investment and the time occurrence of the event. The non-structural losses should be further subdivided in:

- direct economic losses $L_{NS,DE}$: these losses are evaluated similarly to the structural losses and usually refer to the contents losses;

- direct casualties losses $L_{NS,DC}$: they are expressed as the ratio between the number of persons injured over the total number of occupants;
- indirect economic losses $L_{NS,IE}$: these losses are related to different factors, such as business interruptions, relocation expenses and rental income losses;
- indirect casualties losses $L_{NS,IC}$: they are expressed as the ratio between the number of persons injured outside the building over the total population.

For deteriorating systems such as concrete structures exposed to aggressive environments, the loss of functionality results to be time-dependent (Titi & Biondini 2013). In fact, since the structural performance at the occurrence of the extreme event is different, and generally reduced in time, from the original condition of the structure, the functionality loss may vary over time. In fact, an event of the same magnitude could provoke a different loss of functionality if occurring at different time instants. Therefore, the combined effect of seismic damage and deterioration processes has to be taken into account in a life-cycle approach to the assessment of seismic resilience.

4. Recovery models

After an extreme event, the functionality of a system should be restored by recovery interventions aiming to a satisfying level of functionality. The functionality recovery profile varies depending on the magnitude, type and location of the damage caused by an extreme event. Moreover, the rapidity of the recovery interventions is related to the resources available and allocated after the event (Bruneau & Reinhorn 2007). Besides material resources constraints, the effort that the community puts to recover from damage usually depends on the strategic importance that the damaged component has in the system.

For electric and water networks, the recovery curves can be evaluated as the restoration of the service is provided to the customers (Çağnan *et al.* 2007, Chang & Shinozuka 2004, Chang *et al.* 2002, Rose *et al.* 1997, Xu *et al.* 2007). For the particular case of health care facilities, the variables used to evaluate the recovery profile could be the number of beds available, the number of operating rooms and the number of surgeries per day (Cimellaro *et al.* 2010b, 2010c).

For structural systems, considering that in general limited available information does not allow any more specific assumption regarding the shape of the recovery process, the most reasonable assumption for the recovery profile is the linear model (Bocchini *et al.* 2012):

$$Q(t > t_0) = Q_r + H[t - t_0 - \delta_i]\frac{Q_t - Q_r}{\delta_r}(t - t_0 - \delta_i) \tag{5.13}$$

where Q_r is the residual functionality after the extreme event, H[-] represents the Heaviside unit step function, Q_t is the functionality reached after the recovery process, δ_r is the duration of the recovery and δ_i is the idle time between the occurrence of the extreme event and the beginning of the recovery process (Figure 5.13). In most cases, the model is further simplified by assuming $\delta_i = 0$:

$$Q(t > t_0) = Q_r + \frac{Q_t - Q_r}{\delta_r}(t - t_0) \tag{5.14}$$

A key parameter in the definition of the recovery process is the so called "rapidity" r (Cimellaro *et al.* 2010b):

$$r = \frac{Q_t - Q_r}{\delta_r} \tag{5.15}$$

which represents the first derivative of the functionality during the restoration. Bocchini & Frangopol (2012a) considered the slope θ_b of the damage profile function bounded between θ_{max} and θ_{min}. In fact very slow interventions are certainly not convenient and too fast interventions are not realistic. The value θ_{max} can be evaluated by considering the maximum estimated damage and the minimum time required, whereas θ_{min} can be evaluated by considering the minimum estimated damage and the maximum allowable time.

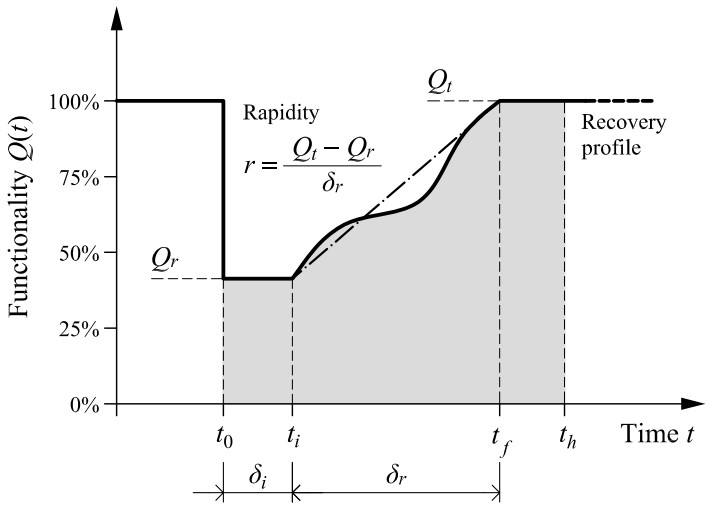

Figure 5.13 – Definition of rapidity and functionality recovery profile (after Bocchini *et al.* 2012, adapted).

Under the hypothesis of neglecting the idle time δ_i, the following recovery models are proposed in literature:

- trigonometric model:

$$Q(t > t_0) = Q_r + \frac{Q_t - Q_r}{2}\left\{1 - \cos\left[\frac{\pi}{\delta_r}(t - t_0)\right]\right\} \tag{5.16}$$

- exponential model (Kafali & Grigoriou 2005), which is suitable for those systems where it is possible to recover quickly most of the functionality but the complete recovery requires a long time:

$$Q(t > t_0) = Q_r + \left\{1 - \exp\left[\frac{-k(t - t_0)}{\delta_r}\right]\right\}(Q_t - Q_r) \tag{5.17}$$

  where k is a shape parameter;

- Gaussian cumulative distribution function (FEMA 2009), where μ and σ are shape parameters that depend on the recovery time (ATC 1985) and *erf*[-] is the error function:

$$Q(t > t_0) = Q_r + \left\{\mathrm{erf}\left[\frac{t - t_0 - \mu}{\delta_r}\right]\right\}(Q_t - Q_r) \tag{5.18}$$

- stepwise functionality recovery function (Padgett & DesRoches 2007): this model is suitable for infrastructure components which can be only in a discrete subset of functionality states, such as bridges where the functionality depends on the number of lanes that are open:

$$Q(t > t_0) = \begin{cases} Q_r & t_0 \le t < t_1 \\ Q_1 & t_1 \le t < t_2 \\ \vdots & \vdots \\ Q_n & t_n \le t < t_0 + \delta_r \\ Q_t & t \ge t_0 + \delta_r \end{cases} \tag{5.19}$$

where Q_1, Q_2, …, Q_n are the discrete values of functionality between Q_r and Q_t achieved at the time instants t_1, t_2, …, t_n respectively.

A model that allows representing different shapes of the recovery profile based on the investigated system and type of damage is proposed in Bocchini *et al.* (2012) and Decò *et al.* (2013). From an analytical point of view, the proposed model is a generalization of the trigonometric model. The variation of six random parameters allows to fit the shape of different recovery processes, ranging from slight to extensive damage and from the cases where the functionality is restored almost entirely at the beginning or at the end of the restoration activities. The parameters are the residual functionality, the idle time, the recovery duration, the target functionality, the flex location and amplitude of the sinusoidal function. The evaluation of the system functionality is performed in a probabilistic approach for different earthquake scenarios.

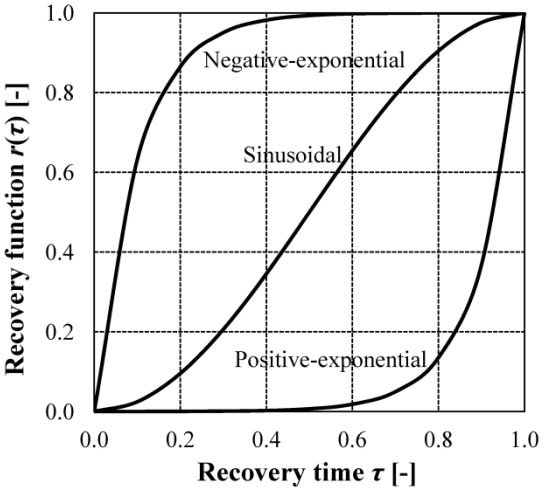

Figure 5.14 – Definition of functionality recovery curves ($k = 10$).

Finally, Titi & Biondini (2013) used the following recovery functions for the evaluation of the seismic resilience of a structure (Figure 5.14):

- positive-exponential:

$$Q(t_i < t < t_f) = e^{-k(1-t+t_i)} \tag{5.20}$$

- sinusoidal:

$$Q(t_i < t < t_f) = \frac{1 - \cos[\pi(t - t_i)]}{2} \tag{5.21}$$

- negative-exponential

$$Q(t_i < t < t_f) = 1 - e^{-k(1-t+t_i)} \tag{5.22}$$

where k is a shape parameter.

These recovery function can describe the case where the system functionality is restored mainly at the end of the recovery process, gradually and quickly after the seismic event respectively.

5. Application: seismic resilience of a concrete bridge exposed to corrosion

The seismic resilience of the concrete bridge presented in Chapter 4, §4 is herein investigated. The resilience of the deteriorating system is evaluated with respect to the structural functionality according to different damage states. The structural performance of the bridge is related to the seismic capacity in terms of total resisting base shear, as indicated in Eqn. 5.11. The damage states are associated with the reaching of prescribed displacement limits, as listed in Chapter 4, Table 4.7. Both system functionality and displacement limits are considered time-variant due to the deterioration process of the concrete members.

First, a probabilistic parametric analysis of the resilience of the bridge is proposed to investigate the effects of the loss of functionality, the target functionality and the adopted recovery function on time-variant resilience within a prescribed time horizon. The efficiency of both the recovery process and the target functionality in improving system resilience is investigated by means of efficiency coefficients. The interaction of seismic damage and environmental deterioration is finally investigated in deterministic terms by nonlinear dynamic analyses to highlight that the residual structural functionality depends on the time of occurrence of the seismic event. Finally the role of uncertainties in a seismic resilience assessment is discussed basing on lifetime probabilistic nonlinear analyses, referring both to the inherent uncertainties of the structural system, the randomness of the deterioration process and the variability of the earthquake excitation.

5.1. Functionality and functionality limit states

The lifetime functionality $Q(t)$ of the bridge is evaluated according to Eqn. 5.11 referring to the time-evolution of the total base shear $F_{base}(t)$ obtained in Chapter 4, §4.4 in probabilistic terms by means of push-over analyses (Figure 4.28). By taking into account the local effects of corrosion damage on the cross-sectional properties of the piers, the time-variant performance of the overall bridge has been defined with respect to increasing system displacement limits, from the yielding displacement up to collapse (Chapter 4, Table 4.7).

Each structural performance level corresponds to a damage state (DS) of the bridge occurring after a seismic event of increasing magnitude. In Table 5.2, a possible failure mechanisms is associated to each damage state, which implies a drop in the of functionality of the bridge system, as qualitatively shown in Figure 5.11b. The probable consequent repair intervention and the outage of the bridge functionality are estimated as well in Table 5.2.

Table 5.2 – Damage states adapted from FEMA (2009) and predicted outage of bridge systems (after Mander *et al.* 2007, adapted).

Damage State	Failure Mechanism	Repair Required	Outage
DS-1	Pre-Yielding	None	*None*
DS-2	Minor Spalling	Inspect, Patch	*< 3 days*
DS-3	Bar Buckling	Repair Components	*< 3 weeks*
DS-4	Bar Fracture	Rebuild Components	*< 3 weeks*
DS-5	Collapse	Rebuild Structure	*> 3 months*

The lifetime functionality of the bridge is evaluated with respect to damage states of increasing severity. For example, the evolution of the functionality for DS-5 is shown in Figure 5.15 over a 50 year lifetime, with indication of mean value μ and standard deviation σ. The distribution of the results is truncated at $Q(t) \leq 1$, since the functionality cannot exceed the value 100% by definition. The scatter around the mean of the bridge functionality at time $t = 0$ is related to the variability of the actual seismic capacity of the bridge at the beginning of lifetime with respect to the nominal properties of the structure. As it can be noticed, the uncertainties related to the deterioration process are added over a 50 year lifetime, thus increasing the standard deviation around the mean functionality.

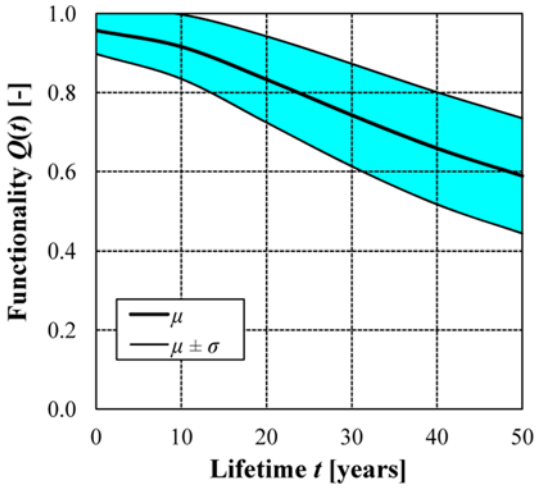

Figure 5.15 – Lifetime functionality of the bridge considering DS-5 (mean μ and standard deviation σ from the mean).

Figure 5.15 highlights also that the functionality of the bridge with respect to the collapse damage state varies significantly after 50 years, with a reduction of about 40%. This clearly indicates how the functionality cannot be considered as a time-independent parameter in the resilience assessment of deteriorating structures. The functionality of the structure referring to the other damage states shows similar trends, as the total base shear corresponding to each structural performance level varies similarly over lifetime (Chapter 4, Figure 4.28).

5.2. Probabilistic assessment of seismic resilience

After the lifetime functionality has been assessed, the evaluation of the corresponding resilience implies the definition of the functionality loss $\Delta Q(t_0)$ at the occurrence of the seismic event and the choice of both a functionality target Q_t and a particular recovery function $r(\tau)$.
Probabilistic parametric analyses are carried out to investigate the effects of these parameters on time-variant resilience based on the following assumptions:

- the loss of functionality $\Delta Q(t_0)$ is imposed as a percentage $\varkappa$ (%)of the current functionality:

$$\Delta Q(t_0) = \kappa Q(t_0) \tag{5.23}$$

  In this way the coupling between environmental and seismic damage is neglected but the drop of functionality is however dependent on the current functionality. This assumption will be removed to investigate the interaction between seismic damage and environmental deterioration;
- the idle time δ_i is neglected ($\delta_i = 0$), thus meaning that the time of occurrence of the seismic event coincide with the initial time of the recovery process ($t_0 = t_i$);
- the recovery profile is fixed a priori assuming as recovery functions positive-exponential, sinusoidal and negative-exponential curves (Eqns. 5.20-5.21-5.22), with a shape parameter k = 10; the recovery functions $r(\tau) \in [0, 1]$ are defined over the time interval Δt by considering:

$$\tau = \frac{t - t_i}{\Delta t} \quad \in [0,1] \tag{5.24}$$

- over the recovery period, the functionality $Q(\tau)$ is assumed to evolve as follows:

$$Q(\tau) = Q_r + H(\tau) r(\tau)(Q_t - Q_r) \tag{5.25}$$

- a time horizon t_h = 12 months is assumed between the occurrence of the seismic event and the recovery of the target functionality: it has been observed that the lifetime seismic resilience does not depend significantly on the recovery time interval, since the major contribution is the loss of functionality $\Delta Q(t_0)$ (Titi & Biondini 2013). Moreover, the parameters involved in the definition of the recovery function $r(\tau)$ are independent on the deterioration processes over lifetime;
- the time horizon is assumed coincident with the reaching of the chosen target functionality ($t_h = t_f$);
- the post-recover functionality Q_t is targeted under the hypothesis of both partial recovery and full recovery: the partial recovery restores the functionality of the system at the level that

the structure had before the occurrence of the event, while the full recovery restores the functionality level at time $t = 0$.

Considering the lifetime properties of the structure in terms of time-variant total resisting base shear $F_{base}(t)$ and varying the time of occurrence t_0 of the seismic event, the resilience of the structure is evaluated over a 50-year lifetime referring to the collapse damage state (DS-5, Table 5.2). The effects of the loss of functionality, the recovery functions and the target functionality are considered separately. The results shown in the following refer to the mean values of the probabilistic results for sake of brevity.

Influence of the loss of functionality

Basing on Eqn. 5.23, the functionality loss $\Delta Q(t_0)$ is dependent on the current system functionality at the occurrence of the seismic event at time $t = t_0$. The influence of the prescribed loss of functionality $\Delta Q(t_0)$ is shown in Figure 5.16, where $\Delta Q(t_0)$ ranges between $0\% Q(t_0)$ and $100\% Q(t_0)$. A sinusoidal recovery function and a partial restoring are assumed. The graph shows that the increase of the drop of functionality results in a reduced resilience at the time of occurrence of the seismic event $t = t_0$. For example, if the seismic event occurs at the beginning of the lifetime ($t_0 = 0$), the resilience of the bridge drops from 0.96 to 0.48, in the case of no seismic damage and full seismic damage respectively. It has to be noticed that the mean value of the resilience $R(t_0 = 0)$ with $\Delta Q(t_0) = 0$ is not equal to 1 for the adopted definition of functionality with a truncated distribution at $Q(t) \leq 1$.

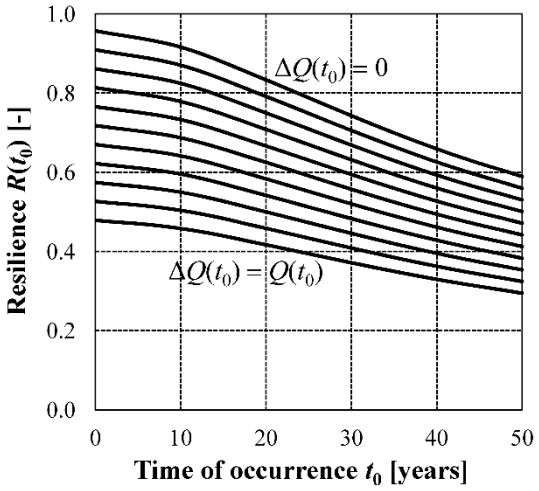

Figure 5.16 –Time evolution of the seismic resilience $R(t_0)$ considering different levels of loss of functionality $\Delta Q(t_0) = \varkappa Q(t_0)$, with $\varkappa = 0\% \div 100\%$, $\Delta\varkappa = 10\%$: sinusoidal recovery profile and partial restoring.

The resilience curve corresponding to $\Delta Q(t_0) = 0$ shows that the resilience of the bridge decreases over time even without the occurrence of seismic damage due to the deterioration processes. If the seismic damage is also considered, it can be noticed that the resilience decreases progressively from

the curve $\Delta Q(t_0) = 0$ to the curve $\Delta Q(t_0) = Q(t_0)$, thus indicating the mutual effects of seismic and environmental damage on resilience.

However, the assumption of a prescribed loss of functionality, which is constant, in percentage with respect to the current functionality, for each resilience curve in Figure 5.16 over the lifetime, seems to be unrealistic. In fact, the functionality drop at the occurrence of the seismic event is dependent on the current deterioration state of the structure related to the actual mechanical properties of the concrete members (Titi & Biondini 2013).

Influence of the adopted recovery function

The functionality recovery profile $r(\tau)$ depends on many factors, including type of systems and components, magnitude and location of damage and restoring techniques. In this study the recovery curves positive-exponential, sinusoidal and negative-exponential indicated in Eqns. 5.20-5.21-5.22 are adopted, with shape factor $k = 10$ (Figure 5.14).

Figure 5.17 shows the time evolution of the seismic resilience considering a positive-exponential profile and a negative-exponential profile. These can be considered limit cases of slow and fast initial recovery respectively, while the above presented case of sinusoidal profile reproduces an intermediate situation of gradual functionality recover (Figure 5.16).

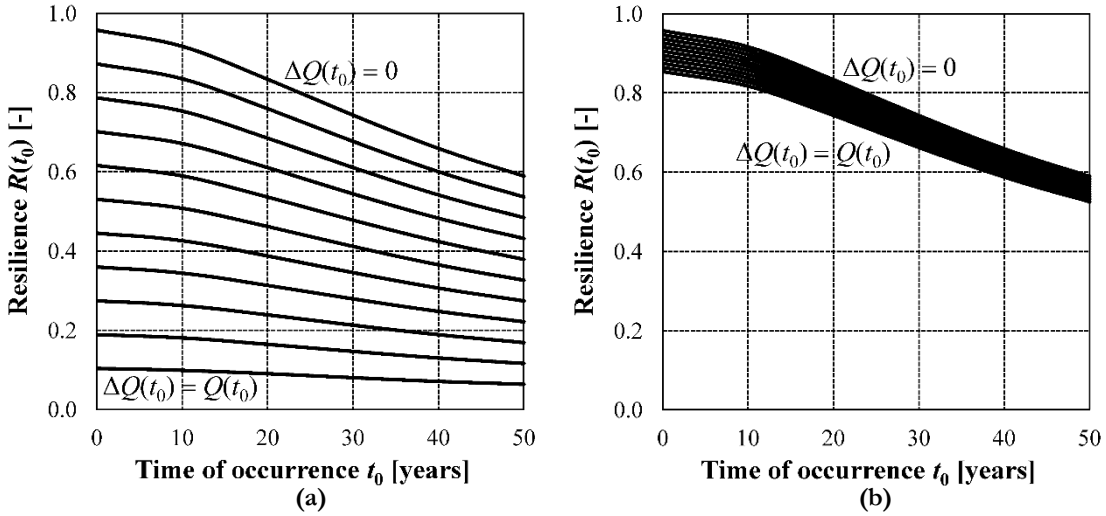

Figure 5.17 – Time evolution of the seismic resilience $R(t_0)$ considering (a) a positive-exponential and (b) a negative-exponential recovery profile: loss of functionality $\Delta Q(t_0) = \varkappa Q(t_0)$, with $\varkappa$ = 0%÷100%, $\Delta\varkappa$ = 10% and partial restoring.

The resilience results to be lower in the case of a positive-exponential recovery profile (Figure 5.17a), where functionality is restored mainly at the end of the recovery process. This may occur when few resources are initially available to repair the structure or when the functionality restore of the structure is not of critical importance among the post-earthquake emergency interventions. On the contrary, the case of a negative-exponential recovery profile reproduces the case of a prompt intervention that restores the greater part of the structural functionality soon after the seismic event. This may occur

for strategic structures where first intervention actions are needed to assure the continuity of the structural functionality.

A comparison between the lifetime resilience evaluated with different recovery profiles is provided in Figure 5.18a. It can be noticed that the seismic resilience significantly depends on the adopted function simulating the recovery process. However, the percentage decrease of resilience over time does not significantly depend on the recovery profiles (Figure 5.18b), indicating that the role of deterioration is not modified by the type of the recovery process. In fact, in all cases the resilience of the structure reduces of about 40% after 50 years of lifetime due to the deterioration processes though being independent on the adopted recovery function.

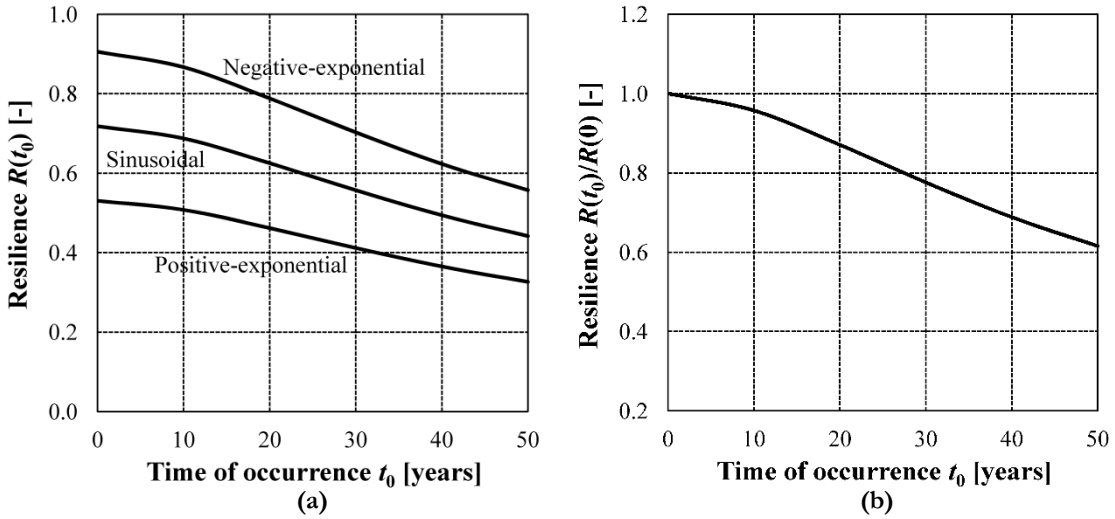

Figure 5.18 – (a) Time evolution of the seismic resilience $R(t_0)$ and (b) percentage decrease $R(t_0)/R(0)$ considering partial restoring and $\Delta Q(t_0) = 50\% Q(t_0)$ for different recovery profiles.

The type of recovery profile is one of the most important factors to ensure suitable levels of lifetime seismic resilience in a timely and efficient manner. In order to evaluate the efficiency of the negative-exponential recovery profile with respect to the positive-exponential recovery profile, the following recovery function efficiency coefficient η_r is proposed:

$$\eta_r = \frac{R_{neg}(t_0, \Delta Q) - R_{pos}(t_0, \Delta Q)}{R_{neg}(t_0 = 0, \Delta Q)} \tag{5.26}$$

where $R_{neg}(t_0, \Delta Q)$ and $R_{pos}(t_0, \Delta Q)$ are the resilience values in case of negative-exponential and positive-exponential recovery profiles respectively, which vary depending on both the time of occurrence of the event and the extent of functionality loss. The value $R_{neg}(t_0 = 0, \Delta Q)$ represents the reference value of seismic resilience at the occurrence of the event at the beginning of the lifetime, considering varying loss of functionality and a negative-exponential recovery profile.

Figure 5.19 shows the trend of the recovery function efficiency coefficient η_r which depends on both the functionality loss ΔQ and the time of occurrence t_0 of the seismic event. The recovery function

efficiency is then evaluated by fixing the time of occurrence and varying the functionality loss (Figure 5.19a) and by imposing the functionality loss and varying the time of occurrence (Figure 5.19b).

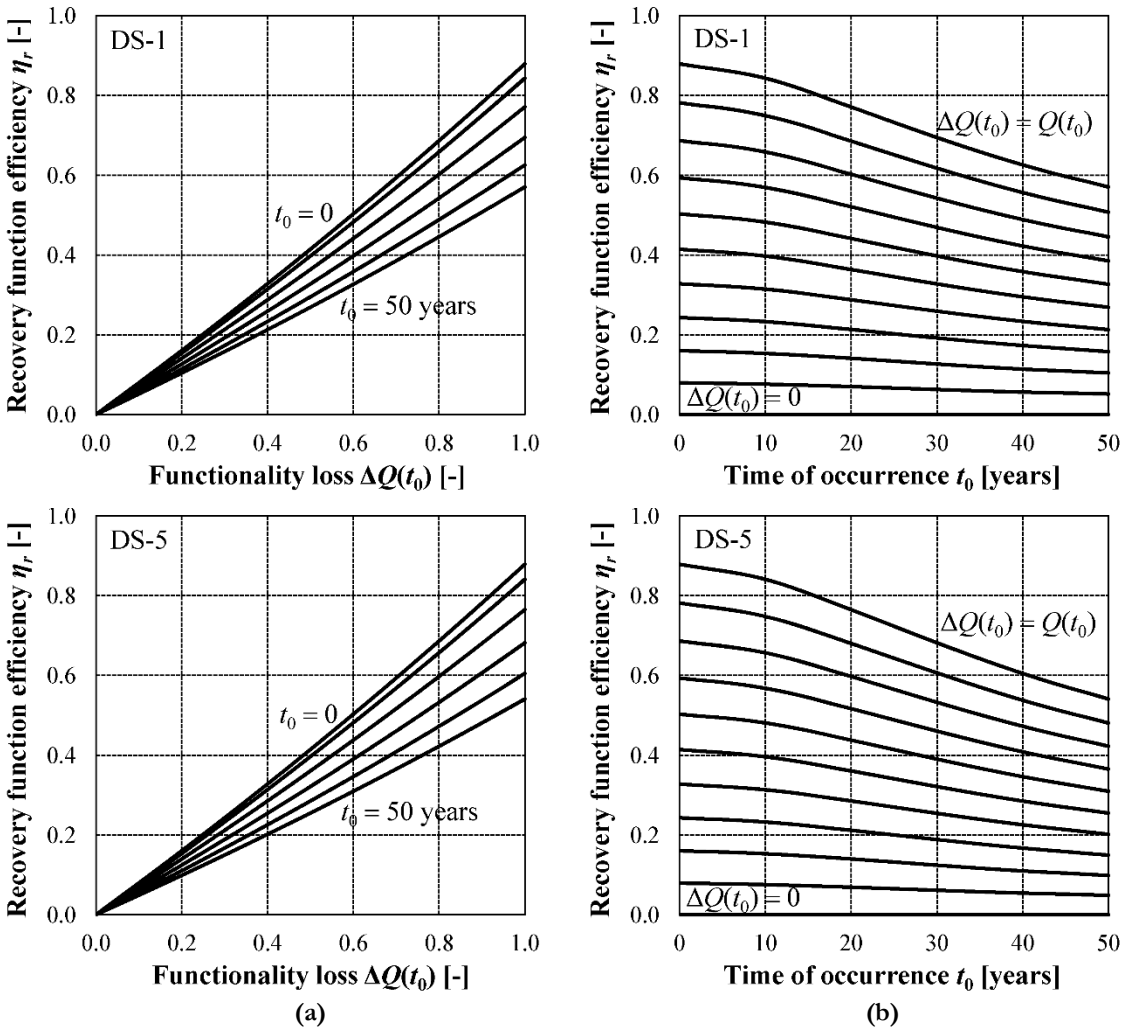

Figure 5.19 – Recovery function efficiency η_r evaluated with respect to (a) the functionality loss $\Delta Q(t_0)$, $\Delta t_0 = 10$ years, and (b) the time of occurrence t_0 of the seismic event ($\Delta Q(t_0) = \varkappa\, \Delta Q(t_0)$, $\Delta\varkappa = 10\%$) for pre-yielding (DS-1) and collapse (DS-5) damage states.

The recovery function efficiency increases as the functionality loss increases from no damage to complete damage (Figure 5.19a). This means that in case of severe seismic damage a prompt intervention, which is modeled by a negative-exponential recovery profile, is more efficient and improves the resilience of the structure.

On the other side, the efficiency of the recovery function decreases as the seismic event occurs after several years of lifetime. This indicates that the gain in terms of resilience given by a rapid recovery intervention is less since the structure is already deteriorated by aging. This is shown also in Figure 5.19b by the decreasing curves of the recovery function efficiency over lifetime, meaning that the effectiveness of rapid recovery actions is inversely proportional to the deterioration of the structure.

These considerations hold for all the considered damage states. In Figure 5.19 pre-yielding (DS-1) and collapse (DS-5) damage states are indicated. It can be noticed that for major damage (DS-5) the recovery function efficiency is lower, which is mainly due to the reduced resilience of the structure associated to increasing levels of damage.

Influence of the target functionality

The functionality targeted Q_t by post-event interventions is a decision-making parameter that may depend on the importance of the structure, on the resources available and on time limitations. The cases of total and partial functionality restoring are herein compared.

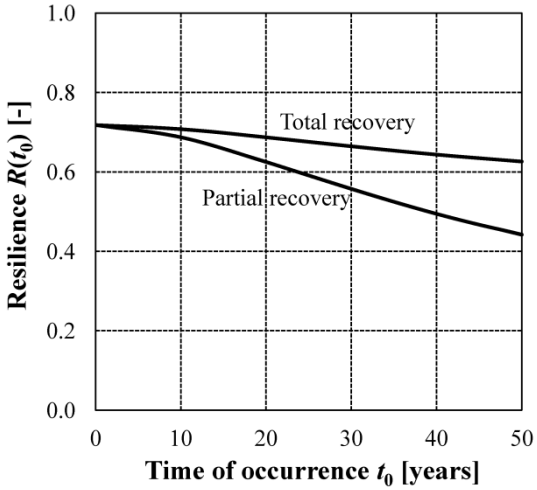

Figure 5.20 – Time evolution of the seismic resilience $R(t_0)$ considering $\Delta Q(t_0) = 50\% Q(t_0)$ and sinusoidal recovery profile for different target functionalities Q_t.

Higher values of resilience are associated with the total functionality recover (Figure 5.20), thus indicating that a full functionality recovery implies the use of major resources then a partial restoring given the same initial conditions of the system. In general, a full functionality recovery implies also a longer recovery time, if the rapidity of the recovery process cannot speed up due to external constraints. On the contrary, the partial restoring takes into account the evolution of system degradation before the occurrence of the seismic event. The recovery interventions are then aimed to restore the pre-event functionality without improving the resilience of the system to possible future events. Moreover, Figure 5.20 shows that the difference between the recovery targets increases over lifetime. This means that on a deteriorated structure the effect of a total recovery in improving the resilience of the system is more significant.

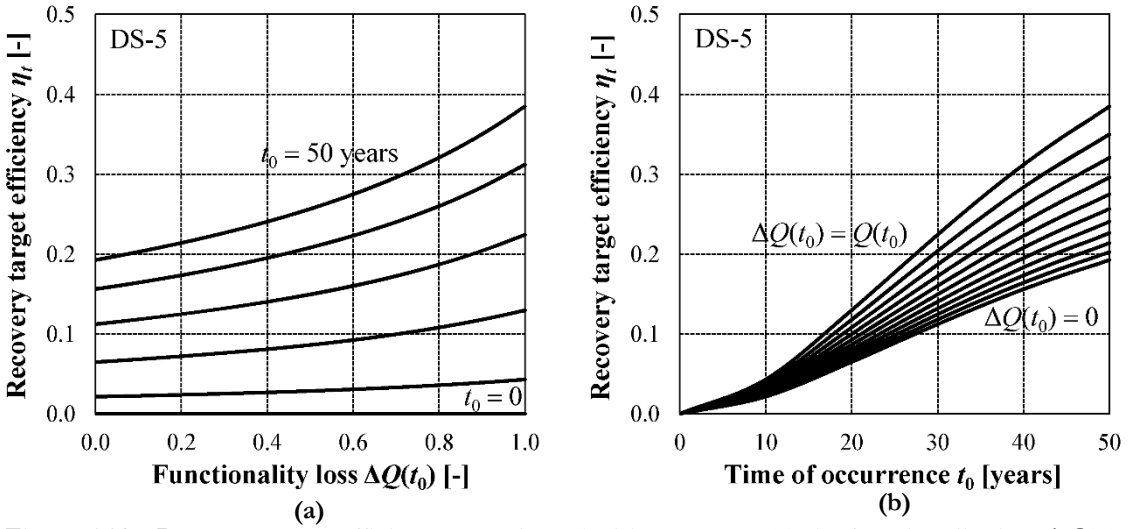

Figure 5.21 – Recovery target efficiency η_t evaluated with respect to (a) the functionality loss $\Delta Q(t_0)$, Δt = 10 years, and (b) the time of occurrence t_0 of the seismic event ($\Delta Q(t_0) = \varkappa\, \Delta Q(t_0)$, $\Delta\varkappa$ = 10%) for collapse (DS-5) damage state.

In this sense, the recovery target efficiency coefficient η_t is proposed as follows:

$$\eta_t = \frac{R_{tot}(t_0, \Delta Q) - R_{part}(t_0, \Delta Q)}{R_{tot}(t_0 = 0, \Delta Q)} \tag{5.27}$$

where $R_{tot}(t_0, \Delta Q)$ and $R_{part}(t_0, \Delta Q)$ are the resilience values in the case of total and partial recovery profiles respectively, which vary depending on both the time of occurrence of the event and the extent of functionality loss. The value $R_{tot}(t_0 = 0, \Delta Q)$ represents the reference value of seismic resilience at the occurrence of the event at the beginning of the lifetime, considering varying loss of functionality and a total recovery profile.

The effectiveness of the total recovery in increasing the seismic resilience is evident in Figure 5.21 with respect to both the functionality loss and the time of occurrence. This means that a total recovery is more efficient as the structure is both more damaged by the seismic event and more deteriorated by aging. However, it has to be considered that a total recovery process implies greater resources and more significant maintenance interventions to restore the original functionality. The major costs associated would be justified by the importance of the structure and by other economic evaluations.

In conclusion, the probabilistic results of the seismic resilience assessment of the bridge for the collapse damage state are shown in terms of mean value μ and standard deviation σ by assuming a functionality loss $\Delta Q(t_0) = 50\% Q(t_0)$, a sinusoidal recovery profile and a partial restoring (Figure 5.22). The trend of the standard deviations is similar to that of functionality of the bridge as discussed for Figure 5.15. Moreover, the trend of mean values μ and standard deviations σ is similar for each damage state considered. It has been also observed that the standard deviations of the results of the probabilistic analyses are not affected by the herein investigated parameter, i.e. the loss of functionality, the recovery profile and the functionality target.

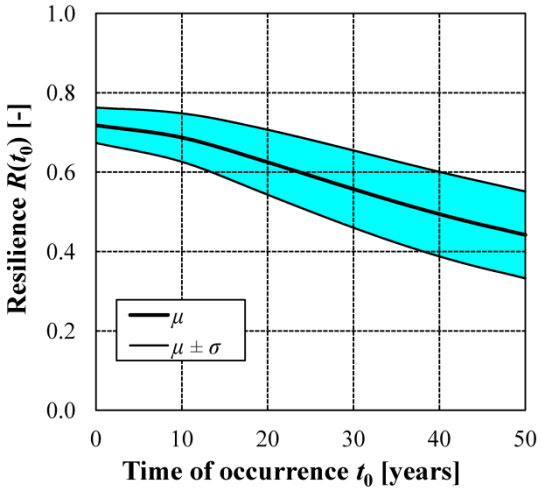

Figure 5.22 – Lifetime seismic resilience $R(t_0)$ with respect to collapse damage state (DS-5) considering $\Delta Q(t_0) = 50\% Q(t_0)$, sinusoidal recovery profile and partial restoring based on system functionality in Figure 5.15 (mean μ and standard deviation σ from the mean).

5.3. Interaction of seismic damage and environmental deterioration

In a seismic resilience analysis, the loss of functionality $\Delta Q(t_0)$ is mainly due to the effects of seismic damage. However, the effects of an earthquake event occurring at time $t = t_0$ may vary over lifetime due to the deterioration processes, which affect the mechanical properties of the structural members. In fact, the functionality loss at the occurrence of a seismic event of same magnitude could be different depending on the time-variant structural capacity related to the environmental exposure. As a consequence, the residual functionality has to be considered a time-dependent parameter as $Q_r = Q_r(t_0)$.

In order to investigate the interaction between environmental deterioration and seismic damage, time-variant nonlinear dynamic analyses of the aging bridge for the nominal configuration have been carried out under ten prescribed ground motions (Chapter 4, Table 4.11) with increasing levels of seismic intensity corresponding to mean PGA = 0.2*g*-0.4*g*-0.6*g* by using OpenSees (Mazzoni *et al.* 2005). The time-variant residual functionality $Q_r(t_0)$ of the damaged structure is then evaluated by post-event nonlinear static analyses. The sequence of nonlinear dynamic and static analyses allows to take directly into account the effects of seismic damage on the structure, which shows time-variant mechanical properties at each time instant $t = t_0$.

Environmental deterioration is accounted for by adopting time-variant moment curvature relationships over a 50-year lifetime (Chapter 4, Figure 4.21a). These relationships, which correspond to the pre-event bending capacity of the piers due to deterioration only, have been linearized as shown in Chapter 4, Figure 4.21b. The quadrilinear stepwise curve is used to define a proper hysteretic rule

implemented in OpenSees (Lowes *et al.* 2003, Mazzoni *et al.* 2005), which accounts for seismic damage in terms of degradation of both stiffness and strength of the piers under cyclic loading.

Seismic damage is evaluated as a function of the load-deformation history under earthquake loading, as proposed in Lowes *et al.* (2003) and Mazzoni *et al.* (2005). The hysteretic damage is simulated through deterioration in unloading stiffness (Figure 5.23a), in reloading stiffness (Figure 5.23b) and in strength (Figure 5.23c). In all the three cases, the damage is evaluated based on the damage index proposed by Park & Ang (1985):

$$\delta_i = \left[\alpha_1 (\widetilde{\Delta}_{\max})^{\alpha_3} + \alpha_2 \left(\frac{E_i}{E_{monotonic}} \right)^{\alpha_4} \right] \tag{5.28}$$

where:

$$\widetilde{\Delta}_{\max} = \max \left(\frac{\Delta_{\max,i}}{\Delta_{u,\max}}; \frac{\Delta_{\min,i}}{\Delta_{u,\min}} \right) \tag{5.29}$$

$$E_i = \int_{load\ history} dE \tag{5.30}$$

In Eqns. 5.28, 5.29, 5.30 i refers to the current displacement increment; δ_i is the damage index, within the range [0; 1] indicating no damage and complete damage respectively; $a_{1\text{-}4}$ are the parameters used to calibrate the damage rule; E is the hysteretic energy with $E_{monotonic}$ equal to the energy required to achieve failure under monotonic loading; $\Delta_{u,\max}$ and $\Delta_{u,\min}$ are the positive and negative deformations at failure; $\Delta_{\max}$ and $\Delta_{\min}$ are the maximum and minimum deformation demand during load history.

In each cycle, degradation due to seismic damage is accounted for as follows:

- unloading stiffness degradation

$$k_i = k_0 (1 - \delta k_i) \tag{5.31}$$

  where k_i is the current unloading stiffness, k_0 is the initial unloading stiffness in the undamaged conditions, and δk_i is the current value of the stiffness damage index;

- reloading stiffness degradation

$$\Delta_{\max,i} = \Delta_{\max,0} (1 + \delta \Delta_i) \tag{5.32}$$

  where $\Delta_{\max,i}$ is the current deformation that defines the end of the reload cycle for increasing deformation demand, $\Delta_{\max,0}$ is the maximum historic deformation demand, and $\delta\Delta_i$ is the current value of the reloading stiffness damage index;

- strength degradation

$$F_{\max,i} = F_{\max,0}(1 + \delta F_i) \tag{5.33}$$

where $F_{\max,i}$ is the current envelope maximum strength, $F_{\max,0}$ is the initial envelope maximum strength in the undamaged condition and δF_i is the current value of the strength damage index. Additional details of this damage model are available in Lowes *et al.* (2003).

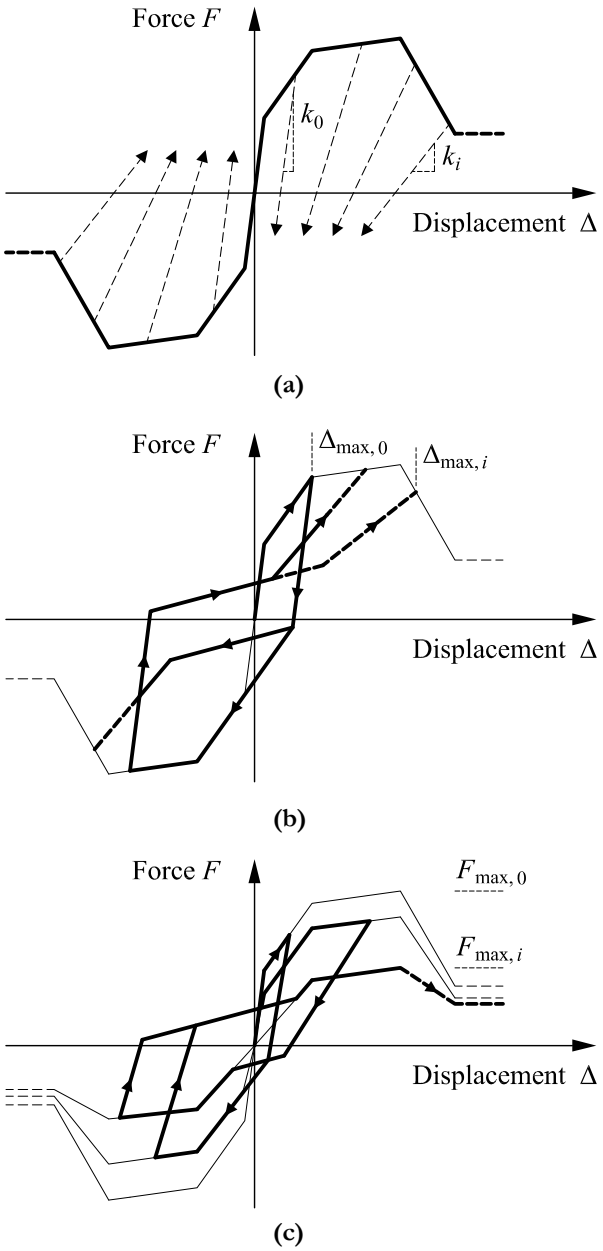

Figure 5.23 – Seismic damage model: (a) Unloading stiffness degradation; (b) Reloading stiffness degradation; (c) Strength degradation (after Lowes *et al.* 2003, adapted).

The seismic event is assumed to occur at each Δt_0 = 10 years over a 50-year lifetime. Figure 5.24 shows the results of the post-event nonlinear static analyses in terms of base shear F_{base} versus top

displacement of the central pier Δ_c in mean values over the ten considered earthquakes scaled at PGA = 0.2*g*-0.4*g*-0.6*g*. These curves evaluate the residual capacity of the structure after the occurrence of the seismic event, thus considering both seismic damage and environmental deterioration. As expected, the post-event seismic capacity decreases at the increase of the PGA level for each time of occurrence t_0. While environmental deterioration is dominant over lifetime in case of a seismic event of PGA = 0.2*g*, an earthquake of PGA = 0.6*g* causes a significant reduction in terms of residual resisting base shear F_{base}, which is added to the progressive decay of the seismic capacity over time. This effect is emphasized after a 50-year lifetime, due to the increasing environmental deterioration level.

Pre-event push-over curves at time instants $t = 0$ and $t = 50$ years are indicated in Figure 5.25 by continuous lines. These curves show the effects that corrosion processes only have on the structure over lifetime. The comparison between pre- and post-event (dashed lines) push-over curves highlights the combined effect of deterioration and mechanical damage. In fact, at time $t_0 = 0$ the decrease of the seismic capacity is due to the seismic damage only, while at time $t_0 = 50$ years the increased effect of the mechanical damage on the deteriorated structure due to environmental aggressiveness is remarkable, especially for the case of PGA = 0.6*g*.

Moreover, the amplified effects of seismic and environmental damage depend also on the earthquake record considered, due to the inherent variability of the seismic excitation. This is evident Figure 5.26, where the pre-event push-over curves are compared to post-event push-over curves obtained for each of the ten considered earthquake records. For increasing levels of PGA, the influence of a specific earthquake record in reducing the residual seismic capacity is significant. This means that both the seismic intensity level and the type of earthquake excitation affect the residual capacity of the structure.

Based on these results, the residual functionality $Q_r(t_0)$ corresponding to collapse limit state (DS5) is evaluated (Figure 5.27a) with respect to the ten considered earthquake records (dashed lines) and compared to the pre-event functionality $Q(t)$ (continuous line). This clearly highlights the influence of deterioration on the effects of seismic damage in the evaluation of the residual functionality $Q_r = Q_r(t_0)$, which depends on both the seismic intensity level and the time of occurrence t_0 of the event. The variability in the seismic excitation is reflected by the different trend of functionality curves referring to the ten earthquake records considered. It is worth noting that at the increase of the seismic damage, observed at PGA = 0.6*g*, the variability in the lifetime trend of the residual functionality $Q_r(t_0)$ for each earthquake record is emphasized. As assessed by the post-event push-over curves, different earthquakes of the same intensity may have different effects on the structure in terms of residual functionality given the time of occurrence t_0.

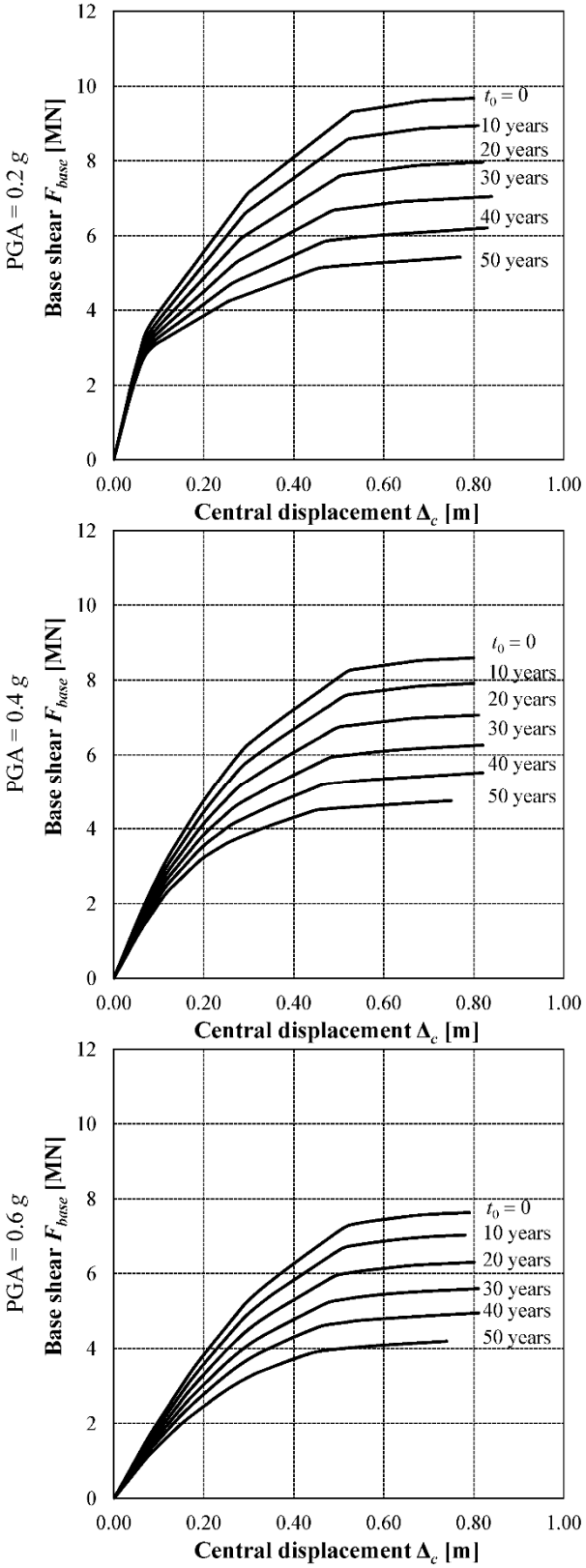

Figure 5.24 –Residual push-over curves of the bridge considering the nominal structure and the mean over ten earthquake records (Chapter 4, Table 4.11) scaled at PGA = 0.2*g*-0.4*g*-0.6*g* over a 50-year lifetime at time intervals Δt_0 = 10 years.

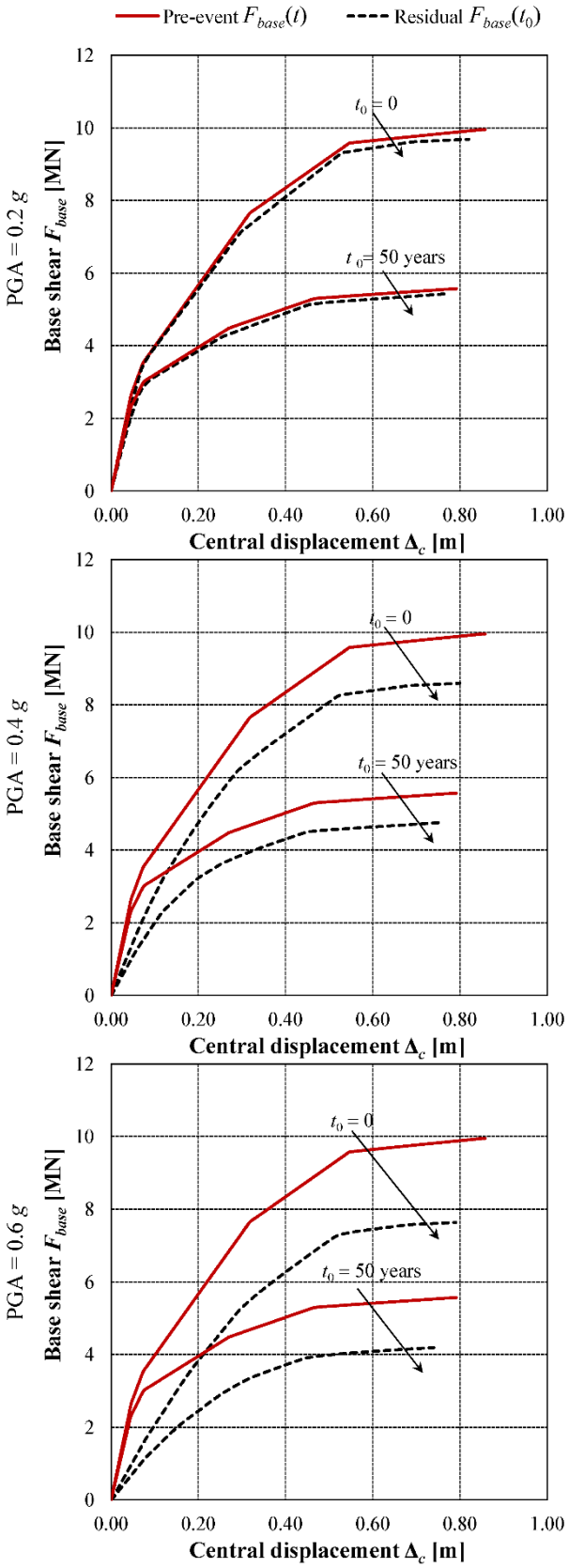

Figure 5.25 – Comparison between the push-over curves of the undamaged (continuous lines) and damaged (dashed lines) structures at the time of occurrence $t_0 = 0$ and $t_0 = 50$ years. Mean values over ten earthquake records (Chapter 4, Table 4.11) scaled at PGA = 0.2*g*-0.4*g*-0.6*g*.

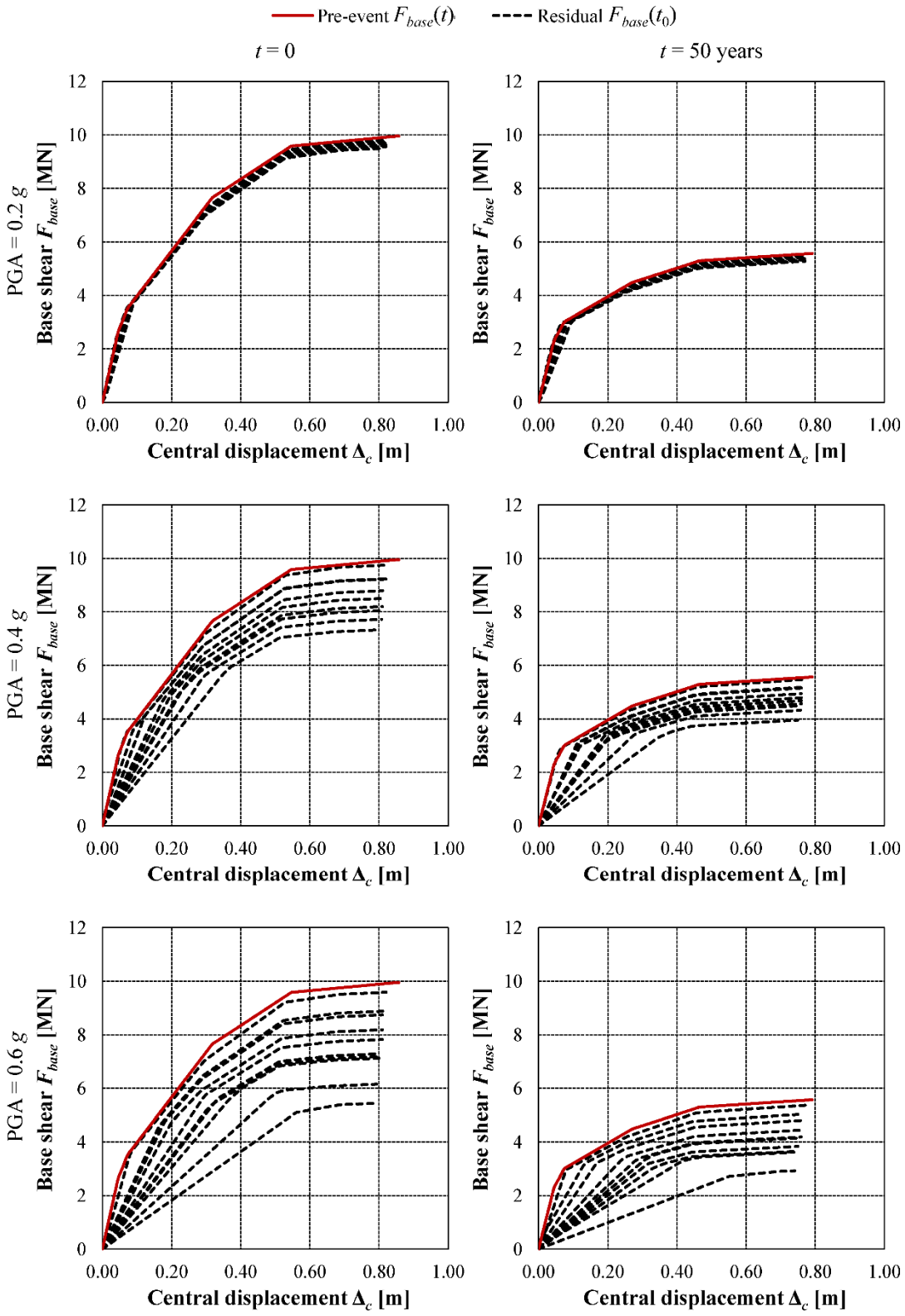

Figure 5.26 – Comparison between pre-event and residual pushover curves (ten earthquake records, Chapter 4, Table 4.11) of the bridge at time instants $t = 0$ and $t = 50$ years for increasing levels of PGA = 0.2g-0.4g-0.6g.

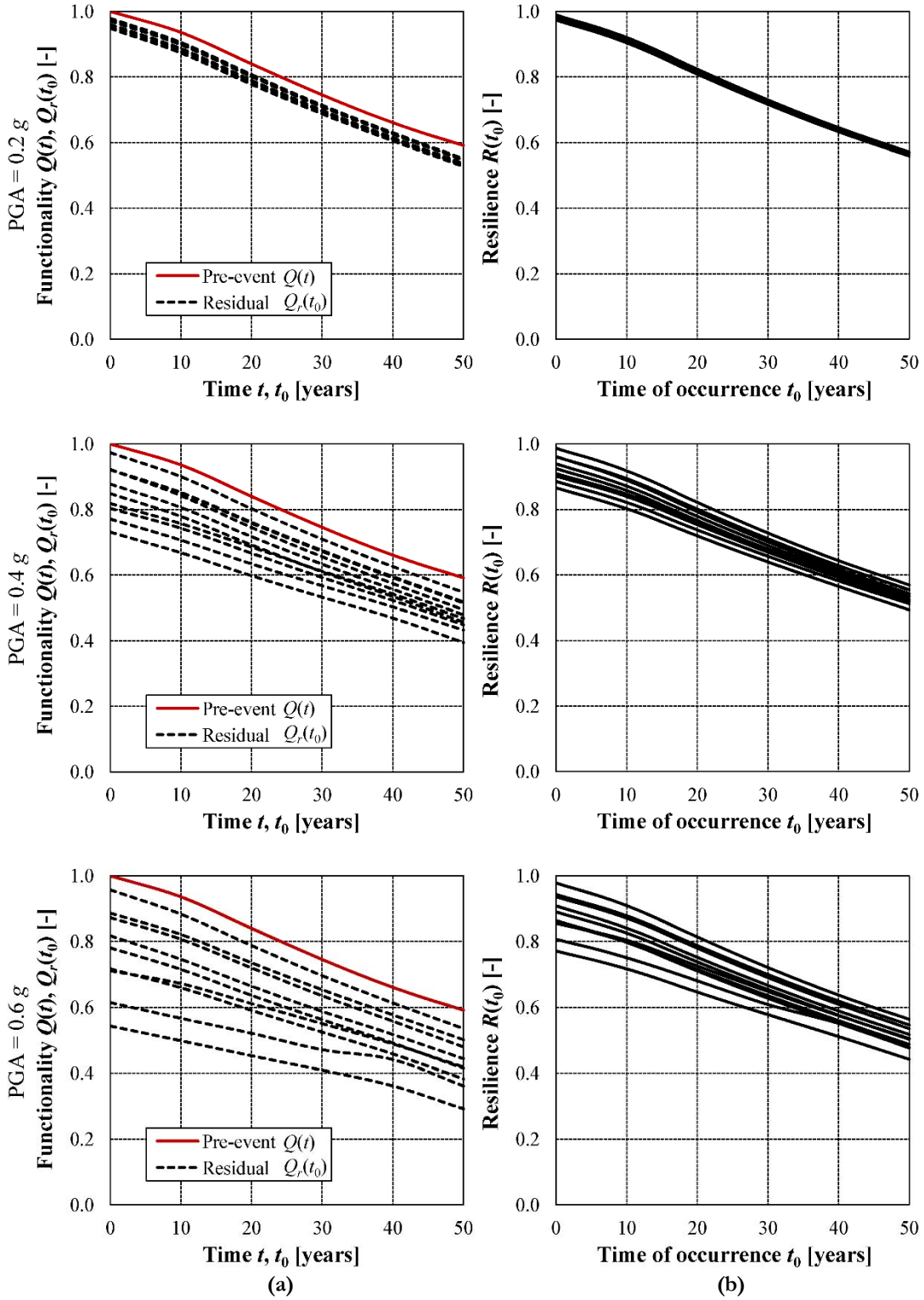

Figure 5.27 – (a) Lifetime functionality $Q(t)$ of the bridge subjected to environmental deterioration (continuous line) and seismic damage $Q_r(t_0)$ under ten earthquake records (dotted lines) with respect to collapse damage state (DS5); (b) Time evolution of the seismic resilience $R(t_0)$ assuming residual functionality $Q_r = Q_r(t_0)$, sinusoidal recovery profile and partial restoring, considering ten earthquake records (Chapter4, Table 4.11).

Table 5.3 – Values of residual functionality $Q_r(t_0)$ and resilience $R(t_0)$ at time $t_0 = 0$ and $t_0 = 50$ for the ten earthquake records (Chapter 4, Table 4.11) scaled at PGA = 0.2*g*-0.4*g*-0.6*g*.

PGA = 0.2*g*

Earthquake record	$Q_r(0)$	$Q_r(50)$	$R(0)$	$R(50)$
EQ1 - Loma Prieta	0.978	0.549	0.989	0.570
EQ2 - Loma Prieta	0.979	0.551	0.990	0.571
EQ3 - Landers	0.960	0.532	0.980	0.561
EQ4 - Landers	0.948	0.527	0.974	0.559
EQ5 - Cape Mendocino	0.960	0.537	0.980	0.564
EQ6 - Superstition Hills	0.967	0.542	0.983	0.567
EQ7 - Northridge	0.954	0.532	0.977	0.562
EQ8 - Northridge	0.979	0.551	0.990	0.571
EQ9 - Northridge	0.975	0.548	0.988	0.570
EQ10 - Northridge	0.971	0.547	0.985	0.569

PGA = 0.4*g*

Earthquake record	$Q_r(0)$	$Q_r(50)$	$R(0)$	$R(50)$
EQ1 - Loma Prieta	0.922	0.515	0.961	0.553
EQ2 - Loma Prieta	0.973	0.547	0.987	0.569
EQ3 - Landers	0.771	0.432	0.885	0.512
EQ4 - Landers	0.731	0.395	0.866	0.493
EQ5 - Cape Mendocino	0.818	0.468	0.909	0.529
EQ6 - Superstition Hills	0.849	0.456	0.924	0.524
EQ7 - Northridge	0.803	0.449	0.902	0.520
EQ8 - Northridge	0.922	0.494	0.961	0.542
EQ9 - Northridge	0.878	0.478	0.939	0.535
EQ10 - Northridge	0.921	0.518	0.961	0.555

PGA = 0.6*g*

Earthquake record	$Q_r(0)$	$Q_r(50)$	$R(0)$	$R(50)$
EQ1 - Loma Prieta	0.873	0.479	0.937	0.535
EQ2 - Loma Prieta	0.957	0.536	0.979	0.563
EQ3 - Landers	0.614	0.361	0.807	0.476
EQ4 - Landers	0.543	0.292	0.772	0.442
EQ5 - Cape Mendocino	0.711	0.419	0.856	0.505
EQ6 - Superstition Hills	0.728	0.365	0.864	0.478
EQ7 - Northridge	0.717	0.383	0.859	0.487
EQ8 - Northridge	0.817	0.444	0.909	0.517
EQ9 - Northridge	0.781	0.415	0.891	0.503
EQ10 - Northridge	0.887	0.502	0.943	0.546

As a consequence, the seismic resilience $R(t_0)$ of the bridge depends on both the time of occurrence of the seismic event t_0 and the actual residual functionality $Q_r(t_0)$. Figure 5.27b shows the ten resilience curves referring to the ten earthquakes considered by assuming the occurrence of the seismic event at Δt_0 = 10 years over a 50-year lifetime. A sinusoidal recovery profile and a partial restoring are assumed. These results can be compared to those in Figure 5.16, where a loss of functionality was fixed a priori without considering the actual seismic damage. The updated results (Figure 5.27b) highlight that the direct evaluation of the effects of seismic damage leads to higher values of resilience at time t_0 = 0, due to a lower loss of functionality, and to lower values of resilience at time t_0 = 50 years, due to the increased level of deterioration of the structure.

This demonstrates the importance of considering the mutual effects of seismic damage and deterioration processes in a lifetime resilience analysis. In particular, high PGA levels significantly affect the resilience of the bridge over time. In fact, it can be noticed that for PGA = 0.2*g* lifetime resilience is mainly affected by the deterioration process, while for PGA = 0.6*g* the role of seismic damage becomes more important.

The values of residual functionality $Q_r(t_0)$ and resilience $R(t_0)$ at time t_0 = 0 and t_0 = 50 for the ten earthquake records (Chapter 4, Table 4.11) scaled at PGA = 0.2*g*-0.4*g*-0.6*g* are listed in Table 5.3. These values refer to functionality and resilience curves shown in Figure 5.27. It can be noticed that the same earthquake record has an increased effect on both functionality and resilience at the increase of the PGA level. In particular, EQ2 results to affect slightly the functionality of the bridge, while EQ4 causes the major damage in terms of reduced functionality and resilience.

In conclusion, a proper evaluation of the interaction between deterioration and seismic damage can be effectively achieved by means of the proposed approach, based on a sequence of nonlinear static and dynamic analysis of pre- and post-event seismic performance. In this study, seismic damage has been evaluated according to the model implemented in OpenSees (Mazzoni *et al.* 2003), in order to demonstrate the practical applicability and effectiveness of the proposed methodology. Further research is needed to formulate appropriate damage models specialized to the evaluation of post-event functionality assessment.

Finally, the above mentioned analyses aimed to assess the interaction between environmental deterioration and seismic damage in the evaluation of the residual functionality $Q_r(t_0)$ are herein carried out in probabilistic terms, in order to investigate the role of uncertainties on seismic damage. The sequence of a nonlinear dynamic analysis for each of the ten earthquake records (EQ, Chapter 4, Table 4.11) and a nonlinear static analysis is repeated for the sample size n = 50,000. The lifetime properties of the structure are based on the probabilistic cross-sectional analysis carried out in Chapter 4, §4.1.

Figure 5.28 shows the mean values μ and standard deviation σ of both the functionality loss $\Delta Q(t_0)$ and resilience $R(t_0)$ depending on the time of occurrence t_0 of the seismic event EQ5. Similar trends are obtained also for the other earthquake records listed in Chapter 4, Table 4.11.

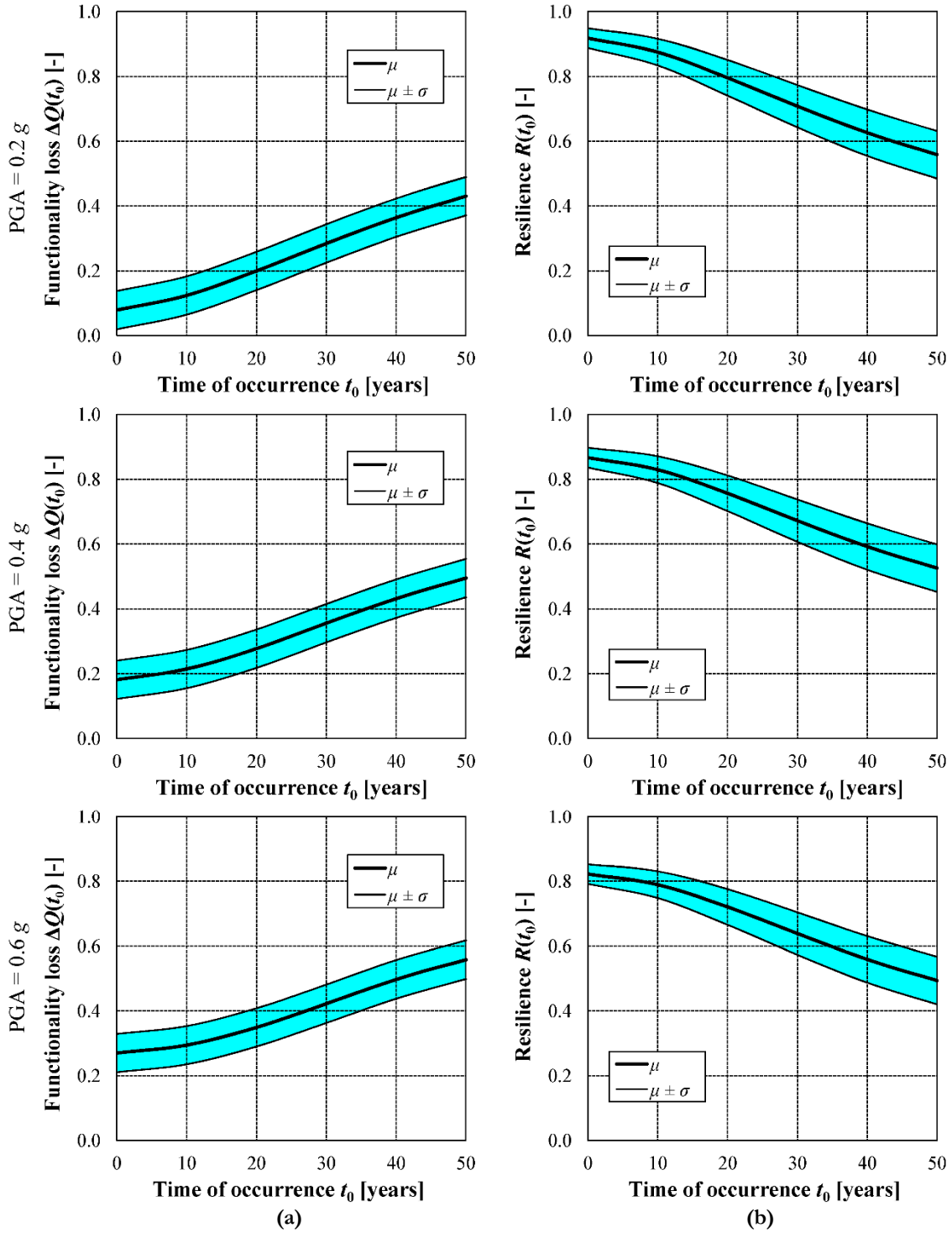

Figure 5.28 – Probabilistic results of (a) functionality loss $\Delta Q(t_0)$ and (b) seismic resilience $R(t_0)$ with respect to collapse damage state (DS5), considering earthquake record EQ5 (Chapter 4, Table 4.11) scaled at levels of PGA = 0.2*g*-0.4*g* -0.6*g*. (mean μ and standard deviation σ from the mean).

6. Conclusions

In general terms, resilience is the ability to recover from shock or to resist being affected by disturbance. This concept has been applied to various fields, including Civil Engineering as well. The aspects of robustness, redundancy, rapidity and resourcefulness contribute to the definition of resilience as the capacity of structures, infrastructure systems and entire communities to withstand and recover efficiently from extreme events.

In this Chapter, the attention has been focused on structural resilience, though a broader investigation on resilience should involve technical, organizational, social and economic aspects. Among these, the technical aspect is the most pertinent to the performance and resilience of critical structural and infrastructural systems, since it refers to the ability of physical systems to perform with acceptable levels when subjected to an extreme event. In this study, earthquakes have been selected among the extreme events that may affect the structures over the service life. In particular, the seismic resilience of deteriorating concrete structures has been investigated. In fact, for such structures damage could also arise progressively in time due to environmental aggressiveness. Therefore, resilience is dependent on the time of occurrence of the seismic event, since the functionality of the structure evolves over time due to deterioration processes.

A probabilistic methodology for lifetime assessment of seismic resilience of concrete structures has been proposed and applied to a bridge structure exposed to both corrosion and seismic damage. A comparison between system functionality, evaluated in terms of seismic capacity, has been carried out by comparing the original state and a perturbed state, in which a mechanical and environmental scenario is applied. It has been shown that lifetime seismic resilience depends on the deterioration process and the combined effect of deterioration and seismic damage. This effect is emphasized at the increase of the seismic intensity level. In fact, both the current functionality state at the occurrence of a seismic event and the considered PGA level determine the loss of functionality of the structure. The effectiveness of recovery interventions as well as the influence of the target functionality have been investigated by means of efficiency coefficients. The type of recovery profile is one of the most important factors to ensure suitable levels of lifetime seismic resilience in a timely and efficient manner. Moreover, a total recovery of the original functionality leads to greater values of the structural resilience, and its effectiveness is more evident as the structure is significantly damaged by the seismic event and deteriorated by aging. Nevertheless, it has to be considered that a greater investment of resources and/or significant maintenance interventions are needed to restore the original functionality timely. Economic evaluations and other aspects, such as the importance of the structure, should then be considered in the decision-making process aimed at selecting the optimal recovery interventions.

The results highlight the need of a life-cycle approach to the probabilistic assessment of seismic resilience of deteriorating structures under seismic and environmental hazards. In a perspective of

risk mitigation, future research should address several issues. Nonlinear functionality indicators based on seismic capacity thresholds, from operational state up to collapse, are needed in order to provide a reliable evaluation of the lifetime resilience. The influence of recovery functions based on the type, magnitude and location of damage should also be investigated. Moreover, the effects of preventive maintenance and repair interventions, which may be planned to guarantee a satisfying resilience target level over lifetime, need to be taken into account. Finally, a complete probabilistic framework for the assessment of lifetime seismic resilience of concrete structures exposed to corrosion should also include the uncertainties related to other parameters such as the idle time, the recovery time, the target functionality and the investigated time horizon.

7. References

Alesch, D.J., Dargush, G.F., Grigoriu, M., Petak, W.J., & von Winterfeldt, D. (2003). Decision models: approaches for achieving seismic resilience. *Research Progress and Accomplishments, 2001-2003*.

ATC (1985). *Earthquake Damage Evaluation Data for California*. Technical Report, Applied Technology Council, ATC-13, Redwood City, CA.

Bocchini, P., Decò, A., & Frangopol, D.M. (2012). Probabilistic functionality recovery model for resilience analysis. *Proceedings of the 6th International Conference on Bridge Maintenance, Safety and Management* (*IABMAS*), July 8-12, Stresa, Lake Maggiore, Italy.

Bocchini, P., & Frangopol, D.M. (2012a). Optimal resilience-and cost-based postdisaster intervention prioritization for bridges along a highway segment. *Journal of Bridge Engineering*, 17(1), 117–129.

Bocchini, P., & Frangopol, D.M. (2012b). Restoration of bridge networks after an earthquake: Multi-criteria intervention optimization. *Earthquake Spectra*, 28(2), 426–455.

Bruneau, M., Chang, S.E., Eguchi, R.T., Lee, G.C., O'Rourke, T.D., Reinhorn, A.M., Shinozuka, M., Tierney, K., Walace, W.A., & von Winterfeldt, D.V (2003). A framework to quantitatively assess and enhance the seismic resilience of communities. *Earthquake Spectra*, 19(4), 733–752.

Bruneau, M., & Reinhorn, A. (2004). Seismic resilience of communities-conceptualization and operationalization. *Proceedings of the International Workshop on Performance-based Seismic-Design, Bled, Slovenia*, June 28-July 1 (Vol. 1).

Bruneau, M., & Reinhorn, A. (2007). Exploring the concept of seismic resilience for acute care facilities. *Earthquake Spectra*, 23(1), 41–62.

Çağnan, Z., Davidson, R. A., & Guikema, S. D. (2006). Post-earthquake restoration planning for Los Angeles electric power. *Earthquake Spectra*, 22(3), 589–608.

Chang, S.E. (2000). Disasters and transport systems: loss, recovery and competition at the Port of Kobe after the 1995 earthquake. *Journal of Transport Geography*, 8(1), 53–65.

Chang, S.E., Pasion, C., Tatebe, K. & Ahmad, R. (2008). *Linking Lifeline Infrastructure Performance and Community Disaster Resilience: Models and Multi-Stakeholder Processes*, Report MCEER-08-0004.

Chang, S.E., & Shinozuka, M. (2004). Measuring improvements in the disaster resilience of communities. *Earthquake Spectra*, 20(3), 739–755.

Chang, S. E., Svekla, W.D., & Shinozuka, M. (2002). Linking infrastructure and urban economy: simulation of water-disruption impacts in earthquakes. *Environment and Planning B: Planning and Design*, 29(2), 281–302.

Cimellaro, G.P., Reinhorn, A.M., & Bruneau, M. (2005). Seismic resilience of a health care facility. *Proceedings of the 2005 ANCER Annual Meeting, Session III*, November 10–13, Jeju, Korea.

Cimellaro, G.P., Reinhorn, A.M., & Bruneau, M. (2006). Quantification of seismic resilience. *Proceedings of the 8th National Conference of Earthquake Engineering*, April 18-22, San Francisco, California, USA.

Cimellaro, G.P., Christovasilis, I.P., Reinhorn, A.M., DeStefano, A. & Kirova, T. (2010a). *L'Aquila Earthquake of April 6, 2009 in Italy: Rebuilding a Resilient City to Multiple Hazard*. Report MCEER-10-0010.

Cimellaro, G.P., Fumo, C., Reinhorn, A.M. & Bruneau, M. (2009) *Quantification of Disaster Resilience of Health Care Facilities*, Report MCEER-09-0009.

Cimellaro, G. P., Reinhorn, A. M., & Bruneau, M. (2010b). Framework for analytical quantification of disaster resilience. *Engineering Structures*, 32(11), 3639–3649.

Cimellaro, G.P., Reinhorn, A.M., & Bruneau, M. (2010c). Seismic resilience of a hospital system. *Structure and Infrastructure Engineering*, 6(1-2), 127–144.

Decò, A., Bocchini, P., & Frangopol, D.M. (2013). A probabilistic approach for the prediction of seismic resilience of bridges. *Earthquake Engineering & Structural Dynamics*. doi: 10.1002/eque.2282.

FEMA (2009). *HAZUS-MH MR4 Earthquake Model User Manual*. Department of Homeland Security, Federal Emergency Management Agency, Washington, D.C., US.

FEMA 356 (2000). *Pre-Standard and Commentary for the Seismic Rehabilitation of Buildings*. Federal Emergency Management Agency and US Army Corps of Engineers.

Kafali, C., & Grigoriu, M. (2005). Rehabilitation decision analysis. G. Augusti, G. Schüeller & M. Ciampoli (eds.), *Safety and Reliability of Engineering Systems and Structures*, Millpress, 2773–2780.

Kafali, C. & M. Grigoriu, M. (2006) *System Performance Under a Multi-Hazard Environment*, Report MCEER-08-0006.

Lowes, L. N., Mitra, N., & Altoontash, A. (2003). *A beam-column joint model for simulating the earthquake response of reinforced concrete frames*. Pacific Earthquake Engineering Research Center, College of Engineering, University of California.

Mander, J.B., Dhakal, R.P., Mashiko, N., & Solberg, K.M. (2007). Incremental dynamic analysis applied to seismic financial risk assessment of bridges. *Engineering Structures*, 29(10), 2662–2672.

Mazzoni, S., McKenna, F. & Fenves, G.L. (2005). *OpenSees command language manual*. Pacific Earthquake Engineering Research (PEER) Center.

Padgett, J.E., & DesRoches, R. (2007). Bridge functionality relationships for improved seismic risk assessment of transportation networks. *Earthquake Spectra*, 23(1), 115–130.

Park, Y.J., & Ang, A.H.S. (1985). Mechanistic seismic damage model for reinforced concrete. *Journal of Structural Engineering*, 111(4), 722–739.

Renschler, C.S., Frazier, A.E., Arendt, L.A., Cimellaro, G.P., Reinhorn, A.M., & Bruneau, M. (2010). Developing the 'PEOPLES' Resilience Framework for defining and measuring disaster

resilience at the community scale. *Proceedings of the 9th US National and 10th Canadian Conference on Earthquake Engineering (9USN/10CCEE)*, July 25-29, Toronto, Ontario, Canada.

Rose, A. (2004). Defining and measuring economic resilience to disasters. *Disaster Prevention and Management*, 13(4), 307–314.

Rose, A., Benavides, J., Chang, S.E., Szczesniak, P., & Lim, D. (1997). The regional economic impact of an earthquake: direct and indirect effects of electricity lifeline disruptions. *Journal of Regional Science*, 37(3), 437–458.

Shinozuka, M. (2009). Resilience and sustainability of infrastructure systems. *Frontier Technologies in Infrastructure Engineering: Structures and Infrastructures Book Series*, 4, 245.

Titi, A., & Biondini, F. (2013). Resilience of concrete frame structures under corrosion. *Proceedings of the 11th International Conference on Structural Safety and Reliability* (*ICOSSAR2013*), June 16-20, New York, NY, USA.

UN/ISDR (2009). *Global assessment report on disaster risk reduction*. United Nations International Strategy for Disaster Reduction, Geneva.

Xu, N., Guikema, S.D., Davidson, R.A., Nozick, L. K., Çağnan, Z., & Vaziri, K. (2007). Optimizing scheduling of post-earthquake electric power restoration tasks. *Earthquake Engineering & Structural Dynamics*, 36(2), 265–284.

CHAPTER 6

CONCLUSIONS

The Thesis presented a probabilistic approach to lifetime assessment of seismic performance and resilience of concrete structures under corrosion. The present work is part of a broad research field aimed to investigate the performance of structural systems under multiple hazards. The investigation moved from the consideration that the combined effects of the deterioration processes affecting concrete structures in aggressive environments and seismic hazard result to be of critical importance in the evaluation of the long-term behavior of structural systems. In fact, huge stocks of existing buildings, bridges and other infrastructure facilities are currently deteriorated showing structural deficiencies, which affect the serviceability of the response of such structures under accidental actions or extreme events. In particular, earthquakes may produce high losses and extensive community disruption.

Among the damage mechanisms affecting concrete structures over time, the effects of chloride-induced corrosion on both reinforcing steel and concrete have been investigated. A simplified one-dimensional model for chloride diffusion has been adopted as a convenient mathematical tool for most of practical applications as suggested by current design codes. Proper damage functions have been adopted to model deterioration at material level. These models accounted for the reduction of

reinforcing steel cross-section area and ultimate strain and degradation of concrete strength. These effects, which depend on the type of corrosion process, have been effectively modeled by time-variant nonlinear stress-strain relationships in the analysis of corroded cross-section. The formulation of a time-variant stiffness matrix accounted then for mechanical nonlinearity as well as material deterioration. The effectiveness of this approach has been validated by comparison between numerical and experimental results of tests carried out on corroded concrete members. Good accuracy has been achieved by using both distributed and lumped plasticity models for the structural analysis.

Lumped plasticity models have been selected for the probabilistic lifetime structural analysis, being accurate though in general less computationally expensive. The structural effects of material deterioration have been effectively modeled by time-variant bending moment versus curvature relationships, which define the flexural behavior of the plastic hinge zones concentrated at beam ends. A reduced structural performance has been observed depending on the corrosion level over time. This is assessed by the time evolution of performance indicators such as the resistant bending moment and curvature ductility at cross-sectional level. As a consequence, the bending capacity and displacement ductility of deteriorated concrete elements has been proved to vary over time.

The structural behavior of deteriorating systems under earthquake loading has been investigated by means of a probabilistic approach accounting for the interaction between environmental and seismic hazard. The lifetime seismic capacity of the structures has been evaluated taking into account the uncertainties related to the material and geometrical properties, the physical models of the deterioration process, and the mechanical and environmental stressors. Randomness in the earthquake events and increasing levels of seismic intensity have been considered as well. This approach allowed a reliable analysis of concrete structures under deterioration. It has been shown that the effects of the local deterioration on the overall seismic performance of concrete structures over time depend on both the type of structure, the exposure scenario and the seismic hazard. The effectiveness of the proposed procedure has been shown through applications, including a multi-story building and a continuous bridge. The lifetime performance of such structures has been investigated by means of nonlinear static and dynamic analyses.

The results obtained for both structures showed a significant reduction of shear strength and a variation of displacement ductility in the overall response to seismic loading. In fact, the time-evolution of the cross-sectional behavior of the plastic hinge zones at the bottom of deteriorated columns and piers has been proved to increase the vulnerability of the structural system to seismic hazard over time. In fact, depending on the exposure of the concrete members and on the structural scheme, the lifetime variation of strength and stiffness of the elements exposed to corrosion may alter the resisting hierarchy and the energy-dissipating failure mode due to the redistribution of

internal forces. In particular, the seismic capacity design criteria adopted for buildings may no longer hold, and the selected collapse mechanism involving the maximum number of stories may not occur after several year of lifetime. For integral bridges, a seismic design based on displacement limit states may become unsatisfactory over time since the structural response under earthquake loading strictly depends on the on the capacity of the piers under deterioration.

These results highlighted that design targeted to satisfy certain performance levels in terms of both forces (over-strength factors) or displacements (drift limits), as stated by recent performance-based design codes, are not sufficient for a reliable assessment of the seismic performance of structural system in aggressive environments. Time-invariant seismic design criteria should hence be revised in order to account for both seismic and environmental hazard by considering increasing seismic intensity and varying exposure aggressiveness. To this aim, the evaluation of the residual capacity of concrete members over time has to be carried out, as suggested in the proposed approach. A proper calibration of limit states and over-strength factors is then needed to ensure suitable levels of performance and safety in a life-cycle oriented design of durable structures. Moreover, proper repair interventions should be planned to restore adequate functionality levels of structurally deficient existing structures.

In a perspective of risk mitigation, the extension of the presented methodology to the assessment of lifetime resilience highlighted the need to improve current resilience analysis procedures, by assuming a time-variant system functionality. In fact, the functionality of deteriorating structural systems shows a progressive decay in time due to aging and environmental aggressiveness. As a consequence, the post-event functionality and seismic resilience resulted to be dependent on the current functionality state of the system and on the seismic intensity level. The application of the procedure for the assessment of lifetime resilience to the case study of the continuous bridge showed a time-variant functionality loss depending on the time of occurrence of the seismic event of the structure for a given exposure scenario. This effect is emphasized at both the increase of the PGA level and the progress of deterioration over lifetime. This confirms the need of a direct evaluation of environmental deterioration and seismic damage. Moreover, the investigation on efficiency coefficients for evaluating the influence of repair actions and post-recovery target functionality showed the effectiveness of prompt interventions and the importance of maintenance in enhancing the resilience of the structure. The type of recovery profile and the post-recovery target functionality has been proved to be important factors to ensure suitable levels of lifetime seismic resilience in a timely and efficient manner.

The present work highlighted the need of incorporating life-cycle concepts in structural design codes in the perspective of service life extension and contributed to a reliable resilience assessment of concrete structures under seismic and environmental hazards. Further investigation about the

interaction between seismic and corrosion hazards is however needed for a reliable time-dependent structural analysis. Different exposure conditions should be considered in order to investigate the effects of increasing environmental aggressiveness and/or localized exposure. A proper calibration of the deterioration model based on experimental data is recommended. The possible recurrence of seismic events should be taken into account as well. Different failure mechanisms, such as shear failure, should by accounted for. Moreover, different structural typologies of frames and bridges should be considered in order to investigate the effects of the structural scheme on the global lifetime performance.

Future research should also address several issues regarding the assessment of seismic resilience of deteriorating structures. Nonlinear functionality indicators based on seismic capacity thresholds should be formulated and recovery functions based on the type, magnitude and location of damage should be implemented. Moreover, the effects of preventive maintenance and repair, which may be planned to guarantee a satisfying resilience target level over lifetime, need to be taken into account. Uncertainties related to other parameters such as the idle time, the recovery time, the target functionality and the investigated time horizon should also be considered in a complete probabilistic framework.

These aspects could be implemented in the proposed general approach for lifetime seismic analysis and resilience assessment of deteriorating structures. In fact, despite the need of further research, the presented methodology has been proved to be a powerful and effective engineering tool aimed at promoting and supporting a life-cycle oriented design to meet the need of resilient structures and infrastructures under seismic and environmental hazards.

REFERENCES

[1] ACI-365 (2000). *Service-life Prediction*. State of the art report, American Concrete Institute, Committee 365.

[2] Akgül, F., & Frangopol, D.M. (2004). Lifetime performance analysis of existing prestressed concrete bridge superstructures. *Journal of Structural Engineering*, 130(12), 1889–1903.

[3] Akiyama, M., & Frangopol, D.M. (2010). On life-cycle reliability under earthquake excitations of corroded reinforced concrete structures. *Proceedings of the Second International Symposium on Life-Cycle Civil Engineering (IALCCE2010)*, Taipei, Taiwan, October 27-31.

[4] Akiyama, M., Frangopol, D.M., & Matsuzaki, H., (2011). Life-cycle reliability of RC bridge piers under seismic and airborne chloride hazards. *Earthquake Engineering and Structural Dynamics*, 40 (15), 1671–1687.

[5] Akiyama, M., Frangopol, D.M., & Suzuki, M. (2011). Integration of the effects of airborne chlorides into reliability-based durability design of reinforced concrete structures in a marine environment. *Structure and Infrastructure Engineering*, 8(2), 125–134.

[6] Akiyama, M., Matsuzaki, H., Dang, H.T., & Suzuki, M. (2012). Reliability-based capacity design for reinforced concrete bridge structures. *Structure and Infrastructure Engineering*, 8(12), 1096–1107.

[7] Alesch, D.J., Dargush, G.F., Grigoriu, M., Petak, W.J., & von Winterfeldt, D. (2003). Decision models: approaches for achieving seismic resilience. *Research Progress and Accomplishments, 2001-2003*.

[8] Al-Harthy, A.S., Stewart, M.G., & Mullard, J. (2011). Concrete cover cracking caused by steel reinforcement corrosion. *Magazine of Concrete Research*, 63(9), 655–667.

[9] Alipour, A., Shafei, B., & Shinozuka, M.S. (2013). Capacity loss evaluation of reinforced concrete bridges located in extreme chloride-laden environments. *Structure and Infrastructure Engineering*, 9(1), 8–27.

[10] Almusallam, A.A., Al-Gahtani, A.S., Aziz, A. R., Dakhil, F.H., & Rasheeduzzafar (1996). Effect of reinforcement corrosion on flexural behavior of concrete slabs. *Journal of Materials in Civil Engineering*, 8(3), 123-127.

[11] Alonso, A., & Andrade, C. (1994). Life time of rebars in carbonated concrete, in *Progress in Understanding and Prevention of Corrosion*, J.M. Costa, A.D. Mercer (Eds.), *Institute of Materials, London*, 634–641.

[12] Alonso, C., Andrade, J., Rodriguez, J., & Diez, J.M. (1998). Factors controlling cracking of concrete affected by reinforcement corrosion. *Materials and Structures*, 31, 435–441.

[13] Alonso, C., Castellote, M., & Andrade, C. (2001). Dependence of chloride threshold with the electrical potential of reinforcements. In *2nd Int. RILEM Workshop on Testing and Modeling the Chloride Ingress into Concrete*, PRO19, 415–425.

[14] Alonso, C., Castellote, M., & Andrade, C. (2002). Chloride threshold dependence of pitting potential of reinforcements. *Electrochimica Acta*, 47(21), 3469–3481.

[15] Andrade, C. (2002). Determination of chloride threshold in concrete. In *Proposal of the Monitoring, Group WG-B3-COST521, Final Report Workshop of COST-521*, Ed. R. Weydert, Luxembourg, 108–119.

[16] Andrade, C., & Alonso, C. (2001). On-site measurements of corrosion rate of reinforcements, *Construction and Building Materials*, 15, 141–145.

[17] Andrade, C., Alonso, M.C., & Gonzalez, J.A. (1990). An initial effort to use the corrosion rate measurement for estimating rebar durability. *Corrosion Rates of Steel in Concrete*, *ASTM STP 1065*, N.S. Berke, V. Chaker and D. Whinting Eds., American Society for Testing and Materials, Philadelphia, 29–37.

[18] Andrade, C., Alonso, C., & Sarrìa, J., (2002). Corrosion rate evolution in concrete structures exposed to the atmosphere, *Cement & Concrete Composites*, 24, 55–64.

[19] Ang, A.H.-S. & Tang, W.H. (2007). *Probability Concepts in Engineering.* 2nd Edition, John Wiley & Sons, Hoboken, NJ, USA.

[20] Angst, U., Elsener, B., Larsen, C.K., & Vennesland, Ø. (2009). Critical chloride content in reinforced concrete – a review. *Cement and Concrete Research*, 39(12), 1122–1138.

[21] Apostolopoulos, C.A., & Papadakis, V.G. (2008). Consequences of steel corrosion on the ductility properties of reinforcement bar. *Construction and Building Materials*, 22(12), 2316–2324.

[22] Arup, H. (1983). The mechanisms of the protection of steel by concrete. *Society of Chemical Industry*, 151–157.

[23] ASCE (2013). *Report card for America's Infrastructure*. American Society of Civil Engineers, Reston, VA. http://www.infrastructurereportcard.org/a/#p/bridges/overview

[24] ATC (1985). *Earthquake Damage Evaluation Data for California*. Technical Report, Applied Technology Council, ATC-13, Redwood City, CA.

[25] Bakker, R. (1994). Prediction of service life reinforcement in concrete under different climatic conditions at given cover. *International Conference on Corrosion and Protection of Steel in Concrete,* Sheffield, UK.

[26] Bakker, R., Van der Wegen, G., & Bijen, J. (1994). Reinforced concrete: an assessment of the allowable chloride content. *Proceedings of CANMET/ACI International* Conference on Durability of Concrete, Nice.

[27] Bamforth, P.B. (1994). Prediction of the onset of reinforcement corrosion due to chloride ingress. *Proceedings of International Conference on Concrete across Borders.*

[28] Bamforth, P.B., & Chapman-Andrews, J.F. (1994). Long term performance of RC elements under UK coastal exposure conditions. *Proceedings of International Conference on Corrosion and corrosion protection of steel in concrete*, R.N. Swamy (Ed.), Sheffield Academic Press, 139–156.

[29] Bamforth, P.B., Price, W.F. (1996) An International Review of Chloride Ingress into Structural Concrete. *Rep. No. 1303/96/9092, Taywood Engineering Ltd., Technology division*, Middlesex, U.K.

[30] Banon, H., Irvine, H.M., & Biggs, J.M. (1981). Seismic damage in reinforced concrete frames. *Journal of the Structural Division*, 107(9), 1713–1729.

[31] Bažant, Z.P. (1979). Physical model for steel corrosion in concrete sea structures. *Journal of the Structural Division, ASCE*, 105(ST6), 1137–1166.

[32] Bentur, A., Diamond, S., & Berke, N.S. (1997). *Steel Corrosion in Concrete, Fundamentals and Civil Engineering Practice*, E&FN Spon Press.

[33] Berry, M.P., & Eberhard, M.O. (2005). Practical performance model for bar buckling. *Journal of Structural Engineering*, 131(7), 1060–1070.

[34] Berto, L., Vitaliani, R., Saetta, A., & Simioni, P., (2009). Seismic assessment of existing RC structures affected by degradation phenomena. *Structural Safety*, 31, 284–297.

[35] Bertolini, L. (2008). Steel corrosion and service life of reinforced concrete structures. *Structure and Infratructure Engineering*, 4(2), 123–137.

[36] Bertolini, L., Elsener, B. Pedeferri, P., & Polder R. (2004). *Corrosion of Steel in Concrete – Prevention, Diagnosis and Repair*. Wiley-VCH, Weinheim.

[37] Bhargava, K., Ghosh, A.K., Mori, Y., & Ramanujam, S. (2007). Corrosion-induced bond strength degradation in reinforced concrete -Analytical and empirical models. *Nuclear Engineering and Design*, 237(11), 1140–1157.

[38] Biczok, I. (1972). *Concrete Corrosion, Concrete Protection*. Akademiai Kiado, Budapest, Wiesbaden.

[39] Biondini, F. (2000). *Strutture da Ponte Soggette ad azioni di Tipo Sismico – Modellazione ed Ottimizzazione*. PhD Dissertation, Department of Structural Engineering, Politecnico di Milano, Milan, Italy.

[40] Biondini, F. (2004). A three-dimensional finite beam element for multiscale damage measure and seismic analysis of concrete structures. *Proceedings of the 13th World Conference on Earthquake Engineering (WCEE)*, August 1-6, Vancouver, BC, Canada: Paper No. 2963.

[41] Biondini, F. (2011). Cellular automata simulation of damage processes in concrete structures. In: *Soft Computing Methods for Civil and Structural Engineering*, Y. Tsompanakis and B.H.V. Topping, (Editors), Saxe-Coburg Publications, Stirlingshire, Scotland, Chapter 10, 229–264.

[42] Biondini, F., Bontempi, F., Frangopol, D.M., & Malerba, P.G. (2004). Cellular automata approach to durability analysis of concrete structures in aggressive environments. *Journal of Structural Engineering, ASCE*, 130(11), 1724–1737.

[43] Biondini, F., Bontempi, F., Frangopol, D.M., & Malerba, P.G. (2004). Reliability of material and geometrically non-linear reinforced and prestressed concrete structures. *Computers & structures*, 82(13), 1021–1031.

[44] Biondini, F., Bontempi, F., Frangopol, D.M., & Malerba, P.G. (2006). Probabilistic service life assessment and maintenance planning of concrete structures, *Journal of Structural Engineering, ASCE*, 132(5), 810–825.

[45] Biondini, F., Camnasio, E., & Palermo, A. (2010). Lifetime seismic performance of concrete bridges. *Proceedings of the Fifth International Conference on Bridge Maintenance, Safety, and Management (IABMAS2010)*, July 11-15, Philadelphia, PA.

[46] Biondini, F., Camnasio, E., & Palermo, A. (2012). Life-cycle performance of concrete bridges exposed to corrosion and seismic hazard. *Proceedings of the Structures Congress 2012 (ASCE2012)*, Chicago, IL, March 29-31.

[47] Biondini, F., Camnasio, E., & Palermo, A. (2013). Lifetime Seismic Performance of Concrete Bridges Exposed to Corrosion. *Structure and Infrastructure Engineering*, ahead-of-print, doi:10.1080/15732479.2012.761248.

[48] Biondini, F., & Frangopol, D.M. (2008). Probabilistic limit analysis and lifetime prediction of concrete structures. *Structure and Infrastructure Engineering*, 4(5), 399–412.

[49] Biondini, F., & Frangopol, D.M. (Eds.) (2008). *Life-Cycle Civil Engineering*. CRC Press, Taylor & Francis Group.

[50] Biondini, F., & Frangopol, D.M. (2009). Lifetime reliability-based optimization of reinforced concrete cross-sections under corrosion. *Structural Safety*, 31(6), 483–489.

[51] Biondini, F., & Frangopol, D.M. (2010). Life-cycle performance of reinforced concrete structures exposed to aggressive agents: Design issues. *Proceedings of the SEI-ASCE Structures Congress 2010*.

[52] Biondini, F., & Frangopol, D.M. (2011). *Life-Cycle of Civil Engineering Systems*. Special Issue of *Structure and Infrastructure Engineering*, 7(1-2), 1–196.

[53] Biondini, F., Frangopol, D.M. & Malerba, P.G. (2008). Uncertainty Effects on Lifetime Structural Performance of Cable-Stayed Bridges, *Probabilistic Engineering Mechanics*, 23(4), 509–522.

[54] Biondini, F., Frangopol, D.M., & Malerba, P.G. (2010). Structural geometry effects on the life-cycle performance of concrete bridge structures in aggressive environments. In *Bridge Maintenance, Safety Management, Health Monitoring and Informatics – IABMAS08: Proceedings of the Fourth International IABMAS Conference*, Seoul, Korea, July 13-17.

[55] Biondini, F., Palermo, A., & Toniolo, G. (2011). Seismic performance of concrete structures exposed to corrosion: case studies of low-rise precast buildings. *Structure and Infrastructure Engineering*, 7(1-2), 109–119.

[56] Biondini, F., & Toniolo, G. (2009). Probabilistic calibration and experimental validation of the seismic design criteria for one-story concrete frames. *Journal of Earthquake Engineering*, 13(4), 426–462.

[57] Biondini, F., Toniolo, G., & Tsionis, G. (2010). Capacity design and seismic performance of multi-storey precast structures. *European Journal of Environmental and Civil Engineering*, 14(1), 11-28.

[58] Biondini, F., & Vergani, M. (2011). Modellazione del degrado di strutture in calcestruzzo armato soggette a corrosione (in Italian). *Giornate AICAP 2011*, Padua, May 19–21.

[59] Biondini, F., & Vergani, M. (2012). Damage modeling and nonlinear analysis of concrete bridges under corrosion. *Proceedings of the Sixth International Conference on Bridge Maintenance, Safety and Management* (*IABMAS 2012*), Stresa, Lake Maggiore, Italy, July 8-12.

[60] Bocchini, P., Decò, A., & Frangopol, D.M. (2012). Probabilistic functionality recovery model for resilience analysis. *Proceedings of the 6th International Conference on Bridge Maintenance, Safety and Management* (*IABMAS*), July 8-12, Stresa, Lake Maggiore, Italy.

[61] Bocchini, P., & Frangopol, D.M. (2012). Optimal resilience-and cost-based postdisaster intervention prioritization for bridges along a highway segment. *Journal of Bridge Engineering*, 17(1), 117–129.

[62] Bocchini, P., & Frangopol, D.M. (2012). Restoration of bridge networks after an earthquake: Multi-criteria intervention optimization. *Earthquake Spectra*, 28(2), 426–455.

[63] Bontempi, F. (1992). Sulla costruzione dei domini di rottura di sezioni in C.A. e C.A.P. soggette a pressoflessione deviata. *Studi e Ricerche*, *Graduate School for Concrete Structures "F.lli Pesenti"*, Politecnico di Milano, Milan, Italy, 13, 261–277 (in Italian).

[64] Bontempi, F., & Malerba, P.G. (1997). The role of softening in the numerical analysis of RC framed structures. *Structural Engineering and Mechanics*, 5(6), 785–801.

[65] Bontempi, F., Malerba, P.G., & Romano, L. (1995). Formulazione diretta secante dell'analisi non lineare di telai in C.A./C.A.P.. *Studi e Ricerche*, *Graduate School for Concrete Structures "F.lli Pesenti"*, Politecnico di Milano, Milan, Italy, 16, 351–386 (in Italian).

[66] Boulfiza, M., Sakai, K., Banthia, N., & Yoshida, H. (2003). Prediction of chloride ions ingress in uncracked and cracked concrete, *ACI Materials Journal*, Title No.100-M5, 38–48.

[67] Broomfield, J.P. (1997). *Corrosion of Steel in Concrete*, Spon Press.

[68] Browne, R.D., Geoghegan, M.P., & Baker, A.F. (1983). *Corrosion of Reinforcements in Concrete Construction*. A.P Crane Ed., Ellis Hordwood Ltd, London, 193–222.

[69] Bruneau, M., Chang, S.E., Eguchi, R.T., Lee, G.C., O'Rourke, T.D., Reinhorn, A.M., Shinozuka, M., Tierney, K., Walace, W.A., & von Winterfeldt, D.V (2003). A framework to quantitatively assess and enhance the seismic resilience of communities. *Earthquake Spectra*, 19(4), 733–752.

[70] Bruneau, M., & Reinhorn, A. (2004). Seismic resilience of communities-conceptualization and operationalization. *Proceedings of the International Workshop on Performance-based Seismic-Design, Bled, Slovenia*, June 28-July 1 (Vol. 1).

[71] Bruneau, M., & Reinhorn, A. (2007). Exploring the concept of seismic resilience for acute care facilities. *Earthquake Spectra*, 23(1), 41–62.

[72] Burks, A.W. & Von Neumann, J. (1966). *Theory of self-reproducing automata*. University of Illinois Press, 1966.

[73] Cabrera, J.G. (1996). Deterioration of concrete due to reinforcement steel corrosion. *Cement & Concrete Composites*, 18, 47–59.

[74] Çağnan, Z., Davidson, R. A., & Guikema, S. D. (2006). Post-earthquake restoration planning for Los Angeles electric power. *Earthquake Spectra*, 22(3), 589–608.

[75] Cairns, J., Plizzari, G.A., Du, Y., Law, D.W., & Franzoni, C. (2005). Mechanical properties of corrosion-damaged reinforcement. *ACI Materials Journal*, 102(4).

[76] Carr, A.J. (2008). *RUAUMOKO Program for Inelastic Dynamic Analysis*. Department of Civil Engineering, University of Canterbury, Christchurch, New Zealand.

[77] CEB (1985). *Model Code for Seismic Design of Concrete Structures*. Bulletin 165.

[78] CEB (1992). *Durable Concrete Structures – Design Guide*. Bulletin 183.

[79] CEB (1997). *New Approach to Durability Design*. Committee Eurointernational du Beton, Bulletin, 283.

[80] CEB (1998). *Seismic Design of Reinforced Concrete Structures for controlled Inelastic Response*. Bulletin 240.

[81] CEN-EN 1992-1-1 (2004). *Eurocode 2 – Design of concrete structures - Part 1-1: General rules and rules for buildings*. European Committee for Standardization, Brussels.

[82] CEN-EN 1992-2 (2006). *Eurocode 2 – Design of concrete structures - Part 2: Concrete bridges – Design and detailing rules*. European Committee for Standardization, Brussels.

[83] CEN-EN 1998-1 (2004). *Eurocode 8: Design of Structures for Earthquake Resistance. Part 1: General rules, seismic actions and rules for buildings*. European Committee for Standardization, Brussels.

[84] Ceravolo, R., De Stefano, A., & Pescatore, M. (2008). Change in dynamic parameters and safety assessment of civil structures. *Mechanics of Time-Dependent Materials*, 12(4), 365–376.

[85] Ceravolo, R., De Stefano, A., & Pescatore, M. (2008). Including structural monitoring activities in safety probabilistic formulations: *Proceedings of the International Symposium on Life-Cycle Civil Engineering* (*IALCCE08*), June 11-14, Varenna, Lake Como, Italy.

[86] Ceravolo, R., Pescatore, M., & De Stefano, A. (2009). Symptom-based reliability and generalized repairing cost in monitored bridges. *Reliability Engineering & System Safety*, 94(8), 1331–1339.

[87] Chang, S.E. (2000). Disasters and transport systems: loss, recovery and competition at the Port of Kobe after the 1995 earthquake. *Journal of Transport Geography*, 8(1), 53–65.

[88] Chang, S.E., Pasion, C., Tatebe, K. & Ahmad, R. (2008). *Linking Lifeline Infrastructure Performance and Community Disaster Resilience: Models and Multi-Stakeholder Processes*, Report MCEER-08-0004.

[89] Chang, S.E., & Shinozuka, M. (2004). Measuring improvements in the disaster resilience of communities. *Earthquake Spectra*, 20(3), 739–755.

[90] Chang, S.E., Svekla, W.D., & Shinozuka, M. (2002). Linking infrastructure and urban economy: simulation of water-disruption impacts in earthquakes. *Environment and Planning B: Planning and Design*, 29(2), 281–302.

[91] Chen, S-S, Frangopol, D.M. & Ang, A-H. S. (2010). *Life-Cycle of Civil Engineering Systems*, Taiwan Building Technology Center, DnE Information Service Net, Taipei, Taiwan, 2010.

[92] Choe, D.E., Gardoni, P., Rosowsky, D., & Haukaas, T. (2008). Probabilistic capacity models and seismic fragility estimates for RC columns subject to corrosion. *Reliability Engineering & System Safety*, 93(3), 383–393.

[93] Choe, D.E., Gardoni, P., Rosowsky, D., & Haukaas, T. (2009). Seismic fragility estimates for reinforced concrete bridges subject to corrosion. *Structural Safety*, 31, 275–283.

[94] Choi, E., DesRoches, R., & Nielson, B. (2004). Seismic fragility of typical bridges in moderate seismic zones. *Engineering Structures*, 26(2), 187–199.

[95] Cimellaro, G.P., Christovasilis, I.P., Reinhorn, A.M., DeStefano, A. & Kirova, T. (2010). *L'Aquila Earthquake of April 6, 2009 in Italy: Rebuilding a Resilient City to Multiple Hazard*. Report MCEER-10-0010.

[96] Cimellaro, G.P., Fumo, C., Reinhorn, A.M. & Bruneau, M. (2009) *Quantification of Disaster Resilience of Health Care Facilities*. Report MCEER-09-0009.

[97] Cimellaro, G.P., Reinhorn, A.M., & Bruneau, M. (2005). Seismic resilience of a health care facility. *Proceedings of the 2005 ANCER Annual Meeting, Session III*, November 10–13, Jeju, Korea.

[98] Cimellaro, G.P., Reinhorn, A.M., & Bruneau, M. (2006). Quantification of seismic resilience. *Proceedings of the 8th National Conference of Earthquake Engineering*, April 18-22, San Francisco, California, USA.

[99] Cimellaro, G. P., Reinhorn, A. M., & Bruneau, M. (2010). Framework for analytical quantification of disaster resilience. *Engineering Structures*, 32(11), 3639–3649.

[100] Cimellaro, G.P., Reinhorn, A.M., & Bruneau, M. (2010). Seismic resilience of a hospital system. *Structure and Infrastructure Engineering*, 6(1-2), 127–144.

[101] Collepardi, M. (2006). *The New Concrete*. Grafiche Tintoretto.

[102] Collepardi, M., Marcialis, A., & Turriziani, R. (1970). Kinetic of penetration of chloride ions into concrete (in Italian). *Industria Italiana del Cemento* 4, 157–164

[103] Collepardi, M., Marcialis, A., & Turriziani, R. (1972). Penetration of chlorides ions into cement paste and concretes. *Journal of American Ceramic Society*, 55, 534–535.

[104] Cornell, C.A., Jalayer, F., Hamburger, R.O., & Foutch, D.A. (2002). Probabilistic basis for 2000 SAC Federal Emergency Management Agency steel moment frame guidelines. *Journal of Structural Engineering*, 128(4), 526–533.

[105] Coronelli, D., & Gambarova, P. (2004). Structural assessment of corroded reinforced concrete beams: Modeling guidelines. *Journal of Structural Engineering*, 130(8), 1214–1224.

[106] Cosenza, E., & Manfredi, G. (2000). Damage indices and damage measures. *Progress in Structural Engineering and Materials*, 2(1), 50–59.

[107] Cosenza, E., Manfredi, G., & Ramasco, R. (1993). The use of damage functionals in earthquake engineering: a comparison between different methods. *Earthquake Engineering & Structural Dynamics*, 22(10), 855–868.

[108] Decò, A., Bocchini, P., & Frangopol, D.M. (2013). A probabilistic approach for the prediction of seismic resilience of bridges. *Earthquake Engineering & Structural Dynamics*. doi: 10.1002/eque.2282.

[109] den Uijl, J.A., & Kaptijn, N. (2002). Structural consequences of ASR: an example on shear capacity. *Heron*, 47(2), 125–139.

[110] Der Kiureghian, A., & Ditlevsen, O. (2009). Aleatory or epistemic? does it matter? *Structural Safety*, 31(2), 105–112.

[111] Dhakal, R.P., & Maekawa, K. (2002). Reinforcement stability and fracture of cover concrete in reinforced concrete members. *Journal of Structural Engineering*, 128(10), 1253–1262.

[112] Dhir, R.K., Jones, M.R., & McCarthy, M.J. (1987). PFA concrete: Chloride induced corrosion. *Magazine of Concrete Research*, 46(169), 269–277.

[113] DM 14 Gennaio 2008. *Norme tecniche per le costruzioni*. Gazzetta Ufficiale della Repubblica Italiana.

[114] Du, Y.G., Clark, L.A., & Chan, A.H.C. (2005). Effect of corrosion on ductility of reinforcing bars. *Magazine of Concrete Research*, 57(7), 407–419.

[115] Duracrete (2000). *The European Union – Brite EuRam III, DuraCrete – Probabilistic Performance Based Durability Design of Concrete Structures*. Final Technical Report of Duracrete Project, Document BE95-1347/R17, CUR, Gouda (NL).

[116] EN 206-1 (2001). *Concrete – Part 1. Specification, Performance, Production and Conformity*, European Committee for Standardization, 2001.

[117] EN 1990 (2002). *Eurocode – Basis of Structural Design*, European Committee for Standardization.

[118] Enright, M.P., & Frangopol, D.M. (1998). Service-life prediction of deteriorating concrete bridges. *Journal of Structural Engineering*, 124(3), 309-317.

[119] ENV 13670-1 (2000). *Execution of Concrete Structures*, European Committee for Standardization.

[120] Estes, A.C., & Frangopol, D.M. (2005). Life-cycle evaluation and condition assessment of structures. *Structural Engineering Handbook*, Chapter 36, 1–51.

[121] Estes, A.C., & Frangopol, D.M. (2001). Bridge lifetime system reliability under multiple limit states. *Journal of Bridge Engineering*, 6 (6), 523–528.

[122] Fang, C., Gylltoft, K., Lundgren, K., & Plos, M. (2006). Effect of corrosion on bond in reinforced concrete under cyclic loading. *Cement and Concrete Research*, 36(3), 548–555.

[123] FEMA (2000). *Planning for a Sustainable Future: The link between Hazard Mitigation and Livability*, Federal Emergency Management Agency, Washington, DC.

[124] FEMA (2000). *Prestandard and commentary for the seismic rehabilitation of buildings*. Report FEMA-356, Department of Homeland Security, Federal Emergency Management Agency, Washington, DC.

[125] FEMA (2009). *HAZUS-MH MR4 Earthquake Model User Manual*. Department of Homeland Security, Federal Emergency Management Agency, Washington, D.C., US.

[126] FEMA 356 (2000). *Pre-Standard and Commentary for the Seismic Rehabilitation of Buildings*. Federal Emergency Management Agency and US Army Corps of Engineers.

[127] *fib* (2006). *Model Code for Service Life Design*. Bulletin, 34.

[128] Frangopol, D.M. (2011). Life-cycle performance, management, and optimisation of structural systems under uncertainty: accomplishments and challenges 1. *Structure and Infrastructure Engineering*, 7(6), 389–413.

[129] Frangopol, D.M., & Akiyama, M. (2011). Lifetime seismic reliability analysis of corroded reinforced concrete bridge piers. In *Computational Methods in Earthquake Engineering*, Springer Netherlands, 527–537.

[130] Frangopol, D.M., Bruhwiler, E. Faber, M.H, & Adey, B. (Eds.). (2004a). *Life-cycle performance of deteriorating structures: Assessment, design, and management*. American Society of Civil Engineers Reston, Virginia.

[131] Frangopol, D.M. & Ellingwood, B.R. (2010). Life-Cycle Performance, Safety, Reliability and Risk of Structural Systems. Editorial, *Structure Magazine*, Joint Publication of NCSEA, CASE, SEI.

[132] Frangopol, D.M., & Furuta, H. (Eds.). (2001). *Life-Cycle Cost Analysis and Design of Civil Infrastructure Systems*. American Society of Civil Engineers, ASCE, Reston, Virginia.

[133] Frangopol, D.M., Kallen, M.J., & Noortwijk, J.M.V. (2004b). Probabilistic models for life-cycle performance of deteriorating structures: review and future directions. *Progress in Structural Engineering and Materials*, 6(4), 197–212.

[134] Frangopol, D.M., Lin, K.Y., & Estes, A.C. (1997). Life-cycle cost design of deteriorating structures. *Journal of Structural Engineering*, 123(10), 1390–1401.

[135] Frangopol, D.M., Lin, K.-Y., & Estes, A. (1997). Reliability of reinforced concrete girders under corrosion attack. *Journal of Structural Engineering*,123(3), 286–297.

[136] Frangopol, D.M., & Liu, M. (2007). Maintenance and management of civil infrastructure based on condition, safety, optimization, and life-cycle cost. *Structure and Infrastructure Engineering*, 3(1), 29–41.

[137] Frederiksen, J. M., Nilsson, L.O., Poulsen, E., Sandberg, P., Sorcnsen, H.E., & Klinghoffer, O. (1996). *HETEK - Chloride penetration into concrete - State of the art. Transport processes, corrosion initiation, test methods and prediction models*, The Road Directorate, Report (53), Copenhagen.

[138] Fukada, Y. (1969). Study on the restoring force characteristics of reinforced concrete buildings. *Proceedings of the Kanto District Symposium*, Tokyo, Japan, Architectural Institute of Japan, 40 (in Japanese).

[139] Ghods, P., Chini, M., Alizadeh, R., Hoseini, M., Shekarchi, M., & Ramezanianpour, A.A. (2005). The effect of different exposure conditions on the chloride diffusion into concrete in the Persian Gulf region. *Proceedings of the ConMAT Conference.*

[140] Ghosh, J., & Padgett, J.E. (2009). Multi-hazards considerations of seismic and aging threats to bridges. *Proceedings of the Structures Conference 2009 (ASCE2009)*, April 30 – May 2, Austin, TX, USA.

[141] Ghosh, J., & Padgett, J.E. (2010). Aging considerations in the development of time-dependent seismic fragility curves. *Journal of Structural Engineering*, 136(12), 1497–1511.

[142] Giberson, M.F. (1967). *The Response of Nonlinear Multi-story Structures Subjected to Earthquake Excitation*. PhD Dissertation, California Institute of Technology, Pasadena, CA.

[143] Giberson, M.F. (1967). *The Response of Nonlinear Multi-story Structures Subjected to Earthquake Excitation*. PhD Dissertation, California Institute of Technology, Pasadena, CA.

[144] Giberson, M.F. (1969). Two nonlinear beams with definitions of ductility. *Journal of the Structural Division*, 95(ST2), 137–57.

[145] Gjørv, O.E. (2009). *Durability Design of Concrete Structures in Severe Environments*, Taylor and Francis.

[146] Glass, G.K., & Buenfeld, N.R. (1997). The presentation of the chloride threshold level for corrosion of steel in concrete. *Corrosion Science*, 39(5), 1001–1013.

[147] Glass, G.K., & Buenfeld, N.R. (2000). The inhibitive effects of electrochemical treatment applied to steel in concrete. *Corrosion Science*, 42(6), 923–927.

[148] Glass, G.K., Page, C.L., & Short, N.R. (1991). Factors affecting the corrosion rate of steel in carbonated mortars. *Corrosion Science*, 32(12), 1283–1294.

[149] Glicksman, M.E. (2000). *Diffusion in solids*. New York, NY: John Wiley & Sons.

[150] Gonzalez, J.A., Andrade, C., Alonso, C., & Feliu, S. (1995). Comparison of rates of general corrosion and maximum pitting penetration on concrete embedded steel reinforcement. *Cement and Concrete Research*, 25(2), 257–264.

[151] Gosain, N.K., Jirsa, J.O., & Brown, R.H. (1977). Shear requirements for load reversals on RC members. *Journal of the Structural Division*, 103(7), 1461–1476.

[152] Gouda, V.K. (1970). Corrosion and Corrosion Inhibition of Reinforcing Steel: I. Immersed in Alkaline Solutions. *British Corrosion Journal*, 5(5), 198–203.

[153] Gowripalan, N., Sirivivatnanon, V., & Lim, C.C. (2000). Chloride diffusivity of concrete cracked in flexure. *Cement and Concrete Research*, 30, 725–730.

[154] Gulikers, J. (2005). Theoretical considerations on the supposed linear relationship between concrete resistivity and corrosion rate of steel reinforcement. *Materials and Corrosion*, 56(6), 393–403.

[155] Hamada, M. (1968). *Proceedings of the Fifth International Symposium of the Chemistry of Cement*, Tokyo, Session III-3, Principal paper, 343–409.

[156] Hausmann, D.A. (1967). Steel corrosion in concrete - How does it occur?. *Materials Protection*, 11, 19–23.

[157] Hou, H-b., & Zhang, G-z. (2004). Assessment on chloride contaminated resistance of concrete with non-steady-state migration method. *Journal of Wuhan University of Technology*, 19(4), 6–8.

[158] Hwang, H., Liu, J.B., & Chiu, Y.H. (2000). *Seismic fragility analysis of highway bridges*. Technical Report No. MAEC RR-4, Mid-America Earthquake Center, Urbana, IL.

[159] Kafali, C., & Grigoriu, M. (2005). Rehabilitation decision analysis. G. Augusti, G. Schüeller & M. Ciampoli (eds.), *Safety and Reliability of Engineering Systems and Structures*, Millpress, 2773–2780.

[160] Kafali, C. & M. Grigoriu, M. (2006) *System Performance Under a Multi-Hazard Environment*, Report MCEER-08-0006.

[161] Kilareski, W.P. (1980). Corrosion induced deterioration of reinforced concrete – an overview, *Materials Performance*, NACE, 19(3), 48-50.

[162] Kobayashi, K. (2006). The seismic behavior of RC members suffering from chloride-induced corrosion. *Proceedings of the 2nd International* fib *Congress*.

[163] Kong, J.S., Ababneh, A.N., Frangopol, D.M., & Xi, Y. (2002). Reliability analysis of chloride penetration in saturated concrete. *Journal of Probabilistic Engineering Mechanics*, 17(3), 302–315.

[164] Krätzig, W.B., Meyer, I.F., & Meskouris, K. (1989). Damage evolution in reinforced concrete members under cyclic loading. *Proceedings of the 5th International Conference on Structural Safety and Reliability (ICOSSAR89)*, San Francisco, CA, 2, 795–804.

[165] Kumar, R., Gardoni, P., & Sanchez-Silva, M. (2009). Effect of cumulative seismic damage and corrosion on the life cycle cost of reinforced concrete bridges. *Earthquake Engineering and Structural Dynamics*, 38, 887–905.

[166] Kunnath, S.K, & Reinhorn, A.M. (1989). *Inelastic three-dimensional response analysis of reinforced concrete structures subjected to seismic loads*. Technical Report No. NCEER-88-0041, University at Buffalo, The State University of New York, NY, USA.

[167] Lee, H.S., Noguchi, T., & Tomosawa, F. (2002). Evaluation of the bond properties between concrete and reinforcement as a function of the degree of reinforcement corrosion. *Cement and Concrete Research*, 32 (8), 1313–1318.

[168] Li, C.Q., Zheng, J.J., Lawanwisut, W., & Melchers, R.E. (2007). Concrete delamination caused by steel reinforcement corrosion, *ASCE Journal of Materials in Civil Engineering*, 19(7), 591–600.

[169] Liu, T., & Weyers, R.W. (1998). Modeling the dynamic corrosion process in chloride contaminated structures. *Cement and Concrete Research*, 28 (3), 365–379.

[170] Lounis, Z., & Amleh, L. (2004). Reliability-based prediction of chloride ingress and reinforcement corrosion of aging concrete bridge decks. *Life cycle performance of deteriorating structures*, 113–222.

[171] Lowes, L. N., Mitra, N., & Altoontash, A. (2003). *A beam-column joint model for simulating the earthquake response of reinforced concrete frames*. Pacific Earthquake Engineering Research Center, College of Engineering, University of California.

[172] Lupoi, A., Franchin, P., & Schotanus, M. (2003). Seismic risk evaluation of RC bridge structures. *Earthquake Engineering & Structural Dynamics*, 32(8), 1275–1290.

[173] Maaddawy, T.E., & Soudki, K. (2007) A model for prediction of time from corrosion initiation to corrosion cracking. *Cement & Concrete Composites*, 29, 168–175.

[174] Malerba, P.G. (Ed.) (1998). *Limit and Nonlinear Analysis of Reinforced Concrete Structures*. International Centre for Mechanical Sciences (CISM), Udine, Italy (in Italian).

[175] Malerba, P.G., & Bontempi, F. (1989). Analisi di telai in C.A. in presenza di non linearità meccaniche e geometriche. *Studi e Ricerche*, *Graduate School for Concrete Structures "F.lli Pesenti"*, Politecnico di Milano, Milan, Italy, 11, 209–224 (in Italian).

[176] Mander, J.B., & Basoz, N. (1999). Seismic fragility curve theory for highway bridges in transportation lifeline loss estimation. *Optimizing post-earthquake lifeline system reliability*, TCLEE monograph no. 16 (Vol. 59) (pp. 315–338). Reston, VA: American Society of Civil Engineering and Design 1980.

[177] Mander, J.B., Dhakal, R.P., Mashiko, N., & Solberg, K.M. (2007). Incremental dynamic analysis applied to seismic financial risk assessment of bridges. *Engineering Structures*, 29(10), 2662–2672.

[178] Mander, J.B., Priestley, M.J.N & Park. R. (1988). Theoretical stress-strain model for confined concrete. *Journal of Structural Engineering*, 114(8), 1804–1826.

[179] Martin-Perez, B., & Lounis, Z. (2003). Numerical modelling of service life of reinforced concrete structures. *In D.J. Naus (Ed.), Actas del 2nd International RILEM Workshop of Life Prediction and Aging Management of Concrete Structures*, 71–79.

[180] Mazzoni, S., McKenna, F. & Fenves, G.L. (2005). *OpenSees command language manual*. Pacific Earthquake Engineering Research (PEER) Center.

[181] Naito, H., Akiyama, M., & Suzuki, M. (2010). Ductility evaluation of concrete-encased steel bridge piers subjected to lateral cyclic loading. *Journal of Bridge Engineering*, 16(1), 72–81.

[182] NCHRP (2006). *Manual on Service Life of Corrosion-Damaged Reinforced Concrete Bridge Superstructure Elements*. National Cooperative Highway Research Program, Report 558, Transportation Research Board, Washington, D.C., USA.

[183] Nielson, B.G., & DesRoches, R. (2007). Seismic fragility methodology for highway bridges using a component level approach. *Earthquake Engineering & Structural Dynamics*, 36(6), 823–839.

[184] Nielson, B.G., & DesRoches, R. (2007). Analytical seismic fragility curves for typical bridges in the central and southeastern United States. *Earthquake Spectra*, 23(3), 615-633.

[185] Nowak, A.S. & Frangopol, D.M. (Eds.) (2005). *Advances in Life-Cycle Analysis and Design of Civil Infrastructure Systems*. Lincoln, Nebraska.

[186] Nürnberger, U. (2002). Corrosion induced failure mechanisms of prestressing steel. *Materials and Corrosion*, 53(8), 591–601.

[187] Ou, Y.C., Tsai, L.L., & Chen, H.H. (2012). Cyclic performance of large-scale corroded reinforced concrete beams. *Earthquake Engineering & Structural Dynamics*, 41(4), 593–604.

[188] Ou, Y.-C., Wang, P.-H., Tsai, M.-S., Chang, K-C., & Lee, G.C. (2010). Large-scale experimental study of precast segmental unbonded post-tensioned concrete bridge columns for seismic regions. *Journal of Structural Engineering*, ASCE, 136(3), 255–264.

[189] Ouglova, A., Berthaud, Y., Foct, F., François, M., Ragueneau, F., & Petre-Lazar, I. (2008). The influence of corrosion on bond properties between concrete and reinforcement in concrete structures. *Materials and Structures*, 41(5), 969–980.

[190] Oyado, M., Kanakubo, T., Sato, T., & Yamamoto, Y. (2011). Bending performance of reinforced concrete member deteriorated by corrosion. *Structure and Infrastructure Engineering*, 7(1-2), 121–130.

[191] Oyado, M., Saito, Y., Yasojima, A., Kanakubo, T., & Yamamoto, Y. (2007). Structural performance of corroded RC column under seismic load. *Proceedings of the First International Workshop on Performance, Protection and Strengthening of Structures under Extreme Loading*, Whistler, Canada, August 20–22.

[192] Padgett, J.E., & DesRoches, R. (2007). Bridge functionality relationships for improved seismic risk assessment of transportation networks. *Earthquake Spectra*, 23(1), 115–130.

[193] Padgett, J.E., & DesRoches, R. (2007). Sensitivity of seismic response and fragility to parameter uncertainty. *Journal of Structural Engineering*, 133(12), 1710–1718.

[194] Padgett, J.E., & DesRoches, R. (2008). Methodology for the development of analytical fragility curves for retrofitted bridges. *Earthquake Engineering & Structural Dynamics*, 37(8), 1157–1174.

[195] Page, C.L., Short, N.R., & El Tarras, A. (1981). Diffusion of chloride ions in hardened cement paste. *Journal of Cement and Concrete Research*, 11(3) 395–406.

[196] Page, C.L., Short, N.R., & Holden, W.R. (1986). The influence of different cements on chloride-induced corrosion of reinforcing steel. *Cement and Concrete Research*, 16(1), 79–86.

[197] Palermo, A., & Pampanin, S. (2008). Enhanced seismic performance of hybrid bridge systems: comparison with traditional monolithic solutions. *Journal of Earthquake Engineering*, 12(8), 1267–1295.

[198] Pampanin, S., Christopoulos, C., & Priestley, M.J.N. (2002). *Residual Deformations in the Performance-Based Seismic Assessment of Frame Structures*. IUSS Press, Pavia, Italy.

[199] Pantazopoulou, S.J., & Papoulia, K.D. (2001). Modeling cover-cracking due to reinforcement corrosion in RC structures. *Journal of Engineering Mechanics*, 127(4), 342–351.

[200] Papia, M., Russo, G., & Zingone, G. (1988). Instability of longitudinal bars in RC columns. *Journal of Structural Engineering*, ASCE, 114(2), 445–461.

[201] Park, R. (1986). Ductile design approach for reinforced concrete frames. *Earthquake Spectra*, 2(3), 565–619.

[202] Park, Y.J., & Ang, A.H.S. (1985). Mechanistic seismic damage model for reinforced concrete. *Journal of Structural Engineering*, 111(4), 722–739.

[203] Park, Y.J., Ang, A.H. S., & Wen, Y.K. (1987a). Damage-limiting aseismic design of buildings. *Earthquake Spectra*, 3(1), 1–26.

[204] Park, R., & Paulay, T. (1975). *Reinforced concrete structures*. New York: John Wiley & Sons.

[205] Park, Y.J., Reinhorn, A.M., & Kunnath, S.K. (1987b). IDARC: Inelastic damage analysis of reinforced concrete frame-shear-wall structures. *Technical Report NCEER-87-0008*, National Center for Earthquake Engineering Research, State University of New York, Buffalo, NY.

[206] Parrott, L.J. (1991). Carbonation, moisture and empty pores. *Advances in Cement Research*, 4(15), 111–118.

[207] Parrott, P.J. (1994). Design for avoiding damage due to carbonation-induced corrosion. *Proceedings of Canmet/ACI International Conference on Durability of Concrete*, Nice, 283.

[208] Pastore, T., & Pedeferri, P., (1994). *La Corrosione e la Protezione delle Opere Metalliche Esposte all'Atmosfera* (In Italian). L'edilizia, December, 75–92.

[209] Pedeferri, P., & Bertolini, L. (1996). *La Corrosione nel Calcestruzzo e negli Ambienti Naturali*, McGraw-Hill.

[210] Pedeferri, P., & Bertolini, L. (2000). *Durability of Reinforced Concrete* (in Italian), McGrawHill Italia, Milan.

[211] Penzien, J. (1993). Seismic design criteria for transporation structures. *Structural Engineering in Natural Hazards Mitigation: Proceedings of the ASCE Structures Congress 1993*, Irvine, CA, 1, 4–36.

[212] Polder, R.B., Peelen, W.H.A., Bertolini, L., & Guerrieri, M. (2002). Corrosion rate of rebars from linear polarization resistance and destructive analysis in blended cement concrete after chloride loading, *15th International Corrosion Congress,* September 22-27, 2002, Granada.

[213] Powell, G.H., & Allahabadi, R. (1988). Seismic damage prediction by deterministic methods: concepts and procedures. *Earthquake engineering & structural dynamics*, 16(5), 719–734.

[214] Priestley, M.J.N., Calvi, G.M., & Kowalsky, M.J. (2007). *Displacement-Based Seismic Design of Structures*. Pavia: IUSS Press.

[215] Priestley, M.J.N., & Paulay, T. (1992). *Seismic Design of Reinforced Concrete and Masonry Buildings*. New York ,NY, USA, John Wiley & Sons.

[216] Priestley, M.N.J., Seible. F., & Calvi, G.M. (1996). *Seismic Design and Retrofit of Bridges*. John Wiley & Sons, New York, NY.

[217] Rasheeduzzafar, Al-Saadoun, S.S., & Al-Gahtani, A.S. (1992). Corrosion cracking in relation to bar diameter, cover, and concrete quality. *Journal of Materials in Civil Engineering*, 4(4), 327–342.

[218] Renschler, C.S., Frazier, A.E., Arendt, L.A., Cimellaro, G.P., Reinhorn, A.M. & Bruneau, M. (2010). *A Framework for Defining and Measuring Resilience at the Community Scale: The PEOPLES Resilience Framework*, Report MCEER-10-0006.

[219] Rodriguez, J., Ortega, L.M., & Casal, J. (1997). Load carrying capacity of concrete structures with corroded reinforcement. *Construction and Building Materials*, 11(4), 239–248.

[220] Rose, A. (2004). Defining and measuring economic resilience to disasters. *Disaster Prevention and Management*, 13(4), 307–314.

[221] Rose, A., Benavides, J., Chang, S.E., Szczesniak, P., & Lim, D. (1997). The regional economic impact of an earthquake: direct and indirect effects of electricity lifeline disruptions. *Journal of Regional Science*, 37(3), 437–458.

[222] Saetta, A.V. (2005). Deterioration of reinforced concrete structures due to chemical–physical phenomena: model-based simulation. *Journal of Materials in Civil Engineering*, 17(3), 313–319.

[223] Saetta, A., Scotta, R., & Vitaliani, R. (1999). Coupled environmental-mechanical damage model of rc structures. *Journal of Engineering Mechanics*, 125(8), 930–940.

[224] Saito, Y., Oyado, M., Kanakubo, T., & Yamamoto, Y. (2007). Structural performance of corroded RC column under uniaxial compression load. *First International Workshop on Performance, Protection & Strengthening of Structures under Extreme Loading*, Whistler, Canada.

[225] Sarja, A. (2000). Durability design of concrete structures – Committee report 130-CSL. *Materials and Structures*, 33(1), 14–20.

[226] Sarja, A., & Vesikari, E. (Editors) (1996). *Durability Design of Concrete Structures*, Manuscript of RILEM Report of TC 130-CSL. RILEM Report Series 14. E&FN Spon, Chapman & Hall.

[227] Schueller, G.I. & Pradlwarter, H.J. (2009). Uncertainty analysis of complex structural systems. *International Journal for Numerical Methods in Engineering*, 80(6-7), 881–913, 2009.

[228] Schneider, U. (1988). Concrete at high temperatures - a general review. *Fire Safety Journal*, 13(1), 55–68.

[229] SEAOC Vision 2000 Committee (1995). *Performance Based Seismic Engineering*. Sacramento, California: Structural Engineers Associate of California.

[230] Shafei, B., Alipour, A., & Shinozuka, M. (2012). Prediction of corrosion initiation in reinforced members subjected to environmental stressors: a finite-element framework. *Cement and Concrete Research*, 42, 365–376.

[231] Sharpe, R.D. (1974). *The Seismic Response of Inelastic Structures*. PhD Thesis, Department of Civil Engineering, University of Canterbury, Christchurch, New Zealand.

[232] Sharp, J.V., & Pullar-Strecker, P. (1980). The United Kingdom concrete-in-the-ocean program. *International Conference on Performance of Concrete in Marine Environment*, ACI SP65, 397–417.

[233] Shinozuka, M. (2009). Resilience and sustainability of infrastructure systems. *Frontier Technologies in Infrastructure Engineering: Structures and Infrastructures Book Series*, 4, 245.

[234] Siemes, T., Han, N., & Visser, J. (2002). Unexpectedly low tensile strength in concrete structures. *Heron*, 47(2), 111–124.

[235] Shinozuka, M., Feng, M.Q., Kim, H.K., & Kim, S.H. (2000). Nonlinear static procedure for fragility curve development. *Journal of Engineering Mechanics*, 126(12), 1287–1295.

[236] Shinozuka, M., Feng, M.Q., Lee, J., & Naganuma, T. (2000). Statistical analysis of fragility curves. *Journal of Engineering Mechanics*, 126(12), 1224–1231.

[237] Sobhani, J., & Ramezanianpour, A.A. (2007). Chloride-induced corrosion of RC structures. *Asian Journal of Civil Engineering (Building and Housing)*, 8(5), 531–547.

[238] Sohanghpurwala, A.A. (2006). *Manual on Service Life of Corrosion-damaged Reinforced Concrete Bridge Superstructure Elements* (Vol. 558). National Cooperative Highway Research Program, Transportation Research Board National Research, Washington, DC, US.

[239] Spacone E., Filippou F.C., & Taucer F.F. (1996). Fibre beam-column element for nonlinear analysis of R/C frames. Part I: Formulation. *Earthquake Engineering and Structural Dynamics*, 25, 711–725.

[240] Spacone, E., & Limkatanyu, S. (2000). Responses of reinforced concrete members including bond-slip effects. *ACI Structural Journal*, 97(6), 831–839.

[241] Stanish, K., Hooton, R. D., & Pantazopoulou, S. J. (1999). Corrosion effects on bond strength in reinforced concrete. *ACI Structural Journal*, 96(6).

[242] Stewart, M.G. (2009). Mechanical behaviour of pitting corrosion of flexural and shear reinforcement and its effect on structural reliability of corroding RC beams. *Structural Safety*, 31, 19–30.

[243] Stewart, M.G., & Rosowsky, D.V. (1998). Time-dependent reliability of deteriorating reinforced concrete bridge decks. *Structural Safety*, 20(1), 91–109.

[244] Strauss, A., Frangopol, D.M. & Bergmeister K. (2012). *Life-Cycle and Sustainability of Civil Infrastructure Systems*, CRC Press, Taylor & Francis Group plc., A. A. Balkema, Boca Raton, London, New York, Leiden.

[245] Thoft-Christensen, P. (1998). Assessment of the reliability profiles for concrete bridges. *Engineering Structures*, 20(11), 1004–1009.

[246] Thomas, M. (1996). Chloride thresholds in marine concrete. *Cement and Concrete Research*, 26(4), 513–519.

[247] Titi, A. (2012). *Lifetime Probabilistic Seismic Assessment of Multistory Precast Buildings*. PhD Thesis, Department of Structural Engineering, Politecnico di Milano, Milan, Italy.

[248] Titi, A., & Biondini, F. (2012). Validation of diffusion models for life-cycle assessment of concrete structures. *Third International Symposium on Life-Cycle Civil Engineering* (*IALCCE 2012*), Vienna, Austria, October 3-6.

[249] Titi, A., & Biondini, F. (2013). Resilience of concrete frame structures under corrosion. *Proceedings of the 11th International Conference on Structural Safety and Reliability* (*ICOSSAR2013*), June 16-20, New York, NY, USA.

[250] Tuutti, K. (1982). *Corrosion of Steel in Concrete*, Swedish foundation for concrete research, Stockholm.

[251] UNI 11104 (2004). *Concrete. Specification, performance, production and conformity - Additional provisions for the application of EN 206-1*. UNI, Ente Nazionale Italiano di Unificazione.

[252] UN/ISDR (2009). *Global assessment report on disaster risk reduction. United Nations International Strategy for Disaster Reduction,* Geneva.

[253] Val, D.V. & Melchers, R.E. (1997). Reliability of deteriorating rc slab bridges. *Journal of Structural Engineering*, 123(12), 1638–1644.

[254] Val, D.V., Stewart, M.G., & Melchers, R.E. (1998). Effect of reinforcement corrosion on reliability of highway bridges. *Engineering Structures*, 20(11), 1010-1019.

[255] Val, D.V., Stewart, M., & Melchers, R.E. (2000). Life-cycle performance of RC bridges: Probabilistic approach. *Computer Aided Civil Infrastructure Engineering*, 15(1), 14–25.

[256] Vassie, P. (1984). Reinforcement corrosion and the durability of concrete bridges. *Proceedings of the Institution of Civil Engineers – Part I*, 76, 713–723.

[257] Vergani, M. (2010). *Modellazione del Degrado di Strutture in Calcestruzzo Armato Soggette a Corrosione* (in Italian). Master Degree Thesis, Politecnico di Milano, Italy.

[258] Vidal, T., Castel, A., & Francois, R. (2004). Analyzing crack width to predict corrosion in reinforced concrete. *Cement and Concrete Research*, 34, 165–174.

[259] Vu, K.A.T., & Stewart, M.G. (2000). Structural reliability of concrete bridges including improved chloride-induced corrosion models. *Structural Safety*, 22(4), 313–333.

[260] Wachtendorf, T., Connell, R., Tierney, K.J., & Kompanik, K. (2002). *Disaster Resistant Communities Initiative: Assessment Of The Pilot Phase – Year 3*. Disaster Research Center, University of Delaware, Newark, DE.

[261] Wang, K., Jansen, D.C., Shah, S.P., & Karr, A.F. (1997). Permeability study of cracked concrete. *Cement and Concrete Research*, 27(3), 381-393.

[262] Wang, X., & Liu, X. (2004). Modeling bond strength of corroded reinforcement without stirrups. *Cement and Concrete Research*, 34(8), 1331–1339.

[263] Williams, M.S., & Sexsmith, R.G. (1995). Seismic damage indices for concrete structures: a state-of-the-art review. *Earthquake Spectra*, 11(2), 319–349.

[264] Wolfram, S. (1983). Statistical mechanics of cellular automata. *Reviews of Modern Physics*, 55(3).

[265] Xi, Y., & Bazant, Z.P. (1999). Modeling of chloride penetration in saturated concrete. *Journal of Materials in Civil Engineering*, 11(1), 58–65.

[266] Xu, N., Guikema, S.D., Davidson, R.A., Nozick, L. K., Çağnan, Z., & Vaziri, K. (2007). Optimizing scheduling of post-earthquake electric power restoration tasks. *Earthquake Engineering & Structural Dynamics*, 36(2), 265–284.

[267] Yalsyn, H., & Ergun, M. (1996). The prediction of corrosion rates of reinforcing steels in concrete. *Cement and Concrete Research*, 26(10), 1593–1599.

[268] Yamamoto, T., Hattori, A., & Miyagawa, T. (2006). Uniaxial compression behavior of confined concrete deteriorated by corrosion of reinforcing steel. *Journal of the Society of Material Science*, 55 (10), 911–916 (in Japanese).

[269] Yamamoto, T., & Kobayashi, K. (2006). Report of research project on structural performance of deteriorated concrete structures by JSCE 331-review of experimental study. *Proceedings of the International Workshop on Life Cycle Management of Coastal Concrete Structures*, Nagoake, Japan, 171-180.

[270] Yuya, S., Oyado, M., Kanakubo, T., & Yamamoto, Y. (2007). Structural Performance of Corroded RC Column under Uniaxial Compression Load. http://rcs.kz.tsukuba.ac.jp/protect2007s.pdf

[271] Zhang, R., Castel, A., & François, R. (2009). Concrete cover cracking with reinforcement corrosion of RC beams during chloride-induced corrosion process, *Cement and Concrete Research*, 40(3), 415–425.

[272] Zienkiewicz, O.C., & Taylor R.L. (2000) *The Finite Element Method, Volume 1: The Basis*. Butterworth-Heinemann.

LIST OF FIGURES

LIST OF TABLES